Spin Sensitive Behavior of Quantum Dots Coupled to Topological Insulators or Superconductors

Von der Fakultät für Elektrotechnik, Informationstechnik, Physik
der Technischen Universität Carolo-Wilhelmina zu Braunschweig

zur Erlangung des Grades eines Doktors

der Naturwissenschaften (Dr. rer. nat.)

genehmigte Dissertation

von Benedikt Gebhard Probst

aus Tübingen

eingereicht am: 19.04.2018

Disputation am: 25.06.2018

1. Referent: Prof. Dr. Patrik Recher
2. Referent: Prof. Dr. Thomas Schmidt

Druckjahr: 2018

Dissertation an der Technischen Universität Braunschweig,
Fakultät für Elektrotechnik, Informationstechnik, Physik

Spin Sensitive Behavior of Quantum Dots Coupled to Topological Insulators or Superconductors

In this thesis we discuss a quantum dot coupled to a helical Luttinger liquid as well as a double dot Josephson junction. In both setups we define a reduced system. We calculate the state of these systems as well as the transport through these systems. Perturbation theory then allows us to identify the relevant processes.

First, we consider a Zeeman-split quantum dot coupled to a helical Luttinger liquid built by the edge states of a quantum spin Hall insulator. The quantum dot is assumed to be in the cotunneling regime containing a single spin $1/2$ electron such that it can be described by the Kondo model. We describe this system using a generalized master equation approach. Applying a bias voltage to the helical Luttinger liquid induces a magnetic field parallel to the spin quantization direction of the helical edge states on the quantum dot. For parallel orientation of the magnetic field and the spin quantization axis in the edge states the spin polarization can be manipulated in strength as well as direction by the bias voltage applied to the edge state. The backscattering conductance shows a resonance when the bias voltage and the Zeeman splitting are equal in magnitude. The strength of this resonance shows a different strength for positive and negative bias. The strength of this asymmetry directly reflects the relative orientation of the magnetic field and the spin quantization direction in the edge state allowing to probe the latter. Using full counting statistics we find that depending on the polarity of the bias voltage the resonance leads to bunching or antibunching. This is interpreted by breaking down the dynamics to the single scattering events. By using bosonization we are able to include electron–electron interaction in the helical edge state. We find that the qualitative features of the system are robust.

Finally, we study the critical Josephson current of a parallel double quantum dot without capacitive or tunnel coupling weakly coupled to two superconductors. In contrast to previous studies we include all charging states of the quantum dots and do not restrict the discussion to the limit of infinite superconducting gaps. We use analytical as well as numerical methods to calculate the ground state of the system treating the on-site interaction exactly. In the limit of infinite superconducting gaps we find that local transport is suppressed and resonant features are clear indicators for nonlocal behavior. We show that reducing the superconducting gaps

can lead to a nonlocal singlet–triplet transition in the ground state which is an inherent nonlocal feature. This singlet–triplet transition leads to an asymmetric peak structure in the critical current. The relevant processes are identified using perturbation theory. To organize the processes used in the perturbative treatment we introduce a diagrammatic scheme. Our findings support the interpretation of recent experiments [R. S. Deacon, A. Oiwa, J. Sailer, S. Baba, Y. Kanai, K. Shibata, K. Hirakawa, and S. Tarucha, Nat. Commun. 6, 7446 (2015)] and also suggest new signatures of nonlocal Cooper pair transport.

Spinsensitives Verhalten von an topologische Isolatoren oder Supraleiter gekoppelten Quantenpunkten

In dieser Dissertation beschäftigen wir uns zum einen mit einem an einen helikalen Randkanal gekoppelten Quantenpunkt und zum anderen mit einem Doppelquantenpunkt Josephson Kontakt. Wir bestimmen den Zustand dieser beiden Systeme und die Eigenschaften des Transportes durch diese Systeme. Dabei benutzen wir jeweils Störungsrechnung, um die relevanten Prozesse zu finden.

Zuerst betrachten wir einen Quantenpunkt mit Zeeman-Aufspaltung, der durch Tunneln an den Rand eines Quanten-Spin-Hall-Isolators gekoppelt ist. Dabei gehen wir davon aus, dass der Quantenpunkt mit einem Spin $1/2$ Fermion einfach besetzt und im Kotunnelregime ist, so dass er im Kondo-Modell beschrieben werden kann. Das System wird mit einer generalisierten Mastergleichung beschrieben. Indem eine Spannung an den Randkanal angelegt wird, wird ein Magnetfeld auf dem Quantenpunkt induziert, das zur Spinquantisierungsachse im Randkanal parallel ist. Sind diese Achsen nicht parallel, kann man die Spinpolarisation auf dem Quantenpunkt sowohl in Stärke als auch in Richtung mit der an den Randkanal angelegten Spannung elektrisch manipulieren. Der Rückstreustrom zeigt dabei eine Resonanz, wenn die Spannung betragsmäßig der Zeeman-Aufspaltung entspricht. Die Stärke dieser Resonanz hängt vom Vorzeichen der Spannung ab. Die Stärke dieser Asymmetrie hängt direkt mit der relativen Orientierung des Magnetfeldes und der Spinquantisierungsachse im Randkanal zusammen. Dieser Zusammenhang läßt Rückschlüsse auf die Richtung der Spinquantisierungsache im Randkanal zu. Mithilfe der Zählstatistik konnten wir zeigen, dass die einzelnen Streuereignisse sich je nach Vorzeichen der Spannung anziehen oder abstoßen. Um dieses Verhalten zu verstehen, wurde die Dynamik in einzelne Streuereignisse und deren Wahrscheinlichkeiten und Raten zerlegt. Durch Bosonisierung konnte die Elektron-Elektron Wechselwirkung im Randkanal berücksichtigt werden. Diese Wechselwirkung beeinträchtigt die qualitativen Beobachtungen nicht.

Zuletzt betrachten wir den kritischen Josephson-Strom eines Doppelquantenpunktes ohne kapazitive Kopplung oder Tunnelkopplung der Quantenpunkte untereinander, der durch Tunneln mit zwei Supraleitern verbunden ist. Im Gegensatz zu bisherigen Arbeiten berücksichtigen wir alle Ladungszustände und beschränken uns nicht auf den Grenzwert einer

großen supraleitenden Bandlücke. Wir benutzen analytische sowie numerische Methoden, um den Grundzustand des Systems zu berechnen. Dabei wird die Wechselwirkung auf dem Quantenpunkt exakt behandelt. Im Grenzfall einer großen supraleitenden Bandlücke finden wir, dass lokaler Transport unterdrückt ist und resonantes Verhalten ein klarer Indikator für nichtlokalen Transport ist. Wir zeigen, dass eine Reduktion der supraleitenden Bandlücke zu einem Singulett–Triplett Übergang im Grundzustand führen kann, welcher eine inhärent nichtlokale Eigenschaft ist. Dieser Singulett–Triplett-Übergang führt zu asymmetrischen Spitzen im kritischen Strom. Die relevanten Prozesse konnten mithilfe von Störungsrechnung bestimmt werden. Um die Menge der beteiligten Prozesse zu ordnen, wurde ein diagrammatisches Schema eingeführt. Unsere Beschreibung bestätigt die Interpretation neuerer Experimente [R. S. Deacon *et al.*, Nat. Commun. 6, 7446 (2015)] und schlägt weitere Signaturen für nichtlokalen Transport vor.

Acknowledgments

First and foremost I would like to thank Prof. Dr. Patrik Recher. He gave me the chance to work on interesting topics in his group. His guidance and ideas allowed me to bring this thesis to the point where it is now. His thoroughness and focus on detail as well as his overview of the field enriched our long discussions, which I will miss.

Next I would like to thank Prof. Dr. Thomas Schmidt for agreeing to co-referee this thesis and Prof. Dr. Peter Lemmens for chairing the defense of this thesis.

Working in the group of Prof. Dr. Patrik Recher was a pleasure and many discussions and seminars helped keeping an overview over the development of the field. Especially I would like to thank Dr. Pauli Virtanen who helped me to set the direction of the QD-HLL project in the beginning and in the FCS part later on. He was an invaluable help and the discussions continued way past his time in Braunschweig. Furthermore, I would like to thank Prof. Dr. Alfredo Levy Yeyati and Dr. Fernando Domínguez for the discussions and their collaboration in the double dot Josephson junction project.

A special thank goes to all my colleagues here at the Institute of Mathematical Physics and the Institute of Theoretical Physics for fun activities and discussions. Cornelia Schmidt deserves a special mentioning. She fought our battles with bureaucracy and welcomed me for countless coffee brakes in her office.

Another special thank deserve my office mates Dr. Alexander Schroer and Alexander Schuray, who always had an open ear to spontaneous discussions and fun projects. Furthermore I would like to thank the group members of the first hour Dr. Anders Ström and Luzie Weithofer with whom we started the group. All these people were not just colleagues but also became friends to me and not only made my time at the institute but also my time in Braunschweig and even a visit in Gothenburg or Ingolstadt a treat.

A city is only the people you meet there. For making my time in Braunschweig memorable I would like to thank the Schokoboller for a lot of fun weekends, the Segelgruppe for rekindling my love for sailing and the Uniorchester for fun music and Stammtisch sessions. I would especially like to thank Dr. Sarah Horst who offered to proofread the thesis last minute.

Finally, I would like to thank my family for their support. My parents and my sister and her family not only supported my decision to do a doctorate but also encouraged me when needed.

List of Publications

- *Controlling spin polarization of a quantum dot via a helical edge state*, B. Probst, P. Virtanen, and P. Recher, Phys. Rev. B **92**, 045430 (2015)
- *Signatures of nonlocal Cooper-pair transport and of a singlet-triplet transition in the critical current of a double-quantum-dot Josephson junction*, B. Probst, F. Domínguez, A. Schroer, A. Levy Yeyati, and P. Recher, Phys. Rev. B **94**, 155445 (2016)

Contents

Chapter 1

Introduction

One of the major changes in the understanding of the properties of electrons and nuclei was to discover that they have an intrinsic magnetic moment called spin. In 1922 W. Stern and O. Gerlach measured the magnetic moment of silver atoms by shooting them through a magnetic field gradient [Ger22c, Ger22b, Ger22a]. To their surprise they found that the resulting distribution was not continuous but showed two distinct orientations and thus was quantized. Moreover, it turned out that this magnetic momentum cannot be explained by the orbital angular momentum of the electrons alone. This meant that the electrons in the atom also needed to have an intrinsic angular momentum which is called spin.

To describe the angular momentum and thus the magnetic moment of electrons properly in quantum mechanics one uses operators with $SU(2)$ symmetry. The smallest representation of this group are the Pauli matrices. These are used to describe the angular momentum of spin $1/2$ particles as for example the electron. One property of the $SU(2)$ symmetry is that the spin operators in different directions will not commute. This makes spin and angular momentum one of the important subjects in quantum mechanics [Sak09].

For a lot of cases the spin in condensed matter systems plays a minor role just adding an extra factor of two due to the degeneracy associated with it. When magnetic fields are involved this degeneracy is lifted by the Zeeman interaction. A simple example for such a behavior is the Pauli paramagnetism that can be obtained by including this shift into the spin dependent density of states [Pau27]. But even without external magnetic fields the spin can play a role when including interaction. Including the Coulomb repulsion one can obtain the Stoner model in mean field theory that has a ferromagnetic phase [Sto38]. Another important role can be played by magnetic impurities. Here spin flip scattering and the degeneracy of the spin states in the lead can lead to a breakdown in perturbation theory. This breakdown is at the heart of the Kondo effect [Hew93].

The effects mentioned above basically do not involve a spin dependent model to begin with but introduce an external field, a spontaneously broken symmetry or an impurity having spin. As soon as the symmetry is broken, ferromagnets can be described by an explicitely spin dependet model which has a different density of states for the two spins and thus a macroscopic magnetic moment. This opens a large variety of phenomena. The most prominent example is the giant magneto resistance (GMR) effect. This effect describes a strong response of the resistance to slight changes in an external magnetic field. The original effect was observed in herterostructures in which two ferromagnets are coupled by a normal metal layer [Bai88, Bin89]. The normal metal mediates an exchange interaction between the magnetic moments of the ferromagnetic layers depending on the thickness of the normal metal layer in an oscillatory manner such that even the sign of the interaction strength can change [Grü86]. This allows to build a device in which the two ferromagnetic layers are coupled antiferromagnetically leading to an antiparallel orientation of the magnetizations. This blocks transport as the majority spin electrons in one ferromagnet are minority spins in the other ferromagnet. Adding a magnetic field will align the magnetizations and thus opens transport channels. These devices are very sensitive probes for magnetic fields. This allowed to increase the data density on hard drives significantly and was awarded a Nobel prize in 2007 to Albert Fert and Peter Grünberg [Grü08, Fer08].

The fact that spin gives another quantum number has a huge impact on the behavior of interacting electrons. Pauli's exclusion principle states that the wave functions of electrons must be odd under exchange of particles. For wave functions that are a product of a spatial and a spin wavefunction this imposes a strong constraint for these two wavefunctions. For two electrons with spin either the spatial wavefunction or the spin wave function has to be odd under exchange of the electrons. The other part then has to be even. If the spin wavefunction is even we can find three different combinations of the individual spins. These states are called the triplet states and correspond to a finite angular momentum. For the odd spin wave function we only find one combination which is called the singlet. The symmetry of these wave functions can have very different implications. Having a closer look at the spatial wave functions we find that in the triplet states with an odd spatial wavefunction the two electrons have no probability to be at the same location and thus tend to have a larger spatial separation. Electrons in the singlet state have a

non vanishing probability to be at the same location and thus are closer to each other [Sak09].

This different separation of the electrons can have very different consequences. In the helium atom, for example, being closer to each other can mean a higher energy due to the Coulomb repulsion of the electrons. When looking at the lowest excited states of the helium atom we find a singlet as well as triplet states. The triplets are here lower in energy than the singlet states as the electrons are further apart and the Coulomb interaction is repulsive [Hak04]. If we find a case where the interaction is attractive the singlet could lower its energy. This is the mechanism which allows the formation of Cooper pairs in superconductors [Tin96]. The attractive interaction can be understood by a retarded interaction mediated by phonons in the lattice of background atoms. This is the starting point for the BCS theory of superconductivity.

From atom physics a lot of concepts to manipulate the spin state of an atom are known. The state of a two level system, for example, can be manipulated with high accuracy using oscillating magnetic or electric fields. Rabi showed that using an oscillating magnetic field perpendicular to a strong static field one can drive transitions between the ground state and an excited state [Rab37]. Such a transition can be understood as a rotation on a Bloch sphere built from the ground state and the excited state [Bra03, Hak04]. A transition from the ground state to the excited state is a rotation by π. The efficiency of this rotation is determined by whether the frequency of the oscillating field matches the energy difference of the states. Ramsey showed that splitting the π rotation into two $\pi/2$ rotations applied with some time in between them not only reduces the width of this resonance but also makes the result more stable against inhomogeneities of the static field [Ram50]. Based on this technique very stable clocks can be built [Bra03]. For spin $1/2$ systems these oscillations not only resemble rotations on some abstract Bloch sphere but correspond to rotations in real space. Having this kind of control would also be interesting in solid state systems and the electrons in those. As these spin $1/2$ systems can also be used to build qubits this is especially of interest for solid state quantum computing [Los98, Han07]. It is, however, not straight forward to isolate and address single electron spins experimentally.

The region where an electron can move can, however, be restricted. In general, most solid state systems are three dimensional by nature. To reduce the effective dimensionality there are several methods. Some systems

are intrinsically reduced in dimensionality. A very famous example for a two dimensional material is graphene [CN09]. In graphene carbon atoms form a hexagonal flat lattice in which the remaining electron can move. Long molecules or atoms arranged at the surface of crystals are a few examples in which one ends up in a one dimensional arrangement of atoms. Another example that plays a particularly important role are semiconductor heterostructures that form two dimensional electron gases (2DEG). In those, two semiconductors with different gaps are joined, forming a two dimensional electron gas whose carrier density can be tuned by shifting the chemical potential [Dat97]. The other method is to put constraint on the motion in one direction. If we roll up graphene for example we enforce periodic boundary conditions in the transversal direction and end up with a one dimensional system with a band for each transversal mode called carbon nanotubes [Sai98, Lai15]. By growing wires with a very small diameter we obtain quantum wires. These now have a confinement in the transversal direction and are effectively one dimensional. Each transversal mode forms one band [Dat97]. Following this idea even further we see that if we now constrain an electron in all directions we obtain effectively a zero dimensional object called a quantum dot [Han07, Lai15]. This quantum dot now serves as a collection of localized energy levels and is sometimes also referred to as an artificial atom.

A special role is played by semiconductor heterostructures. In these systems the existence of mobile electrons depends on the chemical potential. By using top gates the chemical potential can be shifted locally such that the shape of the 2DEG can be modified very conveniently by gates. One can for example define a narrow constriction called a quantum point contact (QPC) [Bee91a]. The width of this constriction can be tuned electrically by metal gates such that the number of transmitting modes can be changed which allows the observation of conductance quantization [vW88]. One can even define quantum dots in such systems [Han07]. One huge advantage is that one has a high level of control on all parameters of the system.

The Coulomb interaction has a very strong effect on the behavior of the quantum dots. It most prominently introduces a charging energy such that the states with different number of electrons on the quantum dot are separated in energy [Soh97, Han07]. If an electron wants to tunnel onto the QD it thus needs energy. If the energy costs are too high the electrons cannot tunnel onto the QD such that no transport is possible. This effect is referred to as Coulomb blockade [Bee91b, Ale02]. By shifting

the energy level or by applying a bias voltage we can reach a situation in which the number of the electrons on the quantum dot can fluctuate. This then opens the possibility for resonant transport by sequential tunneling [Sch97, Han07]. If sequential tunneling is suppressed the transport is only possible via higher order coherent tunnel processes. This transport mechanism is called cotunneling and does not change the number of electrons on the QD [Ave92, Naz09]. The Coulomb interactions thus enables us to tune the transport regime between a regime in which the transport is dominated by the transfer of single electrons to the quantum dot in sequential tunneling and a regime in which coherent transport allows transport through the system without changing the number of electrons on the quantum dot via cotunneling.

This amount of control motivated a lot of ideas how to use those phenomena to manipulate not only the charge current but also the spin current. Recher *et al.* showed that, if a magnetic field is added to the quantum dot such that the ground state has a well defined spin due to the Zeeman interaction, the current through the quantum dot can be spin polarized [Rec01]. In this setup no spin polarization in the leads is required. The magnetic field here leads to the spin dependence of the current.

Another method that drives spin dependent behavior is the use of spin dependent materials. In ferromagnetic leads the density of states of the electrons depend on the spin which leads to a macroscopic polarization. Here the orientation of the ferromagnets plays a crucial role. Already the simple model of aligned ferromagnets with or without magnetic field shows interesting behavior [Wey05b, Wey05a]. When allowing the polarizations to be not aligned the behavior becomes even richer. It was shown that in the sequential tunneling regime the dynamics of the electrons on the quantum dot can be described by a Bloch like equation, accounting for spin accumulation, rotation as well as relaxation [Bra04]. They also showed that besides the external magnetic fields also induced fields from the source and drain lead play a role.

The properties in those systems are mainly characterized by the current of electrons through the system. One of the nice properties of QDs is that the transport is carried by single electrons. In sequential transport the QD fluctuates between two states whose electron numbers differ by one as with each jump one electron is transferred. If a QPC is placed right next to a QD the width of the constriction depends on the number of electrons on the QD. The number of electrons can now be measured

by the conductance of the QPC. This allows to measure the times of the single electron jump events through the QD [Gus06]. In this measurement not only the quantization becomes apparent in the discrete jumps but we also obtain the complete transport statistics. The statistics are referred to as full counting statistics.

In full counting statistics it is exploited that the charge is quantized and that a current can be defined by counting electrons. But in the temporal sequence in which the electrons are transferred there is much more information. When considering the probability that N electrons are transferred in a time interval T the average current is only the first cumulant of this probability distribution. Being able to detect single electron jump events one is able to go well beyond this first cumulant. The most prominent higher cumulant is the current noise which allows already a first insight whether the tunneling events of electrons are independent or not. A simple case where the electron tunnel events are not independent is a QD in the cotunneling regime. If inelastic cotunneling is possible and the cotunneling rate depends on the state of the QD, inelastic processes lead to additional noise which also translates into more irregular transport processes leading to super-Poissonian noise [Suk01].

The probability distribution for the transport of electrons is characterized by its cumulants completely. The cumulants are most conveniently calculated by looking at the cumulant generating function (CGF) which is given by the logarithm of the characteristic function of the distribution. Using these functions cumulants can be obtained as derivatives. Applying this idea to the probability that N electrons are transferred in a time interval T gives an intuitive formalism. In this formalism the argument of the CGF is called the counting field. This is motivated by the fact that it behaves like a field that only couples to terms that change the number of electrons in the lead. These counting fields can be included into most methods commonly used as for example Keldysh Greens functions [Bel03, Lev04, Bel05] or master equations [Bag03]. After using these approaches to calculate the cumulant generating function the cumulants and thus the transport properties can be calculated efficiently.

The high level of control in engineered solid state systems gives a very rich toolbox. It allows to process single spins as well as the control of single charges. This motivates not only to use methods from atom physics but also from quantum optics in the solid state to manipulate and analyze the behavior of these systems. In general one is not restricted to the current alone but can also access higher transport correlations.

Recently new phases of matter gained a lot of interest. In a variety of systems phase transitions were found that were in stark contrast to the phase transitions described by Landau theory. In these phase transitions in neither phase a symmetry was broken. The phase thus differ not in symmetry but in a topological invariant. Here we will focus on the systems being band insulators. One of the first effects that was understood in this way was the quantum Hall (QH) effect. In 1982 Thouless *et al.* used a generalized Bloch theorem to define a band structure for a 2DEG with magnetic field [Tho82]. In this band structure they defined a Berry curvature and using this curvature a topological invariant for the band structure. This topological invariant is protected by the gap in the sense that it cannot change unless the gap is closed. It is identified to be the number of occupied Landau levels. As it is very difficult to close the gap by disorder in strong magnetic fields this helped to understand the robustness of the QH state.

An important property of these topological insulators is that at the boundary of two domains of different topology boundary states exist. This can heuristically be understood by the gap protecting the topological invariant. If we consider the transition between the two topologically different domains to be adiabatic, the gap has to close if the topological invariant has to change. In the QH effect the topological transition is driven by the magnetic field. In a transition from a topological nontrivial to the topological trivial domain the magnetic field has to go from a finite value to zero. Assuming that the magnetic field changes slow enough such that we can use a bulk description locally, at some point the topological invariant needs to change. This cannot happen without the gap closing. This means that somewhere in the bulk gap there has to be a state which is bound to the edge. This behavior is called bulk boundary correspondence. The existence is thus a consequence of a change of the bulk properties and no special property of the finite sample or the nature of the boundary. This argument is rather qualitative but nicely illustrates how powerful the analysis of the topology of the band structure is. In some systems the bound states can be calculated explicitly by assuming a sudden change in the Hamiltonian and matching the wave functions [Kön08, Zho08, Mic12a, Wei13, Sha11, Mic12b]. The existence of a solution is guaranteed by the change of the bulk topology. Because the symmetries are not broken also the boundary state has to respect those symmetries.

One example are two dimensional time reversal invariant topological

insulators. In 2008 Schnyder *et al.* set up a periodic table listing possible topological phases [Alt97, Sch08]. From this table we know that time reversal invariant two dimensional systems have two different topological phases. The problem is now whether a system exhibits the non trivial phase or can be tuned between the phases. In 2005, Kane and Mele already suggested an example for a two dimensional system with time reversal symmetry showing a topological transition. They showed that graphene with spin orbit interaction shows a topologically non trivial phase [Kan05b, Kan05a]. Although the spin orbit interaction turned out to be not large enough in order to observe the effect experimentally they had the right idea. Later, Bernevig *et al.* looked for materials with stronger spin orbit interaction and showed that also in semiconductor heterostructures with spin orbit interaction and an inverted band structure a topological transition is possible [Ber06a, Ber06b]. They showed that one implementation for their model are $HgTe$–$CdTe$ quantum wells in which the thickness of the $HgTe$ quantum well drives the topological transition. These quantum wells could be produced by the Molenkamp group in Würzburg [Kön07, Kön08, Rot09]. In these systems, the band gap was large enough such that they could also show the existence of the edge states and the quantized transport in them.

As already mentioned these edge states have the same symmetries as the bulk. Because this implies time reversal symmetry the edge states have to come in pairs due to Kramers theorem [Haa10]. The two states of the Kramer pair are connected by time reversal symmetry which corresponds to reversal of the momentum as well as changing the spin. These counter propagating states of opposite spin give rise to the quantum spin Hall effect (QSHE). This effect is characterized by a quantized spin Hall conductance and vanishing charge Hall conductance. The vanishing charge Hall conductance comes from the same number of left and right propagating channels on both edges. The quantized spin Hall conductance resembles the fact that the right movers at each edges have opposite spin compared to the respective left mover. Because the origin of these edge states is topological they are very robust against elastic disorder that does not break time reversal symmetry. Because disorder cannot perturb the transport in the edge state the transport should be ballistic and well quantized.

In the experiment, the transport proved to be carried by edge states but still deviated from the expected quantized conductance quite significantly [Kön07, Kön08, Rot09]. There are several attempts to explain the

deviation. As Rashba interaction does not break time reversal symmetry it cannot be the sole source for a reduction of the conductance. If combined with electron-electron interaction [Sch12c] or a nuclear background [DM13] backscattering is possible. If the Rashba interaction is only in a limited region it can be treated as an impurity such that electron-phonon interaction [Bud12] as well as electron-electron interaction [Cré12] might lead to backscattering as well. Another source could be charge puddles in the bulk of the material. Although the band gap is large enough to isolate the edge states it is not very large. Local variations in the electric field thus might push the Fermi level into the bulk bands locally and thus generate charge puddles. In these charge puddles inelastic processes can enable backscattering [Väy13, Väy14]. Nevertheless, other experiments were able to show that the current in the edge state is spin polarized [Bru12].

Being intrinsically spin polarized they are interesting building blocks for spintronic applications. When applying a bias to an edge state the left and right movers have different chemical potentials. Treating both as two separated leads thus means having reservoirs that are totally spin polarized in contrast to ferromagnetic leads in which a minority spin is always present. When treating the edge state in total as a reservoir the edge state acts as a reservoir whose amount of spin polarization is tunable electrically. In the edge states Rashba interaction is allowed if inversion symmetry is broken. A perpendicular electric field breaks this symmetry without breaking TRS which allows us to tune the strength of the Rashba interaction. The linear Rasba effect will only lead to a global rotation of the spin such that besides the amount of spin polarization also the direction of the spin can be tuned to a certain degree.

Because the topological transition in the simple $HgTe$–$CdTe$ quantum wells cannot be switched electronically the devices have to be defined by the buildup of the sample. Domains of trivial and non trivial topology can be defined nevertheless. In order to obtain quantum dot ring structures [Mic11] as well as holes forming an antidot [Sha11] have been considered. By closing the circle bound states form that act as local levels of a quantum dot. By punching a hole into a quantum spin Hall device this defines a quantum dot coupled to both edges. It was shown that such devices can produce spin currents using only electric fields [Dol13]. By shifting the levels electrically the TRS is not broken such that the levels are still spin degenerate and thus doubly occupied. By quickly shifting the energy levels electron pairs can be emitted from these quantum dots

[Inh13]. Depending on how the electrons are measured this becomes an on demand source of spin polarized electrons [Inh13] or of entangled electrons [Dol16]. Using QPCs to measure the spin polarization, these setups can even be used to test a Bell inequality or as beam splitters to test the entanglement of the electrons [Inh13, Dol16]. More involved schemes also allow to generate entangled electrons by post selection [Str15].

The edge states are inherently one dimensional supplying two counter propagating channels which are each not spin degenerate. This renders them an example of a spinless Tomonaga Luttinger liquid which, due to the helical nature of the edge states, is called a helical Luttinger liquid (HLL). This allows the inclusion of interactions in the helical edge states in the calculations exactly. The influence of the interaction onto the Kondo problem [Wu06, Tan11, Mac12] as well as the influence of Rashba interaction onto the Kondo problem [Eri12, Eri13] have been studied using renormalization group methods. The interaction can also be used to include interaction effects in several setups as for example the antidot spin valve [Dol13] or interference devices [Vir11, Dol11, Fer13] or QPCs [Str09, Dol12]. Other ideas directly exploit properties of Luttinger liquids as for example the suppression of electron pair tunneling. This effect can be used to split Cooper pairs already using standard Luttinger liquids [Sat10, Vir12]. Using a HLL, however, the spin is connected to the direction of propagation such that this allows a measurement of spin via charge transport properties and thus a more direct probe of entanglement [Sat10].

In the system we discuss in chapter 2 and chapter 3 we will take the middle road of these approaches. We wanted to understand how a helical edge state interacts with a localized electron. On the one hand we want to have the high control from the semiconductor heterostructures and on the other hand the topological protection and the possibility to include interactions which is possible in HLLs. We thus choose a QD that is tunnel coupled to one helical edge state. This QD is assumed to be otherwise well separated from the environment and to be in the Coulomb blockade regime. This allows us to treat the QD effectively as a spin $1/2$ impurity. Following the instrumental approach of semiconductor heterostructures we describe the behavior of the impurity using a master equation approach. As long as the time reversal symmetry is not violated this will not lead to backscattering. A magnetic field localized on the QD is thus added. To describe the manipulations enabled by this magnetic field we derive a generalized master equation. This generalized master

equation does not only allow us to calculate the state of the impurity but also to calculate the current in the setup. We find that the interplay of the edge state with the magnetic field in the QD results in the opportunity to manipulate the spin of the impurity in direction as well as the strength of the polarization. These manipulations also show signatures in transport where these signatures depend crucially on the relative orientation of magnetic field, polarization of the impurity spin and the orientation of the spins in the edge states. Exploiting this behavior allows us to analyze the spin of the electrons in the edge states using magnetic fields. The generalized master equation can be solved including the interactions in the edge state such that we can also analyze the effect of interactions.

The derivation of the general master equation is given in sections 2.2.3 to 2.2.6. The resulting system parameters for our setup are then given in sections 2.2.7 to 2.2.9. The behavior of the system is then discussed in section 2.3. The current is derived in sections 2.4.1 and 2.4.2 and discussed in section 2.4.3.

Using the standard general master equation we were able to find interesting signatures in transport as well as a possibility to manipulate the impurity. To understand the implications of the helical nature of the edge states better we can also go beyond the average backscattering current and also look at the backscattering current noise. Noise can be a sign for bunching and antibunching which provides some insight on the mechanism behind the backscattering current. In cotunneling through a QD, for example, inelastic scattering events can lead to spin noise on the QD. If now the elastic cotunneling rate depends on the spin of the electron on the QD the spin fluctuations will lead to a switching of these cotunneling rates and thus more irregular transport which then leads to a higher current noise [Suk01].

A technical straightforward method to obtain current noise is using full counting statistics. There zero frequency noise can be identified as the second cumulant of the probability distribution that N electrons are transferred in a time interval T whereas the current is the first cumulant. If the events are independent this distribution is the Poissonian distribution and all cumulants are the same. When we want to know whether the events are independent we thus only have to compare the cumulants. The Fano factor is thus defined as the ratio of the current noise and the current. For rare independent events we expect a Poissonian distribution and this Fano factor is one. Deviations from this value can be signs for correlated transport events. The cumulants are calculated using the cumulant

generating function which can be calculated, as already mentioned from standard methods.

This way we found interesting signatures indicating regimes of super- as well as sub-Poissonian noise. This is commonly used as a sign of bunching and antibunching. Bunching and antibunching can be more directly defined by the joined probability for two events happening within a short time interval. To distinguish them one has to look at temporal correlation functions of two electron transfer events. The behavior at short times then determines the bunching properties. Commonly, bunching leads to super-Poissonian noise and antibunching leads to sub-Poissonian noise although the association is not strict [Ema12]. In order to calculate this correlation function we need to understand the influence of a single event on the system. This analysis allows us to decompose all contributions into simple elementary processes. We found that we can distinguish two types of processes; processes that are enabled by an external magnetic field and those that would also be possible without this field. The second type of process is in general suppressed. If the spin of the impurity itself can block some processes the picture is very different. An interplay of these two observations can lead to deviations from the Poissonian limit. We will derive the cumulant generation function using a master equation approach in section 3.1 and section 3.2 and decompose it into the several electron transfer events in section 3.3. In section 3.4 we then apply these methods to our HLL–QD-system.

By decomposing the noise into the different contributing processes we could understand the super and sub-Poissonian regions by looking at which processes are suppressed. The bias applied to the edge state also dictates the polarization of the impurity. In some regions the impurity state blocks the favored process. Whether the noise is super- or sub-Poissonian now depends on the interplay of this spin blockage with the different mechanisms that lift this blockage or drive a change of polarization of the impurity. By analyzing this interplay we can understand the different regimes.

One of the phenomena mentioned earlier in which spin plays an important role was the possibility for two electrons to reduce their energy by forming a Cooper pair which is a singlet state [Tin96]. This singlet state has the important property that the spin is entangled. Entangled states are inherently quantum mechanical and cannot be understood classically. They play an important role in quantum computing and are at the heart of quantum cryptography [Nie10]. For quantum

cryptography photons are used where the entanglement is well tested [Asp82b, Asp82a, Hen15, Giu15]. To also use entanglement in electronic systems a reliable efficient sources of entangled electrons is needed.

One source of entangled electrons are conventional superconductors. These superconductors are described by the BCS theory. The starting point is the aforementioned mechanism in which two electrons can lower their energy by going into a singlet state called a Cooper pair [Tin96]. In the superconducting state this state is filled by many electrons such that a Cooper pair condensate is established. This Cooper pair condensate is a potential source for entangled electrons. Entanglement describes the correlation between two subsystems measured independently. To obtain entangled electrons we thus have to separate these two electrons without measuring their spin.

There are several proposals how to achieve this. Initial proposals considered energy filters [Les01] or double quantum dots [Rec01]. The latter one was also realized experimentally and showed a very high splitting efficiency [Sch12b]. There are also further suggestions including Luttinger Liquids [Rec02, Ben02] as well as topological edge states found in the QSHE [Sat10] or bilayer graphene [Sch15b]. Splitting the Cooper pairs, however, does not yet show that the electrons are also entangled. A Bell measurement would show the entanglement of the electrons. Bell tests could be done by using a bent carbon nanotube [Bra13] or by transferring the entanglement to photons in two separated cavities and measure the entanglement there [Sch15a, Nig15].

Another idea to use these Cooper pairs is to generate nonlocal entangled states. In 2000, Choi *et al.* considered two quantum dots in between two superconductors in a regime in which each dot is singly occupied. They showed that due to the coupling to the superconductors the electrons of the QDs become entangled in the ground state [Cho00]. The electrons thus are locally separated and still spin entangled. This property still needs to be checked.

This can be achieved using the Josephson current in the system. The Josephson current is the supercurrent that flows between two superconductors if they are coupled. Such a device is called a Josephson junction (JJ). For a JJ it is not important how the superconductors are coupled. The coupling can be achieved for example by a normal metal, an insulator [Lik79] or by more complex systems as for example QDs [Spi91]. Being a supercurrent the current is not driven by a bias applied to the superconductors but by the phase difference between the superconductors. In his

derivation, Josephson showed that the current can be calculated by the phase dependence of the ground state energy of the JJ [Jos62, Jos65]. We shortly summarize his findings in section 4.1. Depending on whether the minimal energy is reached for a phase difference of 0 or π, a JJ is a 0-junction or a π-junction. If a current is pushed through the system the superconductor adjusts the phase difference such that the current flowing through the system is a supercurrent. If the current applied is larger than the maximal current the system can carry, the Josephson junction becomes normal conducting. By tuning the phase and measuring this current the ground state can be examined.

In that light we can identify the setup proposed by Choi *et al.* as a JJ using a double quantum dot (DQD) in which the two dots are coupled via the superconductors. Using the Aharonov–Bohm effect [Cho00, Jac15] or a pilot JJ in a SQUID geometry [Cho00, Wan11] the DQD-JJ ground state can be examined. This allows the identification of signatures of Cooper pair splitting and thus nonlocal transport. Those approaches, however, assume that the two quantum dots forming the JJ are equivalent.

This setup has been realized recently in the group of S. Tarucha [Dea15]. These authors placed two self assembled QDs on top of the gap in between two aluminium leads. They could show that the resulting DQD-JJ is in the single level regime and that there is only a small capacitive coupling between the QDs. They analyzed the supercurrent as a function of the charging states of the two QDs and showed that the result does not agree with the expectations for two independent QDs. In a JJ built from a single level QD the Josephson current switches between a 0-junction and a π-junction behavior depending on the number of electrons on the QD [Spi91, Ish95, Roz01, Lee10]. The reason is the different number of exchanges of fermions needed to transfer a Cooper pair. In their experiment, Deacon *et al.* varied the charging state for one dot and measured the critical current for several fixed charging states of the other dot. They found that changing the state of the second quantum dot does not just contribute an offset to the transport through the first dot which would be the expected behavior for pure local transport. They concluded that this has to be a sign of electron pairs being transported non locally.

In the analysis of a DQD-JJ one has to be very careful because the interplay of the two QDs can be complicated. To illustrate this we can have a short look at JJs made from QDs with multiple levels contributing. When considering several levels on a single QD there are more possible transport paths and the behavior becomes more complicated. The charge

alone is not sufficient anymore to determine the type of JJ [Shi98, vD06]. Because a second quantum dot can be considered to be an independent level we thus have to be very careful in the analysis of this system.

We extend the perturbative approach by Choi *et al.* to be closer to the experiment by Deacon *et al.*. Their experiment deviates in two aspects from the proposal of Choi *et al.*. In the experiment, the charging state of the DQD is changed in a very wide range and their main observation stems from the comparison of the behavior in different charge sectors. Another common assumption for this DQD-JJ is that the superconducting gap is much larger than the energy scales of the DQD. Together with the Coulomb repulsion on the QDs this ensures that Cooper pairs tunnel onto separate QDs and we refer to this regime as the Cooper pair splitter regime. In this regime we can define an effective model for the DQD including injection of Cooper pairs and coupling of the QDs by electron cotunneling. Contribution of higher order in the tunnel coupling than these second order terms are suppressed here [Sch15a]. In the experiment the gap of the superconductor, unfortunately, is not larger than the energies of the DQD such that it is not in this regime.

In order to extend the approach by Choi *et al.* we first include other charging states to the DQD in the Cooper pair splitter regime and then drop the assumption of the large superconducting gap. In the Cooper pair splitter regime we introduce local as well as nonlocal cotunneling and Cooper pair injection terms into the model and calculate the supercurrent by diagonalizing the resulting system. Already in this regime we find that a nonlocal supercurrent will be most prominent in a regime where both QDs are close to a charging transition and not close to charging transitions of one dot only. The detail of this discussion can be found in section 4.4.1.

When dropping the assumption of a large superconducting gap we cannot define an effective model with second order contributions anymore. To describe the system we follow two approaches. We consider the limit of zero bandwidth which basically reduces the superconductors to a single site. This reduces the system size considerably such that the problem can be treated exactly numerically. To interpret the results we also calculate the corrections to the ground state in fourth order in perturbation theory. This enables us to identify the relevant processes and opens up an intuitive interpretation of the results. The perturbative result can furthermore be extended to the wide band limit. In fourth order perturbation theory much more processes play a role than in second order. To keep track of these processes and the associated fermion exchange signs we develop

a simple diagrammatic technique. We thus have an exact method in a simplified model that can be analyzed using a perturbative result that also can be generalized to the full model. All these methods are defined and derived in section 4.3.

The additional processes enabled by reducing the band gap lead to very interesting behavior on the DQD. This is most prominent in the regime where both QDs are singly occupied. In this sector we can have a non local singlet state as well as triplet states. Where in the Cooper pair splitter regime the triplet states could not couple to the superconductors such that the singlet would always be in the ground state now the superconductors can enable a triplet ground state. In fourth order, the picture is different. Here the triplet can also couple to the superconductor. To understand this behavior we have to focus on the processes exchanging the spins of the electrons on the QDs. The effect of this spin exchange directly tests the spin part of the wave function and thus distinguishes singlet and triplets.

It turns out that in contrast to second order, in fourth order there are also processes that favor the triplet ground state. This is very surprising as this means that the superconductor that mostly consists of the singlet Cooper pairs drives a triplet state on the DQD. A careful analysis, however, shows that this triplet state is not driven by Cooper pair injection but by nonlocal cotunneling processes. The tunnel amplitudes can be characterized by a tunneling parity that is characterized by the relative sign of the tunnel couplings. This tunnel parity is directly probed by nonlocal processes and determines whether a triplet ground state is possible.

The switching of these two different ground states has signatures in transport and is a sign for nonlocal transport. The supercurrent contributed by the nonlocal processes distinguishing the triplet and the singlet differs in sign for singlet and triplet whereas local contributions do not change sign. This interplay means that the supercurrent for singlet and triplet is very different. A switching of the ground state thus also leads to a switch in the supercurrent that on the other hand lead to a very asymmetric peak structure. This switching transition and the resulting signatures of non local transport are discussed in section 4.4.3.

To finally get back at a comparison with the experiment by Deacon *et al.* we go back to the zero bandwidth limit and add another level on one QD that differs in its tunnel parity. We choose parameters that are consistent with the experiment. In this way we can reproduce their

findings qualitatively in section 4.5. The number of electrons we have assumed to be on the QDs, however, differs from the number they report. We though think that uncovering the mechanisms behind the interesting behavior still helps to understand their experimental findings.

Chapter 2

Quantum Dot Coupled to a Helical Luttinger Liquid

Topological insulators offer a new interesting state of matter. One example are two dimensional time reversal symmetric topological insulators. In the topological phase edge states exist. As the Hamiltonian obeys time reversal symmetry these edge states appear in pairs. Due to time reversal symmetry these edge states have to be counter propagating and of opposite spin. One consequence is that applying a bias voltage to the edge state leads to a spin polarization in the edge state. The helical edge state thus can serve as a tunable spin polarized reservoir. Because the current in the edge states is directly associated to their spin polarization changing the spin of edge state electrons directly contributes a transport signature. The helical edge states thus are not only interesting spin reservoirs but also state interesting spin measurement devices.

In quantum dots, single electronic states can be isolated such that they offer a high amount of control. One regime that is very sensitive to the spin is the Coulomb blockade regime. In the Coulomb blockade regime the number of electrons cannot change on the quantum dot. This way sequential transport is suppressed and transport is only possible by coherent two-particle cotunneling processes. If the quantum dot is adjusted such that only one electron is on the quantum dot the cotunneling rates strongly depend on the state of this electron and thus also on its spin. This electron thus basically behaves as a spin impurity.

We are interested to see how the rich spin structure of the helical edge states influence the spin state of a quantum dot in the cotunneling regime which offers very spin sensitive behavior. Simply coupling the quantum dot in the cotunneling regime to the helical edge state cannot have a huge effect. The spin might be exchanged between the quantum dot and the helical edge state but as the spin is in general conserved on the quantum dot this might lead to fluctuations in the current but the right movers cannot become left movers and vice versa because this would

mean that they needed to change their spin. If a magnetic field parallel to the spin quantization direction of the electrons in the edge state is introduced the degenerate level on the quantum dot is split but the spin still cannot change. In order to obtain an average effect we need to drive spin transitions on the quantum dot. This can be achieved by adding a magnetic field to the quantum dot that is not aligned with the spin quantization axis of the helical edge state.

To describe the behavior of the quantum dot we use a master equation approach. In a master equation a small system is coupled to a large bath. If this coupling does not disturb the bath the total system can be assumed to be a product state of the small system and an equilibrium bath. By tracing out the bath degree of freedom we obtain the reduced density matrix. A master equation is an equation of motion for this reduced density matrix. This equation of motion will contain the correlation functions of the bath. It can now be solved in different approximations. The most prominent one is the Markov approximation which assumes that the bath has no memory. By applying the secular approximation we obtain a rate equation that allows for a better interpretation of the behavior. As we are interested in the interplay of two different system quantization axes we have to include the off diagonal entries of the density matrix as well and cannot restrict ourselves to a simple Pauli master equation picture.

This way we find that the polarization as well as the direction of the spin polarization can be tuned using the bias voltage in the helical edge state. In general we find two different regimes. One in which the different processes are suppressed energetically and one in which the behavior is dominated by an induced field. The induced field allows the modification of the direction of the spin polarization. Because modifying the direction will also modify the weight of the processes involved it also determines the amount of polarization. All these manipulations also leave traces in the backscattering current. These allow to identify the relative orientation of magnetic field and spin quantization axis in the edge state.

Some of the results presented in this chapter are published by Probst *et al.* [Pro15]. The chapter is structured as follows. In section 2.1 we define the Hamiltonian of the system including the helical edge, the quantum dot and the external magnetic field. In section 2.1.2 we define the coupling to the lead and derive the Kondo Hamiltonian that is used to describe the effective coupling to the helical edge if the quantum dot is in the cotunneling regime. Because the magnetic field is not aligned with the spin quantization axis and the Kondo Hamiltonian conserves spin we have

to compare the two spin quantization axis and the operators defined with respect to those. In section 2.1.3 we thus define the transformation for these spin operators. After we have defined everything we need to describe the system we derive the master equation in section 2.2.3 and extract the steady state in section 2.2.4. Here, we also identify the relevant regimes in which interesting behaviors can be expected.To obtain a rate equation in section 2.2.5 the secular approximation is applied. The general derivation is then applied to our special problem in sections 2.2.7 and 2.2.8. As the results in secular approximation allow the most intuitive interpretation we comment on the validity of this approximation in section 2.2.9. The behavior of the system is then first characterized by the spin polarization of the quantum dot in section 2.3. In section 2.4.1 we comment on the influence that spin flips on the quantum dot have on the helical edge state and derive a current operator. For master equations the current can be calculated from the steady state of the system as is shown in section 2.4.2. The results for our system are then presented in section 2.4.3. These results also include a discussion of the effect of interactions in the helical edge that can be included using bosonization. In section 2.5 we conclude and comment on the experimental feasibility.

2.1 Model

We will consider a helical edge state coupled to a quantum dot in the cotunneling regime. We assume that the coupling preserves spin. The coupling of the quantum dot to the edge state will be described using the Kondo Hamiltonian. The total Hamiltonian is thus

$$H = H_{\mathrm{HLL}} + H_{\mathrm{QD}} + H_K + H_Z, \tag{2.1}$$

where H_{HLL} describes the helical edge state, H_{QD} describes the quantum dot, H_K is the Kondo coupling of those and H_Z describes an additional magnetic field on the quantum dot. Each of these terms needs to be explained in more detail. We will first define H_{HLL} including interactions in section 2.1.1 and then discuss the Kondo Hamiltonian that describes the coupling of the quantum dot to the edge state in section 2.1.2. The magnetic field is not assumed to be parallel to the spin of the edge states. We will thus also give the transformation of spin operators into a different basis corresponding to a different spin quantization axis section 2.1.3.

2.1.1 Helical Edge State

The lead of a QSH insulator can be described by electrons with a linear dispersion relation whose spin is locked to the direction of propagation. As the spin is locked to the direction of propagation the helical edge state can be treated as a spinless Luttinger liquid such that we can add Coulomb repulsion to our model [Wu06]. The resulting model is called a helical Luttinger liquid (HLL) and is described by

$$H_{\mathrm{HLL}} = \hbar v_F \int \mathrm{d}\xi \, : \sum_{\eta=\pm} \Psi_\eta^\dagger(\xi)(-i\eta\partial_\xi)\Psi_\eta(\xi) : + \frac{\lambda}{2}\int \mathrm{d}\xi \, : \Big(\sum_{\eta=\pm} \Psi_\eta^\dagger(\xi)\Psi_\eta(\xi)\Big)^2 :, \quad (2.2)$$

where v_F is the Fermi velocity, $\Psi_\eta^{(\dagger)}(x)$ is the anihilator (creator) of an electron in branch η at position x, λ is the Coulomb parameter and $: \bullet :$ denotes normal ordering. The two branches propagate in different directions and have oposite spin. We associate right movers ($\eta = +$) with spin up and left movers ($\eta = -$) with spin down. When attaching leads to the edge state as illustrated in Fig. 2.1 all right movers come from the left lead and all left movers come from the right lead. The density matrix for the electrons in the helical edge state is thus given by

$$\rho_V = \frac{1}{Z}\exp\Big(-\beta\Big(H_{\mathrm{HLL}} - \frac{eV}{2}(\hat{N}_{\mathrm{R}} - \hat{N}_{\mathrm{L}})\Big)\Big), \quad (2.3)$$

where Z is the partition function ensuring $\mathrm{Tr}(\rho_V) = 1$, $\beta = 1/k_{\mathrm{B}}T$ is the inverse temperature, V is the applied bias voltage and

$$\hat{N}_{R/L} = \int \mathrm{d}\xi \, \Psi_\pm^\dagger(\xi)\Psi_\pm(\xi) \quad (2.4)$$

are the number operators in branch η. Due to spin momentum locking a bias between left and rght movers also implicates a spin bias in the helical edge.

This Hamiltonian can be solved using bosonization. In bosonization a fermionic Fock state with N electrons is generated by adding particle hole excitations to a N-fermion Fermi sea [vD98, Gia07]. These particle hole pairs are bosonic excitations and the Hamiltonian can be diagonalized when written in these bosons. Furthermore the fermions can be written by the bosonic operators. The details of this calculation are summarized

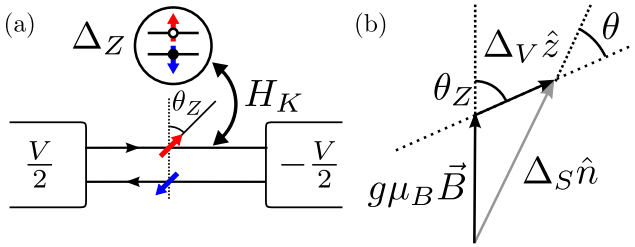

Figure 2.1: Setup considered in this thesis (a) and construction of the effective QD Hamiltonian Eq. (2.1) (b). An HLL is coupled to a QD described by a Kondo Hamiltonian H_K. A magnetic field $\vec{B}$ is applied to the QD, which is tilted with respect to the quantization axis $\hat{z}$ of the helical edge state by an angle θ_Z. The effective system Hamiltonian for the QD is the sum of a Zeeman term $g\mu_B\hbar^{-1}\vec{B}\cdot\vec{S}$ and an induced part $\Delta_V\hat{z}$ that corresponds to the spin polarization of the HLL driven by a bias voltage V. The resulting effective field points along $\hat{n}$ with tilt-angle θ and has strength Δ_S. Figure and caption reproduced from the original publication [Pro15].

in appendix A. In the definition of the bosonic fields a momentum cutoff defined by a length scale α is introduced which restores the continuum limit for $\alpha \to 0$. The interaction can be parameterized using an interaction parameter K. For attractive interactions $K > 1$ whereas $K < 1$ for repulsive and $K = 1$ without interactions. The calculations using bosonization are most convenient when there is no bias voltage applied to the edge state. The bias terms in the density matrix can, however, be gauged into the Hamiltonian such that bosonization can be used [Peç03]. This gauge transformation is presented in appendix B.2.

2.1.2 Quantum Dot and Coupling to the Leads

Here we consider a quantum dot (QD) in the Coulomb blockade regime having an odd number of electrons on the QD. If the levels are well separated only one level determines the properties of the QD coupled to the helical edge state. Such an QD can be described using the single impurity Anderson model. In this model an electrons can occupy a single level where for double occupation Coulomb repulsion needs to be considered. The QD is described by

$$H_{\mathrm{QD}} = \epsilon(d_\uparrow^\dagger d_\uparrow + d_\downarrow^\dagger d_\downarrow) + U d_\uparrow^\dagger d_\uparrow d_\downarrow^\dagger d_\downarrow, \tag{2.5}$$

where $d_\sigma^{(\dagger)}$ is the annihilator (creator) of an electron with spin σ on the QD, ϵ is the single level energy and U is the Coulomb repulsion energy. We are interested in the case in which the QD is singly occupied which corresponds to $\epsilon < 0$ and $\epsilon + U > 0$.

Applying a magnetic field to the QD will add Zeeman interaction to the electrons. The Zeeman Interaction is described by

$$H_Z = \frac{g\mu_B}{\hbar} \vec{S} \cdot \vec{B}, \tag{2.6}$$

where g is the g-factor, μ_B is the Bohr magneton, the spin operators are defined by

$$S^\tau = \frac{\hbar}{2} \sum_{\mu,\nu=\pm} d_\mu^\dagger \sigma_{\mu\nu}^\tau d_\nu, \tag{2.7}$$

σ^τ being the Pauli matrices and $\vec{B}$ is the magnetic field.

Because H_{QD} only contains electron densities it is easy to check, that the Hamiltonian is invariant under rotations of the spin basis. For H_Z, however, we can find a spin basis such that H_Z is diagonal. Defining new spin operators $\vec{S'}$ using this rotated spin direction the Zeeman term can conveniently be written as

$$H_Z = \frac{\Delta_Z}{\hbar} S'^z, \tag{2.8}$$

where $\Delta_Z = g\mu_B|\vec{B}|$ is the Zeeman splitting[1]. Writing the QD with Zeeman interaction in this rotated basis the Hamiltonian is diagonal and has the energies 0, $\epsilon_\downarrow = \epsilon - \Delta_Z/2$, $\epsilon_\uparrow = \epsilon + \Delta_Z/2$ and $2\epsilon + U$. The direction in which the QD Hamiltonian is diagonal is referred to as the spin quantization axis of the QD.

This QD is coupled to the edge state by point like spin conserving tunneling described by

$$H_T = \sum_{\sigma=\pm} t\ \Psi_\sigma(0) d_\sigma^\dagger + \quad \mathrm{h.c.}, \tag{2.9}$$

where t is the coupling strength and $d_\sigma^{(\dagger)}$ is the annihilator (creator) of an electron on the QD whose spin is parallel to the electron in the edge

[1] In general the operators S'^σ are defined such that the complete QD part can be described using only S'^z. Here the quantization direction is only determined by the magnetic field. Later it will also contain induced fields and will thus be redefined.

state. When the other charging states are energetically well separated from the ground state and the temperature and the bias voltage applied is small enough sequential transport is suppressed exponentially because the number of electrons on the QD cannot change. In this regime cotunneling is the dominating transport mechanism. In cotunneling two tunneling events proceed coherently where the other charging states are only used as virtual states such that the suppression is algebraic and not exponential. Because we are interested in manipulating the spin of a single electron we focus on the regime where the QD is singly occupied. In this regime we can now derive an effective model for the low energy space consisting of the lead and the singly occupied QD [Hew93, Sch66]. By applying a Schrieffer-Wolff transformation the tunneling term together with the QD Hamiltonian become a potential scattering term and the famous Kondo Hamiltonian

$$H_K = J\Big(J^+S^- + J^-S^+ + 2J^zS^z\Big), \tag{2.10}$$

where the Kondo coupling is $J = -|t/\hbar|^2U/\epsilon(\epsilon+U)$, the spin operators in the edge state are $J^\pm = J^x \pm iJ^y$ and $J^\tau = \frac{\hbar}{2}\sum_{\mu,\nu=\pm}\Psi^\dagger_\mu(0)\sigma^\tau_{\mu\nu}\Psi_\nu(0)$ and the corresponding QD operators are $S^\pm = S^x \pm iS^y$. The details of this calculation are given in appendix C.1. The potential term can be removed by a transformation which is given in appendix C.2.

2.1.3 Spin Rotations

In the previous sections we gave the definitions of H_{HLL} as well as the Kondo Hamiltonian H_K. When writing down the operators we implicitly assumed that the spins of the electrons on the QD are quantized along the same direction as the spins of the electrons in the helical edge state. When applying a magnetic field, however, a change of basis for the spins on the QD is helpful as then the QD Hamiltonian becomes diagonal and the Zeeman term takes a very simple form. This spin rotation will only be applied to the QD as the spin in the helical edge has a different meaning. Here the spin is locked to the direction of propagation which is very important for transport interpretations. We will thus focus on how the spin operators on the dot change if we change the spin basis on the dot only.

In order to get the transformed spin operators we first need to give the effect of a spin rotation for the operators on the QD. We adopt a notation in which the subscript of the fermionic operators denote whether the spin is parallel to the spin quantization axis in the edge state ($\pm$) or whether

the spin is parallel to the quantization axis in the QD ($\uparrow$ / $\downarrow$). These two spin bases are connected by a general $SU(2)$ transform U [Sak09]

$$\begin{pmatrix} d_\uparrow \\ d_\downarrow \end{pmatrix} = U \begin{pmatrix} d_+ \\ d_- \end{pmatrix} \equiv \begin{pmatrix} e^{i(\phi+\gamma)/2}\cos(\theta/2) & -e^{-i(\phi-\gamma)/2}\sin(\theta/2) \\ e^{i(\phi-\gamma)/2}\sin(\theta/2) & e^{-i(\phi+\gamma)/2}\cos(\theta/2) \end{pmatrix} \begin{pmatrix} d_+ \\ d_- \end{pmatrix}, \tag{2.11}$$

where ϕ, γ and θ are the Euler angles of the corresponding rotation. The angle ϕ is the initial rotation around the z-axis whereas θ is the following rotation around the x-axis that tilts the z direction. The angle γ is a rotation around the resulting z-axis. The angle ϕ thus determines in which direction the z'-axis is tilted and θ determines how much it is tilted. As the system will be rotation invariant around this resulting z-axis the remaining parameter γ will not show up in the final result.

To understand that this transformation corresponds to a spin rotation we consider a two level system that can be interpreted as a spin $1/2$ system. Such a system with a level splitting of Δ can be described in general by

$$H_2 = \frac{\Delta}{2} \begin{pmatrix} d_\uparrow^\dagger & d_\downarrow^\dagger \end{pmatrix} \hat{n} \cdot \vec{\sigma} \begin{pmatrix} d_\uparrow \\ d_\downarrow \end{pmatrix}, \tag{2.12}$$

where $\hat{n}$ is a vector of unit length and $\vec{\sigma}$ is the vector of Pauli matrices and $d_\sigma^\dagger$ creates a fermion in level σ on the QD. A vector of unit length can be parameterized by spherical coordinates by

$$\hat{n} = \begin{pmatrix} \sin\theta\cos\phi \\ \sin\theta\sin\phi \\ \cos\theta \end{pmatrix}, \tag{2.13}$$

where θ is the polar angle and ϕ is the azimuthal angle with respect to the x axis. These angles correspond directly to the Euler angles when choosing $\hat{n}$ as the transformed z'-axis. By inserting Eq. (2.13) into Eq. (2.12) we find the matrix representation of $\hat{n} \cdot \vec{\sigma}$

$$H_2 = \frac{\Delta}{2} \begin{pmatrix} d_\uparrow^\dagger & d_\downarrow^\dagger \end{pmatrix} \begin{pmatrix} \cos\theta & \sin\theta\, e^{-i\phi} \\ \sin\theta\, e^{i\phi} & \cos\theta \end{pmatrix} \begin{pmatrix} d_\uparrow \\ d_\downarrow \end{pmatrix}. \tag{2.14}$$

Because $\hat{n}$ corresponds to the resulting z'-axis after the rotation defined by the Euler angles θ and ϕ the matrix should be diagonal when written

using the $d_\pm$ operators. Rewriting the Hamiltonian by

$$H_2 = \frac{\Delta}{2}\begin{pmatrix} d_+^\dagger & d_-^\dagger \end{pmatrix} U^\dagger \begin{pmatrix} \cos\theta & \sin\theta\, e^{-i\phi} \\ \sin\theta\, e^{i\phi} & \cos\theta \end{pmatrix} U \begin{pmatrix} d_+ \\ d_- \end{pmatrix} \tag{2.15a}$$

$$= \frac{\Delta}{2}\begin{pmatrix} d_+^\dagger & d_-^\dagger \end{pmatrix} \sigma_z \begin{pmatrix} d_+ \\ d_- \end{pmatrix} \tag{2.15b}$$

this can be shown by explicit calculation. By choosing $\hat{n}$ as the spin quantization axis we can thus diagonalize Hamiltonians of the form Eq. (2.12).

In the definition of the Kondo Hamiltonian Eq. (2.10) the spin operators are given with respect to the spin quantization axis in the edge state. To find the effect of these spin flips in the basis in which the QD is diagonal we have to find the effect of the spin rotation on the spin operators by inserting U

$$S^\tau = \frac{\hbar}{2}(d_+^\dagger\ d_-^\dagger)\sigma^\tau \begin{pmatrix} d_+ \\ d_- \end{pmatrix} = \frac{\hbar}{2}(d_\uparrow^\dagger\ d_\downarrow^\dagger)U^\dagger\sigma^\tau U \begin{pmatrix} d_\uparrow \\ d_\downarrow \end{pmatrix}. \tag{2.16}$$

The resulting transformation can now be summarized by

$$S^\tau = \sum_{\mu=z,\pm} (\mathscr{D}(U))_{\tau\mu} S'^\mu \tag{2.17a}$$

$$\mathscr{D}(U) = \begin{pmatrix} \cos\theta & -\frac{z_\gamma}{2}\sin\theta & -\frac{z_\gamma^*}{2}\sin\theta \\ z_\phi \sin\theta & z_\phi z_\gamma \cos^2\frac{\theta}{2} & -z_\gamma^* z_\phi \sin^2\frac{\theta}{2} \\ z_\phi^* \sin\theta & -z_\gamma z_\phi^* \sin^2\frac{\theta}{2} & z_\gamma^* z_\phi^* \cos^2\frac{\theta}{2} \end{pmatrix}, \tag{2.17b}$$

where $z_\phi = e^{i\phi}$, $z_\gamma = e^{i\gamma}$ and

$$S'^\tau = \frac{\hbar}{2} \sum_{\mu,\nu=\uparrow/\downarrow} d_\mu^\dagger \sigma_{\mu\nu}^\tau d_\nu \tag{2.18}$$

are the spin operator in the spin quantization axis of the QD. For convenience we define the coefficients $c_{ij} \equiv (\mathscr{D}(U))_{ij}$.

2.2 Derivation of the GME

One common way to describe QD systems coupled to electric leads is using a master equation. This is a technique from open quantum systems in which the system is divided into two parts that are coupled; a small system which can be solved exactly and a large bath with many degrees

of freedom. As the bath is large the coupling to the system does not perturb the bath. Furthermore the relaxation into the equilibrium state is very effective meaning that the bath is always in equilibrium. The system part can then be described by a density matrix for the impurity only. The equation of motion for this reduced density matrix is then the master equation.

Here we will carefully repeat the derivation of this master equation. The reason is that we need to drop a common assumption on the interaction done usually. We will start by commenting on the separation of system and bath. Then we will introduce some notation that allows a simple formulation of the dynamics of density matrices. Finally we will derive the generalized master equation (GME) in several approximations.

2.2.1 System and Bath Partitioning

The main idea behind a master equation is to separate the total system into a small part that can be treated exactly and a large bath that has may degrees of freedom such that it is not changed by the coupling to the small part. This allows to describe the system dynamics exactly and treat the interaction to the bath perturbatively. The total Hilbert space $\mathcal{H}$ is thus separated into a system space $\mathcal{H}_S$ and a bath spacs space $\mathcal{H}_B$ such that $\mathcal{H} = \mathcal{H}_S \otimes \mathcal{H}_B$.

The bath is assumed to have a lot of degrees of freedom and an effective relaxation mechanism. Perturbations in this bath thus do not change the state of the bath and when perturbed the bath will relax to the equilibrium state quickly. This ensures that the bath is always in equilibrium and that the density matrix of the total system ρ_{tot} can be decomposed into a direct product of a bath and a system density matrix. The system part is the reduced density matrix which is defined by $\rho \equiv \mathrm{Tr}_B(\rho_{\mathrm{tot}})$, where the trace is over the bath degrees of freedom. The total system density matrix is then $\rho_{\mathrm{tot}} = \rho \otimes \rho_V$.

After splitting the Hilbert space into a system and a bath we need to split the Hamiltonian, too. The Hamiltonian H is separated into three parts; one part describing the bath H_B, one describing the system H_S and one describing the interaction H_I such that

$$H = H_S + H_B + H_I. \tag{2.19}$$

The system Hamiltonian and the bath Hamiltonian act on the respective parts of the Hilbert space only whereas the interaction Hamiltonian couples those two Hilbert spaces. In the standard derivation of the master

equation the interaction is assumed to vanish when the bath is traced out $\mathrm{Tr}_B(H_I\rho_V) = 0$ [Bre02, Kol10].

In our special case this is not directly the case. The Kondo coupling Eq. (2.10) contains spin flip terms but also one term proportional to the spin polarization of the edge state, which will be our bath. Applying a bias voltage to the helical edge state will introduce a spin bias which renders this term finite and thus disqualifies the Kondo Hamiltonian from being a valid interaction Hamiltonian in that sense. In the derivation of the master equation we will thus keep the terms that include a trace of H_I over the bath and keep them in the equation. We will see that we can include them naturally in the master equation. They will even allow us an interpretation of this behavior in section 2.2.5.

We can deal with the problem in a simple way. If we subtract the operator we obtain when tracing out the bath from the interaction Hamiltonian we obtain an interaction Hamiltonian that vanishes when tracing out the bath degree of freedom. In the operator we subtracted all degrees of freedom of the bath are traces out such that only the QD degrees of freedom are left. We thus can compensated for it by adding a term to the system Hamiltonian. For our example this leads to

$$H_B = H_{\mathrm{HLL}} \tag{2.20a}$$
$$H_S = H_Z + 2J\langle J^z\rangle_V S^z \tag{2.20b}$$
$$H_I = H_K - 2J\langle J^z\rangle_V S^z, \tag{2.20c}$$

where $\langle\bullet\rangle_V \equiv \mathrm{Tr}_B(\bullet\rho_V)$. For convenience we want to write the interaction Hamiltonian $H_I = \sum_{k=\pm,z} A_k B_k$ by defining

$$A_\pm \equiv JJ^\mp \qquad A_z \equiv 2J\big(J^z - \langle J^z\rangle_V\big) \tag{2.21a}$$
$$B_\pm \equiv S^\pm \qquad B_z \equiv S^z. \tag{2.21b}$$

This redefinition of the interaction simplifies the calculations. In this definition of the system, the bath and the interaction operators we chose our separation into a bath and a system. When introducing the secular approximation later we will see that this separation will be crucial.

It is convenient to express the system part not as a sum of two spin operators as defined in Eqs. (2.20) but to use the resulting spin operator. By introducing $\Delta_V \equiv 2J\hbar\langle J^z\rangle_V$ and introducing appropriate spin operators $\vec{S}'$ the system Hamiltonian is

$$H_S = \frac{\Delta_Z}{\hbar}\hat{n}_B\cdot\vec{S} + \frac{\Delta_V}{\hbar}S^z = \frac{\Delta_S}{\hbar}S'^z, \tag{2.22}$$

where $\hat{n}_B$ is the unit vector pointing in the direction of the magnetic field. The resulting rotation angles and the resulting splitting Δ_S will be discussed in section 2.2.7.

2.2.2 Dynamics of Density Matrices

The dynamics of density matrices are defined by the von Neumann equation. The von Neumann equation for the total density matrix is given by

$$\dot{\rho}_{\mathrm{tot}}(t) = -\frac{i}{\hbar}[H, \rho_{\mathrm{tot}}]. \tag{2.23}$$

This equation can conveniently be written using a superoperator describing the commutator. For two Hermitian operators X and Y this operator is defined by

$$\mathcal{L}_X Y = \frac{1}{\hbar}[X, Y]. \tag{2.24}$$

The von Neumann equation is then simply

$$\dot{\rho}_{\mathrm{tot}}(t) = -i\mathcal{L}_H \rho_{\mathrm{tot}}. \tag{2.25}$$

By vectorizing the density matrix we can represent superoperators by matrices. The von Neumann equation can thus also be solved by a matrix exponential. Using the Baker-Campbell-Hausdorff formula the matrix exponential is

$$\exp(i\mathcal{L}_X t)Y = \exp(iXt/\hbar)\; Y \exp(-iXt/\hbar). \tag{2.26}$$

Coming back to the von Neumann equation Eq. (2.25) we see that this equation can formally be solved using a matrix exponential. When using Eq. (2.26) to write down the effect of the exponential on a density matrix we see that the exponentials on the r.h.s become time evolution operators which then yields the well known form of the time propagation of the density matrix.

The exponential of $i\mathcal{L}_H t$ will in general always place time propagation operators around the operator it is applied to. This can be used to write operators in the Heisenberg picture as

$$X(t) = e^{i\mathcal{L}_H t} X. \tag{2.27}$$

In the same way we can use this notation to give the connection between operators in the Schrödinger picture and operators in the interaction picture. In the definition of the operators in the interaction picture the free

evolution is included in the definition of the operator. For our system the definition of an operator in the interaction picture is thus

$$X^I(t) = e^{i(\mathcal{L}_{H_S}+\mathcal{L}_{H_B})t}X, \tag{2.28}$$

where X is the operator in the Schrödinger picture.

The equation of motion for operators and density matrices in the interaction picture is very similar to the one for operators in the Heisenberg picture with the difference that the evolution is not driven by the full Hamiltonian but by the interaction Hamiltonian in the interaction picture. We generalize the notation to the interaction picture and thus define

$$\mathcal{L}_X^I(t')Y^I(t) = \frac{1}{\hbar}[X^I(t'), Y^I(t)]. \tag{2.29}$$

This notation allows us to express the equations of motion in a very compact way. Using this definition the von Neumann equation in the interaction picture can be written as

$$\dot{\rho}^I_{\mathrm{tot}}(t) = -i\mathcal{L}_I^I(t)\rho^I_{\mathrm{tot}}(t), \tag{2.30}$$

where we used the shorthand notation $\mathcal{L}_I \equiv \mathcal{L}_{H_I}$.

2.2.3 Derivation of the GME

The starting point for the derivation of the master equation is the von Neumann equation in the interaction picture Eq. (2.30). A formal integration of this equation yields

$$\rho^I_{\mathrm{tot}}(t) = \rho^I_{\mathrm{tot}}(t_0) - i\int_{t_0}^{t} \mathrm{d}\tau\, \mathcal{L}_I^I(\tau)\rho^I_{\mathrm{tot}}(\tau). \tag{2.31}$$

Reinserting this result into Eq. (2.30) we obtain

$$\dot{\rho}^I_{\mathrm{tot}}(t) = -i\mathcal{L}_I^I(t)\rho^I_{\mathrm{tot}}(t_0) - \int_{t_0}^{t} \mathrm{d}\tau\, \mathcal{L}_I^I(t)\mathcal{L}_I^I(\tau)\rho^I_{\mathrm{tot}}(\tau). \tag{2.32}$$

Because of the assumption of a large bath we can now use that the total density matrix can be decomposed into a product of the reduced density matrix and the bath. By tracing out the bath we obtain

$$\begin{aligned}\dot{\rho}^I(t) = &-i\mathrm{Tr}_B\Big(\mathcal{L}_I^I(t)\big(\rho^I(t_0)\otimes\rho_V\big)\Big)\\ &- \int_{t_0}^{t} \mathrm{d}\tau\, \mathrm{Tr}_B\Big(\mathcal{L}_I^I(t)\mathcal{L}_I^I(\tau)\big(\rho^I(\tau)\otimes\rho_V\big)\Big).\end{aligned} \tag{2.33}$$

Because we redefined the interaction in Eq. (2.21) the first term on the right hand side would vanish. We will, however, keep these terms here as this gives a more general result and shows how the redefinition Eq. (2.21) and the validity of the secular approximation are connected.

The expression still depends on the initial state of the density matrix at t_0. By tracing out the bath in Eq. (2.31) we can express $\rho(t_0)$ using only the density matrix at later times. Reinserting into Eq. (2.33) we obtain

$$\begin{aligned}\dot{\rho}^I(t) = &-i\mathrm{Tr}_B\Big(\mathcal{L}_I^I(t)\big(\rho^I(t)\otimes\rho_V\big)\Big)\\ &-\int_{t_0}^{t}\mathrm{d}\tau\,\mathrm{Tr}_B\Big(\mathcal{L}_I^I(t)\mathcal{L}_I^I(\tau)\big(\rho^I(\tau)\otimes\rho_V\big)\Big)\\ &-\int_{t_0}^{t}\mathrm{d}\tau\,\mathrm{Tr}_B\Big(\mathcal{L}_I^I(t)\Big(\mathrm{Tr}_B\Big(\mathcal{L}_I^I(\tau)\big(\rho^I(\tau)\otimes\rho_V\big)\Big)\otimes\rho_V\Big)\Big). \quad (2.34)\end{aligned}$$

This expression is the generalization of Eq. (30) from Koller *et al.* [Kol10] or Eq. (3.116) from Breuer and Petruccione [Bre02] with the additional terms that appear for $\langle H_I\rangle_V \neq 0$. Following the notation by Koller *et al.* [Kol10] we define

$$\dot{\rho}^I(t) = -i\mathrm{Tr}_B\Big(\mathcal{L}_I^I(t)\rho(t)\otimes\rho_V\Big) - \int_{t_0}^{t}\mathrm{d}\tau\,\mathcal{K}^I(t,\tau)\rho^I(\tau), \quad (2.35)$$

where the kernel of the integration is

$$\begin{aligned}\mathcal{K}^I(t,\tau)\rho^I(\tau) = &\,\mathrm{Tr}_B\Big(\mathcal{L}_I^I(t)\mathcal{L}_I^I(\tau)\rho^I(\tau)\otimes\rho_V\Big)\\ &-\mathrm{Tr}_B\Big(\mathcal{L}_I^I(t)\mathrm{Tr}_B\big(\mathcal{L}_I^I(\tau)\rho^I(\tau)\otimes\rho_V\big)\otimes\rho_V\Big). \quad (2.36)\end{aligned}$$

Inserting the definition of $\mathcal{L}_I^I$ and H_I^I we obain the explicit expression for this kernel. Because A_η as well as B_η contain an even number of fermionic operators they can be exchanged without obtaining an additional sign such that the system and bath part factorizes. Using that the trace

allows cyclic permutations of the operators we find

$$\begin{aligned}\mathcal{K}^I(t,\tau)\rho^I(\tau) = \frac{1}{\hbar^2}\sum_{\alpha,\beta=\pm,z}\Bigg(\Big(&\mathrm{Tr}_B\big(A^I_\alpha(t)A^I_\beta(\tau)\rho_V\big)\\ &-\mathrm{Tr}_B\big(A_\alpha\rho_V\big)\mathrm{Tr}_B\big(A_\beta\rho_V\big)\Big)[B^I_\alpha(t),B^I_\beta(\tau)\rho^I(\tau)]\\ +\Big(&\mathrm{Tr}_B\big(A^I_\beta(\tau)A^I_\alpha(t)\rho_V\big)-\mathrm{Tr}_B\big(A_\alpha\rho_V\big)\mathrm{Tr}_B\big(A_\beta\rho_V\big)\Big)\\ &\times[\rho^I(\tau)B^I_\beta(\tau),B^I_\alpha(t)]\Bigg).\end{aligned}\tag{2.37}$$

We will first focus on the lead part of this equation. Because all degrees of freedom are traced out here this term imposes the most constrains on the expression. One of the most prominent properties is that the lead Hamiltonian itself is spin conserving and time independent. Due to the time independence the lead part only depends on the difference $t-\tau$. The lead part thus can always be written via the lead correlation function

$$G_{\alpha\beta}(t) = \mathrm{Tr}_B\Big(A^I_\alpha(t)A^I_\beta(0)\rho_V\Big) - \mathrm{Tr}_B\big(A_\alpha\rho_V\big)\mathrm{Tr}_B\big(A_\beta\rho_V\big).\tag{2.38}$$

The operators $A_\pm$ are defined to be spin flip operators where the spin quantization direction in this definition is the spin quantization direction of the edge state. This correlation function only has finite values for $\alpha=-\beta$. Inserting this constraint and the defined correlation function the kernel can be written in a very compact way

$$\begin{aligned}\mathcal{K}^I(t,\tau)\rho^I(\tau) = \frac{1}{\hbar^2}\sum_{\alpha=\pm,z}\Big(&G_{\alpha\bar\alpha}(t-\tau)[B^I_\alpha(t),B^I_{\bar\alpha}(\tau)\rho^I(\tau)]\\ &+G_{\bar\alpha\alpha}(\tau-t)[\rho^I(t)B^I_{\bar\alpha}(\tau),B^I_\alpha(t)]\Big),\end{aligned}\tag{2.39}$$

where $\bar\alpha=-\alpha$ and $\bar z=z$.

Up to this point the derivation is the same for the standard generalized master equation [Bre02, Blu96]. The next step would be a reformulation of the integration variable and then performing the Markov and secular approximation. This route will be followed in section 2.2.9. Here we will, for now, follow another route that allows us to circumvent the secular approximation as described by Koller *et al.* [Kol10].

2.2.4 Steady State in the GME

The advantage of the interaction picture is that the evolution is driven by the interaction and that the free system is already included in the definition of the operators. The price we pay is that in the definition of the operators a reference point in time t_0 is chosen. This leads to a nontrivial time dependence of the operators such that $\mathcal{K}^I(t,\tau)$ is a function of two times and cannot be written as a function of $t-\tau$ alone. This can, however, be achieved by going back to Schrödinger picture. The density matrix in Schrödinger picture is given by $\rho(t) = e^{-iH_S t}\rho^I(t)e^{iH_S t}$. Calculating $\dot{\rho}(t)$ from this expression and inserting Eq. (2.35) we find the master equation in Schrödinger picture

$$\dot{\rho}(t) = -i\mathcal{L}_{S,\text{eff}}\rho(t) - \int_{t_0}^{t} \mathrm{d}\tau\, \mathcal{K}(t-\tau)\rho(\tau), \tag{2.40}$$

where

$$\begin{aligned}\mathcal{K}(t-\tau)\rho(\tau) &\equiv e^{-iH_S t}\mathcal{K}^I(t-\tau)\rho^I(\tau)e^{iH_S t}\\ &= \frac{1}{\hbar^2}\sum_{\alpha=\pm,z}\Big(G_{\alpha\bar{\alpha}}(t-\tau)\Big(B_\alpha e^{-iH_S(t-\tau)}B_{\bar{\alpha}}\rho(\tau)e^{iH_S(t-\tau)}\\ &\quad - e^{-iH_S(t-\tau)}B_{\bar{\alpha}}\rho(\tau)e^{iH_S(t-\tau)}B_\alpha\Big) + G_{\bar{\alpha}\alpha}(\tau-t)\\ &\quad\times\Big(e^{-iH_S(t-\tau)}\rho(\tau)B_{\bar{\alpha}}e^{iH_S(t-\tau)}B_\alpha\\ &\quad - B_\alpha e^{-iH_S(t-\tau)}\rho(\tau)B_{\bar{\alpha}}e^{iH_S(t-\tau)}\Big)\Big)\end{aligned} \tag{2.41}$$

and $\mathcal{L}_{S,\text{eff}}\rho(t) = \mathcal{L}_S\rho(t) + \mathrm{Tr}_B\big(\mathcal{L}_I\rho(t)\otimes\rho_V\big)$ is an effective system Liouvillian. In this expression the spin operators B_α of the QD are still in the basis in which the spins are parallel to the operators in the edge state. As the system is not diagonal the time evolution of the system is nontrivial. We use Eq. (2.17) to replace the B_α operators by S'^α operators that

have a very simple time evolution. For the kernel we obtain in this basis

$$\begin{aligned}\mathcal{K}(t-\tau)\rho(\tau) = \frac{1}{\hbar^2}\sum_{k,l=\pm,z}\Bigg(\mathcal{G}_{kl}(t-\tau)\Big(&S'^k e^{-iH_S(t-\tau)}S'^l\rho(\tau)e^{iH_S(t-\tau)} \\ &- e^{-iH_S(t-\tau)}S'^l\rho(\tau)e^{iH_S(t-\tau)}S'^k\Big) + \mathcal{G}_{lk}(\tau-t) \\ &\times\Big(e^{-iH_S(t-\tau)}\rho(\tau)S'^l e^{iH_S(t-\tau)}S'^k \\ &- S'^k e^{-iH_S(t-\tau)}\rho(\tau)S'^l e^{iH_S(t-\tau)}\Big)\Bigg),\end{aligned} \tag{2.42}$$

where the correlation function

$$\mathcal{G}_{kl}(t) \equiv \sum_{\alpha=\pm,z} c_{\alpha k}c_{\bar{\alpha}l}G_{\alpha\bar{\alpha}}(t) \tag{2.43}$$

is defined such that it contains the geometrical factors $c_{\alpha k}$. In this basis the time evolution is then given by

$$e^{i\Delta_S S'^z t} = \begin{pmatrix} e^{i\Delta_S t/2\hbar} & 0 \\ 0 & e^{-i\Delta_S t/2\hbar}\end{pmatrix} \tag{2.44}$$

such that the time evolution just adds phase factors to the matrix elements of $\mathcal{K}$. The explicit form of this term is given in appendix D.

The general master equation Eq. (2.40) now is a self-consistency equation for the reduced density matrix. The equation is, however, mathematically given by a convolution of the kernel $\mathcal{K}$ and the reduced density matrix ρ. Doing a Laplace transform such a convolution becomes the product of the Laplace transform of $\mathcal{K}$ and ρ. This enables us to calculate the Laplace transform of the reduced density matrix. The inverse transform is not as straight forward as for the Fourier transform [Arf13]. For some properties, however, the Laplace transform at specific values is sufficient.

One of this properties is the long time behavior which can be determined by the finial value theorem. For convenience we define the Laplace transform $F(z)$ of a function $f(t)$ as

$$F(z) \equiv \int_0^\infty e^{izt/\hbar}f(t)\,\mathrm{d}t\,. \tag{2.45}$$

Using this definition the final value theorem reads [Bee03]

$$\lim_{t\to\infty} f(t) = \lim_{z\to i0^+}\frac{izF(z)}{\hbar}. \tag{2.46}$$

The final value theorem thus allows us to extract the long time limit from the Laplace transform at $z = 0$.

This can be used to determine the steady state of the general master equation. The steady state is the static state that the system relaxes to. The steady state $\bar{\rho}$ is thus

$$\lim_{t\to\infty} \rho(t) = \lim_{z\to i0^+} \frac{iz\rho(z)}{\hbar} = \bar{\rho} \tag{2.47}$$

and has the property

$$\lim_{t\to\infty} \dot{\rho}(t) = 0. \tag{2.48}$$

The rate of change $\dot{\rho}$ is determined by the generalized master equation Eq. (2.40). The long time limit, however, is most conveniently determined in Laplace space. Bringing Eq. (2.40) to Laplace space we find

$$\dot{\rho}(z) = -i\mathcal{L}_S\rho(z) - i\mathrm{Tr}_B(\mathcal{L}_I\rho(z)\otimes\rho_V) - \mathcal{K}(z)\rho(z). \tag{2.49}$$

Applying the final value theorem to Eq. (2.48) and inserting Eq. (2.49) we find

$$0 = \lim_{t\to\infty} \dot{\rho}(t) = \lim_{z\to i0^+} \frac{iz\dot{\rho}(z)}{\hbar} \tag{2.50a}$$

$$= \lim_{z\to i0^+} \big(-i\mathcal{L}_{S,\mathrm{eff}} - \mathcal{K}(z)\big)\frac{iz\rho(z)}{\hbar} \tag{2.50b}$$

$$= \big(-i\mathcal{L}_{S,\mathrm{eff}} - \mathcal{K}(0)\big)\bar{\rho} \tag{2.50c}$$

which reduces the problem of finding the steady state to finding the kernel of a linear mapping.

Using this method allows us to obtain a steady state without doing further approximations than the Markov approximation. We can especially avoid the secular approximation usually done in order to obtain a generalized master equation. When dealing with different directions of spin quantization axes this is, however, a crucial point as the resulting spin quantization axis in not clear in the beginning. We will see that in the secular approximation the choice of the proper system bath separation is crucial. For the expression in Eq. (2.50) the right choice of the system is not that crucial such that the result can serve as a benchmark for the result we obtain in secular approximation. In the next chapter we will have a closer look at the secular approximation and the implication of the choice of a specific system.

2.2.5 Secular Approximation

The basic idea behind the secular approximation is to identify terms that are oscillating fast compared to the relaxation dynamics of the density matrix due to the coupling to the bath and neglect them. We, however, have to distinguish between the fast oscillation of the off diagonal elements of the density matrix and the fast oscillations of the couplings in the master equation.

By going to the interaction picture the unperturbed part of the evolution is included in the definition of the states of the system. The resulting dynamics is now driven by the perturbation. This dynamics is now described by the master equation. By including the free evolution in the definition of the states itself we get rid of the part of the coherent evolution that is driven by the unperturbed system. The oscillating behavior of the off diagonal entries of the density matrix in Schrödinger picture is driven by the coherent dynamics and thus is absent in the interaction picture. Formally we can compare Eq. (2.40) to Eq. (2.35) and find that one major difference is that Eq. (2.35) lacks the $\mathcal{L}_S$ term which drives the oscillations of the off diagonal elements of the density matrix. Because we assumed that the interaction term does not vanish if the bath is traced out we still have an additional term that has been included in the definition of $\mathcal{L}_{S,\mathrm{eff}}$.

To understand how this term can be removed we transform Eq. (2.40) into an interaction picture where we leave the unperturbed system $\bar{H}_S$ not yet chosen. The corresponding density matrix is defined as $\rho^{\bar{I}} = \exp(i\bar{H}_S t/\hbar)\rho(t)\exp(-i\bar{H}_S t\hbar)$. Using the master equation in the Schrödinger picture Eq. (2.40) we can also give a master equation in this new interaction picture corresponding to $\bar{H}_S$

$$\dot{\rho}^{\bar{I}}(t) = i\big(\mathcal{L}_{\bar{H}_S} - \mathcal{L}^{\bar{I}}_{S,\mathrm{eff}}\big)\rho^{\bar{I}} - \int_0^t \mathrm{d}\tau\, e^{i\bar{H}_S t/\hbar}\big(\mathcal{K}(t-\tau)\rho(\tau)\big)e^{-i\bar{H}_S t/\hbar}, \quad (2.51)$$

where the second term defines the transformed integration kernel. In this form we see that by choosing $\bar{H}_S = H_S$ we can remove the $\mathcal{L}_S$ term from the master equation. In general we are able to remove all terms that describe coherent dynamics by choosing $\bar{H}_S$ accordingly.

At this point we can come back to the definitions Eqs. (2.20). The first term in Eq. (2.40) describes the coherent dynamics. In the interaction picture we can remove this term by carefully choosing the Hamiltonian we

consider to be the unperturbed system and thus removing the first term in Eq. (2.51). If we chose the wrong system we are left with remainder coherent dynamics. If we choose the partition into system and bath such that $\langle H_I \rangle_V = 0$ then we already chose a system that removes the coherent oscillation in the interaction picture. If we choose the naive partitioning we would end up with a remainder term that drives coherent dynamics that then drive oscillation on the off diagonal terms.

In the naive partitioning we would have ended up with

$$\mathcal{L}_{S,\text{eff}}\rho = \frac{1}{\hbar}[H_Z + 2J\langle J^z \rangle_V S^z, \rho]. \tag{2.52}$$

In order to remove the coherent dynamics in the interaction picture we then needed to choose $\bar{H}_S = H_Z + 2J\langle J^z \rangle_V S^z$, which again brings us back to the definition we did in Eq. (2.20). Because in this light this Hamiltonian includes an effective field induced by the lead we call it the effective Hamiltonian $H_{\text{eff}} \equiv \bar{H}_S$.

For the secular approximation we start with the master equation in the interaction picture Eq. (2.35) and its kernel Eq. (2.39) and insert explicit expressions for the operators in the interaction picture. Those are given in the Schrödinger picture by

$$B^I_\alpha(t) = \sum_{k=\pm,z} c_{\alpha k} e^{i\sigma_k \Delta_S t/\hbar} S^k \tag{2.53}$$

where $\sigma_+ = -\sigma_- = 1$, $\sigma_z = 0$ and Eq. (2.22) was inserted into the definition of the operators in the interaction picture. Inserting these into Eq. (2.39) we obtain

$$\begin{aligned}\mathcal{K}^I(t,\tau)\rho^I(\tau) = \frac{1}{\hbar^2} \sum_{k,l=\pm,z} & e^{i\Delta_S(\sigma_k+\sigma_l)t/\hbar} e^{-i\Delta\sigma_l(t-\tau)/\hbar} \\ & \times \left(\mathcal{G}_{kl}(t-\tau)[S^k, S^l\rho^I(\tau)] + \mathcal{G}_{lk}(\tau-t)[\rho^I(\tau)S^l, S^k]\right).\end{aligned} \tag{2.54}$$

In the next step we do the Markov approximation. For the Markov approximation we assume that the correlation in the leads decay fast and that thus the correlation functions of the leads are δ-like and we can assume that $\rho^I(\tau) \approx \rho^I(t)$. By this approximation the equation becomes time local in t and we are independent of the history of the evolution of the system.

In Markov approximation the integral in Eq. (2.35) can now be carried out yielding

$$\dot{\rho}^I(t) = -\frac{1}{\hbar^2}\sum_{k,l=\pm,z} e^{i\Delta_S(\sigma_k+\sigma_l)t/\hbar} \times \left(\mathcal{F}^+_{kl}(-\Delta_S\sigma_l)[S^k, S^l\rho^I(t)] + \mathcal{F}^-_{lk}(-\Delta_S\sigma_l)[\rho^I(t)S^l, S^k]\right), \quad (2.55)$$

where

$$\mathcal{F}^\sigma_{kl}(z) = \int_0^\infty \mathrm{d}\tau\, e^{iz\tau/\hbar}\mathcal{G}_{kl}(\sigma\tau) \quad (2.56)$$

are the half sided Fourier transforms of the correlation functions $\mathcal{G}_{kl}(\tau)$. Note that as the integral is not over the whole real axis the sign of the time argument of $\mathcal{G}_{kl}(\tau)$ plays a role.

The master equation in Markov approximation now being time local still contains some fast oscillating terms. The oscillating terms oscillate on the scale $\tau_s \approx \hbar/\Delta_S$ of the system. For the density matrix the terms that drive coherent oscillations that are on the same order, however, are removed such that the dynamics of the density matrix are determined by the coupling to the bath alone. This coupling to the bath has a relaxation time scale $\tau_R \propto \hbar\beta(J/v_F\hbar)^{-2}$ which we assume to be larger than τ_S. As the density matrix in interaction picture changes on the scale of τ_R it is approximately constant on the scale τ_S such that the fast oscillations do not contribute. We thus neglect terms for which $\sigma_k + \sigma_l \neq 0$. The resulting equation

$$\dot{\rho}^I(t) = -\frac{1}{\hbar^2}\sum_{k=\pm,z} \left(\mathcal{F}^+_{k\bar{k}}(\Delta_S\sigma_k)[S^k, S^{\bar{k}}\rho^I(t)] + \mathcal{F}^-_{\bar{k}k}(\Delta_S\sigma_k)[\rho^I(t)S^{\bar{k}}, S^k]\right), \quad (2.57)$$

is now local in time and does not contain oscillating terms anymore.

The secular approximation is obtained by neglecting fast oscillating terms. The oscillations in these terms needed to be fast compared to the relaxation dynamics of the system. For the validity of the approximation it is important that the dynamics of the system are only given by relaxation as these processes are slow. Therefore it was important to remove any additional coherent oscillations. If any coherent oscillations were left the separations in fast and slow oscillation would have been obscured. The choice of the unperturbed system is thus of great importance for the validity of the secular approximation.

The master equation in secular approximation can be written in a standardized form[2]; the Lindblad form. This form guarantees the conservation of the trace and thus is the standard form of the Markovian dynamics of open systems. This form will be given in the next chapter. Finally we will then compare the result of Eq. (2.50) to the result obtained from Eq. (2.57) before continuing with the calculation of transport properties.

2.2.6 Master Equation in Lindblad Form

It can be shown that all quantum dynamical semigroups can be described in a standardized form [Bre02]. For this standardized form the Liouvillian is written in the Lindblad form

$$\dot{\rho}(t) = \mathcal{L}_{\mathrm{LF}}\rho(t) = -\frac{i}{\hbar}[H,\rho] + \frac{1}{\hbar^2}\sum_{k=1}^{N^2-1}\gamma_k\Big(W_k\rho(t)W_k^\dagger - \frac{1}{2}\Big(W_k^\dagger W_k\rho(t) + \rho(t)W_k^\dagger W_k\Big)\Big), \quad (2.58)$$

where N is the dimension of the Hilbert space and W_k are the Lindblad operators and γ_k are positive coefficients and H is a Hermitian operator. This equation can be written in a more convenient form

$$\mathcal{L}_{\mathrm{LF}}\rho(t) = -i\mathcal{L}_H\rho(t) + \mathcal{D}[\rho(t)], \quad (2.59)$$

where the dissipator $\mathcal{D}$ is defined by

$$\mathcal{D}[\rho(t)] = \frac{1}{\hbar^2}\sum_{k=1}^{N^2-1}\gamma_k\Big(W_k\rho(t)W_k^\dagger - \frac{1}{2}\{W_k^\dagger W_k,\rho(t)\}\Big), \quad (2.60)$$

and $\{A,B\} = AB + BA$ is the anticommutator. Using the dissipator the master equation can be written in a very compact form. It is, however, important to mention that the Hermitian operator need not be the system Hamiltonian.

We will now bring the master equation in secular approximation Eq. (2.57) into the Lindblad form and determine the operators H, W_k as well as the

[2] In general this is not possible for all master equations. Breuer and Petruccione argue that for functions of positive type this form can always be obtained [Bre02]. The correlation functions here fulfill this condition.

coefficients γ_k. By carrying out the commutators in Eq. (2.57) we obtain

$$\dot{\rho}^I(t) = -\sum_{k=\pm,z} \Big(\mathcal{F}^+_{k\bar{k}}(\Delta_S \sigma_k) S^k S^{\bar{k}} \rho^I(t) + \mathcal{F}^-_{k\bar{k}}(-\Delta_S \sigma_k) \rho^I(t) S^k S^{\bar{k}} - \mathcal{F}_{k\bar{k}}(\Delta_S \sigma_k) S^{\bar{k}} \rho^I(t) S^k \Big), \quad (2.61)$$

where the Fourier transform $\mathcal{F}_{kl}(\omega)$ is defined by

$$\mathcal{F}_{kl}(\omega) = \mathcal{F}^+_{kl}(\omega) + \mathcal{F}^-_{kl}(-\omega). \quad (2.62)$$

In order to cast this equation in Lindblad form we use

$$a\hat{X}\hat{Y} + b\hat{Y}\hat{X} = \frac{a+b}{2}[\hat{X}, \hat{Y}] + \frac{a-b}{2}\{\hat{X}, \hat{Y}\}, \quad (2.63)$$

where $\hat{X}$ and $\hat{Y}$ are operators and $a, b \in \mathbb{R}$. The master equation can then be written in Lindblad form by

$$\dot{\rho}(t)^I = -\frac{i}{\hbar}[H_{\mathrm{LS}}, \rho^I(t)] + \mathcal{D}[\rho^I(t)] \quad (2.64)$$

$$H_{\mathrm{LS}} = -i \sum_{k=\pm,z} \frac{\mathcal{F}^+_{k\bar{k}}(\Delta_S \sigma_k) - \mathcal{F}^-_{k\bar{k}}(-\Delta_S \sigma_k)}{2\hbar} S^k S^{k\dagger} \quad (2.65)$$

$$\mathcal{D}[\rho^I(t)] = \frac{1}{\hbar^2} \sum_{k=\pm,z} \mathcal{F}_{\bar{k}k}(-\Delta_S \sigma_k) \Big(S^k \rho^I(t) S^{k\dagger} - \frac{1}{2}\{S^{k\dagger} S^k, \rho^I(t)\} \Big), \quad (2.66)$$

where we used that $S^{\bar{k}} = S^{k\dagger}$ and H_{LS} is the Lamb shift Hamiltonian. Transforming this equation back to the Schrödinger picture only reintroduces the commutator with the system Hamiltonian such that the dissipator as well as the Lamb shift Hamiltonian have the same shape.

The Lamb shift Hamiltonian gives second order corrections to the effective system Hamiltonian. For our case the resulting matrix for the Lamb shift terms only has diagonal entries as

$$S^+S^- = \hbar^2 \begin{pmatrix} 1 & 0 \\ 0 & 0 \end{pmatrix} \qquad S^zS^z = \hbar^2 \begin{pmatrix} 1/4 & 0 \\ 0 & 1/4 \end{pmatrix}$$
$$S^-S^+ = \hbar^2 \begin{pmatrix} 0 & 0 \\ 0 & 1 \end{pmatrix} \quad (2.67)$$

such that the Lamb shift will not alter the direction of the quantization axis and only shifts the energy and changes the splitting of the effective QD levels. The splitting is the only term that has an effect on the system and would enter in the dissipator and thus only in higher order terms. This is in contrast to the first order terms which need to be respected as they change the direction of quantization and thus are important for the validity of the secular approximation. Here we will ignore this Lamb shift term.

In this form we can write down the equations of motion in the Schrödinger picture in a particular simple form. Changing to the Schrödinger picture only reintroduces the commutator that was removed by going to the interaction picture. Inserting the matrix representation of the spin operators into Eq. (2.64) we obtain the equations of motion for the entries of the density matrix

$$\dot{\rho}_{\uparrow\uparrow}(t) = -\Gamma_{\downarrow\uparrow}\rho_{\uparrow\uparrow}(t) + \Gamma_{\uparrow\downarrow}\rho_{\downarrow\downarrow}(t) \tag{2.68a}$$

$$\dot{\rho}_{\downarrow\downarrow}(t) = \Gamma_{\downarrow\uparrow}\rho_{\uparrow\uparrow}(t) - \Gamma_{\uparrow\downarrow}\rho_{\downarrow\downarrow}(t) \tag{2.68b}$$

$$\dot{\rho}_{\uparrow\downarrow}(t) = (-i\Delta_S/\hbar - \Gamma_{\mathrm{deph}})\rho_{\uparrow\downarrow}(t) \tag{2.68c}$$

$$\dot{\rho}_{\downarrow\uparrow}(t) = (i\Delta_S/\hbar - \Gamma_{\mathrm{deph}})\rho_{\downarrow\uparrow}(t), \tag{2.68d}$$

where $\Gamma_{\uparrow\downarrow} \equiv \mathcal{F}_{-+}(-\Delta_S)$, $\Gamma_{\downarrow\uparrow} \equiv \mathcal{F}_{+-}(\Delta_S)$, $\Gamma = \Gamma_{\uparrow\downarrow} + \Gamma_{\downarrow\uparrow}$ and $\Gamma_{\mathrm{deph}} \equiv \mathcal{F}_{-+}(-\Delta_S) + \mathcal{F}_{+-}(\Delta_S) + \mathcal{F}_{zz}(0)/2$. The diagonal and off diagonal entries thus decouple and the equation of motion can be interpreted as a rate equation for the diagonal entries and dephasing for the off diagonal entries. This representation allows us to interpret the behavior in an intuitive way. The behavior of the system will now be an interplay of the spin flip rates $\Gamma_{\sigma\bar{\sigma}}$ and the parameters of the effective system. Before we can discuss the behavior of the system we thus need to discuss the properties of the effective system.

2.2.7 Effective System Parameters

In Eq. (2.22) we introduced an additional term in the system that we later identified as the induced field due to the coupling to the lead in Eq. (2.52). We also argued that this additional term is equivalent to the redefinition of system and coupling in Eq. (2.20). In the derivation of the master equation we used the coefficients defined in Eq. (2.17) to write the spin operators S^σ in a basis that diagonalizes the system such that their time evolution is simple. This transformation is parameterized by the two angles θ and ϕ as discussed in section 2.1.3. There we also

showed that these angles can be determined by representing the resulting effective magnetic field in spherical coordinates.

In Fig. 2.1b) the geometry of the effective Hamiltonian is shown. The effective system is the sum of the splitting due to the magnetic field $g\mu_B\vec{B}$ and an induced splitting $\Delta_V\hat{z}$, where $\hat{z}$ is the spin quantization direction of the edge state electrons. Those two fields are tilted by θ_Z with respect to each other. The resulting effective field is modified in strength and in direction. We need to determine those new parameters.

The transformation between the operators for the spin in the edge state and the effective quantization direction in the effective system can most conveniently be calculated by writing down the effective system Hamiltonian H_{eff} in the spin basis in which the z axis is parallel to the spin of the right movers. In this basis the direction of the magnetic field can be parameterized by two angles; the polar angle θ_Z and the azimuthal angle ϕ_Z of the magnetic field.The induced field points along the z axis such that

$$H_{\text{eff}} = \frac{1}{\hbar}\begin{pmatrix}\Delta_Z \sin\theta_Z \cos\phi_Z \\ \Delta_Z \sin\theta_Z \sin\phi_Z \\ \Delta_Z \cos\theta_Z + \Delta_V\end{pmatrix} \cdot \vec{S} = \frac{\Delta_S}{\hbar}\begin{pmatrix}\sin\theta\cos\phi \\ \sin\theta\sin\phi \\ \cos\theta\end{pmatrix} \cdot \vec{S}, \quad (2.69)$$

where θ and ϕ are the polar and azimuthal angles parameterizing the effective system direction $\hat{n}$ and Δ_S is the effective splitting of the system.

The effective splitting in the system can be determined by calculating the norm of the vectors on both sides of the equation. This leads to

$$\Delta_S = \sqrt{\Delta_Z^2 + \Delta_V^2 + 2\Delta_Z\Delta_V\cos\theta_Z}, \quad (2.70)$$

where we chose the splitting Δ_S to be positive. The parameter ϕ only appears in the first two components. By choosing $\phi = \phi_Z$ we can get rid of these factors. The third component then yields

$$\theta = \arccos\Big(\frac{\Delta_Z\cos\theta_Z + \Delta_V}{\Delta_S}\Big). \quad (2.71)$$

By using $\sin(\arccos(x)) = \sqrt{1-x^2}$, which is valid for $-1 < x < 1$ we can check that this angle also fulfills the first two components because

$$\sqrt{1 - \Big(\frac{\Delta_Z\cos\theta_Z + \Delta_V}{\Delta_S}\Big)^2} = \sqrt{\frac{\Delta_Z^2}{\Delta_S^2}\sin^2\theta_Z} = \frac{\Delta_Z}{\Delta_S}\sin\theta_Z, \quad (2.72)$$

where we used that $\Delta_Z, \Delta_S > 0$ and that $0 \leq \theta_Z < \pi$.

For a fixed angle θ_Z the interplay between Δ_V and Δ_Z determines the properties of the effective system. In general we can distinguish three interesting regimes; the regime in which the Zeeman splitting dominates $\Delta_Z \gg \Delta_V$, the regime of large bias voltage in which $|\Delta_V| \gg \Delta_Z$ and the regime where the two contributions cancel each other $\Delta_V \approx -\Delta_Z \cos\theta_Z$. Because $\Delta_V \propto JV$ and $\Delta_Z \propto B$ these regimes can either be switched by changing the magnetic field or by changing the bias. Depending on which contribution it is larger and will dominate the behavior.

For small bias voltage we find $\Delta_V \ll \Delta_Z$. Because we assume that J is small and $\Delta_V \propto JV$ this condition is met for a large bias voltage range when Δ_Z is not zero. This especially also includes the cases in which $eV \approx \Delta_Z$. In this regime $\Delta_S \approx \Delta_Z$ and thus $\theta \approx \theta_Z$. The effective field aligns with the magnetic field and the splitting is given by the Zeeman splitting.

For large bias voltage when $|\Delta_V| \gg \Delta_Z$ we find that $\Delta_S \approx |\Delta_V|$. The angle on the other hand then is $\theta = \arccos(\mathrm{sgn}(eV\beta)) = (1 - \mathrm{sgn}(eV\beta))\pi/2$. For large bias voltage the system thus aligns with the lead quantization axis. The sign of the bias then decides whether the system aligns or antialigns. In Fig. 2.1 this corresponds to the case where Δ_V pushes the system into the right upper or left lower direction.

For the intermediate bias voltage the resulting system is in between those two cases. It also includes the point where $\Delta_V \approx -\Delta_Z \cos\theta_Z$. At this point the resulting splitting is minimal. In this regime the effect of the bias voltage on the direction of the effective field is very strong and the direction can be changed without really affecting the splitting.

2.2.8 Correlation Functions of the HLL

In section 2.2.6 we saw that the transition rates between the diagonal elements of the density matrix contain the Fourier transforms of the lead correlation functions. These correlation functions can be calculated using bosonization including the Coulomb interaction of the electrons in the helical edge. The details of these calculations are given in appendix B. Here we would like to summarize the most important properties of the correlation functions needed to interpret the behavior of the transition rates.

In section 2.2.3 we introduced the correlation function $G_{kl}(\tau)$. Due to number conservation in the system only three correlation functions play a role $G_{zz}(\tau)$ and $G_{\pm\mp}(\tau)$. Following [Peç03] the bias voltage in the

density matrix ρ_V can be gauged into the lead operators such that

$$G_{\alpha\bar{\alpha}}(\tau) = e^{-i\sigma_\alpha eVt/\hbar}\mathrm{Tr}_B(\rho_{\mathrm{HLL}}A_\alpha(t)A_{\bar{\alpha}}(0)), \tag{2.73}$$

where $\rho_{\mathrm{HLL}} = \exp(-\beta H_{\mathrm{HLL}})/Z_{\mathrm{HLL}}$ and $Z_{\mathrm{HLL}} = \mathrm{Tr}_B(\rho_{\mathrm{HLL}})$. The details of this transformation is summarized in appendix B.2. The correlation function can thus be decomposed into an oscillating prefactor and an expectation value for a system without bias. The correlation functions are

$$G_{\pm\mp}(\tau) = \left(\frac{J}{\beta v}\right)^2 e^{\mp ieVt/\hbar}\ \frac{(\sin a)^{2K}}{(2a)^2}\left(\frac{i}{\sinh(ia - \frac{\pi t}{\hbar\beta})}\right)^{2K} \tag{2.74a}$$

$$G_{zz}(\tau) = \left(\frac{J}{\beta v}\right)^2 \frac{1}{2K}\left(\frac{i}{\sinh(ia - \frac{\pi t}{\hbar\beta})}\right)^2, \tag{2.74b}$$

where $a \equiv \pi\alpha/\hbar\beta v$, α is the cutoff and K the interaction parameter of the bosonization and $v \equiv v_F K$ is the Fermi velocity.

The interaction influences $G_{zz}(\tau)$ and $G_{\pm\mp}(\tau)$ differently. The continuum limit $a \to 0$ is well behaved for $G_{zz}(\tau)$ whereas it cannot be carried out for $G_{\pm\mp}(\tau)$ for $K \neq 1$ as a the prefactor has an algebraic divergence with an exponent of $2K - 2$. When interaction in the leads is included we thus cannot carry out the continuum limit and have to keep the cutoff parameter a finite.

In both cases the time argument leads to a decay that is characterized by the dimensionless time $\pi t/\hbar\beta$. For larger temperatures the decay is exponential and the correlation function is well localized in time. For smaller temperatures, however, the hyperbolic sine can be approximated linearly and we find that the decay is algebraic and in the case of $G_{\pm\mp}(\tau)$ is non universal.

For the transition rates we need to calculate the Fourier transforms of these correlation functions. We define these Fourier transforms by

$$F_z(\omega) = \int_{-\infty}^{\infty} \mathrm{d}\tau\ e^{i\omega\tau/\hbar}\ G_{zz}(\tau) \tag{2.75a}$$

$$F_{\sigma\bar{\sigma}}(\omega) = \int_{-\infty}^{\infty} \mathrm{d}\tau\ e^{i\omega\tau/\hbar}\ G_{\sigma\bar{\sigma}}(\tau). \tag{2.75b}$$

These integrals can be carried out analytically by using a generalized binominal formula. For small a the resulting expressions can be simplified

and we obtain

$$F_z(\omega) = \frac{1}{\hbar\beta}\left(\frac{\hbar J}{v}\right)^2 \frac{\omega\beta}{2\pi K}\frac{e^{\beta\omega/2}}{\sinh(\omega\beta/2)} \tag{2.76a}$$

$$F_{\sigma\bar{\sigma}}(\omega) = F(\omega - \sigma eV) \tag{2.76b}$$

$$F(\omega) = \frac{1}{\hbar\beta}\left(\frac{\hbar J}{v}\right)^2 \frac{(2\sin a)^{2K}}{(2a)^2} \frac{\pi}{\Gamma(K)|\Gamma(1-K+i\omega\beta/2\pi)|^2}\frac{e^{\omega\beta/2}}{\cosh\omega\beta - \cos 2\pi K}. \tag{2.76c}$$

As the bias voltage only appears in an oscillating prefactor in Eq. (2.74a) the bias voltage just shifts the frequency and to understand the behavior of $F_{\sigma\bar{\sigma}}(\omega)$ it is sufficient to discuss the properties of $F(\omega)$.

For the GME the half sided Fourier transforms also play a role. These can also be calculated analytically. The result, however, is more complicated and not very intuitive. They only appear in the GME result. Most of the interpretations of the result can be done using the GME in secular approximation which only contains the Fourier transforms. We thus give these transforms in appendix B and only discuss the Fourier transforms here.

For the interpretation of the result the dependence on the bias voltage plays an important role. The bias voltage or also the Zeeman splitting only has an significant influence if they are larger than k_BT as otherwise the thermal widening will hide all structures. We are thus especially interested in frequencies of $\omega\beta > 1$. For $|\omega\beta| \gg 1$ we can use Stirling's formula to show that

$$|\Gamma(1-K+i\omega\beta/2\pi)|^2 \approx 2\pi(|\omega|\beta/2\pi)^{1-2K}e^{-|\omega|\beta/2}e^{-2+2K}. \tag{2.77}$$

Inserting this into Eq. (2.76c) we obtain for $\omega\beta \gg 1$ and $a \ll 1$

$$F(\omega) \approx \frac{1}{\hbar\beta}\left(\frac{\hbar J}{v}\right)^2 \frac{4\pi^2}{\Gamma(K)e^{-2+2K}}\ (2a)^{2K-2}\ (\omega\beta/2\pi)^{2K-1}\ e^{(\omega-|\omega|)\beta/2} \tag{2.78}$$

We thus find that for negative frequencies the Fourier transform decays exponentially whereas for positive frequencies it behaves algebraically with an exponent of $2K-1$. For $K=1$ the Fourier transform $F(\omega)$ shows the same functional behavior as $F_z(\omega)$.

2.2.9 Validity of Secular Approximation

In section 2.2.5 we introduced the secular approximation. Its central idea was to neglect terms in the equation which just introduce fast oscillations that vanish when averaged over a time longer than the period of these oscillations. The important assumption was that the time scale of the relaxation τ_R is large compared to the time scale of this oscillations which is given by the timescale of the oscillations of the system τ_S. In the last section we introduced the effective system parameters and also listed some properties and different regimes. The master equation in secular approximation allows for an intuitive interpretation. It is thus important to understand in which regime the secular approximation is reliable as this opens up a very strong tool for the interpretation of the system.

In the last section we showed that the induced field cannot only modify the effective splitting itself but also the direction. Each of these regimes were characterized by a specific relation between Δ_V and Δ_Z. To get a feeling for the influence on the validity for the secular approximation we need to estimate τ_S and τ_R.

The system time scale can be estimated by the relaxation rates. In general these relaxation rates are small as they are of second order in the coupling which is small. The rates also contain the Fourier transform of the lead correlation function which follows a power law with exponent $2K-1$ for large bias voltage βV. On the one hand we can thus estimate the timescale of the relaxation by

$$\frac{1}{\tau_R} = \left(\frac{\hbar J}{v_F}\right)^2 \frac{1}{\hbar\beta}(eV\beta)^{2K-1}. \tag{2.79}$$

The timescale of the system, on the other hand, can be estimated by $\hbar/\Delta_S$, which can be estimated by

$$\frac{\hbar}{\tau_S} = \Delta_S \approx \max(\Delta_V, \Delta_Z). \tag{2.80}$$

These simple estimates allow to determine in which regime $\tau_R \gg \tau_S$.

In the regime where the bias voltage is of the order of the Zeeman splitting we find

$$\frac{\tau_S}{\tau_R} \approx \left(\frac{\hbar J}{v_F}\right)^2 (eV\beta)^{2K-2} \ll 1. \tag{2.81}$$

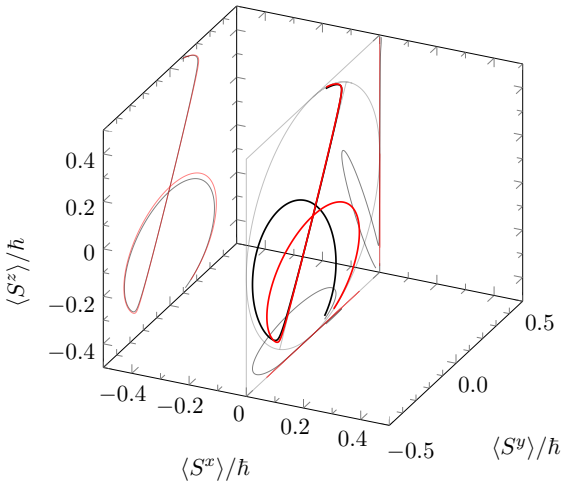

Figure 2.2: Spin expectation values of the QD spin using the steady state calculated for the GME (black) and the GME in secular approximation (red) for $\Delta_Z\beta = 0.5$, $\hbar J/v_F = 0.1$, $\theta_Z = \pi/6$ and $K = 1$. The bias voltage eV goes from $-150k_\mathrm{B}T$ to $100k_\mathrm{B}T$, which is the same bias voltage range also shown in Fig. 2.3, where the same parameters are used. In grey the plane defined by $x = 0$, the direction of the magnetic field as well as the circle defining full polarization are added to guide the eye. On the walls of the box the projections onto these surfaces are shown. We see that for large positive and negative bias voltage the spin of the QD aligns with the lead quantization axis. For lower bias the system aligns with the magnetic field and switches polarization for $eV \approx \Delta_Z$. For growing negative bias voltage the quantization axis rotates and the polarization anti aligns with the lead quantization axis. During this rotation the spin expectation value in secular approximation deviates from the polarization using the full GME as the spin expectation value rotates out of the plane.

We can thus expect the secular approximation to hold. In this bias voltage range the splitting is not altered crucially. The splitting of the system thus protects the approximation.

In the case where $\Delta_Z \approx -\Delta_V$ the system timescale is of order $(\hbar J/v_F)^{-1}$ such that a more careful analysis is necessary. Using $\Delta_V = -\hbar JV/4\pi v_F$ we find

$$\frac{\tau_S}{\tau_R} = \frac{\hbar J}{v_F} 4\pi \ (eV\beta)^{2K-2}, \tag{2.82}$$

which is now only first order in the small parameter such that the secular approximation is not as safe as for smaller bias. This regime is realized either by a small Zeeman splitting, a strong coupling or a high bias voltage applied to the edge state. In the first two cases the splitting in the system is reduced and thus the approximation is not as good anymore. In the third case the rates are large such that the relaxation dynamics are faster rendering fast oscillation more important. In this case the effective angle is close to $\pi/2$. The spin of the impurity thus cannot have a large influence as no spin direction is preferred.

In the regime of $|\Delta_V| \gg \Delta_Z$ the bias voltage and thus the relaxation rates are large and also generate the same problems as mentioned above. The difference however is that in this case $\theta \approx 0$ or $\theta \approx \pi$. Looking closer at the secular entries in $\mathcal{K}$ we see that all those entries are multiplied by $\sin\theta$ or $\sin^2\theta$ which is small. In order to understand how small they are we insert Eq. (2.71) into the sine and obtain

$$\sin\theta = \sin\left(\arccos\left(\frac{\Delta_V + \Delta_Z\cos\theta_Z}{\Delta_S}\right)\right) = \sin\theta_Z\left|\frac{\Delta_Z}{\Delta_S}\right|. \tag{2.83}$$

Because $\Delta_S \approx \Delta_V$ this term add another factor of Δ_Z/Δ_S, which is of order of $1/eV$ leading to an additional suppression. The secular approximation thus is aided by the suppression of the oscillating terms because the system quantization direction aligns with the electrons in the lead.

Using the GME we can calculate the steady state density matrix which is completely determined by the spin expectation values. To understand the influence of the secular approximation we calculated the spin polarization using the full kernel as well as using the secular approximation. In the regime of $|eV| \approx \Delta_Z$ we found no crucial deviations of the two results as is expected from our estimates. The result for a small Zeeman splitting is shown in Fig. 2.2. In Fig. 2.3 the same results for the polarization in secular approximation is shown as a function of the bias voltage V. We see that the results coincide well for positive bias voltage as well as

very negative bias voltage. They deviate in the regime where the bias voltage is such that it changes the direction of the quantization axis of the effective system. This is also the regime where the effective splitting is small. Above we argued that this is also the regime in which we expect the secular approximation to be worse. The polarization using the full GME rotates out of the plane which is a sign of the precession in the system. If one focuses on the projection to the y-z-plane, however, the qualitative behavior is still good.

The polarization in secular approximation and the result using the full GME coincide in a wide range of parameters. The only regime in which they deviate is the regime in which $\Delta_V \approx -\Delta_Z \cos\theta_Z$. There the effective splitting is small compared to the relaxation, which is fast due to the high bias voltage, making the secular approximation less accurate. The qualitative features, however, still coincide. We will thus use the secular result to interpret the results qualitatively but have to check whether the result in secular approximation still reproduces the result from the full GME sufficiently well.

2.3 Behavior of the Quantum Dot

In the previous section we discussed several properties of the correlation functions and the effective system as well as the validity of the secular approximation. The secular approximation showed to be valid in all relevant regimes such that we can use it to interpret the behavior of the system. We will now look at the behavior of the system and interpret it using the properties of the rates and the geometry. For this we will focus on the polarization. We first investigate the case of $\Delta_Z \gg \Delta_V$ and continue with the case of $\Delta_Z \approx -\Delta_V$.

The spin polarization of the QD is determined by two factors; the polarization of the QD and the direction of the spin quantization axis. In Eq. (2.68) we have a simple solvable rate equation. It is, however, only that simple when choosing the basis to be the effective system. In this description the steady state density matrix is always diagonal. From the point of view of the helical edge state this state then will have off diagonal entries in the density matrix. Because the steady state in the effective system is diagonal it can be completely parameterized by $\langle S'^z \rangle$

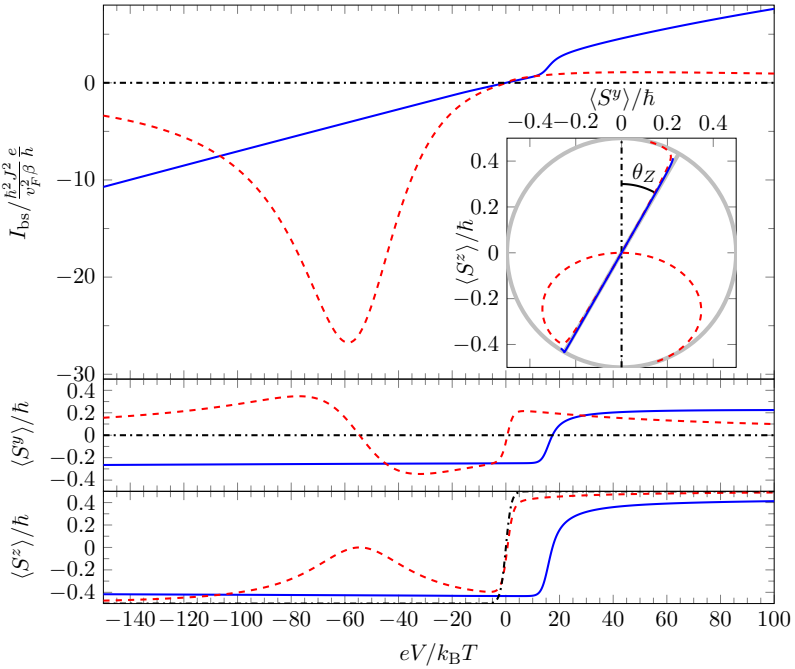

Figure 2.3: Backscattering current and QD spin polarization in y and z direction, where the z direction is the spin quantization axis of the edge state, for $\hbar J/v_F = 0.1$, $\theta_Z = \pi/6$, $\Delta_Z = 15 k_{\mathrm{B}}T$ (blue, solid), $\Delta_Z = 0.5 k_{\mathrm{B}}T$ (red, dashed) and $\Delta_Z = 0 k_{\mathrm{B}}T$ (black, dash dotted) as a function of the bias voltage V and for $K = 1$. The inset shows the spin polarization in the y-z plane. For illustration, the Bloch sphere as well as the direction of the magnetic field is added in gray. When $|eV|$ is comparable with Δ_Z and thus $\Delta_Z \ll \Delta_V$, the spin polarization aligns with the magnetic field. If Δ_V becomes comparable to Δ_Z the spin polarization starts to align with the lead quantization axis. For a sufficiently small magnetic field or a sufficient large bias voltage we see that the spin quantization axis rotates while the quantum dot is still polarized such that the spin polarization forms a loop before again aligning with the lead quantization axis. Without magnetic field the induced field is parallel to the lead quantization axis such that the polarization in z direction changes sign at $eV = 0$. Figure and caption reproduced from the original publication [Pro15].

and the spin polarization in the edge state system is then

$$\langle S^x\rangle = \cos\theta\langle S'^z\rangle \tag{2.84a}$$
$$\langle S^y\rangle = \cos\phi\sin\theta\langle S'^z\rangle \tag{2.84b}$$
$$\langle S^z\rangle = \sin\phi\sin\theta\langle S'^z\rangle. \tag{2.84c}$$

The spin polarization in the effective system $\langle S'^z\rangle$ on the other hand is determined by the steady state of Eq. (2.68). A closer look at this equation shows that diagonal and off diagonal entries decouple. Because we chose a basis in which the system is diagonal we do not have transitions between the off diagonal entries. Besides the system splitting driving oscillations we also find a damping term that describes dephasing. In the long time limit the off diagonal entries thus do decay such that the steady state density matrix is diagonal in this basis and thus given by

$$\bar{\rho} = \begin{pmatrix} \Gamma_{\uparrow\downarrow}/\Gamma & 0 \\ 0 & \Gamma_{\downarrow\uparrow}/\Gamma \end{pmatrix} = \begin{pmatrix} 1/2 + \langle S'^z\rangle/\hbar & 0 \\ 0 & 1/2 - \langle S'^z\rangle/\hbar \end{pmatrix}. \tag{2.85}$$

The total spin polarization is thus an interplay of the direction of the effective system and the polarization in this effective frame of reference. We will start to focus on a regime in which the direction is fixed first and then discuss the case in which the direction changes significantly as a function of the bias voltage.

For $\Delta_V \ll \Delta_Z$ we showed in section 2.2.7 that the direction of the effective system aligns with the magnetic field. For our discussion it is thus sufficient to understand the behavior of Eq. (2.85). Therefore we write down the two rates

$$\Gamma_{\downarrow\uparrow} = \cos^4\frac{\theta}{2}F(\Delta_S - eV) + \sin^4\frac{\theta}{2}F(\Delta_S + eV) + \frac{1}{4}\sin^2\theta F_z(\Delta_S) \tag{2.86a}$$
$$\Gamma_{\uparrow\downarrow} = \sin^4\frac{\theta}{2}F(-\Delta_S - eV) + \cos^4\frac{\theta}{2}F(-\Delta_S + eV) + \frac{1}{4}\sin^2\theta F_z(-\Delta_S). \tag{2.86b}$$

Each of the terms in the sum is a product of a term depending on θ which represents the geometry and a term that depends on Δ_S and eV which represents energy conservation.

First we have a closer look at the term representing energy conservation. In Fig. 2.4 a process is illustrated in which the system is excited by making

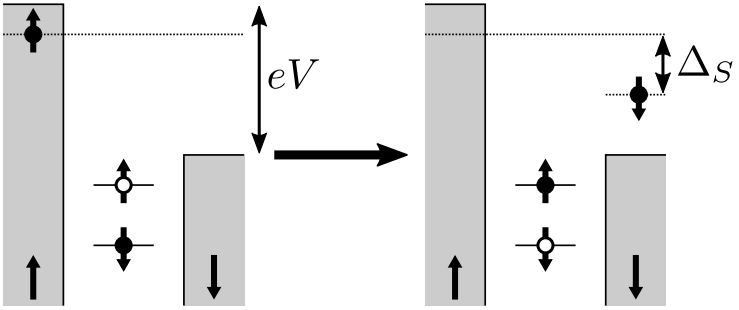

Figure 2.4: Spin conserving cotunneling event contained in H_I. The right and left movers are represented as two different reservoirs and the system by its two states. A spin up electron is scattered to a spin down electron by exciting the QD. To excite the system it has to supply an energy of Δ_S. This process is thus possible for $eV > \Delta_Z$. Because in this process the spin of the impurity is increased and the spin in the lead is decreased this process is spin conserving.

a right mover (spin up) a left mover (spin down). For now we will assume that the magnetic field is aligned with the lead quantization axis. Exciting the system means increasing the spin such that the spin of the edge electron needs to be reduced. In order to excite the system the lead has to supply an energy of Δ_S meaning that the electron that is put back in the lead needs to be inserted at a lower energy than the electron removed from the lead. For $eV < \Delta_S$ this process is thus only possible for finite temperature and exponentially suppressed and only strong for $eV > \Delta_Z$.

The situation changes if the magnetic field is not exactly aligned with the spin quantization axis of the edge state. If the magnetic field is slightly tilted the right movers (spin up) have a large overlap with the spin up electrons on the QD but also a small finite overlap with the spin down electrons on the QD. If we now only focus on the diagonal entries of the density matrix this would seem to be a spin conservation violating process. In the master equation the off diagonal entries, however, decay such that although the Hamiltonian is spin conserving the resulting transition rates seem to violate spin conservation. Now, also spin flips in the lead are possible without flipping the spin of the impurity or flipping the impurity in the same direction.

We will thus distinguish processes that violate spin conservation and processes that conserve spin conservation. The spin conservation violating

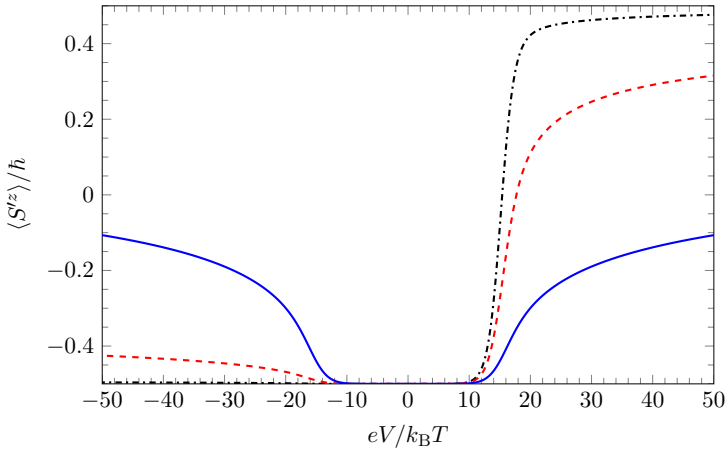

Figure 2.5: Polarization in the effective system for $\hbar J/v_F = 0.1$, $\Delta_Z = 15 k_{\mathrm{B}} T$, $\theta_Z = \pi/6$ (black, dash dotted), $\theta_Z = \pi/3$ (red, dashed) and $\theta_Z = \pi/2$ (blue, solid).

processes are enabled by the overlap of an edge state electron with the opposite spin in the system. In the case of $\theta_Z = \pi/2$ the overlap of the lead electrons and the states in the QD is such that no spin direction is preferred. When going from $0 \leq \theta_Z < \pi/2$ to $\pi/2 \leq \theta_Z < \pi$ the effective system spin quantization axis flips over in the reference frame of the edge state and the spin conserving and spin conservation violating processes exchange their meaning.

When looking at Eq. (2.86) we can identify terms that correspond to spin conserving processes and terms that correspond to spin conservation violating processes. The spin conserving terms are also present without a tilt in the magnetic field and thus are the terms involving a cosine whereas the terms violating spin conservation involve a sine. The spin conserving and spin conservation violating terms differ only by their effect in the leads where they flip the spin in different directions such that energy conservation demands a change of sign in the bias. We will thus restrict our discussion on cases $0 < \theta_Z < \pi/2$.

We will now have a closer look at the effect of the different processes on the polarization which is shown in Fig. 2.5 for several angles θ_Z. Looking at Eq. (2.86) we find that for $\Gamma_{\uparrow\downarrow}$ all terms are exponentially suppressed for $|eV| < \Delta_S$ whereas for $\Gamma_{\downarrow\uparrow}$ no term has this suppression.

The QD thus relaxes into its spin down state, being its ground state, as can be seen for all angles in Fig. 2.5. For $|eV| > \Delta_S$ one of the two first terms in Eq. (2.86a) becomes strong; for $eV > \Delta_S$ the spin conserving process and for $eV < -\Delta_S$ the spin conservation violating process. As the rate to excite the QD is now finite the spin expectation value increases. The strength of the spin conservation violating process compared to the spin conserving process is controlled by the angle θ_Z. Looking at Fig. 2.5, we see that for small tilt angles the spin conserving processes excite the QD effectively for $eV > \Delta_S$ whereas there is hardly any effect for $eV < \Delta_S$. Increasing the angle will reduce the effect of the spin conserving processes and strengthen the spin conservation violating processes such that the polarization of the QD for $eV > \Delta_Z$ is less effective but more effective for $eV < \Delta_S$. When we reach a point where the magnetic field is perpendicular to the spin quantization axis in the lead the spin conserving and spin conservation violating processes are equivalent and the result for positive and negative bias voltage is the same.

In Eq. (2.86) we find also one term, the last one, that depends on the bias voltage only via Δ_S. This term corresponds to spin flip processes that are independent of the state of the lead. Such a process is possible if an electron jumps onto the QD and the electron from the dot jumps back into the hole the first electron left. Because we assume only one level on the QD these electrons must have opposite spin and this process is only possible because the electron jumping to the dot has a finite overlap with both states. This is also a spin non conserving process.

For now the interpretation of the different types of processes helps us to understand the behavior of the rates. In chapter 3.3 this idea will be formalized and extended to interpret the transport properties. For now it is important to understand that for $|eV| \approx \Delta_S$ two processes set in and that the relative strength is controlled by the tilt angle θ_Z.

Until now we focused on the case where the tilt angle of the effective system θ is independent of the bias voltage V. This case already offers the interesting perspective of manipulating the state of the QD electrically by changing the strength of the polarization. The direction of the polarization is, however, fixed. In order to manipulate the direction of the impurity we need to go into a regime in which $-\Delta_V \approx \Delta_Z$ which directly yields $-eV \gg \Delta_Z$. In this regime the angle depends on the bias V. As a consequence of the bias voltage being large we can approximate

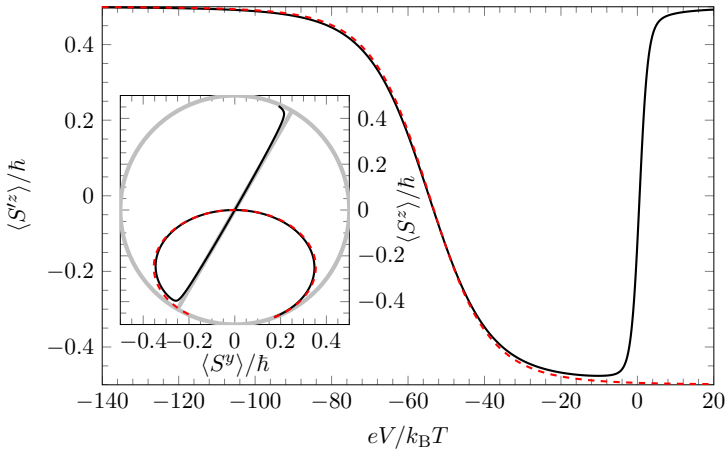

Figure 2.6: Spin expectation value (black, solid) and approximation from Eq. (2.88) (red, dashed) in the effective system for $\hbar J/v_F = 0.1$, $\theta_Z = \pi/6$ and $\Delta_Z = 0.5 k_\mathrm{B} T$. In the inset the resulting spin polarization in the edge state system is shown. The direction of the magnetic field and the Bloch sphere are shown for illustration.

the rates by

$$\Gamma_{\downarrow\uparrow} \approx \cos^4 \frac{\theta}{2} F(-eV) \qquad \Gamma_{\uparrow\downarrow} \approx \sin^4 \frac{\theta}{2} F(-eV) \tag{2.87}$$

because the other terms are exponentially suppressed or of the order of Δ_S. This approximation yields a particular simple expression for the spin excitation value in the effective system

$$\langle S'^z \rangle = \frac{\hbar}{2} \frac{\Gamma_{\uparrow\downarrow} - \Gamma_{\downarrow\uparrow}}{\Gamma} \approx \frac{\hbar}{2} \frac{\sin^4 \theta/2 - \cos^4 \theta/2}{\sin^4 \theta/2 + \cos^4 \theta/2} = \hbar \frac{2\cos\theta}{\cos^2\theta + 1}. \tag{2.88}$$

It is interesting that in this regime the behavior is only given by the geometry of the problem and not by the lead correlation functions because the functional dependence for both rates is the same.

The resulting spin polarization is shown in Fig. 2.6. We can see that the simple approximation does not describe the change of the spin polarization at $eV \approx \Delta_Z$ but describes the increase of polarization for negative bias very well. The change of the polarization is thus an effect of the rotation of the angle between the lead quantization axis and the effective system quantization axis. In the effective system this rotation shifts the weight from the spin conserving to the spin conservation violating processes such that the excitation rate increases again. As at the same time the effective system flips over the resulting polarization in the reference frame of the edge state is pointing into the negative z direction. This is illustrated in the inset of Fig. 2.6.

We discussed the behavior of the QD and understood how the bias voltage applied to the edge state and the tilt of the magnetic field together influence the behavior of the system. We found that processes violating spin conservation play an important role in the interpretation of the behavior. This reflects the fact that the spin of the electrons can change due to the magnetic field. This means that the magnetic field could now also drive a backscattering current which was prohibited by time reversal symmetry without magnetic field.

2.4 Transport Properties Using the GME

In section 2.2 we focused on the derivation of a generalized master equation in order to describe the behavior of the system and obtained a method for determining the steady state density matrix. In section 2.3 we then looked at the polarization as this is one method of parameterizing the

density matrix. We could identify several regimes in which we found interesting behavior. Until now we have, however, not discussed the effect on the lead. Due to the dynamics of the system the number of left and right movers now can be changed. This leads to signatures of the system behavior in the transport through the edge state.

In the edge state time reversal symmetry prohibits elastic backscattering from impurities that do not violate time reversal symmetry. In a simple picture this can be understood as a consequence of the fact that the electron cannot change its spin. In section 2.3 we argued that an electron can change its spin by jumping on the dot such that the QD makes it possible to make right left movers and vice versa, leading to backscattering.

Here we will derive an expression for the current that allows the calculation of the current for the GME as well as for the GME in secular approximation. In chapter 3 we will use a different method to calculate the current that also allows the calculation of higher cumulants.

2.4.1 Current Operator

The edge states form at a domain boundary between domains of different topology. Here we consider a topological insulator in which time reversal symmetry is not violated. This means that also the edge state is time reversal symmetric. Kramer's theorem ensures that in a spin $1/2$ system each eigenvalue is at least twofold degenerate and each eigenstate has a time reversal partner [Haa10]. These pairs of eigenstates are Kramer pairs. The edge states are such Kramer pairs propagating in different directions. Without breaking time reversal symmetry elastic backscattering is thus forbidden [Xu06, Wu06]. Using the Landauer-Büttiger formalism the conductance for each edge is

$$G_0 = \frac{e^2}{h}, \tag{2.89}$$

because each edge has one mode, which is not spin degenerate and the transmission can be assumed to be perfect as backscattering is forbidden.

Coupling the QD in the cotunneling regime to this edge state now allows single electrons to jump onto the QD while simultaneously the electron sitting on the impurity is pushed back into the edge state. We can now treat the left and the right movers in the edge state as two different independent reservoirs. The spin of the electrons in these reservoirs is then antiparallel.

Considering the case where the spin is conserved the right mover (spin up) can only scatter if the QD is in its ground state (spin down). After this scattering event the QD stays in its excited state (spin up). During this scattering process a right mover is removed and a left mover is added. As the QD is now excited the only possible process is the reverse process. This means that when averaging over time the number of right movers does not change.

The situation changes if the processes are not spin conserving anymore. If a right mover (spin up) scatters here the impurity could also stay in its ground state. The process is thus not blocked anymore by spin conservation. This process then reduces the number of right movers also on average.

The current in the edge state, however, is not completely determined by this scattering events but by the bias voltage applied to it. The bias voltage applied to the edge state drives an occupation imbalance of right and left movers ultimately leading to the quantized conductance mentioned above. Adding backscattering events to this picture will now modify this ballistic current. C. S. Peça *et al.* showed this by gauging the bias voltage into the operators and found that the current operator obtains an offset that corresponds to this ballistic contribution and the operator describing the deviations from this ballistic value [Peç03]. I. Safi and H. J. Schulz showed that if a right mover is injected into a Luttinger liquid it will end up in the right reservoir [Saf96]. If a scattering event generates a left mover from a right mover this means an electron is injected into the left lead. As series of these events generate a current that is on top of the ballistic current and can be interpreted as a backscattering current.

Following this argument we identified the rate of injection of left movers as the backscattering current. In the context of a GME we will treat the left and the right movers as two separate reservoirs of electrons each having their own chemical potential differing by eV. In this respect the setup we consider is similar to a setup where a QD is coupled to Spin polarized antiparallel reservoirs. The important difference here is, however, that these two reservoirs are realized in the same edge states but can nevertheless be probed separately by reservoirs on the left and right. This also holds even if interactions are present in the helical edge state.

We consider the current to be positive for electrons going left to right. The right movers and left movers are treated as two separate reservoirs.

The current into these reservoirs are defined as

$$\hat{I}_\eta(t) \equiv \dot{\hat{N}}_\eta = \frac{ie}{\hbar}[H_I(t), \hat{N}_\eta(t)] = \frac{ie}{\hbar}\sigma_\eta \sum_{\alpha=\pm} \sigma_\alpha A_\alpha(t) B^\alpha(t), \quad (2.90)$$

where $\hat{N}_\eta$ is the number of electrons moving in branch η as defined in Eq. (2.4) and $\sigma_R = -\sigma_L = 1$. As the QD in Coulomb blockade cannot accumulate charge the current coming from the right movers is the same as the current going to the left movers.

We do not consider a sudden quench such that we are interested in the current in the steady state. The current is thus defined as the expectation value at long times when the system has relaxed into the steady state

$$I_\eta = \lim_{t\to\infty} \mathrm{Tr}(\hat{I}_\eta(t)\rho_{\mathrm{tot}}(t)). \quad (2.91)$$

We choose the backscattering current such that a positive backscattering current reduces the current compared to the ballistic value. Furthermore, we define the backscattering current by its long time limit where it is defined by the steady state such that it is given by the expectation value

$$I_{\mathrm{bs}} = I_L. \quad (2.92)$$

The backscattering current is thus given by the rate at which left movers are added to the helical edge state. In the reminder of this chapter we will always discuss this backscattering current.

2.4.2 Current from GME

In section 2.4.1 we identified the current between the reservoir of the right and left movers as the backscattering current and also defined a current operator for this current. Here we will use the result from the GME to calculate the backscattering current Eq. (2.92). For this we evaluate Eq. (2.91) in the interaction picture

$$\begin{aligned} I_\eta(t) &= \mathrm{Tr}(I_\eta^I \rho_{\mathrm{tot}}^I(t)) \\ &= i\int_{t_0}^{t} \mathrm{d}\tau\, Tr\Big(I_\eta^I(t)\mathcal{L}_I^I(\tau)\rho_{\mathrm{tot}}^I(\tau)\Big) + \mathcal{O}(J^3). \end{aligned} \quad (2.93)$$

When calculating the current up to second order and rewriting it using the cyclic property of the trace we can cast this equation into a form that is very similar to our GME

$$I_\sigma(t) = \frac{i}{\hbar}\int_{t_0}^{t} \mathrm{d}\tau\, \mathrm{Tr}\left(\frac{1}{2}\Big\{\hat{I}_\eta^I(t), [H_I^I(\tau), \rho^I(\tau)]\Big\}\right). \quad (2.94)$$

In this form the equation is very similar to Eq. (2.35) up to the fact that the current operator is not associated with a commutator but with an anti commutator. We exploit this similarity and define $\mathcal{L}^I_{I_\eta}(t)\bullet = \frac{1}{2}\{I^I_\eta(t), \bullet\}$. Using this definition the current can now be written by the current kernel $\mathcal{K}^I_{I_\eta}(t,\tau)$ defined by

$$\mathcal{K}^I_{I_\eta}(t,\tau)\rho^I(\tau) = i\mathrm{Tr}_B(\mathcal{L}^I_{I_\eta}(t)\mathcal{L}^I_I(\tau)\rho^I(\tau)\otimes\rho_V) \tag{2.95}$$

such that the current then can be written as

$$I_\eta(t) = \int_{t_0}^{t} \mathrm{Tr}_S(\mathcal{K}^I_{I_\eta}(t,\tau)\rho^I(\tau)). \tag{2.96}$$

The expression in the trace can be brought back to the Schrödinger picture the same way as discussed for the kernel $\mathcal{K}^I$ in section 2.2.4. Following the same procedure we obtain

$$\begin{aligned}
\mathcal{K}_{I_\eta}(t-\tau)\rho(\tau) = \\
\frac{e}{\hbar^2}\frac{1}{2}\sum_{k,l=\pm,z}\Bigg[&\mathcal{G}^{I_\eta}_{k,l}(t-\tau)\Big(S'^k e^{-iH_S(t-\tau)}S'^l\rho(\tau)e^{iH_S(t-\tau)} \\
&+ e^{-iH_S(t-\tau)}S'^l\rho(\tau)e^{iH_S(t-\tau)}S'^k\Big) \\
&+ \mathcal{G}^{I_\eta}_{kl}(\tau-t)\Big(e^{-iH_S(t-\tau)}\rho(\tau)S'^k e^{iH_S(t-\tau)}S'^l \\
&+ S'^l e^{-iH_S(t-\tau)}\rho(\tau)S'^k e^{iH_S(t-\tau)}\Big)\Bigg],
\end{aligned} \tag{2.97}$$

where

$$\mathcal{G}^{I_\eta}_{kl}(\tau) \equiv \sum_{\alpha=\pm}\sigma_\alpha\sigma_\eta\ c_{\alpha,k}c_{\bar{\alpha},l}G_{\alpha\bar{\alpha}}(\tau). \tag{2.98}$$

This expression is very similar to Eq. (2.42). The current superoperator has some important differences to the tunnel operator Eq. (2.9). It is built using an anti commutator instead of a commutator such that the terms are added up and not subtracted. The sum in the definition of $\hat{I}_\eta$ excludes the $A_z B_{\tilde{z}}$ term and has an alternating sign. This is reflected in the definition of $\mathcal{G}^{I_\eta}_{kl}(\tau)$ where the sum is only over the $\pm$ components and the sign of the terms in the sum alternate in sign. This alternating sign corresponds to the direction of current that a certain process contributes. This will be discussed in more detail in section 3.3.

Because for the calculation of the current the trace of Eq. (2.97) is needed, the resulting expression can be simplified using the cyclic property

of the trace. Using this property the two time propagation operators can be arranged around the S'^k operators and the operators can be arranged to the right of the density matrix yielding

$$I_\eta(t) = \frac{e}{\hbar^2}\int_{t_0}^{t} \mathrm{d}\tau \sum_{k,l=\pm,z} \Big(\mathcal{G}_{kl}^{I_\eta}(t-\tau) e^{i\sigma_k \Delta_S (t-\tau)/\hbar} + \mathcal{G}_{kl}^{I_\eta}(\tau - t) e^{i\sigma_l \Delta_S (t-\tau)/\hbar} \Big) \mathrm{Tr}_S(\rho(\tau) S'^k S'^l). \quad (2.99)$$

In order to obtain the long time limit we can use the final value theorem. For this we need to perform the Laplace transform defined in Eq. (2.45) and determine the $z \to i0^+$ limit. As Eq. (2.99) is a convolution the result is

$$I_\eta(z) = \frac{e}{\hbar^2} \sum_{k,l=\pm,z} \Big(\mathcal{F}_{kl}^{I_\eta +}(z + \sigma_k \Delta_S) + \mathcal{F}_{kl}^{I_\eta -}(z + \sigma_l \Delta_S) \Big) \mathrm{Tr}_S(\rho(z) S'^k S'^l), \quad (2.100)$$

where

$$\mathcal{F}_{kl}^{I_\eta \sigma}(z) \equiv \int_0^\infty \mathrm{d}\tau\, e^{iz\tau/\hbar} \mathcal{G}_{kl}^{I_\eta}(\sigma\tau) = \sum_{\alpha=\pm} \sigma_\alpha \sigma_\eta c_{\alpha,k} c_{\bar{\alpha},l} F_{\alpha\bar{\alpha}}^{\sigma}(z), \quad (2.101)$$

and $F_{\alpha\bar{\alpha}}^{\sigma}(z)$ is the half sided Fourier transform of $G_{\alpha\bar{\alpha}}(\sigma\tau)$. Inserting this into the final value theorem we find

$$I_\eta = \frac{e}{\hbar^2} \sum_{k,l=\pm,z} \Big(\mathcal{F}_{kl}^{I_\eta +}(\sigma_k \Delta_S) + \mathcal{F}_{kl}^{I_\eta -}(\sigma_l \Delta_S) \Big) \mathrm{Tr}_S(\bar{\rho} S'^k S'^l), \quad (2.102)$$

where we used that the steady state density matrix is given by $\lim_{z\to i0^+} \rho(z)/\hbar$. Using Eq. (2.102) we can now calculate the current resulting for the steady state obtained from Eq. (2.50) or from Eq. (2.68).

For diagonal density matrices only terms with $\sigma_k = -\sigma_l$ contribute to Eq. (2.102) such that the result takes on the relative simple form

$$I_\eta = -\sigma_\eta e \Big[\cos^4\frac{\theta}{2} (F_{-+}(-\Delta_S)\bar{\rho}_{\downarrow\downarrow} - F_{+-}(\Delta_S)\bar{\rho}_{\uparrow\uparrow}) + \sin^4\frac{\theta}{2} \left(F_{-+}(\Delta_S)\bar{\rho}_{\uparrow\uparrow} - F_{+-}(-\Delta_S)\bar{\rho}_{\downarrow\downarrow}\right) + \frac{\sin^2\theta}{4}(F_{-+}(0) - F_{+-}(0)) \Big]. \quad (2.103)$$

For the steady state in secular approximation we can thus give an analytical result for the current because the steady state is represented by a diagonal density matrix and can be given analytically. The current for using the full steady state from the GME again gives us the possibility to benchmark our analytical result. Here we will, however, not focus on this comparison but rather on the properties of the transport.

The current formula can also be calculated using full counting statistics as is shown in chapter 3. This formalism then also allows us to calculate noise and interpret the properties by breaking down the current to simple events.

2.4.3 Results

Before we discuss the transport signatures of the behavior discussed in section 2.3 we first discuss as a benchmark the case of aligned spin quantization axis in the edge and the system. As discussed in section 2.2.7 this includes two cases; the case of aligned magnetic field $\theta_Z = 0$ and the case of large bias $|\Delta_V| \gg \Delta_Z$. After discussing the influence of the angle θ_Z in various regimes we will also discuss the influence of interaction in the helical edge.

The two aligned scenarios are somewhat different. We will first discuss the case of a magnetic field that is aligned with the spin quantization axis in the edge and then show that in the high bias voltage regime with a small tilted magnetic field transport also vanishes. If $\theta_Z = 0$ the rates $\Gamma_{\sigma\bar{\sigma}}$ simplify substantially as spin conservation violating processes are forbidden and we find

$$\Gamma_{\downarrow\uparrow} = F_{+-}(\Delta_S) \qquad \Gamma_{\uparrow\downarrow} = F_{-+}(-\Delta_S). \tag{2.104}$$

For $\theta_Z = 0$ also the angle $\theta = 0$ and the backscattering current reduces to

$$\begin{aligned} I_{\mathrm{bs}} &= eF_{-+}(-\Delta_S)\bar{\rho}_{\downarrow\downarrow} - eF_{+-}(\Delta_S)\bar{\rho}_{\uparrow\uparrow} \\ &= e\Big(F_{-+}(-\Delta_S) - F_{+-}(\Delta_S)\frac{\bar{\rho}_{\uparrow\uparrow}}{\bar{\rho}_{\downarrow\downarrow}}\Big)\ \bar{\rho}_{\downarrow\downarrow}. \end{aligned} \tag{2.105}$$

From Eq. (2.85) we find that

$$\bar{\rho}_{\uparrow\uparrow}/\bar{\rho}_{\downarrow\downarrow} = \Gamma_{\uparrow\downarrow}/\Gamma_{\downarrow\uparrow} = F_{-+}(-\Delta_S)/F_{+-}(\Delta_S) \tag{2.106}$$

and thus that the current vanishes. For $\theta_Z = 0$ a closer look at the kernel of the GME Eq. (D.5) shows that the resulting matrix coincides with

the matrix defining the rate equation Eq. (2.68) as all terms combining diagonal and off diagonal entries vanish. The same reasoning thus also applies for the GME result.

For $|\Delta_V| \gg \Delta_Z$ the reasoning is similar but we have to be more careful because for large bias voltage θ approaches 0 but on the other hand the rates are also very large as they can be proportional to $(eV\beta)^{2K-1}$. It is thus not clear whether the product vanishes or whether we obtain a finite value in the limit $|eV| \to \infty$. We start by looking at the polarizations at large bias. Because only one Fourier transform in Eq. (2.86) is not suppressed exponentially we find for $eV \gg \Delta_Z$

$$\rho_{\downarrow\downarrow} \approx \frac{\sin^4 \frac{\theta}{2}}{\cos^4 \frac{\theta}{2} + \sin^4 \frac{\theta}{2}} \qquad \rho_{\uparrow\uparrow} \approx \frac{\cos^4 \frac{\theta}{2}}{\cos^4 \frac{\theta}{2} + \sin^4 \frac{\theta}{2}}, \tag{2.107}$$

whereas for $-eV \gg \Delta_Z$ we find

$$\rho_{\downarrow\downarrow} \approx \frac{\cos^4 \frac{\theta}{2}}{\cos^4 \frac{\theta}{2} + \sin^4 \frac{\theta}{2}} \qquad \rho_{\uparrow\uparrow} \approx \frac{\sin^4 \frac{\theta}{2}}{\cos^4 \frac{\theta}{2} + \sin^4 \frac{\theta}{2}}. \tag{2.108}$$

It is important to notice that in the case of $|\Delta_V| \gg \Delta_Z$ and thus $\Delta_S \approx \Delta_V$ we find that $eV \gg \Delta_S$ such that $F(\sigma\Delta_S \pm eV) \approx F(\pm eV)$ and the last term in Eq. (2.86) can be neglected. In the regime discussed here the sign of the bias voltage decides whether the effective system aligns or anti aligns with the lead polarization axis. Its only effect is thus to exchange $\rho_{\uparrow\uparrow}$ and $\rho_{\downarrow\downarrow}$. Because a change of the sign in the bias voltage also changes whether $F_{+-}(\omega)$ or $F_{-+}(\omega)$ vanishes we find for the current in the case $\pm eV \gg \Delta_Z$

$$I_\eta = -\eta\, e\, \mathrm{sign}(eV) F(|eV|) \left(\frac{\cos^4 \frac{\theta}{2} \sin^2 \frac{\theta}{2}}{\cos^4 \frac{\theta}{2} + \sin^2 \frac{\theta}{2}} + \frac{\sin^2 \theta}{4} \right). \tag{2.109}$$

This result now separates the geometrical factors from the lead correlation function. The effects of the electron–electron interaction in the lead is also restricted to the lead correlation function in this result.

The case in which the system quantization axis aligns with the lead quantization axis goes further than this and even requires $\Delta_Z/\Delta_V \ll 1$. We thus can expand the trigonometric functions in Δ_Z/Δ_V. Inserting

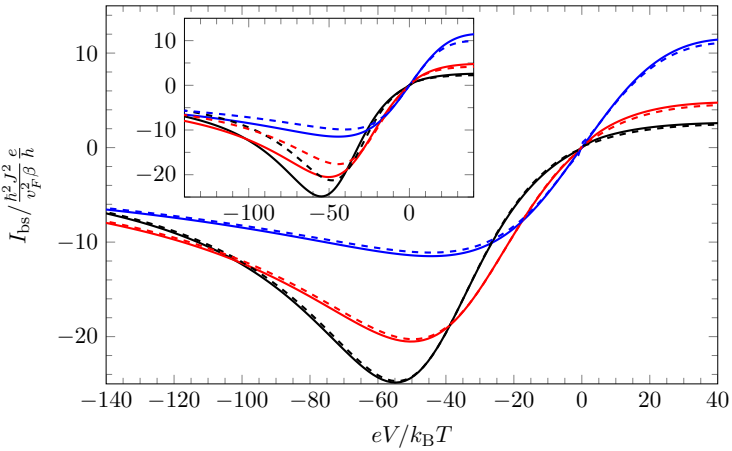

Figure 2.7: Backscattering current for $\hbar J/v_F = 0.1$, $\Delta_Z = 0.5 k_{\mathrm{B}}T$, $\theta_Z = \pi/6$ (black), $\theta_Z = \pi/3$ (red) and $\theta_Z = \pi/2$ (blue) using the secular approximation (solid) and approximation Eq. (2.111) (dashed). In the inset the backscattering current is shown for the same parameters using the secular approximation (solid) and the result using the GME (dashed). We see that despite the deviations the qualitative behavior coincides.

Eq. (2.71) we find

$$\sin^2\frac{\theta}{2} = \frac{1}{2}\left(1 - \frac{\Delta_Z\cos\theta_Z + \Delta_V}{\Delta_S}\right) \approx \frac{\sin^2\theta_Z}{4}\left(\frac{\Delta_Z}{\Delta_V}\right)^2 \tag{2.110a}$$

$$\cos^2\frac{\theta}{2} = \frac{1}{2}\left(1 + \frac{\Delta_Z\cos\theta_Z + \Delta_V}{\Delta_S}\right) \approx 1 - \frac{\sin^2\theta_Z}{4}\left(\frac{\Delta_Z}{\Delta_V}\right)^2 \tag{2.110b}$$

$$\sin\theta = \frac{\Delta_Z}{\Delta_S}\sin\theta_Z \approx \sin\theta_Z\frac{\Delta_Z}{\Delta_V} - \cos\theta_Z\sin\theta_Z\left(\frac{\Delta_Z}{\Delta_V}\right)^2, \tag{2.110c}$$

where higher orders in Δ_Z/Δ_V have been neglected. Inserting this into Eq. (2.109) we find that the trigonometric terms decay at least as $(eV\beta)^{-2}$ and thus the current decays at least with $1/eV\beta$. This shows that although the bias voltage and thus the rates are large the spin of the impurity still blocks the current because the system aligns fast enough.

Using Eq. (2.109) we could show that the current vanishes if the bias voltage is large enough such that the effective system aligns with the lead quantization axis. In the calculation we only used $|eV| \gg \Delta_Z$ and only

used in the end that also $|\Delta_V| \gg \Delta_Z$. The equation itself however only relies on the fact that the rates Eq. (2.86) are each dominated by one term. This means Eq. (2.109) is also valid when dropping the assumption that $|\Delta_V| \gg \Delta_Z$. Inserting Eq. (2.110) we find

$$I_\eta = -\eta\, e\, \mathrm{sign}(eV)\, F(|eV|) \times \frac{1}{4}\left(\frac{\Delta_Z^2 \sin^2\theta_Z}{\frac{\cos^2\theta_Z+1}{2}\Delta_Z^2 + \Delta_V^2 + 2\Delta_Z\Delta_V\cos\theta_Z}\right). \quad (2.111)$$

The current for small Δ_Z and large bias voltage is shown in Fig. 2.7 for several angles θ_Z. We see that on the one hand for $eV < 0$ a strong minimum in the backscattering current develops. The minimum is most pronounced for small tilt angles. For $eV > 0$ on the other hand we see a very washed out maximum that is small for a small tilt angle. Increasing the tilt angle the minimum becomes less pronounced and moves closer to $eV = 0$. For $eV > 0$ the transport becomes stronger up to the point where at $\theta_Z = \pi/2$ the curve is symmetric.

In section 2.3 we argued that the rotation of the effective system leads to the exchange of spin conserving and spin non conserving processes when the system tips over. In the reference frame of the lead the impurity seems to flip when going from large to very negative bias voltage. In the reference frame of the effective QD system, however, we found that the polarization relaxes to the ground state for $eV \approx \Delta_Z$ but then becomes excited again as soon as the effective system quantization axis is rotated and thus exchanges the meaning of relaxation processes and processes exciting the system. The processes that drive this repolarization then contribute a current. When the impurity is fully polarized the transport is blocked again.

For the interpretation of this transport feature we used the secular approximation. In section 2.2.9 we analyzed the validity of this approximation and found that in the regime discussed here there are qualitative deviations in the polarization. To see these deviations appear in the current we show the current using the GME and the secular approximation in the inset of Fig. 2.7. The results agree qualitatively. In the secular approximation the current is overestimated in general. The rotation out of the y-z plane seems to lead to a transport blockade of the dot.

Until now we discussed the cases in which the bias voltage compared to the Zeeman splitting is either so large that the system aligns with the lead quantization axis or that the system starts to rotate. We could show that

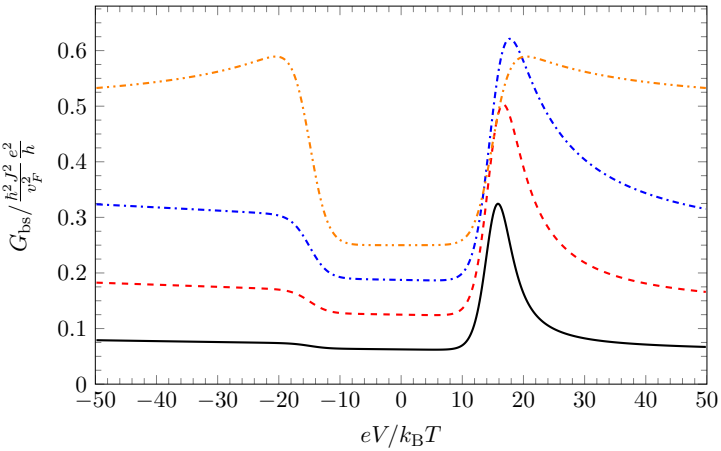

Figure 2.8: Differential conductance for $\hbar J/v_F = 0.1$, $\Delta_Z = 15 k_{\mathrm{B}}T$, $\theta_Z = \pi/6$ (black, solid), $\theta_Z = \pi/4$ (red, dashed), $\theta_Z = \pi/3$ (blue, dash dotted) and $\theta_Z = \pi/2$ (orange, dash double dotted). Elastic processes that transfer electrons without changing the state of the QD lead to transport for $|eV| < \Delta_Z$ whereas for $|eV| > \Delta_Z$ also spin flip processes contribute. Increasing the angle θ_Z also increases the current due to elastic processes. The spin flip processes show a different strength for positive and negative bias. The asymmetry is stronger for small θ_Z and vanishes for $\theta_Z = \pi/2$.

these phenomena can be understood by the change of the orientation of the effective system with respect to the edge state polarization and the resulting change in overlaps alone. The Fourier transforms characterizing the lead correlations are in the high frequency regime where the behavior is completely dominated by the bias voltage such that any change comes from the geometric factors. Furthermore we chose $\Delta_Z < k_\mathrm{B}T$. Because we need $\hbar J/v_F$ to be small this helps us to find the phenomena in a reasonable bias voltage range.

Now we will discuss the case in which $eV \approx \Delta_Z$ and $\Delta_Z > k_\mathrm{B}T$. In this regime the direction of the effective field hardly depends on the bias. Transitions between regions in which energy conservation prohibits or enables processes are now well separated and can be identified. To understand the behavior of the QD in this regime we distinguished between spin conserving and spin conservation violating processes. We argued that without violation of spin conservation the system can only be excited for $eV > \Delta_Z$ whereas it can only relax to the ground state for $|eV| < \Delta_Z$. The tilt of the quantization axis then enables spin conservation violating processes and thus also excitation for $-eV > \Delta_Z$. For $|eV| < \Delta_Z$, however, all excitation processes, no matter whether they conserve spin or not, are forbidden energetically. The quantum dot is locked in the ground state and one would expect no transport.

To discuss the transport in the system we have a look at the differential conductance G. In Fig. 2.8 we show the differential conductance for several tilt angles θ_Z. Looking at the region $|eV| < \Delta_Z$ we find a constant conductance although no excitation is possible. For $|eV| > \Delta_Z$ we find transport signatures that can be explained by onset of excitation processes.

Where the onset of transport at $|eV| > \Delta_Z$ is expected the transport for $|eV| < \Delta_Z$ is unexpected as the QD cannot change its state there. Responsible for this transport is the last term in Eq. (2.103) which is independent of the state of the QD. This current is contributed by processes that change the spin of an electron in the helical edge state without changing the spin of the electron on the QD. Such a process could be an electron tunneling onto the QD and back to the edge state. As the electron in the edge state has a finite overlap with both states of the QD it can change the spin in one of those tunneling events. This does not change the spin of the electron on the QD and the electron thus does not have to absorb or deposit any energy in the QD. It can happen as soon as a bias voltage is applied to the edge states and there are free states to

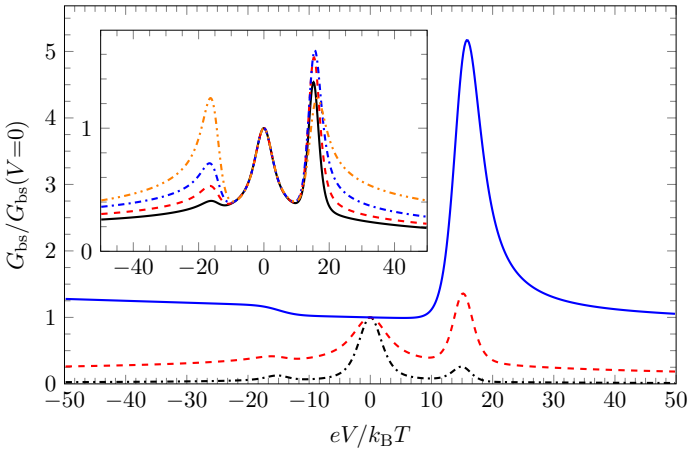

Figure 2.9: Renormalized differential conductance as a function of bias voltage V for different HLL interaction strengths: $K = 0.6$ (black dash dotted), $K = 0.8$ (red dashed) and $K = 1$ (blue solid), $\Delta_Z = 15\ k_{\rm B}T$, $\hbar J/v_F = 0.1$, $\alpha/\hbar\beta v_F = 10^{-3}$, and $\theta_Z = \pi/6$. The inset shows the renormalized differential conductance for the parameters and line styles as in Fig. 2.8 but now with $K = 0.8$. Figure and caption reproduced from the original publication [Pro15].

scatter into.

For $|eV| > \Delta_Z$ processes exciting the QD are now allowed energetically and processes flipping the spin on the QD and the edge states simultaneously contribute to the current. In section 2.3 we learned that the QD is in its ground state for $|eV| < \Delta_Z$ such that only processes exciting the QD are possible. Looking at Eq. (2.103) we find that this means that the onset at $eV \approx \Delta_Z$ is weighted by a cosine term whereas the onset at $-eV = \Delta_Z$ is weighted by a sine and thus suppressed for[3] $0 \leq \theta_Z < \pi/2$. This reflects the fact that exciting the system at positive bias voltage can be done conserving the spin whereas it can only be done by violating spin conservation for negative bias. Because the spin conservation is violated this means that the sign of the current is negative. When $\theta_Z = \pi/2$ the meaning of spin conservation vanishes as the overlap with electrons in the edge state with both states on the QD is the same. The onset of transport thus is symmetric.

The rates in our approach are given by the Fourier transform of the lead

[3]The missing range in the angle can be obtained by inverting the sign of the bias voltage as already mentioned in section 2.3

correlation functions. Using bosonization we can calculate these correlation functions and their Fourier transforms also including the interactions of the electrons in the edge state. The corresponding rates were also given in section 2.2.8. There we saw that $F_z(\omega)$ and $F(\omega)$ behave differently when interaction is introduced. Interaction only renormalizes $F_z(\omega)$ whereas it leads to an algebraic behavior with non universal exponent as well as a divergent dependence on the regularization parameter a in $F(\omega)$. This divergent behavior makes it difficult to compare different interactions with each other. We will thus renormalize the differential conductance to the differential conductance at $V = 0$.

The results are shown in Fig. 2.9 where the renormalized conductance is shown for several interaction parameters $K \leq 1$. The range of values shown there and the special value of $K = 0.8$ used later corresponds to values observed in cleaved edge nanowires in $GaAs$–$AlGaAs$ heterostructures [Aus00, Aus02]. Furthermore this value was also predicted for $HgTe$–$CdTe$ quantum wells [Teo09]. We can see that three distinct peaks develop; two peaks at the onset of transport at $|eV| \approx \Delta_Z$ and another peak at $eV = 0$. At these voltages the phase oscillation, that are driven by the Zeeman field and due to the spin flip, are compensated by the oscillations driven by the bias voltage. The electron–electron interaction will lead to divergences at these points that are cut by temperature. To understand this behavior better we have a closer look at Eq. (2.78) and find that the rate shows a $|\omega\beta|^{2K-1}$ behavior where the bias voltage is contained in ω. The derivative with respect to the frequency thus diverges at $\omega = 0$. This divergence is cut by the temperature. For $K = 1$ we obtain a linear frequency dependence of the rate resulting in a constant conductance. For $K < 1$ the weight of the rates shifts closer to the point where $\omega = 0$ due to the divergent behavior. This then leads to the peaks in the differential conductance.

The interaction will change the correlation functions but not the effective Hamiltonian. Especially the tilt angle θ between the edge state spins and the effective spin quantization direction is the same as in the $K = 1$ case. This means that besides the rates being concentrated around the points $eV = 0$ and $|eV| = \Delta_Z$ the geometry prefactors are not altered. This can be seen in the inset of Fig. 2.9 where the renormalized differential conductance is plotted for several angles. Comparing the height of the peaks at $eV \approx \pm\Delta_Z$ we find again the asymmetric behavior that is controlled by the tilt angle.

For now we could use the notion of spin conserving and spin con-

servation violating processes to understand the transport properties. In section 3.3 we will decompose the master equation into the single processes and analyze their effect on the lead. This will not only allow us to understand the current in more detail but also to interpret the noise behavior.

2.5 Conclusion

In this chapter we discussed the behavior of a quantum dot in the Coulomb blockade regime coupled to a helical edge state. To this setup we added a magnetic field that is not necessarily aligned to the spin quantization axis of the helical edge state. If the magnetic field is not aligned to the spin quantization axis in the helical edge state it can drive nontrivial behavior of the impurity spin.

To describe the behavior of the system we set up a generalized master equation. This master equation is investigated within two approaches. In a first approach, we expanded the time evolution of the reduced density matrix in the interaction picture, transformed it back to the Schrödinger picture and were able to obtain the long time limit from the resulting equation using the final value theorem. In a second approach, we applied the secular approximation in the interaction picture and obtained a rate equation for the entries of the density matrix. The advantage of the first approach is that we obtain the steady state without the need for the secular approximation. In contrast to this approach, we obtain a dynamical equation using the secular approximation which allows us to interpret the behavior by a rate equation.

In the derivation of the result in secular approximation we found that it is essential to choose the appropriate system Hamiltonian in order to remove leading order terms in the Kondo coupling in the interaction picture. The chosen system can be interpreted as an effective system that contains the external magnetic field as well as the induced field due to the coupling to the helical edge state. The induced field is a consequence of the spin bias in the helical edge state and thus linear in the bias voltage applied to the edge state.

For the validity of the secular approximation we need to assume that the system dynamics is fast compared to the relaxation time of the system. The relaxation in the system is fast for large rates and the system dynamics are fast for a large splitting of the effective states of the quantum dot. This is fulfilled for $|eV| \approx \Delta_Z$ and we find that the secular

approximation is good in this regime. For a larger bias voltage the induced field becomes comparable to the external magnetic field. In this case the rates are large and depending on the sign of the bias voltage the external magnetic field and the induced field can cancel each other partially reducing the effective splitting. We found that in this case the secular approximation is less justified but still reproduces the qualitative features. The result using the secular approximation can thus be used to interpret the behavior at least qualitatively in the whole parameter range.

In secular approximation we find that the off diagonal entries of the reduced density matrix decay and that the quantum dot spin thus aligns with the effective spin quantization direction. For the diagonal entries we obtain a rate equation. If the effective spin quantization axis of the quantum dot and the spin quantization axis in the helical edge are not aligned a simultaneous spin flip conserving the total spin will populate the off diagonal entries of the reduced density matrix. As these decay the spin gets effectively projected onto the diagonal entries. Because now both spin components of the quantum dot are affected it seems that spin conservation violating processes are possible. Distinguishing spin conserving processes and spin conservation violating processes allows for a better understanding. Spin conservation violating processes are enabled by the tilt of the effective quantum dot spin quantization axis and are thus weaker than spin conserving processes. Compared to the spin conserving processes a spin flip on the quantum dot violating the spin conservation has the opposite effect in the helical edge.

For different bias voltages the behavior of the system is defined by different mechanisms. If the bias voltage applied to the helical edge state is of the order of the Zeeman splitting this bias voltage determines whether spin flip processes are possible or suppressed on the quantum dot. If the bias voltage is so large that the induced field is of the order of the external magnetic field then the direction of the effective field depends on the voltage and the geometrical factors in the GME determine the behavior of the quantum dot. These two effects allow us to manipulate the spin polarization of the quantum dot in the strength as well as in the direction.

In the first case the bias voltage is considered to be of the order of the Zeeman splitting. In this regime the effective system is dominated by the Zeeman term and thus aligns with the external magnetic field and the splitting is given by the Zeeman splitting Δ_Z. In the edge states spin flips processes can be selectively suppressed by applying a bias voltage. By

blocking the spin flip processes in the edge state the corresponding spin flip on the quantum dot can thus be suppressed. This allows to directly tune the spin flip rates on the quantum dot using the bias voltage in the edge state. Because the spin polarization is determined by the relative strength of the two spin flip rates of the quantum dot spin the spin polarization of the quantum dot can be adjusted using the bias voltage in the edge state. As the effective spin quantization axis of the quantum dot is not aligned with the spin quantization axis in the helical edge spin conservation violating processes are possible and can be switched separately using the bias voltage. For $|eV| < \Delta_Z$ the quantum dot is in its ground state and for $|eV| \approx \Delta_Z$ starts to become excited. This increase of the spin is driven by different spin flip processes for $\pm eV$ so that it is asymmetric in the bias voltage. This asymmetry is a consequence of the helical structure of the edge together with the tilt of the magnetic field. The spin of the quantum dot itself will, however, still be aligned with the magnetic field.

In the case of $-\Delta_V \approx \Delta_Z$ the direction of the effective spin quantization direction can be tuned by the applied bias voltage. Because the coupling is considered to be weak this case is a high bias voltage case and $|eV| \gg \Delta_Z$. In the large bias voltage case one type of spin flip in the helical edge state is strongly suppressed. The geometry of the effective spin quantization axis of the quantum dot now determines which process on the quantum dot is associated to this process. As the spin quantization axis on the quantum dot now starts rotating the spin conserving and spin conservation violating processes exchange their meaning. The result is that the spin polarization of the quantum dot will follow the effective system quantization axis forming a loop and eventually aligning with the lead quantization axis for the case of a dominant induced field. This provides a handle to also adjust the direction of the spin polarization electronically. The amount of polarization is also determined by the geometric factors such that it cannot be tuned independently from the direction.

Because the spin flip processes on the quantum dot are also associated with spin flip processes in the helical edge state these manipulations also have signatures in the backscattering current. The two cases discussed above have different signatures which can be understood by the relative orientation of the effective spin quantization axis of the quantum dot and the spin quantization axis in the lead. In the low bias voltage case $|eV| \approx \Delta_Z$ the rates of spin conserving and spin conservation violating processes

change in relative strength. For large bias voltage where $-\Delta_V \approx \Delta_Z$ only one component contributes to the rate and the geometry of the effective system quantization axis decides whether this corresponds to a spin conserving or a spin conservation violating process.

One type of spin conservation violating process enabled by the tilted magnetic field are processes that change the spin of an electron in the edge state without changing the spin of the quantum dot. These processes are called elastic processes whereas processes changing the quantum dot are inelastic processes. In the low bias voltage case we found that for $|eV| < \Delta_Z$ the elastic tunneling processes drive a current and that for $|eV| > \Delta_Z$ spin flip processes drive an additional current. The elastic processes are possible irrespective of the state of the quantum dot. For the case of a noninteracting helical edge their contribution to the conductance is a constant offset.

The inelastic processes become possible for $|eV| \approx \Delta_Z$ as in this process energy needs to be absorbed from or deposited in the helical edge states. The sign of the bias voltage determines whether they are enabled by conserving spin or not. The spin conserving process is possible for $eV > \Delta_Z$ whereas the spin conservation violating process is only possible for $eV < -\Delta_Z$. The relative strength of these two processes can thus be obtained by comparing the strength of the onset of transport. The asymmetry of the two peaks associated with the onset of these two transport channels in the conductance thus enables us to learn something on the relative orientation of the external magnetic field and the spin quantization axis. When changing the external magnetic field one could try to find the configuration in which the transport signatures are symmetric. This would be a definite sign that the field is oriented perpendicular to the spin quantization axis in the helical edge state. A quantum dot thus could be used as a spin polarization probe using the external field to adjust the direction and the backscattering current as a readout.

This behavior is in principle unaltered when interaction in the edge state is included. By including the interaction in the edge state we found that three peaks develop in the conductance. Each peak corresponds to one type of process; one elastic process and two inelastic processes. The geometry of the effective system quantization axis is independent of the interaction such that the height of the peaks is again determined by the relative orientation of the lead spin quantization axis and the effective system quantization axis. The peak origins from the divergence of the lead correlation function cut by the temperature.

For high bias voltage the effective system quantization axis starts to align with the lead quantization axis. For a perfectly aligned effective field the interplay between spin polarization of the quantum dot and the lead correlation function will block transport. For large bias voltage the lead correlation functions can become large. We showed that if the effective system quantization axis aligns with the edge state quantization axis the spin polarization is stronger than the increase of the lead correlation function such that the blockage in the aligned case is restored even with small magnetic fields. For $\Delta_Z \approx -\Delta_V$ we found that the spin conserving processes and spin conservation violating processes are similar in strength such that the quantum dot depolarizes. The reason was the rotation of the effective spin quantization. Because now also inelastic processes are not blocked by spin polarization anymore we find a strong maximum in the current. The rotation of the effective spin quantization axis thus leads to strong backscattering.

In our proposal we assume that a freely tunable magnetic field is applied to the quantum dot. In realistic experimental setups it is very difficult to generate magnetic fields restricted to small regions of a sample. There are nevertheless some proposals how this can be achieved. By coupling the quantum dot to a magnetic insulator a field can be induced on the quantum dot [Ted86, Los98, Mia15]. Using a magnetic insulator generates an induced field similar to the helical edge state in our proposal. External fields cannot be limited locally in general on the scales needed to address a single quantum dot. It has, however, been demonstrated that, using the stray fields of nanomagnetic elements, magnetic fields can be controlled on a submicrometer length scale [McN10].

Limiting the magnetic field to the quantum dot might be challenging and the amount of tunability might be limited. The alternative would be to expose the complete quantum spin Hall sample to an external magnetic field. This will break time reversal symmetry such that the transport might not be ballistic anymore and become diffusive. Ballistic transport can then only be expected on length scales of the mean free path. For $HgTe$–$CdTe$ quantum wells mobilities of $1.5 - 4.9 \times 10^5\,\mathrm{cm^2 V^{-1} s^{-1}}$ have been observed [Rot09, Ger10]. Assuming an effective mass of $m^* = 0.007 m_e$ [Rot10] this corresponds to mean free paths of $0.3 - 1.1\,\mu\mathrm{m}$. If the edge state of the device is shorter than this mean free path we still can expect to obtain ballistic transport.

By exposing the edge states to a magnetic field they are subjected to the Zeeman effect as well as to orbital effects. The orbital effect was

studied by G. Tkachov and E. M. Hankiewicz [Tka10]. They found that close to the Dirac points still two bands exist but that one of these bands flattens out for higher energies leading to a chiral edge state and thus a quantum Hall regime. Around the Dirac points the two bands, however, are approximately helical such that we still expect the quantum spin Hall effect for energies close to the Dirac point. Several other studies also found that the helical edge states persist up to several Tesla [Tka10, Tka11, Sch12a, Pik14, Pik14].

The orbital effect itself can be estimated by comparing the bulk penetration length $l_\lambda = \hbar v_F/D \approx 37\,\mathrm{nm}$ to the magnetic length $l_B = |e\vec{B}/\hbar|^{-1/2}$. By $l_\lambda = l_B$ we can now define a critical magnetic field. For the penetration depth mentioned above we find a critical magnetic field of $0.5\,\mathrm{T}$ which corresponds to a Zeeman splitting of $\Delta_Z/k_\mathrm{B} \approx 18.5\,\mathrm{K}$ assuming $g^* \approx 55$. The Zeeman effect opens a gap of ϵ_gap at the Dirac point. The effect of this gap, however, becomes smaller further away from the Dirac point. Above the gap the two edge states are not perfectly antiparallel anymore. The overlap of the states is of the order of $\mathcal{O}(\epsilon_\mathrm{gap}/\hbar v_F k_F)$ where k_F is the Fermi momentum. Due to this overlap a scalar impurity of strength V_0 would lead to a backscattering rate in the order of $\mathcal{O}\big((V_0\epsilon_\mathrm{gap}/\hbar^2 v_F^2 k_F)^2\big)$. In this chapter the Zeeman splitting was assumed to be comparable to or smaller than the bias voltage which itself has to be smaller than the band width D. Therefore, we assume that it should be possible to avoid the vicinity of the Dirac point in the choice of the chemical potential thus reducing the effect from backscattering due to scalar impurities.

For $HgTe$–$CdTe$ quantum wells the bulk band gap in the topological phase is $D \approx 10\,\mathrm{meV}$. Using this bulk band gap we find for the short distance cutoff $\alpha \approx \hbar v_F/D$ used in this chapter a temperature of $T \approx 116\,\mathrm{mK}$. The Kondo temperature $T_K \approx (D/k_B)\exp(-\pi v_F/\hbar J)$ for the parameters we used is much lower such that our perturbative treatment is justified. At these temperatures the currents we found are in the order of several pico ampere. These currents as well as the temperatures are experimentally accessible. Novel materials with higher band gaps [Zho14, Zha14, Xu13, Xia11] would allow for higher temperatures and thus larger transport signatures.

Chapter 3

Full Counting Statistics for the QD-HLL System

Full counting statistics is a very convenient method to obtain the transport properties of a system. The starting point is the probability $P(N,T)$ that N electrons are transferred in a time interval T. This probability is of special interest as its cumulants are connected to the current and the current noise. Namely the expectation value of N is connected to the average current and the variance is connected to the current noise. In order to calculate these cumulants it is most convenient to use the cumulant generating function (CGF). This CGF is basically defined as the logarithm of the Fourier transform of the probability $P(N,T)$. The CGF has the interesting property that the nth cumulant is given by the nth derivative by the frequency which is called counting field χ here. The motivation for this name stems from the fact that only terms that transfer an electron depend on this counting field meaning only they couple to this field. If we have the CGF calculating the cumulants thus is only a matter of calculating derivatives.

The CGF can be calculated by several methods by including counting fields. It can be calculated using scattering matrices [Kli03], non equilibrium Greens functions [Bel03, Bel05] and master equations [Bag03]. The main interest in this chapter is on a closer analysis of the behavior found in chapter 2 and include higher cumulants into the analysis. We will thus focus on how to obtain the CGF from a generalized master equation.

In order to distinguish if the single electrons have been transferred independently or whether they are correlated a very common observable is the Fano factor. The Fano factor is the ratio of the first and the second cumulant. It already allows some insight into the statistics of the transport. For uncorrelated rare events one can expect a Poissonian distribution which is characterized by a Fano factor of one. If the Fano factor is larger than one, one speaks of super-Poissonian noise, whereas one speaks of sub-Poissonian noise if the Fano factor is smaller than one.

One property of large interest is whether the electrons have a tendency to follow right next after each other or whether they have the tendency to avoid each other in subsequent tunneling events. This is called bunching and antibunching. In general bunching is considered to lead to super-Poissonian noise whereas antibunching is considered to lead to sub-Poissonian noise. This association, however, is not always appropriate. If the dynamics is more involved this association does not apply [Ema12]. To understand if two events bunch or not we have to discuss the joined probability of two electrons being transferred within a certain time. This joined probability can be characterized by the $g^{(2)}$-function. This function allows to distinguish bunching from antibunching even if it does not show in the Fano factor.

To analyze the behavior observed in chapter 2 and the underlying mechanisms in more detail we investigate the bunching behavior of the electrons scattered. For this we first follow the argument of Bagrets and Nazarov [Bag03] to derive an expression for the CGF using the master equation in section 3.1. If the measurement time T is chosen long enough the CGF takes a very simple form which is given in section 3.1.1. In section 3.2 this result is then used to obtain the transport properties by doing a perturbative expansion in the counting field. To calculate the $g^{(2)}$-function we have to understand the effect of a single electron scattering event. In section 3.3 we expand the propagation for the reduced density matrix for short times and then define superoperators corresponding to the scattering of an electron in the edge state. This enables us to calculate the $g^{(2)}$-function in section 3.3.1.

In section 3.4 these methods are then applied to the system from chapter 2. For this system we first calculate the noise and the Fano factor in section 3.4.1. There we find an asymmetric Fano factor with respect to the bias voltage in the helical edge state exhibiting a transition from a super-Poissonian to a sub-Poissonian value. In order to understand this we decompose the Fano factor into a contribution from uncorrelated events and correlated events in section 3.4.2. This shows that the sub-Poissonian noise comes from correlated events which are then analyzed in section 3.4.3 using single scattering events. We then also discuss the influence of interaction in section 3.4.4 and find that we still find antibunching which is, however, not always visible in the Fano factor.

3.1 FCS and Master Equations

The central probability distribution $P(N,T)$ was introduced rather generally. We did not yet specify what we mean by N. In general, N would be the number of electrons added to a specific part of the system, for example a reservoir or a lead. This means that we can define a counting field for each reservoir. Bagrets and Nazarov discussed this in more detail [Bag03]. They derive a master equation with counting fields for QDs in the Coulomb blockade regime including several leads. The derivation given here is strongly motivated by their approach. We use, however, a generalized von Neumann equation as a starting point. Furthermore, we have the special case that we only have two reservoirs; the right movers and the left movers. In the regime considered here the QD cannot accumulate charge or change its charging state, such that it is sufficient to discuss only one of the two reservoirs. We will choose this reservoir to be the one of the left movers in section 3.2. Here we will derive the basic equations for one counting field χ counting a general number of electrons N. If one would be interested in several leads one could easily exchange this field by a vector of several fields and the electron number by a vector of numbers.

To see how to introduce the counting fields into a master equation we derive the CGF in an open system context. We start with the definition of the CGF

$$e^{-S(\chi,T)} = \sum_N e^{i\chi N} P(N,T) \tag{3.1}$$

as the Fourier transform of the probability $P(N,T)$. Writing the final and the initial state in a Fock basis one can rewrite the expression as [Kli03]

$$e^{-S(\chi,T)} = \mathrm{Tr}\Big(\rho_0 e^{-i\chi\hat{N}}\mathcal{U}(0,T)e^{i\chi\hat{N}}\mathcal{U}(T,0)\Big), \tag{3.2}$$

where $\mathcal{U}(t,t')$ is the time propagator, $\hat{N}$ is the number operator for the electrons counted and the initial state ρ_0 is the initial state that is assumed to be diagonal in the electron number basis. As the initial state is diagonal in the number of electrons the expression can be rewritten such that

$$e^{-S(\chi,t)} = \mathrm{Tr}\Big(\rho_{\mathrm{tot}}(\chi;t)\Big) \tag{3.3a}$$

$$\rho_{\mathrm{tot}}(\chi;t) = \mathcal{U}\big(\chi/2;t,0\big)\rho_0\mathcal{U}\big(-\chi/2;0,t\big) \tag{3.3b}$$

$$\mathcal{U}(\chi;t,t') = e^{i\chi\hat{N}}\mathcal{U}(t,t')e^{-i\chi\hat{N}}. \tag{3.3c}$$

The CGF is thus given by the trace of a density matrix which now depends on the counting field χ via the time propagator. Since the counting field and the number operator do not contain an explicit time dependence we can gauge it into the Hamiltonian such that

$$\mathcal{U}(\chi;t,t') = e^{i\chi\hat{N}}\left(\mathcal{T}e^{i\int_t^{t'} H\mathrm{d}\tau}\right)e^{-i\chi\hat{N}} = \mathcal{T}e^{i\int_t^{t'} H(\chi)\mathrm{d}\tau}, \tag{3.4}$$

where $\mathcal{T}$ denotes time ordering and

$$H(\chi) \equiv e^{i\chi\hat{N}}He^{-i\chi\hat{N}}. \tag{3.5}$$

In this formulation it is clear that the time derivative of $\mathcal{U}$ is again given by the Hamiltonian now including the counting field. The resulting von Neumann equation for the density matrix $\rho(\chi,t)$ is thus simply

$$\dot{\rho}_{\mathrm{tot}}(\chi;t) = -i\mathcal{L}_H(\chi)\rho_{\mathrm{tot}}(\chi;t) \tag{3.6a}$$

$$\mathcal{L}_H(\chi)X = \frac{1}{\hbar}(H(\chi/2)X - XH(-\chi/2)), \tag{3.6b}$$

where a Liouvillian $\mathcal{L}_H(\chi)$ including the counting field has been defined.

By gauging the counting field into the Hamiltonian and defining a Liouvillian that includes the counting field we managed to reestablish a von Neumann equation including counting fields that looks the same as the von Neumann equation[1] in Eq. (2.30). Instead of using Eq. (2.30) as a starting point we will use Eq. (3.6) to derive a master equation. Before we continue we will, however, have a closer look at $H(\chi)$.

The counting field terms in Eq. (3.5) only affect terms of the Hamiltonian that do not commute with $\hat{N}$ and thus change the number of electrons. In our model neither the system nor the bath Hamiltonian change the number of electrons in the reservoir. Using the decomposition into a system and a bath part Eq. (2.19) we can thus see that the interaction Hamiltonian is the only term depending on the counting field

$$H(\chi) = H_B + H_S + H_I(\chi). \tag{3.7}$$

Going to the interaction picture thus will not introduce further dependencies on the counting field such that the von Neumann equation in the interaction picture looks the same as in Eq. (2.30) with the Liouvillian taking care of the counting field.

[1] Note that the von Neumann equation in Eq. (2.30) is already in the interaction picture.

We can now repeat the derivation of the generalized master equation using the Liouvillian defined in Eq. (3.6). For simplicity we also assume that we are in the interaction picture with respect to the effective system defined in the previous chapter such that the equivalent expression to Eq. (2.34) is now

$$\dot{\rho}^I(\chi;t) = -\int_{t_0}^{t} \mathrm{d}\tau \ \mathrm{Tr}_B\Big(\mathcal{L}_I^I(\chi;t)\mathcal{L}_I^I(\chi;\tau)(\rho^I(\chi;\tau)\otimes\rho_V)\Big). \tag{3.8}$$

Starting from this expression we will now derive the master equation in secular approximation.

3.1.1 Long Time Limit

In section 2.2 we were able to calculate the long time behavior of the reduced density matrix from the spectral properties of the superoperator that defined the GME. When considering $P(N,T)$ we explicitely have a time dependence in the definition and thus need the dynamical behavior of the density matrix. The dynamics of the density matrix can most conveniently be obtained from an equation of motion. In secular approximation the GME is time local and can be interpreted as an equation of motion and is no self-consistency equation anymore. We will thus restrict ourselves to the GME in secular approximation. For $\chi = 0$ the initial state can be decomposed into the steady state and deviations from this steady state which decay exponentially. For long times the density matrix thus relaxes to the steady state. This situation changes for $\chi \neq 0$ as there this steady state now also decays. If the measurement time T used in the definition of $P(N,T)$, however, is long enough the CGF simplifies significantly [Bag03].

In secular approximation and the Markov approximation the resulting equation is time local and the dynamics can be calculated. The GME can then be written using a Liouvillian $\mathcal{L}^I$ by

$$\dot{\rho}^I(\chi;t) = -\mathcal{L}^I(\chi)\rho^I(\chi;t). \tag{3.9}$$

A formal solution of this equation can be obtained by

$$\rho^I(\chi;t) = e^{-t\mathcal{L}^I(\chi)}\rho_0(\chi) = \Omega(t)\rho_0(\chi), \tag{3.10}$$

where $\Omega(t) \equiv \exp(-i\mathcal{L}^I(\chi)t)$ is the propagator for the density matrix and $\rho_0(\chi)$ is now the initial reduced density matrix. Here, the solution is given in the interaction picture. It can be transformed back to the Schrödinger

picture. This, however, makes only a difference on the off diagonal entries of the density matrix. We will later see that for the interpretation of the transport properties only diagonal entries play a role and the behavior can be interpreted using a rate equation approach.

For longer measurement times T the CGF can be calculated from the spectral properties of $\mathcal{L}^I(\chi)$. To see this we need to have a closer look at the spectrum of $\mathcal{L}^I(\chi)$. For $\chi = 0$ we will have one eigenvalue 0 that corresponds to the steady state. All other eigenvalues have a positive real part, meaning the corresponding eigenstates decay and thus lead to relaxation to the steady state. If the eigenvalues have a finite imaginary part this corresponds to a resulting coherent evolution such that we also have to find a complex conjugated partner. Those eigenvalues come from the coherent dynamics as for example seen in the Lamb shift term.

This situation changes for a finite counting field. If the counting field is finite all eigenstates lead to decaying solutions. The dependence on the counting field is continuous such that we can identify the eigenvalue with the smallest real part $\Lambda_0(\chi)$ as the eigenvalue that is connected to the steady state at $\chi = 0$ such that $\Lambda_0(0) = 0$, which is the steady state $\bar{\rho}$. When representing the initial state using the eigenstates of $\mathcal{L}^I$ the density matrix will be dominated by the contribution of this space for long times as this state decays slower than the others. Inserting this into the definition of the CGF we find [Bag03]

$$S(\chi; t) \approx -\ln \mathrm{Tr}\big(e^{-\Lambda_0(\chi)t}\rho_0(\chi)\big) \approx \Lambda_0(\chi)t. \tag{3.11}$$

For long times the analytical structure of the CGF is thus given by the analytical structure of Λ_0. These analytical properties now determine the transport properties.

3.2 Transport Properties

In the previous section we discussed how to obtain the CGF from a master equation approach. The CGF is one possibility to characterize the probability $P(N, T)$. This probability carries the information on how many electrons have been transferred and thus determines the transport properties. The important step is to connect the cumulants of this probability distribution to transport properties [Naz03]. This can be done by using that the current is the rate of total change of the number of left movers and thus the change of the number of left movers is the integrated current.

The average current $\bar{I}$ and the current noise S_I are defined as

$$\bar{I} \equiv \frac{1}{T}\int_0^T \mathrm{d}\tau\, I_L(\tau) \qquad S_I \equiv \int_{-\infty}^{\infty} \mathrm{d}\tau\, \langle \delta I_L(\tau)\delta I_L(0)\rangle, \tag{3.12}$$

where $\delta\hat{I}_\eta \equiv \hat{I}_\eta - \langle \hat{I}_\eta \rangle$. In appendix E we show that these are connected to the cumulants of $P(N,T)$ and thus to the CGF via

$$\bar{I} = i\frac{e}{T}\frac{\partial}{\partial\chi}S(\chi,T) \qquad S_I = \frac{e^2}{T}\frac{\partial^2}{\partial\chi^2}S(\chi,T), \tag{3.13}$$

where T is the duration of the measurement. This measurement time is assumed to be long compared to all correlation times in the system.

For long measurement times T, we can now use Eq. (3.11) to calculate $\bar{I}$ and S_I by expanding Λ_0 in χ up to second order. Instead of using the exact expression for Λ_0 we use perturbation theory up to second order in the counting field to calculate the average current and the noise. On the one hand we are not interested in higher cumulants and on the other hand a perturbative treatment opens up more possibilities for the interpretation of the physical processes that contribute.

In standard perturbation theory the perturbation is linear in the small parameter and the operator is Hermitian. The Liouvillian describing the GME is not Hermitian and depends nonlinearly on the counting field. The operator not being Hermitian means that the left and right eigenvectors are not just connected via adjungation. When setting up the perturbative treatment we thus have to be careful. We thus will generalize the perturbation theory for non-Hermitian matrices in which the superoperator is a matrix and the density matrix is a vector. But first we will discuss the nonlinear dependence of $\mathcal{L}$ on the counting field.

In standard perturbation theory usually only a term linear in the perturbation is considered. The Liouvillian $\mathcal{L}(\chi)$, however, via Eq. (3.7) contains an exponential function in H_I, such that we cannot restrict ourselves to linear order. If we want to calculate the quadratic contributions we also have to expand the Liouvillian up to second order by

$$\mathcal{L}(\chi) = \mathcal{L}(0) + \chi\mathcal{L}'(0) + \frac{\chi^2}{2}\mathcal{L}''(0) + \mathcal{O}(\chi^3), \tag{3.14}$$

where the primes denote derivatives with respect to the counting field χ. The first term is the unperturbed system which corresponds to the GME of the system. The other terms will be treated in perturbation theory.

The unperturbed state is the steady state where $\Lambda_0(0) = 0$. This steady state $\bar{\rho}$ is represented by a vector $|\phi_0\rangle$. The master equation and hence the Liouvillian conserve the trace of a density matrix. Thus the left eigenvector for $\Lambda_0(0)$ is given by the linear form that is representing the trace $\langle\tilde{\phi}_0|$. To avoid irritations left eigenvalues have a tilde.

These eigenstates can now be used to define the projector onto the steady state $\mathcal{P} = |\phi_0\rangle\langle\tilde{\phi}_0|$ and the projector onto the complement of the steady state $\mathcal{Q} = \mathbb{1} - |\phi_0\rangle\langle\tilde{\phi}_0|$. As an expansion for the eigenvalue Λ_0 we find

$$\Lambda_0(\chi) \approx \Lambda_0(0) + \chi\Lambda_0'(0) + \frac{\chi^2}{2}\Lambda_0''(0) + \mathcal{O}(\chi^3) \tag{3.15}$$

and can now determine the expansion coefficients in perturbation theory using the projectors we just defined

$$\Lambda_0'(0) = \langle\tilde{\phi}_0|\mathcal{L}'|\phi_0\rangle \tag{3.16a}$$

$$\Lambda_0''(0) = \langle\tilde{\phi}_0|\mathcal{L}''|\phi_0\rangle - \langle\tilde{\phi}_0|\mathcal{L}'\mathcal{Q}\frac{2}{\mathcal{L}(0) - \Lambda_0(0)}\mathcal{Q}\mathcal{L}'|\phi_0\rangle. \tag{3.16b}$$

In the second term of the second equation we used the inverse of a singular linear operator. For this to be well behaved the kernel of this operator is projected out such that this inverse is well defined and we obtain a pseudoinverse. The details of the calculation can be found in appendix F.

Because of Eq. (3.11) these coefficients are directly connected to $\bar{I}$ and S_I via

$$\bar{I} = e\langle\langle i\mathcal{L}'\rangle\rangle \tag{3.17a}$$

$$S = e^2\left(\langle\langle\mathcal{L}''\rangle\rangle - 2\langle\langle\mathcal{L}'\mathcal{Q}\frac{1}{\mathcal{L}(0) - \Lambda_0}\mathcal{Q}\mathcal{L}'\rangle\rangle\right), \tag{3.17b}$$

where $\langle\langle\bullet\rangle\rangle \equiv \mathrm{Tr}(\bullet\rho_0) = \langle\tilde{\phi}_0| \bullet |\phi_0\rangle$. In order to calculate the current we now just need the steady state and the Liouvillian including the phase factor from the counting field dependence. In section 3.4 we will use the explicit example of a Kondo coupling to show that the resulting current is the same as the current derived in section 2.4.2. Before we continue with calculating the current and the noise in our system we will first have a closer look at the interpretation of the phase factor including the counting field and its interpretation.

3.3 Electron Scattering Operators

In the last section we analysed the transport properties for long measurement times. For those long times the CGF was given by the spectral properties of the Liouvillian but not the dynamical structure of the GME. To characterize the dynamic behavior we want to calculate the probabilities for the transfer of an electron and the joint probability for two successive electron transfers. In quantum optics the probabilities that an atom absorbs a photon are used to characterize the field as well correlations in the field [Scu97]. By discussing those single events and their correlations the bunching properties are more clear than via the noise. Furthermore, this discussion opens up another possibility to interpret the noise behavior by means of the effect of a single jump.

Before we can analyze the effect of an electron jump event we will first establish an interpretation for the counting field dependence in the Liouvillian. Looking at the definition of the propagator $\mathcal{U}(\chi; t, t')$ in Eq. (3.3) we see that only the parts of the propagator which obtain a phase dependence are the terms changing the number of left movers. The time evolution of the density matrix $\rho(\chi; t)$ itself is then composed of a time forward and a time backward evolution, where in the time backward evolution the counting field needs to change sign. Because the counting field is spread on time forward and backward propagator the phase dependence is $\chi/2$ in Eqs. (3.3) and (3.6). If we interpret ρ_0 as an initial state and $\rho(\chi; t)$ as the final state a phase dependence indicates that the number of left movers has changed during the propagation of the density matrix. The von Neumann equation defined by Eq. (3.6) now gives us a definition for the propagator of the density matrix. When deriving the master equation from Eq. (3.6) we obtain a time local description of the reduced density matrix that still contains the phase dependence despite not containing the lead part anymore. The phase dependence, however, still indicates the change in number of left movers in the lead and allows us to identify the parts of the evolution of the reduced density matrix that changed the number of left movers in the edge state. We thus decompose the Liouvillian from Eq. (3.9) into three parts by

$$\mathcal{L}(\chi) = \mathcal{L}_0 + e^{i\chi}\mathcal{J}_+ + e^{-i\chi}\mathcal{J}_-, \tag{3.18}$$

such that the phase dependence is split into separate operators. Here, $\mathcal{L}_0$ is the part of the evolution which did not change the number of left movers in the lead whereas $\mathcal{J}_\pm$ represents processes that changed the number of left movers in the edge state.

In order to understand the different terms in the Liouvillian we first focus on the time evolution for short times and especially on the cases in which the number of left movers has changed in this short time. For short times δt we can expand the propagator from Eq. (3.9) by

$$e^{-\mathcal{L}(\chi)\delta t} \approx \mathbb{1} - \delta t\ \mathcal{L}(\chi) = (\mathbb{1} - \delta t\ \mathcal{L}_0) - e^{i\chi}\delta t\ \mathcal{J}_+ - e^{-i\chi}\delta t\ \mathcal{J}_-. \quad (3.19)$$

Following the interpretation from above we can now identify the effect of the processes that changed the number of left movers and those that did not on the reduced density matrix. If we now observe that the number of left movers changed during this short time by one this restricts the dynamics to those parts that have a phase dependence of $e^{i\chi}$. The state after such a scattering event is then given by applying $\mathcal{J}_\pm$ to the initial density matrix. The resulting density matrix then needs to be renormalized due to the partial collapse of the wavefunction due to the observation done in the lead. The probability for this process, however, is obtained by summing over the final states. The restriction of the final states to those that differ by one in the number of left movers from the initial state is done by restricting the dynamics to the part with the right phase factor.

Using this decomposition of the Liouvillian we can now obtain the density matrix after we observed an event in the edge state which allows us to calculate the probability of these events as well as the properties of the impurity after such an event. In the next section we will calculate the probability for scattering events as well as the joined probability for two scattering events. After this we will use these probabilities to calculate transport properties. Finally we will connect the probabilities to the perturbative expressions Eq. (3.17). This allows us to interpret the noise and current by the scattering events and their probabilities.

3.3.1 Correlation in Electron Transport

The most direct measure of the independence of events is to calculate the joint probability of those two events and compare it to the probability for the single events. This approach is also used to characterize the light field in quantum optics, where this approach is applied to atoms absorbing photons from the field [Scu97]. Here we will use the dynamics of the QD system to determine the joint probability for the transfer of electrons.

We start by giving the probability for a single electron transfer. In general one would calculate this probability by calculating the overlap between an initial state after some propagation with all final state that

differ from the initial state by one electron in the lead part. Here we can, just from the counting field dependence, see which part of the evolution will contribute. This means that we do not have to restrict the set of possible final states but can just choose the corresponding part from $\mathcal{L}(\chi)$ driving the dynamics that we are interested in. The probability to observe a backscattering event in a time interval δt is thus given by

$$w_1^{\pm} \equiv -\delta t \langle\langle \mathcal{J}_{\pm} \rangle\rangle, \tag{3.20}$$

where the system is assumed to be in the steady state initially[2].

To determine if two events are independent the joint probability needs to be calculated. This means we need to calculate the probability that after an electron transfer at time t another electron is transferred at time $t + \tau$. We need to adjust the propagation accordingly. The propagator fulfills the group property such that the propagation can be written by a sequence of a scattering event followed by a free evolution and another scattering event. The propagation during a scattering event is described using Eq. (3.19) whereas the free evolution is described by Eq. (3.10). Note that free evolution does not imply that the system is isolated but that electrons exchanged with the edge state are not observed. The correlation is between two observed scattering events. The joined probability is thus given by

$$w_2^{\eta\nu}(\tau) = \delta t^2 \frac{\langle\langle \mathcal{J}_\eta e^{-\tau\mathcal{L}(0)} \mathcal{J}_\nu \rangle\rangle}{w_1^\nu} \tag{3.21}$$

where we already used that the problem only depends on τ.

Starting from this joined probability we can define a second order correlation function that compares the joined probabilities to the probabilities of the single events

$$g_{\mu\nu}^{(2)}(\tau) = \frac{w_2^{\mu\nu}(\tau)}{w_1^\mu} = \frac{\langle\langle \mathcal{J}_\mu e^{-\tau\mathcal{L}(0)} \mathcal{J}_\nu \rangle\rangle}{\langle\langle \mathcal{J}_\mu \rangle\rangle \langle\langle \mathcal{J}_\nu \rangle\rangle}, \tag{3.22}$$

whose short time behavior determines the bunching behavior of the events. Bunching leads to $g_{\mu\nu}^{(2)}(0) > 1$ whereas antibunching means $g_{\mu\nu}^{(2)}(0) < 1$.

This is the most general definition of bunching and antibunching. The characterization using the Fano factor can be derived from this definition for many systems. We will now express the current and the current noise using those probabilities and the $g^{(2)}$-function which allows us to interpret the noise behavior by single and successive scattering events.

[2]Note that the negative sign comes from the definition of the exponent of the propagator Eq. (3.10).

3.3.2 Connection to Transport Noise

In our perturbative expansion Eq. (3.17b) we need the expansion of the Liouvillian $\mathcal{L}$ in the counting field χ. Using Eq. (3.18) we find

$$\mathcal{L}' = i(\mathcal{J}_+ - \mathcal{J}_-) \tag{3.23a}$$
$$\mathcal{L}'' = -(\mathcal{J}_+ + \mathcal{J}_-). \tag{3.23b}$$

Especially the first expression has a simple interpretation. When calculating the current we find that

$$\bar{I} = e\frac{w_1^+ - w_1^-}{\delta t} \tag{3.24}$$

such that the current is given by the difference of the probabilities that during a time δt an electron is scattered to a left mover and the one that it is scattered to a right mover. Motivated by this interpretation we define the current superoperator by

$$\mathcal{I} \equiv \mathcal{J}_- - \mathcal{J}_+. \tag{3.25}$$

The backscattered current is then defined as $\bar{I} = e\langle\langle\mathcal{I}\rangle\rangle$. We define the rate of a flip event by $I_\sigma \equiv -\langle\langle\mathcal{J}_\sigma\rangle\rangle$. Note that we use the notation of a current although it lacks the charge here[3]. The rate of flip events is always positive. They can, however, be used to obtain the electrical current.

In order to connect the noise calculated using FCS to the $g^{(2)}$-function we write the pseudoinverse in the perturbative expansion Eq. (3.16) to the propagator. The pseudoinverse of a linear operator is characterized by being 0 on the kernel of this linear operator and the inverse everywhere else. This idea of projecting out the kernel of a linear map can also be generalized to the propagator by defining the irreducible propagator $\mathcal{R}(t) \equiv \mathcal{Q}\Omega(t)\mathcal{Q}$ where the steady state part is projected out. Using this irreducible propagator the pseudoinverse can be written as

$$\mathcal{Q}\frac{1}{\mathcal{L}(0)}\mathcal{Q} = \int_0^\infty dt\ \mathcal{R}(t). \tag{3.26}$$

which allows to associate the irreducible propagator $\mathcal{R}(t)$ to the pseudoinverse of the Liouvillian $\mathcal{L}(0)$.

[3]Note that this notation must not be confused with the currents in section 2.4.1. The notation can be distinguished by the subscript as there we use R/L and here $\pm$.

We can now use Eqs. (3.23) and (3.25) to express the noise from Eq. (3.17b) using electron jump operators and the reduced propagator yielding

$$\frac{S}{e^2} = I_+ + I_- + 2\int_0^\infty \mathrm{d}\tau\, \langle\langle \mathcal{I}\mathcal{R}(\tau)\mathcal{I}\rangle\rangle. \tag{3.27}$$

The integrand can now be rewritten by inserting the definition of the current Eq. (3.25) and expressing the result using the definition of the $g^{(2)}$-function Eq. (3.22) yielding

$$\begin{aligned}\langle\langle \mathcal{I}\mathcal{R}(\tau)\mathcal{I}\rangle\rangle = I_+^2(g_{++}^{(2)}(\tau)-1) + I_+^2(g_{--}^{(2)}(\tau)-1)\\ - I_+I_-(g_{+-}^{(2)}(\tau) + g_{-+}^{(2)}(\tau) - 2).\end{aligned} \tag{3.28}$$

Because for long times the two scattering events are independent the $g^{(2)}$ functions approach one and we can define the integral

$$G_{\mu\nu}^{(2)} \equiv \int_0^\infty \mathrm{d}\tau\, \big(g_{\mu\nu}^{(2)}(\tau) - 1\big). \tag{3.29}$$

Using these factors the Fano factor defined as $F = S/|e\bar{I}|$ can conveniently be written as

$$\begin{aligned}F = \frac{I_+ + I_-}{|I_+ - I_-|} + \frac{2|\bar{I}|}{e}\Bigg(\frac{e^2I_+^2}{\bar{I}^2}G_{++}^{(2)} + \frac{e^2I_-^2}{\bar{I}^2}G_{--}^{(2)}\\ - \frac{e^2I_+I_-}{\bar{I}^2}(G_{+-}^{(2)} + G_{-+}^{(2)})\Bigg).\end{aligned} \tag{3.30}$$

This expression is a generalisation of the result from [Ema12] where a similar derivation was done in the large bias voltage limit. It is composed of two parts. The first term describes the Poissonian noise due to independent scattering events. The second term describes the contribution to the noise from correlated scattering events.

The second term is composed of two components. First, there is a weight factor which weights the contribution of a type of process to the transport and a factor that characterizes the independence of the events. The sign of the $G^{(2)}$-factor determines whether the Fano factor is reduced or enhanced. The Fano factor thus depends on the integral over time and not only on the short time behavior of the $g^{(2)}$-function. If the system dynamics are more involved the Fano factor cannot determine the bunching behavior anymore [Ema12]. If the dynamics of the system does not change the sign of $g^{(2)}(t) - 1$ the discussion of the short times behavior is sufficient to determine the sign of the Fano factor.

3.4 Application to the Spin Impurity Coupled to the HLL

In the previous sections we derived the master equation including the counting fields and derived expressions for the current and the current noise. The dynamics have been decomposed into the different scattering processes to allow for a better interpretation of the average current and the current noise. Here we will now give the explicit form for the impurity coupled to the helical edge state. We will calculate the current noise and analyze the behavior using single scattering events.

In order to obtain a master equation including the counting fields we need to calculate $H_I(\chi)$ first. Using the Baker-Campbell-Hausdorff theorem we find

$$H_I(\chi) = e^{i\chi\hat{N}} H_I e^{-i\chi\hat{N}} \tag{3.31a}$$
$$= J(e^{-i\chi} A_+ B_+ + e^{i\chi} A_- B_- + A_z B_z) \tag{3.31b}$$
$$= \sum_{\alpha=\pm,z} A_\alpha(\chi) B_\alpha, \tag{3.31c}$$

where $A_\alpha(\chi) \equiv e^{-i\sigma_\alpha\chi} A_\alpha$. From this point we can directly give the equivalent expression to Eq. (2.39). The only point we need to take special care of is the sign of the counting field. This sign depends on whether the Hamiltonian has been added on the left or on the right of the density matrix. Writing out the double commutators in Eq. (2.39) we find

$$K^I(\chi;t,\tau)\rho^I(\chi;\tau) = \frac{1}{\hbar^2} \sum_{\alpha=\pm,z} G_{\alpha\bar{\alpha}}(t-\tau) B^I_\alpha(t) B^I_{\bar{\alpha}}(\tau) \rho^I(\tau)$$
$$+ G_{\alpha\bar{\alpha}}(\tau-t) \rho^I(\tau) B^I_{\bar{\alpha}}(\tau) B^I_\alpha(t) + e^{i\sigma_\alpha\chi} \Big(G_{\alpha\bar{\alpha}}(\tau-t) B^I_{\bar{\alpha}}(t) \rho^I(\chi;\tau) B^I_\alpha(\tau)$$
$$+ G_{\alpha\bar{\alpha}}(t-\tau) B^I_{\bar{\alpha}}(\tau) \rho^I(\chi;\tau) B^I_\alpha(t) \Big). \tag{3.32}$$

The counting field factor thus only attaches to the correlation function $G_{\alpha\bar{\alpha}}(\tau)$ and only for terms in which the two system operators are on different sides of the density matrix. From this point we can repeat the derivation and obtain the master equation in secular approximation including counting fields. Defining

$$\mathcal{F}_{k,l}(\chi;\omega) \equiv \sum_{\alpha=\pm,z} c_{\alpha k} c_{\bar{\alpha} l} e^{i\sigma_\alpha\chi} F_{\alpha\bar{\alpha}(\omega)} \tag{3.33}$$

this master equation is given by

$$\dot{\rho}^I(\chi;t) = -\frac{i}{\hbar}[H_{\mathrm{LS}}, \rho^I(\chi;t)] + \frac{1}{\hbar^2}\sum_{k=\pm,z}\Big(\mathcal{F}_{\bar{k}k}(\chi;-\Delta_S\sigma_k)S^k\rho^I(\chi;t)S^{k\dagger} - \frac{1}{2}\mathcal{F}_{\bar{k}k}(0;-\Delta_S\sigma_k)\{S^kS^{k\dagger},\rho^I(\chi;t)\}\Big), \quad (3.34)$$

where the Lamb shift Hamiltonian is independent of the counting field.

Introducing a counting field will not add new terms but only add phase factors to the existing terms such that due to the secular approximation the diagonal and off diagonal entries decouple again. It is thus sufficient to give a rate equation for the diagonal entries which have the same form in the interaction picture and the Schrödinger picture. Representing the density matrix by

$$\rho = \begin{pmatrix}\rho_{\uparrow\uparrow}\\ \rho_{\downarrow\downarrow}\end{pmatrix} \quad (3.35)$$

the master equation is

$$\dot{\rho}(\chi;t) = -\mathcal{L}(\chi)\rho(\chi;t), \quad (3.36)$$

where

$$\mathcal{L}(\chi)\begin{pmatrix}\rho_{\uparrow\uparrow}\\ \rho_{\downarrow\downarrow}\end{pmatrix} = \begin{pmatrix}\Gamma_{\downarrow\uparrow}-\Gamma_{00}(\chi) & -\Gamma_{\uparrow\downarrow}(\chi)\\ -\Gamma_{\downarrow\uparrow}(\chi) & \Gamma_{\uparrow\downarrow}-\Gamma_{00}(\chi)\end{pmatrix}\begin{pmatrix}\rho_{\uparrow\uparrow}\\ \rho_{\downarrow\downarrow}\end{pmatrix} \quad (3.37)$$

and

$$\Gamma_{00}(\chi) = \frac{1}{4}\sum_{\alpha=\pm} c_{z,\alpha}c_{z,\bar{\alpha}}(e^{i\sigma_\alpha\chi}-1)F_{\alpha\bar{\alpha}}(0) \quad (3.38a)$$

$$\Gamma_{\uparrow\downarrow}(\chi) = \sum_{\alpha=\pm,z} c_{+\alpha}c_{-\bar{\alpha}}e^{i\sigma_\alpha\chi}F_{\alpha\bar{\alpha}}(-\Delta_S) \quad (3.38b)$$

$$\Gamma_{\downarrow\uparrow}(\chi) = \sum_{\alpha=\pm,z} c_{-\alpha}c_{+\bar{\alpha}}e^{i\sigma_\alpha\chi}F_{\alpha\bar{\alpha}}(\Delta_S) \quad (3.38c)$$

are the transition rates, where $\Gamma_{\sigma\bar{\sigma}} \equiv \Gamma_{\sigma\bar{\sigma}}(0)$.

To understand the meaning of the rates $\Gamma_{\sigma\bar{\sigma}}(\chi)$ and $\Gamma_{00}(\chi)$ we have to understand their influence on the dynamics of the impurity. The dynamics of the impurity are retained for $\chi = 0$. The entries of the matrix in Eq. (3.37) then tell to which type of process the rate is associated to. A

counting field dependence of a rate indicates that an electron has been transferred in the process. We can thus identify what the corresponding process does to the impurity and whether an electron has been transferred.

The off diagonal entries are spin flip processes described by the rate $\Gamma_{\sigma\bar{\sigma}}(\chi)$. They stem from the terms with $k = \pm$ in Eq. (3.34). Due to the structure of the dissipation part only the off diagonal entries have a counting field dependence. The same terms also appear on the diagonal of $\mathcal{L}$ but this time without a counting field dependence. These terms ensure that for $\chi = 0$ the trace of ρ is preserved. Because in these processes the impurity is changed these terms are called inelastic processes and the rates are the inelastic cotunneling rates.

On the diagonal there are further terms described by $\Gamma_{00}(\chi)$ that stem from the $k = z$ terms in Eq. (3.34). Looking at the $\chi = 0$ case we see that $\Gamma_{00}(0) = 0$ such that these terms vanish and do not contribute to the dynamics of the impurity. As they do not change the impurity those processes are called elastic processes. The rate, however, has a phase dependence indicating that an electron can be transferred. The rate $\Gamma_{00}(\chi)$ is the elastic cotunneling rate. For our special case we also see that the elastic rate is the same on both diagonal entries. The elastic processes are therefore independent of the state of the impurity.

This can be elaborated by setting up the decomposition defined in Eq. (3.18). For this we split up the rates by the phase dependencies by

$$\Gamma_{\sigma\bar{\sigma}} = \Gamma^0_{\sigma\bar{\sigma}} + e^{i\chi}\Gamma^+_{\sigma\bar{\sigma}} + e^{-i\chi}\Gamma^-_{\sigma\bar{\sigma}}, \tag{3.39}$$

where $\Gamma^0_{\sigma\bar{\sigma}}$ are transitions in the system without changing the number of left movers, $\Gamma^+_{\sigma\bar{\sigma}}$ corresponds to a process that increases the number of left movers, whereas $\Gamma^-_{\sigma\bar{\sigma}}$ decreases those. Using these rates the electron jump operators and $\mathcal{L}_0$ are given by

$$\mathcal{J}^{\pm} = \begin{pmatrix} -\Gamma^{\pm}_{00} & -\Gamma^{\pm}_{\uparrow\downarrow} \\ -\Gamma^{\pm}_{\downarrow\uparrow} & -\Gamma^{\pm}_{00} \end{pmatrix} \quad \mathcal{L}^0 = \begin{pmatrix} \Gamma_{\downarrow\uparrow} - \Gamma^0_{00} & -\Gamma^0_{\uparrow\downarrow} \\ -\Gamma^0_{\downarrow\uparrow} & \Gamma_{\downarrow\uparrow} - \Gamma^0_{00} \end{pmatrix}, \tag{3.40}$$

where the rates are given by

$$\Gamma^0_{00} = -\frac{1}{4}\sin^2\theta\,\Big(F_{+-}(0) + F_{-+}(0)\Big) \tag{3.41a}$$

$$\Gamma^+_{00} = \frac{1}{4}\sin^2\theta\; F_{+-}(0) \qquad \Gamma^-_{00} = \frac{1}{4}\sin^2\theta\; F_{-+}(0) \tag{3.41b}$$

$$\Gamma^0_{\uparrow\downarrow} = \frac{1}{4}\sin^2\theta\; F_{zz}(-\Delta_S) \qquad \Gamma^0_{\downarrow\uparrow} = \frac{1}{4}\sin^2\theta\; F_{zz}(\Delta_S) \tag{3.41c}$$

$$\Gamma^+_{\uparrow\downarrow} = \cos^4\frac{\theta}{2}\; F_{+-}(-\Delta_S) \qquad \Gamma^+_{\downarrow\uparrow} = \sin^4\frac{\theta}{2}\; F_{+-}(\Delta_S) \tag{3.41d}$$

$$\Gamma^-_{\uparrow\downarrow} = \sin^4\frac{\theta}{2}\; F_{-+}(-\Delta_S) \qquad \Gamma^-_{\downarrow\uparrow} = \cos^4\frac{\theta}{2}\; F_{-+}(\Delta_S). \tag{3.41e}$$

This decomposition allows us an interpretation of each term individually on the one hand by its effect on the Impurity as well as by its effect on the leads. In general, the subscripts indicate the effect on the dot, 0 meaning no change, whereas the superscript indicates the effect on the edge state where 0 also means no change and $\pm$ means increase/decrease of left movers.

Before we continue to an analysis of the noise we first check that the results presented here coincide with the results from section 2.4.2. The best way to see this is to use the Liouvillian in the form it is defined in Eq.(3.34). Using this form we find

$$\langle\langle \mathcal{L}' \rangle\rangle = \frac{1}{\hbar^2}\sum_{k=\pm,z} \partial_\chi \mathcal{F}_{k\bar{k}}(\chi;\Delta_S\sigma_k)\mathrm{Tr}_S(\bar{\rho}S^k S^{k^\dagger}), \tag{3.42}$$

where the derivative by the counting field needs to be evaluated at $\chi = 0$. This needs to be compared to the result from using the secular approximation in Eq. (2.102). The secular approximation implies $l = \bar{k}$ such that the half sided Fourier transforms become a Fourier transform which is given by

$$\mathcal{F}^{I_\eta}_{k\bar{k}}(\omega) \equiv \sum_{\alpha=\pm} \sigma_\alpha\sigma_\eta\; c_{\alpha k}c_{\bar{\alpha}\bar{k}}F_{\alpha\bar{\alpha}}(\omega). \tag{3.43}$$

Note that the sum is only over $\alpha = \pm$. Comparing this to Eq. (3.33) we see that the derivative by χ kills the $\alpha = z$ term in the sum and introduces the sign of α into the sum. The derivative of the correlation function $\mathcal{F}_{k\bar{k}}(\chi;\omega)$ thus directly produces the correlation functions[4]

[4]The additional factor of i we did not mention here is then cancelled by the i in the definition of the current superoperator.

$\mathcal{F}^{I_\eta}_{k\bar{k}}(\omega)$. The FCS and the GME in secular approximation thus produce the same current. The FCS result, however, allows a closer inspection of the contributing processes.

After we have now given the electron jump operators and the Liouvillian we just need the pseudoinverse to calculate the noise and the $g^{(2)}$-functions. Also here the steady state can be obtained by diagonalising the Liouvillian in Eq. (3.37) and yields

$$\rho_0 = \frac{1}{\Gamma}\begin{pmatrix}\Gamma_{\uparrow\downarrow}\\ \Gamma_{\downarrow\uparrow}\end{pmatrix}, \tag{3.44}$$

where $\Gamma \equiv \Gamma_{\uparrow\downarrow} + \Gamma_{\downarrow\uparrow}$. As we describe the system using only two states the irreducible propagator and the pseudoinverse take a very simple form. Both project out the steady state and have a simple behavior on the complement of the steady state. The irreducible propagator gives an exponential decay

$$\mathcal{R}(t) = \mathcal{Q}e^{-\Gamma t} \tag{3.45}$$

whereas the pseudoinverse gives a factor of $1/\Gamma$ such that it is

$$\mathcal{Q}\frac{1}{\mathcal{L}(0)}\mathcal{Q} = \frac{\mathcal{Q}}{\Gamma}. \tag{3.46}$$

The projector on the complement itself is

$$\mathcal{Q} = \begin{pmatrix}\Gamma_{\downarrow\uparrow}/\Gamma & -\Gamma_{\uparrow\downarrow}/\Gamma\\ -\Gamma_{\downarrow\uparrow}/\Gamma & \Gamma_{\uparrow\downarrow}/\Gamma\end{pmatrix}. \tag{3.47}$$

The propagator and the pseudoinverse now allow the calculation of the noise current as well as the $g^{(2)}$-function. The irreducible propagator has a rather simple form and shows an exponential decay and no further complex dynamics. As the time scale of the decay is given by Γ the $G^{(2)}_{\mu\nu}$-factors can be calculated and are

$$G^{(2)}_{\mu\nu} = \frac{1}{\Gamma}(g^{(2)}_{\mu\nu}(0) - 1) = \frac{1}{\Gamma}\frac{\langle\langle \mathcal{J}^\mu \mathcal{Q} \mathcal{J}^\nu\rangle\rangle}{\langle\langle \mathcal{J}^\mu\rangle\rangle\langle\langle \mathcal{J}^\nu\rangle\rangle}. \tag{3.48}$$

Using the definition of $\mathcal{Q}$ we arrive at the most handy form of these factors

$$G^{(2)}_{\mu\nu} = \frac{1}{\Gamma}\frac{\langle\langle \mathcal{J}^\mu \mathcal{J}^\nu\rangle\rangle - \langle\langle \mathcal{J}^\mu\rangle\rangle\langle\langle \mathcal{J}^\nu\rangle\rangle}{\langle\langle \mathcal{J}^\mu\rangle\rangle\langle\langle \mathcal{J}^\nu\rangle\rangle}. \tag{3.49}$$

This term compares the probability of two successive flips following instantaneously after each other to the probability for two individual flips. For the interpretation we need to look at the results.

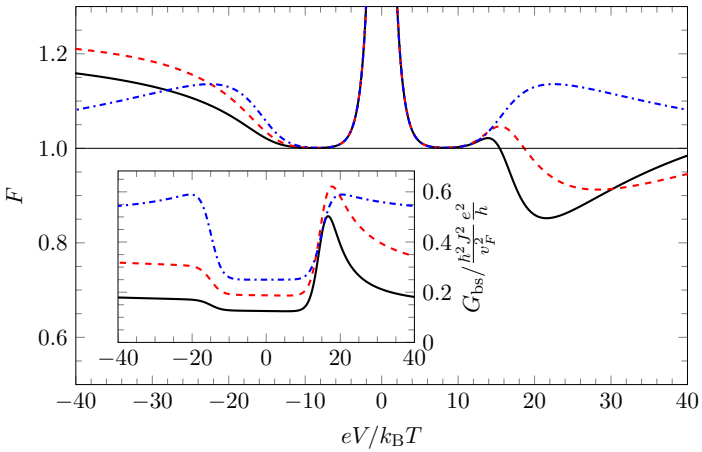

Figure 3.1: Fano factor for $\hbar J/v_F = 0.1$, $\Delta_Z = 15k_BT$, $\theta_Z = \pi/2$ (blue, dashdotted), $\theta_Z = \pi/3$ (red, dashed) and $\theta_Z = \pi/4$ (black, solid). The inset shows the corresponding backscattering conductance. This conductance shows an asymmetry as a function of bias voltage polarity in the onset of transport for $eV \approx \Delta_Z$ compared to $eV \approx -\Delta_Z$ which was discussed in section 2.4.3. For $\theta_Z = \pi/2$ the contribution to the Fano factor of cotunelling is super-Poissonian. If the magnetic field is neither aligned with nor perpendicular to the spin quantization axis in the edge state, however, cotunneling leads to a region of sub-Poissonian noise.

3.4.1 Noise Behavior of the System

The current noise allows insights into the behavior of the system the current itself does not give. An impurity or a tunnel barrier will lead to fluctuations in the occupation of the states in a conductor which leads to fluctuations in the current. One important question is whether the scattering or tunneling events are independent or whether they are correlated. If the events are not correlated and rare the distribution $P(N,T)$ is the Poisson distribution. For a Poissonian distribution all cumulants are the same. We define the Fano Factor as the ratio between second and first cumulant

$$F = \frac{S}{e|\bar{I}|}. \tag{3.50}$$

For a Poissonian distribution this ratio is one, indicating that the events are not correlated. One example are two terminal conductors without interaction in the weak transmission regimes. The Fano factor there is $F = 1 - T$ such that for low transmission and thus rare events the Fano factor is approximately one [Bla00]. For rare events the events are independent and thus we expect a Poissonian distribution.

3.4.2 Decomposition of Noise

To discuss the noise behavior we look at the Fano factor of the backscattering current in the impurity edge state system. In Fig. 3.1 the Fano factor is plotted for several tilt angles θ_Z. In the inset also the conductance already discussed in section 2.4.3 is shown for support of the discussion. For the symmetric case of $\theta_Z = \pi/2$ we see that the backscattering conductance as well as the Fano factor are symmetric as a function of the bias voltage eV and thus only depend on $|eV|$. When the angle is changed to a non perpendicular orientation we found in section 2.4.3 that the conductance becomes asymmetric and that there is a stronger onset of transport for $eV \approx \Delta_Z$ compared to $eV \approx -\Delta_Z$. The noise, however, despite being super-Poissonian in general develops a sub-Poissonian region. To identify the relevant processes we need to look closer at the different contributions to the noise.

To interpret the noise behavior we need to understand the contributions to the different terms in Eq. (3.30) as this also allows us to identify the processes that are responsible for the sub- and super-Poissonian contributions. In Fig. 3.2 the total Fano factor as well as the contribution due to the first term containing the Poissonian contributions and the other terms

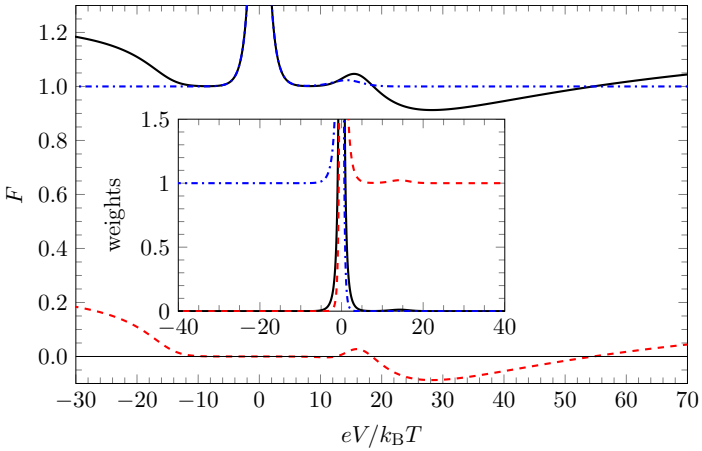

Figure 3.2: Full Fano factor (black, solid), first term (blue, dashdotted) and second term from Eq. (3.30) (red, dashed) for $\hbar J/v_F = 0.1$, $\Delta_Z = 15k_BT$ and $\theta_Z = \pi/3$. The inset shows $(eI_+/\bar{I})^2$ (red, dashed), $(eI_-/\bar{I})^2$ (blue, dashdotted) and $(e^2I_+I_-/\bar{I}^2)$ (black, solid) for the same values. The first term of Eq. (3.30) describes the Poissonian contribution of cotunelling and the thermal noise arround $eV = 0$ whereas the other terms show super- as well as sub-Poissonian noise. The $e^2I_+I_-/\bar{I}^2$ terms can only contribute around $eV = 0$ as only there both rates are not suppressed. For larger bias voltages only one of the two terms weighted by $eI_+/\bar{I}$ or $eI_-/\bar{I}$ dominates. The noise contribution S_I is thus given by electron jumps into the same direction whereas jumping back and forth only contributes for small bias voltage.

containing the correlations are shown. We see that the contribution of the first term describes the thermal noise as well as the Poissonian shot noise whereas the other terms describe the deviation from the Poissonian value. The contribution of the second term changes its sign and thus leads to sub-Poissonian noise. In order to understand this behavior better we need to analyze the correlation terms in Eq. (3.30) closer. These three terms are given by a weight factor of $e^2 I_\sigma I_\tau / \bar{I}^2$ and a correlation function of the flip operators $G^{(2)}_{\sigma\tau}$. Each of these weights thus describes the weight of a certain type of process to the transport[5]. The correlation function then tells us how these processes contribute to the noise. In the inset of Fig. 3.2 the weight factors are plotted. We see that $eI^+/|\bar{I}|$ and $eI^-/|\bar{I}|$ are close to one for positive or negative bias voltage respectively. They diverge at $eV = 0$ as there is still a probability for electrons to backscatter but no current is contributed. As these two weight factors have a step shape the product of the weight factors will only have contributions around $eV = 0$. The noise of electrons jumping back and forth thus only contributes here whereas for $eV > k_B T$ the electrons mostly scatter into the same direction such that the noise is dominated by the contribution of two successive jumps of electrons into the same direction. The noise behavior in this regime thus can be understood by studying the factors $G^{(2)}_{\pm\pm}$.

For a closer understanding of these successive jump events we insert the explicit definition of the electron jump operators Eq. (3.40) into Eq. (3.49) and obtain

$$G^{(2)}_{\sigma\sigma}\Gamma {I_\sigma}^2 = \Gamma^\sigma_{\downarrow\uparrow}\Gamma^\sigma_{\uparrow\downarrow} - (\Gamma^\sigma_{\uparrow\downarrow}\rho_{\downarrow\downarrow} + \Gamma^\sigma_{\downarrow\uparrow}\rho_{\uparrow\uparrow})^2. \tag{3.51}$$

The first term corresponds to processes in which a spin flips up and down and vice versa when two electrons jump, whereas the second term summarizes the probability for a spin flip event. Because a spin flip flop event is possible by the same rates irrespective of the initial state of the impurity this term does not depend on $\rho_{\uparrow\uparrow}$ or $\rho_{\downarrow\downarrow}$. We find that the bunching properties are solely determined by spin flip processes and that elastic tunneling events do not play a role. Because they are independent of the state of the impurity they contribute the same way to the correlated scattering events as they also contribute to the square of the probability

[5]Note that the weights here might be larger than one. This is due to the fact that the current is not a measure of total events but the difference of the two processes.

of a single scattering event and cancel in this expression. Elastic processes thus cannot correlate scattering events.

Before we go into the details of Eq. (3.51) we take a closer look at the implications of the spin rotation onto the rates. When introducing the rotated operators to the Hamiltonian we obtain terms that seemingly violate spin conservation. When setting up the GME we found that the off diagonal entries decouple from the diagonal entries and decay. This seemingly spin conservation violation thus leads to processes that do not conserve spin and processes that conserve spin. The reason is that an electron in the edge has a finite overlap with both spin directions in the impurity. When $0 < \theta_Z < \pi/2$ the overlap with the same spin is larger such that spin conserving processes are preferred over processes violating spin conservation.

By defining the electron jump operators we cannot only categorize a process by its effect on the QD but can also identify the process that is associated in the helical edge state. This allows us to split the spin flip rates of the QD into three contributions each associated with a specific scattering event in the helical edge state; two different types of backscattering events and one in which the number of left movers is not changed. Each of the backscattering events will change the spin of an electron in the edge state. A backscattering event scattering a left (right) mover will increase (decrease) the spin of the edge state electron. The rates can thus be spin conserving ($\Gamma^-_{\downarrow\uparrow}$, $\Gamma^+_{\uparrow\downarrow}$) or spin conservation violating ($\Gamma^+_{\downarrow\uparrow}$, $\Gamma^-_{\uparrow\downarrow}$, Γ^σ_{00}). The spin non conserving processes are enabled by a finite spin overlap with the edge electrons but suppressed compared to the spin conserving processes.

This preferred spin direction can directly be seen in the bias voltage dependencies of the flip rates shown in the insets of Fig. 3.3. The flip rates are zero up to a voltage determined by the level splitting on the QD and then the increase is linear[6]. In Fig. 3.3 (a) right movers with spin up are scattered to left movers with spin down. By flipping the impurity the right movers can only gain an energy of Δ_Z. As for $eV < -\Delta_Z$ all energetically available states of left movers are mostly filled, the flip rates are small. If $eV > -\Delta_Z$ the right movers can gain energy by flipping the impurity from $\uparrow$ to $\downarrow$ and scatter back. By scattering back their spin also flip from $\uparrow$ to $\downarrow$ such that this is a spin non conserving process. As the

[6] In a more general case including electron-electron interaction the increase is given by a power law with the exponent $2K-1$. The suppression, however, is in all cases exponential.

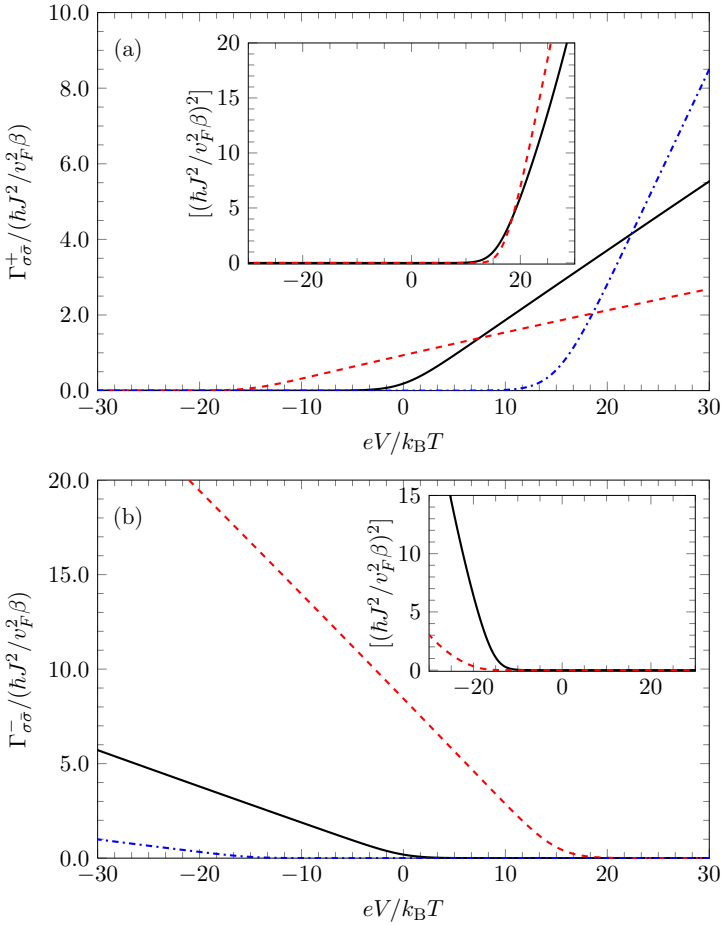

Figure 3.3: Rates Γ^{σ}_{00} (black, solid), $\Gamma^{\sigma}_{\uparrow\downarrow}$ (blue, dashdotted) and $\Gamma^{\sigma}_{\downarrow\uparrow}$ (red, dashed) for $\sigma = +$ (a) and $\sigma = -$ (b) for $\hbar J/v_F = 0.1$, $\Delta_Z = 15k_BT$ and $\theta_Z = \pi/3$. In the insets the corresponding contributions $\Gamma^{\sigma}_{\downarrow\uparrow}\Gamma^{\sigma}_{\uparrow\downarrow}$ (black, solid) and $(\Gamma^{\sigma}_{\downarrow\uparrow}\rho_{\uparrow\uparrow} + \Gamma^{\sigma}_{\uparrow\downarrow}\rho_{\downarrow\downarrow})^2$ (red, dashed) to the Eq. (3.51) for $G^{(2)}_{++}\Gamma I^2_{+}$ (a) and $G^{(2)}_{--}\Gamma I^2_{-}$ (b) are shown. We see that up to a threshold the rates are suppressed and then start to increase linearly. In (a) we see that the order of the dominant rate changes whereas it does not in (b). When weighting the rates with the probability of the initial states we can see in the insets that the dominant contribution to Eq. (3.51) does not change in (b) whereas it changes in (a) leading to a crossover between super and sub-Poissonian noise.

matrix element is suppressed the slope of the linear part is decreased. For $eV > \Delta_Z$ backscattering of a right mover is also possible by flipping the impurity from $\downarrow$ to $\uparrow$ which matches the flip of spins in the helical edge. This process conserves spin and the slope of the linear part is larger. In elastic processes the state of the QD and thus the energy of the scattered electron does not change such that the onset of transport is at $eV = 0$.

For scattering a left mover to a right mover the interpretation is equivalent although now the spin flips are suppressed for large bias. The onset of the flips is determined by the flip process on the dot. As the electron in the edge is now scattered in the opposite direction the spin flip is also inverted such that the rate starting a linear increase is also the rate corresponding to the inverted spin flip. Looking at Fig. 3.3 (b) the dominant rate sets in for $eV < \Delta_Z$ such that the relevant voltage is the same for both spin conserving spin flip rates. The order of the flip rates does thus not change and the rate $\Gamma^-_{\downarrow\uparrow}$ is always the largest rate.

To determine whether the noise is super- or sub-Poissonian we need to compare $\Gamma^\sigma_{\uparrow\downarrow}\Gamma^\sigma_{\downarrow\uparrow}$ to $(\Gamma^\sigma_{\downarrow\uparrow}\rho_{\uparrow\uparrow} + \Gamma^\sigma_{\uparrow\downarrow}\rho_{\downarrow\downarrow})^2$ which is done in the insets of Fig. 3.3 (a) and (b). There, the order of these contributions only changes for positive bias leading to sub-Poissonian noise.

To understand this behavior we need to look at the polarization of the impurity shown in Fig. 3.4. For $eV < \Delta_Z$ the impurity is relaxed to its ground state and thus in the spin down state. For $eV > \Delta_Z$ the rate $\Gamma_{\downarrow\uparrow}$ is blocked energetically such that the impurity cannot relax to its ground state anymore and stays in the excited state. For $eV < -\Delta_Z$ an additional excitation mechanism is possible due to spin non conserving processes which are, however, suppressed such that the excitation of the impurity is weak. When the polarization is negative the contribution of the spin flip process $\Gamma^\sigma_{\downarrow\uparrow}$ is suppressed by the spin polarization. For $eV < -\Delta_Z$ the dominant contribution in $(\Gamma^\sigma_{\downarrow\uparrow}\rho_{\uparrow\uparrow} + \Gamma^\sigma_{\uparrow\downarrow}\rho_{\downarrow\downarrow})^2$ thus comes from a spin conservation violating process exciting the QD which is weak. This term thus is small in Fig. 3.3 (b). For $eV > \Delta_Z$, however, the excitation rate becomes the dominant rate. This excitation process is now the spin conserving process and is not blocked by the spin polarization of the QD such that we find a regime in which $(\Gamma^\sigma_{\downarrow\uparrow}\rho_{\uparrow\uparrow} + \Gamma^\sigma_{\uparrow\downarrow}\rho_{\downarrow\downarrow})^2$ is dominated by this favored spin conserving process.

The factors $\Gamma^\sigma_{\uparrow\downarrow}\Gamma^\sigma_{\downarrow\uparrow}$ for $\sigma = \pm$ only differ in the sign of eV such that the contribution in Fig. 3.3 (a) and (b) are the same up to a change in the sign of the bias. This factor is always composed of a spin conserving and a spin non conserving process. In the $(\Gamma^\sigma_{\downarrow\uparrow}\rho_{\uparrow\uparrow} + \Gamma^\sigma_{\uparrow\downarrow}\rho_{\downarrow\downarrow})^2$ term only

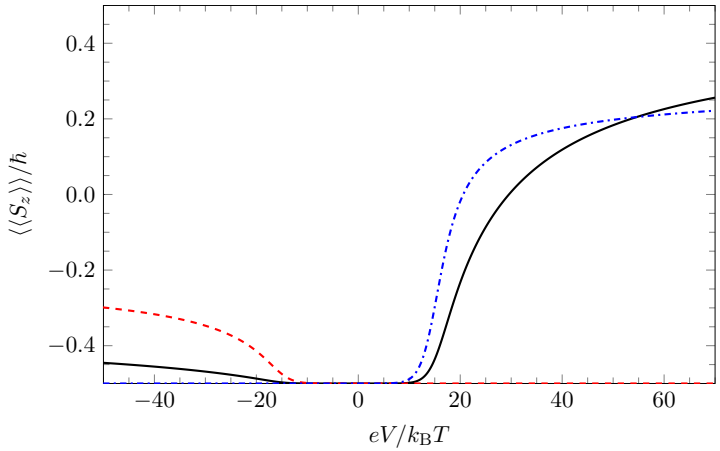

Figure 3.4: Polarization of the impurity (black, solid) and polarization after a scattering event increasing the number of left movers (blue, dash dotted) or decreasing the number of left movers (red, dashed) for $\hbar J/v_F = 0.1$, $\Delta_Z = 15 k_{\mathrm{B}}T$ and $\theta_Z = \pi/3$. We see that for negative bias voltage the polarization of the impurity after a scattering event is closer to the unpolarized state whereas for positive bias voltage the polarization of the impurity might even change sign after a scattering event. If the dot is strongly polarized, spin conserving processes are blocked and all processes violate spin conservation. For positive bias voltage the polarization does not block the spin conserving process such that the polarization can even change sign for $eV \approx \Delta_Z$. For larger bias voltage the polarization again blocks the spin conserving processes.

one of the two summands can be a spin conserving process whereas the other has to violate spin conservation. If the spin conserving process is not suppressed by the spin of the impurity it dominates this term. If it is suppressed, however, the rate for the suppressed spin conservation violating process is squared. Comparing this to a term that contains a spin conserving as well as a spin conservation violating process means that switching between this two cases in which spin conservation violating or spin conserving processes dominate directly means a change of sign of the right hand side of Eq. (3.51). This way we can understand the crossover between super- and sub-Poissonian noise from a formal point of view. Here the rate for flip flop processes are compared to the rate for transport processes squared. One can also understand the behavior by analyzing the events directly.

3.4.3 Effect of Scattering Events

To understand why the electrons bunch for $eV < -\Delta_Z$ and antibunch for some range for $eV > \Delta_Z$ we calculate the spin of the impurity after an electron jump event. To find the spin of the impurity after such a scattering event we need to restrict the time evolution to processes that change the number of left movers in the lead. Applying this restricted dynamics to the density matrix means that the trace is not conserved such that we have to renormalize the density matrix after the scattering event (see introduction of section 3.3). The spin of the system after an electron jump thus is given by $\langle\langle S^z \mathcal{J}^\sigma \rangle\rangle / \langle\langle \mathcal{J}^\sigma \rangle\rangle$ which is plotted in Fig. 3.4. We see that in general by an electron transfer event the spin of the impurity increases. This might be counterintuitive for $eV < 0$ as on the one hand a scattering event increases the spin of the electron in the edge state and on the other hand the spin of the impurity is also increased. The reason is that the spin polarization blocks the spin conserving processes and only processes that do not conserve the spin will occur. These processes then increase the spin. As the blockage due to the polarization is now weakened a successive jump conserving spin is now more probable leading to bunching.

For $eV > \Delta_Z$ the situation is different. There the polarization is also increased but now due to the spin conserving process. Increasing the polarization thus does not open a channel previously blocked. On the contrary, when the polarization becomes positive after a flip event a successive flip increasing the impurity spin is suppressed. The flip back

down, however is a spin non conserving process and thus suppressed. This means that two successive flips are less likely leading to antibunching. For larger bias voltage the impurity approaches a full polarization again suppressing the favored spin conserving process. Then the electron backscattering event will reduce the polarization and thus facilitating a successive scattering event again leading to bunching as can be seen by comparing Fig. 3.2 and Fig. 3.4.

The spin of the impurity after the scattering event shows some unexpected behavior in the regions where the scattering event is blocked. In Fig. 3.4 we see that the polarization after a electron scattering event is alway $-1/2$. To understand this behavior we have to have a closer look at the rates in Fig. 3.3 (a) and (b). In the region in which the rates are exponentially suppressed the largest rate is always $\Gamma^{\sigma}_{\downarrow\uparrow}$. Because the exponential suppression sets in later it is exponentially larger than the other rates. In a region where hardly any events happen this is thus the dominant rate such that the dot after such a rare event is always polarized in the down state.

The interplay of the spin polarization of the QD and the switch of the strength of different scattering rates determines the bunching behavior. To understand this better we assume that the polarization of the dot can be tuned freely. In general two successive scattering events are associated by two events on the QD. For simplicity we will focus on the spin flip flop processes. The polarization of the QD will now determine whether the first spin flip is an excitation or a relaxation process. For positive polarization the first spin flip will be a relaxation process and the second an excitation process and vice versa for negative polarization. To determine whether we expect bunching or antibunching we have to compare the rates for these events. Looking at Fig. 3.3 (b) we see that for scattering to a right mover the relaxation is always the dominating process. For scattering to a left mover, however, we see that the relaxation sets in already at $eV \approx -\Delta_Z$ but excitation only at $eV \approx \Delta_Z$ as can be seen in Fig. 3.3 (a). Because the excitation process is the spin conserving process the corresponding rate quickly becomes larger than the one corresponding to the relaxation process. So in general we can argue that for $eV < \Delta_Z$ relaxation dominates and negative polarization leads to bunching whereas for $eV > \Delta_Z$ excitation dominates such that negative polarization leads to antibunching.

The polarization of the QD is not only driven by scattering events but also by events that are not connected to scattering events. For this

reason the QD is also influenced by events not recognized in transport. The transport events thus do not completely determine the polarization of the QD. For negative bias voltage we see only negative polarization such that the mechanism described above will lead to bunching. For positive bias voltage the impurity is not instantaneously repolarized and still in its down state. At $eV \approx \Delta_Z$ the excitation rate becomes larger allowing for antibunching which is also observed due to the negative polarization of the QD. If the polarization becomes positive the picture changes and antibunching becomes possible.

In simple terms one could argue that the question is whether the first event releases a spin blockage or drives the system into a blocking state. The smaller the tilt of the magnetic field is, the stronger the effect of the spin blockage affects the behavior. This leads to the very strong sub-Poissonian region for small tilt in Fig. 3.1. If the magnetic field is oriented perpendicular to the spin quantization axis in the helical edge all rates are equivalent such that we cannot obtain a blocking state. The noise thus is purely super-Poissonian.

3.4.4 Effect of Interaction

In a next step we will also look at the effect of interactions. By introducing interactions into the bath we find that the correlation functions change. Instead of an exponential suppression for negative frequencies and linear behavior for positive frequencies we showed in section 2.2.8 that instead of the linear frequency dependence we find algebraic behavior with an exponent of $2K - 1$ for positive frequencies. The effect on the system is shown in Fig. 3.5. The most notably effect of the interaction is the bump in the Fano factor at $eV \approx \Delta_Z$. This bump is not coming from the correlated scattering events but is already apparent in the Poissonian part. It is, however, also not an effect of interactions but it is already present without interaction but more prominent with interactions. In Fig. 3.2 it is hardly visible. In Fig. 3.3 (a) we also miss this small bump because it is reduced further as we show the squares of $eI_\sigma/\bar{I}$.

To understand where this bump comes from we have a closer look at I_σ which can be written as

$$I_\sigma = \Gamma^\sigma_{00} + \Gamma^\sigma_{\downarrow\uparrow}\rho_{\uparrow\uparrow} + \Gamma^\sigma_{\uparrow\downarrow}\rho_{\downarrow\downarrow}. \tag{3.52}$$

Responsible for the bump is the term $\Gamma^-_{\downarrow\uparrow}\rho_{\uparrow\uparrow}$ which is plotted for the interacting case in Fig. 3.6 (b). Looking at Fig. 3.6 (a) we see that $\rho_{\uparrow\uparrow}$

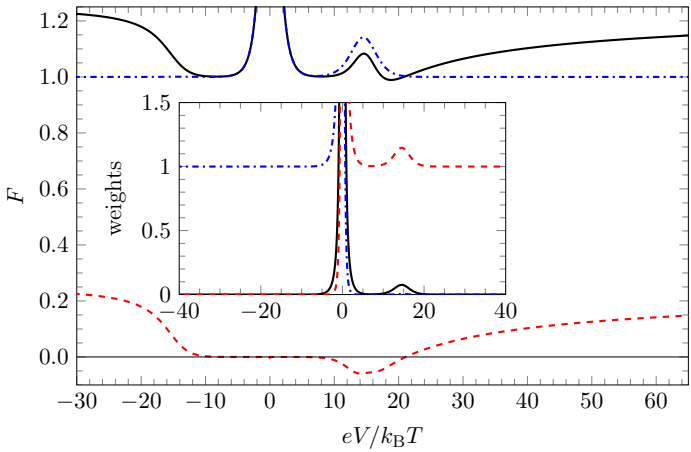

Figure 3.5: Fano factor (black, solid) as well as Poissonian contribution (blue, dash dotted) and the contributions of correlated events for $\hbar J/v_F = 0.1$, $\Delta_Z = 15k_BT$, $\theta_Z = \pi/3$, $\alpha/\hbar\beta v_F = 10^{-3}$ and $K = 0.8$. The Poissonian part and contributions by correlations are given by the first and the second term in Eq. (3.30). In the inset the corresponding weight factors I_+^2/I^2 (red, dashed), $e^2I_-^2/\bar{I}^2$ (blue, dash dotted) and $e^2I_-I_+/\bar{I}^2$ (black, solid) are shown. We see that $eI_+/\bar{I}$ as well as the Poissonian contribution develop a bump at $eV = \Delta_Z$. On closer inspection we see that this bump has its origin in a recurrence of eI_- which then decreases $\bar{I}$. Details of this recurrence are shown in Fig. 2.9.

is exponentially decaying towards $eV \approx 0$ and increases exponentially towards $|eV| \approx \Delta_Z$. As $\rho_{\uparrow\uparrow} = \Gamma_{\uparrow\downarrow}/\Gamma$ this exponential behavior comes from $\Gamma_{\uparrow\downarrow}$. From Fig. 3.3 (a) and (b) we can see that both rates $\Gamma^{\pm}_{\uparrow\downarrow}$ are algebraic for $\pm eV > \Delta_Z$ and decay exponentially for $\pm eV < \Delta_Z$. There is thus a window $|eV| < \Delta_Z$ where the larger exponential of $\Gamma^{+}_{\downarrow\uparrow}$ and $\Gamma^{-}_{\downarrow\uparrow}$ dominates over $\Gamma_{\downarrow\uparrow}$. In this window Γ is linear in the bias voltage. The polarization thus shows this exponential behavior. The exponential behavior is not altered by the interaction such that the behavior seen in Fig. 3.6 is in principle also present in Fig. 3.3. Coming back to $\Gamma^{-}_{\downarrow\uparrow}\rho_{\uparrow\uparrow}$ we see that in the regime where the rate is still algebraic the probability of a scattering event with a spin flip $\Gamma^{-}_{\downarrow\uparrow}\rho_{\uparrow\uparrow}$ is suppressed exponentially by $\rho_{\uparrow\uparrow}$. This probability is only suppressed exponentially for $eV > \Delta_Z$ but $\rho_{\uparrow\uparrow}$ already increases exponentially for $0 < eV < \Delta_Z$ such that it is not strong enough to suppress the rate at $eV \approx \Delta_Z$ and a bump can be seen. As introducing interactions leads to an exponent smaller than one the weight in the rate shifts towards $eV \approx \Delta_Z$ without changing the exponential behavior the height of the bump is increased. It is thus a phenomenon that occurs due to the transition from the exponential to the algebraic behavior. The width of the range in the bias voltage in which we can see this bump is thus of the order of $k_{\mathrm{B}}T$.

This deviation of the Fano factor from the Poissonian value thus is no sign of correlation of the events. For $eV \approx \Delta_Z$ the spin of the impurity starts to change its polarization. In this process not only processes that increase the number of left movers increase but also processes that increase the number of right movers become strong again around $eV \approx \Delta_Z$ despite the bias voltage being positive. This reverse current is not observed in chapter 2 as at the same time a stronger current increasing the number of left mover sets in. These events increase the number of events and thus the noise but reduce the current. The current is thus no good measure for the number of events. By defining the Fano factor using the average current $\bar{I}$ we obtain a value $F > 1$ although the events are uncorrelated because we underestimate the number of total events.

Looking at the contribution of the correlated events to the Fano factor in Fig. 3.5 also with interaction we see antibunching. Because now all rates are power laws with an exponent smaller than one the behavior known from the noninteracting case is basically compressed to the points where $|eV| = \Delta_Z$ and $eV = 0$. For $eV \approx \Delta_Z$ we find that the Fano factor develops a region where it is larger than one due to uncorrelated events. Unfortunately, the interaction now pushed the region in which we

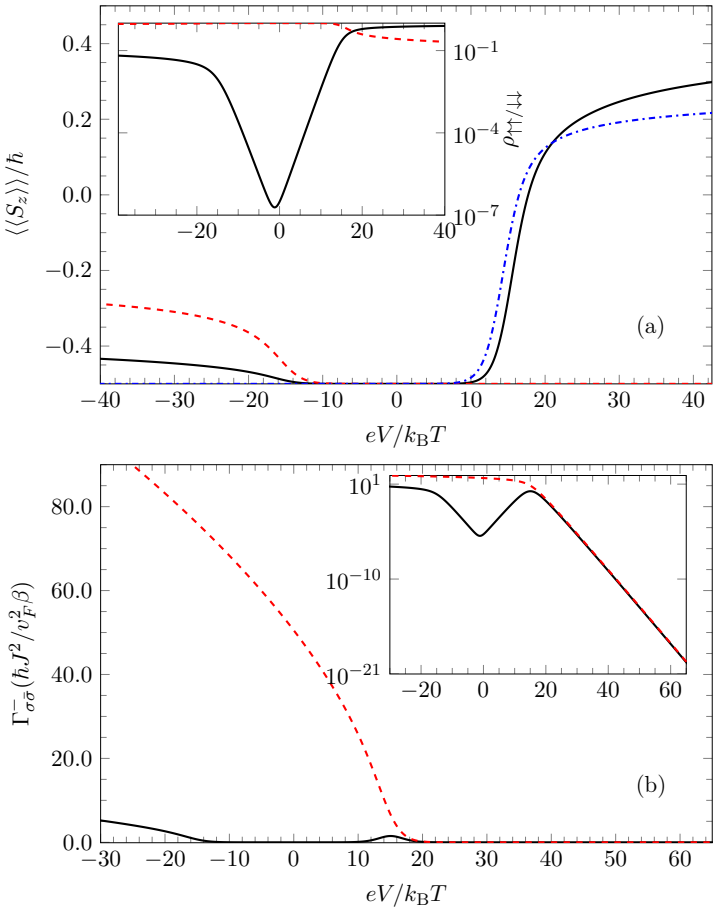

Figure 3.6: Polarization of the impurity (a) as well as scattering rates (b) for $\hbar J/v_F = 0.1$, $\Delta_Z = 15k_BT$, $\theta_Z = \pi/3$, $\alpha/\hbar\beta v_F = 10^{-3}$ and $K = 0.8$. In (a) the polarization (black, solid) as well as the polarization after a scattering event increasing (blue, dash dotted) and decreasing (red, dashed) the number of left movers. In the inset the entries of the density matrix $\rho_{\uparrow\uparrow}$ (black, solid) and $\rho_{\downarrow\downarrow}$ (red, dashed) are shown on a logarithmic scale. We observe that the suppression of $\rho_{\uparrow\uparrow}$ is exponential in $|eV|$ and ends when $|eV| > \Delta_Z$. In (b) the rate $\Gamma^-_{\downarrow\uparrow}$ (red, dashed) as well as $\Gamma^-_{\downarrow\uparrow}\rho_{\uparrow\uparrow}$ (black, solid) is shown. We see that $\Gamma^-_{\downarrow\uparrow}$ is suppressed exponentially for $eV > \Delta_Z$ and algebraic for $eV < \Delta_Z$. For $|eV| < \Delta_Z$ we see in $\Gamma^-_{\downarrow\uparrow}\rho_{\uparrow\uparrow}$ the exponential behavior of $\rho_{\uparrow\uparrow}$. For $eV \approx \Delta_Z$ this suppression is weak. Because the interaction shifts the weight in the rate towards this point a recurrence of $\Gamma^-_{\downarrow\uparrow}\rho_{\uparrow\uparrow}$ becomes visible.

find antibunching just into this region such that the antibunching cannot be seen in the Fano factor.

The sub-Poissonian regime, however, is controlled by the polarization. By using Sterling's formula in Eq. (2.78) we could show that the rates can be written by power laws in the frequency. This can be used to show that the polarization mostly[7] depends on eV/Δ_Z. The bias voltage region in which antibunching can be found thus becomes larger by increasing the Zeeman splitting. The width of the bump that hides the antibunching in the Fano factor, however is given by $k_\mathrm{B}T$ and thus is independent of Δ_Z. For larger Zeeman splitting the antibunching thus becomes visible again in the Fano factor.

3.5 Conclusion

In this chapter we calculated the current and the current noise using full counting statistics and our master equation from chapter 2. We started from the general definition of the cumulant generating function from the probability $P(N,T)$ that N electrons are transferred in a time interval T. This cumulant generating function could be represented by the trace over a density matrix whose time evolution included the counting fields. From this expression we derived a master equation that now contains counting fields. The long time behavior of the cumulant generating function is then connected to the spectral properties of the Liouvillian that describes this master equation and its counting field dependence. The current and noise were then calculated using perturbation theory in the counting field for this Liouvillian.

By expanding the propagator for the reduced density matrix for short times we could identify the parts of the evolution that are associated with a transfer of electrons between the helical states of opposite propagation direction. Using these parts we defined superoperators which allowed us to describe the effect of an electron scattering event on the reduced density matrix.

To study the bunching behavior we calculated the joint probability of two scattering events using the superoperators describing the effect of these scattering events. The bunching behavior is then characterized by

[7] For $K = 1$ this is exact as $F_z(\omega) \propto \omega$ and $F(\omega) \propto \omega$ for $\omega > 0$ there. With interaction only $F(\omega)$ becomes algebraic. This different behavior prohibits a pure eV/Δ_Z dependence. For larger bias voltage the $F_z(\omega)$ term can be neglected such that the dependence on eV/Δ_Z is restored.

a generalized $g^{(2)}$-function. Using the behavior at small times of this $g^{(2)}$-function bunching and antibunching can directly be distinguished. This $g^{(2)}$-function then was also connected to the Fano factor defined as the ratio of noise and current. This directly allowed us to identify which contribution comes from independent and which comes from correlated events.

By decomposing the Liouvillian of the master equation into the superoperators describing scattering events we were able to analyze the dynamics not only by the effect a process has on the quantum dot but also by the effect the process has on the helical edge state. This allows a better understanding of the processes involved also in chapter 2 but especially in the correlations of two events.

This method then was applied to the quantum dot coupled to the helical edge also discussed in chapter 2. We showed that using full counting statistics we could reproduce the expression for the current from chapter 2.4.2. For the noise we found thermal noise for $eV = 0$ which corresponds to current fluctuations due to the spin noise of the quantum dot that is not associated with an average charge current. For $|eV| < \Delta_Z$ we found Poissonian noise from the independent elastic tunneling events. In general, we found super-Poissonian noise for $|eV| > \Delta_Z$. For tilt angles $0 < \theta_Z < \pi/2$ we found a region with sub-Poissonian noise for $eV \approx \Delta_Z$.

This sub-Poissonian behavior could be interpreted using the rates for a spin flip which is associated with a scattering event in the edge state. The spin of the quantum dot played an important role in the understanding of the bunching behavior. We could show that the bunching behavior is determined by events flipping the spin of the quantum dot twice. As the impurity has spin $1/2$ these processes are flip-flop processes. Depending on whether the first or the second flip event is more probable we find antibunching or bunching. If the first event is less probable and the second process is more probable we find bunching as the disturbance from the first event relaxes quickly. If the second process would have been less probable we would have observed antibunching.

The spin polarization of the quantum dot determines what the first event of the flip-flop process is. For positive spin polarization the first event will be a relaxation event and for negative polarization an excitation event. The relative strength of the rates for relaxation and excitation changes at $eV \approx \Delta_Z$. The spin of the quantum dot only changes its spin for $eV > \Delta_Z$. The change of the relative strength of excitation and relaxation rates thus also leads to a crossover from bunching to

antibunching. The smaller the tilt in the magnetic field direction is the stronger is the difference of excitation and relaxation rate and thus the antibunching. For perpendicular orientation the difference vanishes and we find only bunching.

Because the edge state can be treated as a helical Luttinger liquid we also could include electron-electron interaction in the edge state. As also seen in the previous chapter 2 we found that the rates shifted the weight to the crucial points $\pm eV = \Delta_Z$ and $eV = 0$.

This amplified a phenomenon also present without interaction. For $eV \approx \Delta_Z$ the number of electrons transferred in the direction favored by the bias voltage increases strongly. The number of electrons being transported against the polarity of the bias voltage, however, also increases in a small bias voltage region. Such processes are enabled in the crossover between two regimes by finite temperature. We still find a positive backscattering current but the average current is now a bad measure for the total number of events. As this current was used in the definition of the Fano factor this leads to a super-Poissonian region in the contribution from uncorrelated events.

From the analysis of the $g^{(2)}$-function we found that we still have bunching behavior. The interaction alters the functional dependence on the bias voltage of the rates but the overall strength of the rates is a direct consequence of the tilt of the magnetic field which is not altered by the interaction. Due to the power law the width of the region where antibunching is found is smaller. The spin polarization, however, depends mostly on eV/Δ_Z such that this region is larger for larger Zeeman splitting.

In the Fano factor the signatures of the super-Poissonian noise for uncorrelated events and the sub-Poissonian contribution of the correlated events cancel each other. This is a consequence of the interaction shifting the weight towards $eV \approx \Delta_Z$. This enhances the flow of electrons against the bias voltage and compresses the regime in which antibunching is observed into the same region. The width of the super-Poissonian region in the contribution of the uncorrelated events, however, is given by the temperature whereas the width of the region in which antibunching is observed is given by the Zeeman splitting. If the Zeeman splitting is large compared to the temperature the antibunching then also leads to sub-Poissonian noise which is also reflected in the Fano factor.

Chapter 4

Double Dot Josephson Junction

The creation of mobile spin-entangled electron pairs in solid-state transport setups has been the subject of intensive research in recent years [Rec01, Les01, Rec02, Ben02, Rec03, Pra04, Oli02, LY07, Cay08, Sat10, Sch15b, Ami16, Bur16, Hus16]. The interest stems from the nonlocal properties of these entangled electrons that could be an interesting ingredient for quantum computing or other devices. The key idea in these setups is to use Cooper pairs and split them creating a nonlocal pair of electrons and injecting them into Fermi liquid leads. In the experiment the nonlocal transport features are observed. Whether these electrons are still entangled is still an open question.

In a previous proposal Choi *et al.* [Cho00] already showed that in a double quantum dot Josephson junction nonlocal correlations on the two quantum dots are induced. The nonlocal correlations can be probed by measuring the supercurrent in a SQUID setup [Cho00, Wan11]. This Josephson current is only possible for coherent transport of the Cooper pairs in contrast to the Cooper-pair splitters. Although in these setups the Cooper pair cannot be split they nevertheless offer the possibility to show nonlocal coherent transport.

Recently this setup was realized in an experiment by Deacon *et al.* [Dea15]. In their setup they measured the critical current in a Josephson junction made from two self assembled quantum dots which are in the single level regime. In their setup they claim to observe nonlocal transport signatures. They obtain these signatures by switching the charging state of each quantum dot and find signatures that are in contrast to the behavior expected for two independent dots. The change of the charging state of one quantum dot, however, is not included in the discussion of Choi *et al.* [Cho00]. In this chapter we will thus extend their proposal to include all charging states of the quantum dot. In order to be even closer to the experiment we will also decrease the superconducting gap.

As we will not assume that the Coulomb repulsion or the superconduct-

ing gap is large compared to the single particle energies of the quantum dots the methods need to be adjusted slightly. We will compare three approaches. In a first approach we will assume zero bandwidth in the superconductors reducing each of them to a single site. This reduces the complexity such that the resulting Hamiltonian can be diagonalized numerically exact in the whole parameter range. If the superconducting gap is large we use an effective model where the coupling to the superconductors is included by second-order corrections corresponding to electron tunneling between the quantum dots as well as injection of Cooper pairs. This model can also be diagonalized numerically exactly but relies on a large superconducting gap. In the third approach we proceed without this assumption and directly calculate the fourth-order corrections to the ground state. The third approach offers the advantage that it can be applied to the zero-bandwidth limit as well as to a finite bandwidth model of the two superconductors. Besides the possibility to extend the observations to a model with finite bandwidth in the superconductors we can also attribute the behavior observed to specific processes for interpretation. As the superconducting gap is reduced, more processes start to contribute leading to a richer behavior.

For an infinite superconducting gap we find that only nonlocal resonances in transport can lead to resonances in the critical current as local resonances are absent in the ground state. By reducing the superconducting gap the behavior becomes more complex. On the one hand local transport is enhanced but on the other hand nonlocal processes drive a singlet triplet transition not present in the case of infinite gap in the superconductors. Using perturbation theory we can identify the relevant processes and show that a coupling to a singlet superconductor can drive triplet ground states. We analyze this nonlocal behavior and show that the switching between the two spin states shows clear transport signatures.

We start this chapter with a short discussion of the dc-Josephson effect in section 4.1. Next, we introduce the system Hamiltonian in section 4.2. Here, we also introduce the coupling to the superconductors and comment on the influence the local wave functions of the levels have on the tunnel coupling amplitude and how we gauge the phases of the superconductors into the tunnel couplings. In section 4.3 we then introduce the methods we use. Namely the zero-bandwidth approximation in section 4.3.1 and quasi degenerate perturbation theory in section 4.3.2. The quasi degenerate perturbation theory is then used to set up the effective

model for infinite superconducting gap in section 4.3.3 and to calculate the fourth-order corrections to the ground state directly in section 4.3.4. In section 4.4 we then discuss the behavior we find. We begin with the behavior for an infinite superconducting gap in section 4.3.3 and then show how reducing the superconducting gaps lead to a singlet–triplet transition in section 4.4.2. This singlet–triplet transition then leads to asymmetric peak structures discussed in section 4.4.3. These ideas are then extended to a multilevel setup producing behavior similar to the experiment in section 4.5 before we conclude this chapter.

This chapter is based on an original publication by Probst *et al.* [Pro16]. This publication is the result of a close collaboration with Dr. Fernando Domínguez from Madrid, who contributed the numerical data for the model in zero-bandwidth approximation and the multi level quantum dot, and Dr. Alexander Schroer from Braunschweig, who contributed the calculations for the second order effective model called Cooper pair splitter regime here. The fourth order perturbation theory calculations and the diagrammatic scheme was the contribution of the author of this thesis.

4.1 dc-Josephson Effect

In 1962 B. Josephson showed that a current between two superconductors can flow without any bias voltage applied [Jos62, Jos65] if they are coupled but separated by a barrier. He showed that the supercurrent called Josephson current I_J is given by

$$I_J = I_c \sin \Delta\varphi, \tag{4.1}$$

where the critical current I_c is the maximum current that can be driven by a difference in the phase of the superconductor $\Delta\varphi$. This contribution to the current is present whether the junction of the two superconductors is normal conducting or an insulator as long as the order parameters of the superconductor penetrate into the other superconductor.

He also showed that the Josephson current can be obtained from the free energy of the barrier F by

$$I_J = \frac{2e}{\hbar} \frac{\partial F}{\partial \Delta\varphi}. \tag{4.2}$$

As a direct consequence we find for $T = 0$ that the Josephson current is given by the dependence of the ground state to the phase difference $\Delta\varphi$.

We want to elaborate on the result from Eq. (4.2) in more detail. In his derivation Josephson used thermodynamical arguments in equilibrium. The same result can also be derived using a tunneling Hamiltonian which corresponds to the approach used in the DQD Josephson junction. We follow the derivation given by Bruus and Flensberg [Bru04].

In the BCS theory the superconductor ν is described by

$$H_\nu^{\mathrm{BCS}} = \sum_{\mathbf{k}\sigma} \varepsilon_{\mathbf{k}\nu} c^\dagger_{\mathbf{k}\nu\sigma} c_{\mathbf{k}\nu\sigma} + \sum_{\mathbf{k}} \Delta_\nu e^{-i\varphi_\nu} c^\dagger_{\mathbf{k}\nu\uparrow} c^\dagger_{-\mathbf{k}\nu\downarrow} + \mathrm{h.c.}, \tag{4.3}$$

where $c_{\mathbf{k}\nu\sigma}$ annihilates an electron with momentum $\mathbf{k}$ and spin σ in superconductor ν, $\varepsilon_{\mathbf{k}\nu}$ is the energy of these electrons and Δ_ν and φ_ν are the absolute value and the phase of the superconducting order parameter.

These two superconductors are now coupled by a barrier. This barrier can be an insulator or a metal but also a more complicated system like a quantum dot or even a double quantum dot. In general we refer to this system as a barrier. This barrier is described by the Hamiltonian H_{barrier}. The electrons of the superconductor can now tunnel into the barrier. The phase of the superconductor can now be used to describe the tunneling current. The tunnel operator can in general be defined by

$$H'_T = \sum_{\mathbf{k},\sigma,\nu} t_{\mathbf{k}\sigma\nu} f^\dagger_\sigma c_{\mathbf{k}\sigma\nu} + \mathrm{h.c.}, \tag{4.4}$$

where f_σ annihilates a fermion in the barrier and $t_{\mathrm{k}\sigma\nu}$ is the tunneling amplitude. In general the tunneling transfers the electron into a state in the barrier. The case of an insulating barrier here is a special case. In this case the barrier does not have a state for the electron to tunnel into. Because the electrons have a finite overlap with the electrons in the other superconductor the electrons tunnel directly into the other superconductor.

The phase of the order parameter here plays the role of a counting field similar to the counting field in chapter 3 because it also indicates terms changing the number of electrons. To make the correspondence of counting field and superconducting field more obvious we gauge the phase of the order parameter into the fermions of the superconductor by

$$c_{\mathbf{k}\nu\sigma} \to e^{-i\varphi_\nu/2} c_{\mathbf{k}\nu\sigma}. \tag{4.5}$$

This way the order parameter becomes purely real and the tunneling Hamiltonian obtains the same phase factor as in chapter 3.

In order to emphasize the connection of the tunneling Hamiltonian, the current operator and the phase of the order parameter we write the current into the superconductor ν in analogy to Eq. (2.90) by

$$\hat{I}_\nu = e\dot{\hat{N}}_\nu = \frac{ie}{\hbar}[H'_T, \hat{N}_\nu]. \tag{4.6}$$

Inserting the tunneling Hamiltonian including the phase dependence we find by a simple calculation

$$\begin{aligned}\hat{I}_\nu &= i\frac{e}{\hbar}\sum_{\mathbf{k}\sigma}\left(t^*_{\mathbf{k}\sigma\nu}e^{-i\varphi_\nu/2}f^\dagger_\sigma c_{\mathbf{k}\sigma\nu} - t^*_{\mathbf{k}\sigma\nu}e^{i\varphi_\nu/2}c^\dagger_{\mathbf{k}\sigma\nu}f_\sigma\right)\\ &= -\frac{2e}{\hbar}\frac{\partial H'_T}{\partial\varphi_\nu}\end{aligned} \tag{4.7}$$

which shows that this phase also practically can be used as a counting field.

When considering two superconductors both coupled to the barrier this gauge transformation can be carried out on both sides. As the tunneling operator conserves charge and the barrier itself also conserves charge, the current out of the one superconductor has to be the same as the current into the other. This means that all results only can depend on the difference of the two phases $\Delta\varphi$. This is also the only gauge invariant quantity. The resulting current operator $\hat{I}_S$ between two superconductors thus is given by

$$\hat{I}_S = \frac{2e}{\hbar}\frac{\partial H'_T}{\partial\Delta\varphi}. \tag{4.8}$$

In the gauge we chose the dependence on the phase is in the tunneling Hamiltonian only. The total Hamiltonian is thus defined by

$$H = \sum_\nu H^{\mathrm{BCS}}_\nu + H_{\mathrm{barrier}} + H'_T(\Delta\varphi). \tag{4.9}$$

Because the only phase dependence of H is via $H'_T(\Delta\varphi)$ we can safely replace the tunnel Hamiltonian by the total Hamiltonian H in Eq. (4.8). This allows us to obtain the supercurrent from the free energy.

The free energy of the system is defined by

$$F(\Delta\varphi) = -\beta^{-1}\ln\mathrm{Tr}\Big(\exp\big(-\beta H(\Delta\varphi)\big)\Big), \tag{4.10}$$

where $\beta = 1/k_{\mathrm{B}}T$ is the inverse temperature. It is now straight forward to check that

$$\frac{\partial F}{\partial\Delta\varphi} = \frac{\hbar}{2e}\langle\hat{I}_S\rangle, \tag{4.11}$$

where the expectation value over the canonical ensemble defined by the Hamiltonian H. This way we could show that the phase acts as a counting field and also reproduces Eq. (4.2). For $T = 0$ the supercurrent is determined by the ground state.

This expression gives us the supercurrent as a function of the applied phase difference. In order to characterize the dc-junction usually a current is pushed through the system. The system then adjusts the phase difference such that it can carry this current without resistance. The amount of current the system can carry in its superconducting state, however, can be limited. When pushing more current through the system it thus has to become normal conducting. This threshold current is the critical current

$$I_c = \frac{2e}{\hbar} \max_{\Delta\varphi} \left(\frac{\partial F}{\partial \Delta\varphi} \right). \tag{4.12}$$

For simple systems where the critical current is sinusoidal as in Eq. (4.1) the maximum is always at $\Delta\varphi = \pi/2$. If the phase dependence of the ground state is more complicated or the ground state changes, the situation is more complicated and we have to be more careful.

To calculate the free energy or in the $T = 0$ limit the ground state energy we have to diagonalize H. In section 4.3.1 we do this exactly for a simplified model. In many cases the superconducting gap is so large that excitations in the superconductors are energetically expensive. We can thus use quasi degenerate perturbation theory to decouple the low energy part of the Hilbert space without excitations in the superconductor and the high energy part. This way we obtain an effective low energy model. For low temperatures we can ignore the phase dependence of the effective high energy part such that then the free energy is given by the free energy of the effective low energy system alone. If the superconducting gap is larger than all energies of the barrier the effective low energy system contains corrections second order in the tunnel coupling. In section 4.3.3 we include this second-order terms and diagonalize the resulting effective low energy Hamiltonian to obtain the ground state. If the energies of the barrier are also large, we can directly do perturbation theory for the ground state in fourth order to obtain its phase dependence. This is done in section 4.3.4 to obtain the supercurrent.

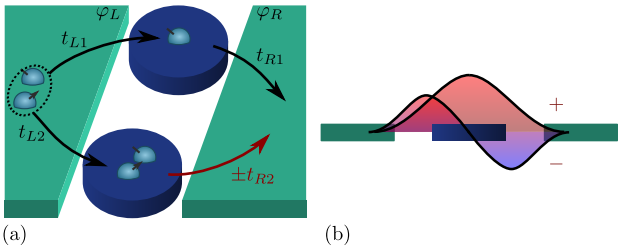

Figure 4.1: Double-quantum-dot Josephson junction. (a) The Josephson current is carried by Cooper pairs which tunnel coherently between two superconducting leads with superconducting phases φ_L and φ_R. Microscopically, this involves four single-particle tunneling events with amplitudes $t_{\nu i}$. Local transport (both electrons of a Cooper pair tunnel through a single quantum dot) can be distinguished from nonlocal transport (the two electrons of a Cooper pair tunnel through different quantum dots). (b) The symmetry of the orbital wave functions on the quantum dots is captured in the total tunnel parity $\mathcal{P} = \mathrm{sign}(t_{L1}t_{L2}t_{R1}t_{R2})$, or, equivalently, in $\pm t_{R2}$, and has distinctive signatures in the critical current. Figure and caption reproduced from the original publication [Pro16].

4.2 Model

Following [Cho00, Wan11] we consider the geometry depicted in Fig. 4.1 (a). Two quantum dots (QDs) $i = 1, 2$ are tunnel coupled in parallel to two s-wave superconductors $\nu = L, R$ at $\mathbf{x} = 0$ with amplitudes $t_{\nu i}$, which are chosen real in the absence of a magnetic field. Each QD contains only a single spin-degenerate level, $\sigma = \uparrow, \downarrow$, with energy ε_i and with the local Coulomb repulsion U_i, which is relevant for transport. There is no direct crosstalk between the QDs or between the superconductors. The Hamiltonian is

$$H = H_1 + H_2 + H_L + H_R + H_T \tag{4.13}$$

with the QD contributions

$$H_i = \sum_\sigma \varepsilon_i d_{i\sigma}^\dagger d_{i\sigma} + U_i d_{i\uparrow}^\dagger d_{i\downarrow}^\dagger d_{i\downarrow} d_{i\uparrow}, \tag{4.14}$$

the superconducting lead contributions

$$H_\nu = \sum_{\mathbf{k}\sigma} \varepsilon_{\mathbf{k}\nu} c_{\mathbf{k}\nu\sigma}^\dagger c_{\mathbf{k}\nu\sigma} + \sum_{\mathbf{k}} \Delta e^{-i\varphi_\nu} c_{\mathbf{k}\nu\uparrow}^\dagger c_{-\mathbf{k}\nu\downarrow}^\dagger + \mathrm{H.c.}, \tag{4.15}$$

and their tunnel coupling

$$H_T = \sum_{i\sigma\nu} t_{\nu i} d_{i\sigma}^\dagger \psi_{\nu\sigma}(0) + \text{H.c.} = \sum_{i\mathbf{k}\sigma\nu} t_{\nu i} d_{i\sigma}^\dagger c_{\mathbf{k}\nu\sigma} + \text{H.c.}, \tag{4.16}$$

where the $d_{i\sigma}$ operators annihilate electrons localized on the QDs and where the $c_{\mathbf{k}\nu\sigma}$ and the $\psi_{\nu\sigma}(\mathbf{x})$ operators annihilate spin-σ electrons in lead ν with momentum $\mathbf{k}$ or at position $\mathbf{x}$, respectively. The normal-state dispersion in the leads is $\varepsilon_{\mathbf{k}\nu}$. We assume the two superconducting leads to be of the same material with the same superconducting energy gap Δ and same dispersion relation $\varepsilon_{\mathbf{k}\nu}$. The superconducting phases φ_ν are not equal and only the difference between the superconducting phases, $\Delta\varphi = \varphi_L - \varphi_R$ is a gauge-invariant quantity, which enters the physical observables as mentioned in section 4.1.

The tunneling amplitudes depend strongly on the wave function of the electron on the QD. As illustrated in Fig. 4.1 (b) the relative sign of the wave function on the left and the right can be positive or negative, depending on the parity of the wave function. Without magnetic fields we know that $t_{L1}t_{L2}^* t_{R1} t_{R2}^*$ has to be a real number. We can thus summarize this sign by defining the total tunnel parity

$$\mathcal{P} = \text{sgn}(t_{L1}t_{L2}t_{R1}t_{R2}). \tag{4.17}$$

This parity summarizes all signs that can be induced locally by the wave function.

Following section 4.1 we choose a gauge that makes the amplitude of the superconducting pairing term in Eq. (4.15) real by

$$c_{\mathbf{k}\nu\sigma} \to e^{-i\varphi_\nu/2} c_{\mathbf{k}\nu\sigma}. \tag{4.18}$$

This gauge then adds a phase factor to the tunnel amplitudes in Eq. (4.16).

All these effects can be summarized very conveniently by gauging all signs and phase factors into the right side. By gauging the operators of the DQD the amplitudes t_{Li} cannot only be made real but also positive such that the tunnel parity sign $\mathcal{P}$ now only appears in the tunnel amplitudes of the right superconductor. By shifting the phase of the right superconductor we can choose a gauge such that

$$t_{R1} \to t_{R1} e^{i\Delta\varphi/2} \qquad t_{R2} \to \mathcal{P} t_{R2} e^{i\Delta\varphi/2}, \tag{4.19}$$

where all $t_{\nu i} > 0$. This way we gauged the superconducting phase difference into the tunnel coupling to the right superconductor and the tunnel

parity sign $\mathcal{P}$ into the coupling of the second QD to the right lead. In general we could have gauged this sign into an arbitrary tunneling barrier and have chosen the junction of the second dot and the right superconductor.

We discuss the case in which both QDs are in the single-level and Coulomb-blockade regime where the level broadening due to the tunnel couplings to the leads, $\Gamma_{\nu i} = 2\pi N(\varepsilon_F)|t_{\nu i}|^2$ with $N(\varepsilon_F)$ the normal-state density of states at the Fermi level, is much smaller than the level spacing $\delta\varepsilon_i$ and the Coulomb repulsion U, $\Gamma_{\nu i} \ll \delta\varepsilon_i, U_i$. For each dot this ensures a well defined charge.

In a DQD the QDs can also hybridize amongst each other either by exchanging an electron or by injection of a Cooper pair. The charge state of the DQD (N_1, N_2) is, however, well defined away from the transport resonances driven by these processes. The different charging states in the ε_1-ε_2 plane are illustrated in Fig. 4.2 where the singlet (S) and triplet (T) are both $(1,1)$ states and will be defined in detail in section 4.3.4.

For transport in systems with superconductivity we have to distinguish transport features for single electrons and pairs of electrons. If the gap is larger than the temperature single electron transport is blocked in the gap. We will nevertheless discuss the single particle transport resonances as this also helps to understand the behavior of the system, because the DQD is characterized by its charging states which are directly connected to single particle transitions. These transitions are also used to characterize the device of Deacon *et al.* [Dea15] and helps to understand the behavior of the system.

For normal conducting leads single particle transport is facilitated via sequential tunneling if two states differing by one electron are nearly degenerate such that transitions between the states are allowed. For single electron transport the QDs can be treated separately such that these resonances occur at $\varepsilon_i = 0$ and $\varepsilon_i = -U_i$. These lines then also coincide with the change of ground state.

The fact that the change of ground state coincides with the onset of single particle transport means that transport signatures in the Josephson current occur in the same region in the $\varepsilon_1 - \varepsilon_2$ plane. To see this we need to understand which states of the DQD are coupled by the superconductors. These resonances, which come from the coupling to the superconductors, do not involve a ground states and thus cannot be observed in the critical current. The most significant features in the Josephson current are those of switching ground states. The different types of resonances are discussed in detail in section 4.4.1.

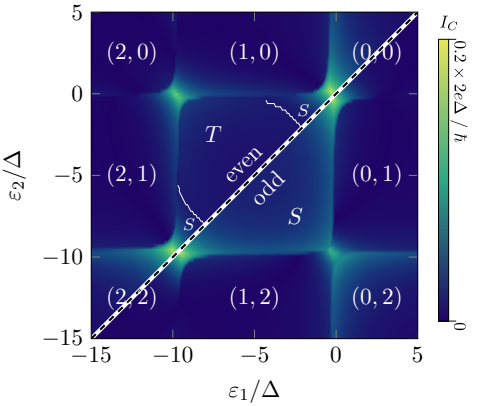

Figure 4.2: Critical current across the junction at zero temperature as a function of the quantum-dot level energies $\varepsilon_{1/2}$ obtained in the zero-bandwidth approximation. The upper-left half of the plot shows the critical current at even tunnel parity and the lower-right half at odd tunnel parity. The critical current becomes large close to ground-state transitions where the charge of the quantum dots (N_1, N_2) fluctuates. At even tunnel parity a transition between a nonlocal singlet (S) and a triplet (T) ground state in the $(1, 1)$ sector emerges. The parameters are $|t| = 0.5\Delta$ and the Coulomb repulsion $U = 10\Delta$, where Δ is the magnitude of the superconducting gap in the leads. Figure and caption reproduced from the original publication [Pro16].

4.3 Methods

We will discuss the result of three different methods. First, we use a method introduced by Affleck *et al.* [Aff00] where the superconductor is integrated out reducing it to a single superconducting site corresponding to the zero-bandwidth approximation. This reduces the size of the Hilbert space significantly such that we can diagonalize the system exactly.

In the second method we exploit that the superconducting gap is large and use quasi degenerate perturbation theory to obtain an effective model for the DQD. In the third model we do direct quasi degenerate perturbation theory for the ground state.

If Δ is large compared to all energy scales of the DQD we are in the regime where Cooper-pair splitting dominates transport [Cho00, Sch15a]. Using quasi degenerate perturbation theory we can derive an effective model for the DQD containing local as well as nonlocal Cooper-pair injection terms and a cotunneling term which allow an electron to change the QD [Sch15a]. These terms are of second order in the tunneling and higher order terms are suppressed by the large superconducting gap. The resulting Hamiltonian can then be diagonalized exactly numerically. The resulting energy phase relation then contains all orders of the second-order corrections. As the phase dependent terms in the Hamiltonian are already second order in the tunneling the resulting effect on the ground state energy, and thus the Josephson current, is of fourth order in the tunneling. This method stays valid in the vicinity of the resonances and also describes the hybridization of the DQD states due to the superconductor.

The third method directly calculates the fourth-order corrections to the ground state energy. Compared to the Cooper-pair splitter regime this method does not depend on the gap being larger than the DQD energy scales and thus allows a wider range of parameters and is also closer to the regime described by Deacon *et al.* [Dea15]. This method, however, cannot be valid in the vicinity of a change of ground states and thus will not cover the resonances that are used in the Cooper-pair splitting regime. In exchange it allows to access a regime in which more processes are possible that show interesting behavior and that are also interesting in the non resonant regime. It can furthermore also be applied to the zero-bandwidth case allowing the interpretation of the behavior seen there.

4.3.1 Zero-Bandwidth Approximation

In 2000 Affleck *et al.* [Aff00] used a model in which they integrated out the superconducting leads such that they are reduced to a boundary contribution. This corresponds to a single superconducting site, yielding the effective lead Hamiltonian

$$H_\nu^{\mathrm{zbw}} = \Delta_b c_{\nu\uparrow}^\dagger c_{\nu\downarrow}^\dagger + \mathrm{H.c.} \tag{4.20}$$

where now renormalized tunnel parameters $t_{\nu i} \to t_{\nu i}^b$ and a renormalized pairing amplitude Δ_b are used. The Hilbert space of this model is small enough to be handled numerically such that the eigenenergies can be calculated exactly. This model was used in calculations for single QDs coupled to superconductors and showed good qualitative agreement to mean field calculations. It is able to describe the competition of Kondo correlations and superconducting pairing correlations in these systems [Vec03, Ber07].

The renormalized parameters Δ_b and $t_{\nu i}^b$ need to be calculated self-consistently [Aff00]. In section 4.4 we will use fourth order perturbation theory to interpret the results of the zero-bandwidth model as well as the original Hamiltonian Eq. (4.15). Using bare couplings $\Delta_b = \Delta$ and $t_{\nu i}^b$ we find already good qualitative agreement for weak coupling. The difference can be accounted for by a global prefactor proportional to the energy density of states of the normal leads.

4.3.2 Quasidegenerate Perturbation Theory

When considering the superconducting gap to be larger than the on-site energies of the DQD and tunnel couplings $\Delta \gg \varepsilon_j, t_{\mu j}$ excitations in the superconducting leads are highly unfavorable. We can thus assume that states with no excitations in the leads are energetically well separated from states with excitations in the leads. We can thus use quasi degenerate perturbation theory. We will sketch the results here and refer to [Win03] for the details of the derivation.

For quasi degenerate perturbation theory we have to define a low energy space and a high energy space. The Hamiltonian is then decomposed into two parts

$$H = H^0 + H', \tag{4.21}$$

where H^0 is a Hamiltonian whose eigenenergies E_n as well as eigenstates are known and a coupling Hamiltonian H' that contains all couplings between the high and low energy space. To decouple the low and the high

energy space we use a canonical transformation. This transformation is then chosen such that it removes the coupling to higher energies order by order such that the Hamiltonian becomes block diagonal and the remaining coupling to higher energies becomes higher order in the tunnel coupling. As pushing the coupling to higher order the low and the high energy space decouple and we are left with an effective Hamiltonian for the low energy space.

In our case we want to exploit that excitations in the lead cost a lot of energy. The tunneling operators generate these excitations and thus are the coupling operator H' in our case. As each tunneling process involves an excitation there are no matrix elements within the low energy space but only matrix elements to the high energy space or within the high energy space. This will allow us to simplify the expressions significantly.

Removing the coupling up to second order we obtain for the matrix elements of the effective Hamiltonian

$$H_{\text{eff}} = H^{(0)} + H^{(2)} + H^{(4)}, \tag{4.22}$$

where $H^{(n)}$ are the corrections nth order in the tunnel coupling to the unperturbed Hamiltonian $H^{(0)}$. The corrections up to second order are given by

$$H^{(0)}_{mm'} = H^{0}_{mm'} \tag{4.23a}$$

$$H^{(2)}_{mm'} = \frac{1}{2}\sum_{l} H'_{ml}H'_{lm'}\left(\frac{1}{E_m - E_l} + \frac{1}{E_{m'} - E_l}\right), \tag{4.23b}$$

where H'_{ml} are the matrix elements of the coupling with respect to the eigenstates of H_0, m and m' are low energy states and the sum over l is over the high energy states. Here we already used that $H'_{mm'} = 0$ as mentioned above. When evaluating the matrix elements of H' we have to be careful and take care of signs that might arise due to the exchange of electrons.

This expansion allows us to set up effective Hamiltonians without further assumptions on the low energy Hamiltonian and coupling. Especially degeneracies are not problematic in contrast to standard perturbation theory. Using quasi degenerate perturbation theory one obtains the matrix elements that will lift the degeneracy and can diagonalize the resulting effective Hamiltonian afterwards.

One extreme choice of low energy state is to chose the ground state only. If the ground state is not degenerate this simply reproduces the

expression for standard perturbation theory. If the ground state is degenerate, however, quasi perturbation theory simplifies finding the two energies when the degeneracy is lifted. For degenerate low energy states the fourth-order corrections take the sufficiently simple form

$$H^{(4)}_{mm'} = -\frac{1}{2}\sum_{l,l',m''} H_{ml}H_{lm''}H_{m''l'}H_{l'm'} \times \left(\frac{1}{(E_m-E_l)^2(E_m-E_{l'})}+\frac{1}{(E_m-E_l)(E_m-E_{l'})^2}\right) + \sum_{l,l',l''} H_{ml}H_{ll'}H_{l'l''}H_{l''m'}\frac{1}{E_m-E_l}\frac{1}{E_m-E_{l'}}\frac{1}{E_m-E_{l''}}, \quad (4.24)$$

where the sum over l and l' is over the high energy states and $H'_{ll'}$ is the corresponding matrix element and the sum over m'' is over the low energy states. In order to obtain the effective Hamiltonians we just need to find the matrix elements H'_{ml}. Because the states l have to be eigenstates we first need to diagonalize the superconducting lead.

The superconducting lead can be diagonalized by a Bogoliubov transformation [Tin96]. We will summarize this procedure here for the Hamiltonian Eq. (4.15). This method also applies to the zero-bandwidth Hamiltonian Eq. (4.20) as there only the sum over $\mathbf{k}$ is dropped, which is not essential to the diagonalization. The Bogoliubov transformation is defined by

$$c_{\mathbf{k}\nu\uparrow} = u^*_{\mathbf{k}\nu}\gamma_{\mathbf{k}\nu 0} + v_k\gamma^\dagger_{\mathbf{k}\nu 1} \qquad c^\dagger_{-\mathbf{k}\nu\downarrow} = -v^*_{\mathbf{k}\nu}\gamma_{\mathbf{k}\nu 0} + u_k\gamma^\dagger_{\mathbf{k}\nu 1}, \quad (4.25a)$$

where $|u_{\mathbf{k}\nu}|^2 + |v_{\mathbf{k}\nu}|^2 = 1$ ensures fermionic commutation relations for $\gamma_{\mathbf{k}\nu\eta}$. Inserting this into Eq. (4.15) and removing diagonal terms we find

$$v_{\mathbf{k}\nu}u^*_{\mathbf{k}\nu} = \frac{\Delta_\nu}{2E_{\mathbf{k}\eta}} \qquad |v_{\mathbf{k}\nu}|^2 = 1-|u_{\mathbf{k}\nu}|^2 = \frac{1}{2}\left(1-\frac{\varepsilon_{\mathbf{k}\nu}}{E_{\mathbf{k}\nu}}\right), \quad (4.26)$$

where $E_{\mathbf{k}\nu} = \sqrt{\Delta_\nu^2+\varepsilon^2_{\mathbf{k}\nu}}$ is the energy of the excitations defined by[1] $\gamma_{\mathbf{k}\nu\eta}$. The resulting Hamiltonian is then given by

$$H_\nu = \sum_{\mathbf{k}} E_{\mathbf{k}\nu}(\gamma^\dagger_{\mathbf{k}\nu 0}\gamma_{\mathbf{k}\nu 0} + \gamma^\dagger_{\mathbf{k}\nu 1}\gamma_{\mathbf{k}\nu 1}), \quad (4.27)$$

[1] Note that $u_{\mathbf{k}\nu}$ and $v_{\mathbf{k}\nu}$ are real here as we gauged the phase of the superconductor into the tunnel coupling. If we had not done this the phase factor would appear in the $v_{\mathbf{k}\nu}u^*_{\mathbf{k}\nu}$ term.

where we dropped a constant term. We will thus use a basis in which the excitations in the lead are described by the Bogoliubons which are the excitations generated by $\gamma^\dagger_{\mathbf{k}\nu\eta}$.

Using this formalism we will now discuss two cases. The first case is the Cooper pair splitter regime. In this regime the superconducting gap is larger than the on-site energies of the DQD and tunnel couplings $\Delta \gg \varepsilon_j, t_{\mu j}$ such that the low energy space is given by all DQD states without any excitations in the leads. In second order the effective Hamiltonian then contains terms for local as well as nonlocal Cooper-pair injection as well as cotunneling terms. After this we will allow the superconducting gap to be of the order of the on-site energies of the DQD such that the low energy space now only consists of a possibly degenerate ground state. For this case we then do fourth order perturbation theory. As there are a lot of possible processes we will give a simple diagrammatic scheme to take care of all the fermion exchange signs that may occur.

4.3.3 Cooper-Pair-Splitter Regime

In 2000 Choi *et al.* discussed a Josephson junction with a DQD in between two superconductors and showed that nonlocal correlations are induced on the DQD and calculated the Josephson current [Cho00]. In 2001 Recher *et al.* [Rec01] used two normal leads instead of a second superconductor and were able to show that for large superconducting gap the nonlocal processes dominate. A large superconducting gap will also enhance nonlocal correlations in a DQD Josephson junctions which then also leads to nonlocal transport of Cooper pairs. We thus call this regime the Cooper-pair splitter regime. By having a nonlocal supercurrent one is even able to demonstrate that the Cooper pairs not only are transported nonlocally but also coherently.

In the original suggestion for a Cooper-pair splitter [Rec01] it was shown that for large superconducting gap the dominant transport channel is nonlocal and thus splits the Cooper pairs. Probing the entanglement of these Cooper pairs is, however, difficult as spin measurement for single electrons is difficult. There were several ideas how to transfer the entanglement to photons and probe them for entanglement. One suggestion uses a LASER to excite the split Cooper pair to a higher level such that the following relaxation generates entangled photons [Nig15]. Another approach suggest a DQD in between a p-type and a n-type superconductor which allows to transfer the entanglement of the Cooper pair to photons in a cavity by

recombination of the electrons from the two superconductors [Sch15a]. They also derived an effective model for the DQD including superconducting pairing terms. Here we will revisit this model from the point of view of nonlocality in the Josephson current.

In this model the superconducting gap is considered significantly larger than the on-site energies of the DQD and the tunnel couplings $\Delta \gg \varepsilon_j, t_{\mu j}$ and excitations in the superconducting leads are highly unfavorable. The low energy space is thus given by all DQD states without any excitations in the lead. Using the quasi degenerate perturbation theory summarized above[2] the effective Hamiltonian in for large Δ can be written as

$$H_{\text{eff}} = \sum_{i\sigma} \varepsilon_i d_{i\sigma}^\dagger d_{i\sigma} + \sum_i U_i d_{i\uparrow}^\dagger d_{i\downarrow}^\dagger d_{i\uparrow} d_{i\downarrow} + \sum_{ij\sigma\nu} \tilde{t} \mathcal{P}_{ij\nu} d_{i\sigma}^\dagger d_{j\sigma} + \sum_{ij\nu} \left(\tilde{\Delta}_{ij} \mathcal{P}_{ij\nu} e^{-i\varphi_\nu} (d_{i\uparrow}^\dagger d_{j\downarrow}^\dagger - d_{i\downarrow}^\dagger d_{j\uparrow}^\dagger) + \text{H.c.} \right), \quad (4.28)$$

where $\tilde{\Delta}_{ij}$ is the effective amplitude to inject a local ($i = j$) or a nonlocal ($i \neq j$) Cooper pair and $\tilde{t}$ describes cotunneling. The parity enters via $\mathcal{P}_{ij\nu} = 1$ if $\nu = L$ or $i = j$ and $\mathcal{P}_{ij\nu} = \mathcal{P}$ if $\nu = R$ and $i \neq j$. For the explicit form of $\tilde{\Delta}_{ij}$ and $\tilde{t}$ we refer to [Sch15a] and treat them here as effective parameters. They can also be calculated using the technique given in section 4.3.5.

As the particle number in the superconductor is conserved modulo two the effective Hamiltonian can be separated into two decoupled blocks; an even block in which an even number of electrons on the DQD and an odd block in which the number of electrons on the DQD are odd.

One special even state is the $(1,1)$-charge state. This state can be represented by a nonlocal singlet state and three nonlocal triplet states. Because the Cooper pairs in the superconductor are singlets the triplets decouple as they cannot interact with the superconductor. The singlet, however, is coupled to higher other charging states. When treating this coupling in second-order perturbation theory in $\tilde{\Delta}_{ij}$ and $\tilde{t}$, that is fourth

[2] Schroer *et al.* [Sch15a] use the Schrieffer-Wolff transformation as introduced by Hewson [Hew93] that facilitates projections onto the low energy space and a simple algebraic operation. This method, however, assumes that we know the exact energy. In leading order this is not very problematic, but it becomes more complicated when extended to higher orders. We thus stick to the method described by Winkler [Win03].

order in the tunnel coupling, these states repel each other such that the singlet state is lowered and the triplets are always higher or same in energy as the singlet. In section 4.3.5 we will show this in an example.

4.3.4 Ground State in Perturbation Theory

Assuming a large superconducting gap in the leads simplifies the expressions for the coefficients $\tilde{\Delta}_{ij}$ and $\tilde{t}$ in Eq. (4.28). It also suppresses cotunneling compared to Cooper-pair injection thus making it a Cooper-pair splitter. In the experiment by Deacon *et al.*, however, the gap is not significantly larger than the energy differences of the DQD states [Dea15]. We thus want to drop this assumption. This means we now cannot neglect cotunneling anymore in general. Excitations of the DQD system now are similar in energy to excitations in the leads and thus also have to be treated as high energy states. The low energy space is thus only given by the possibly degenerate ground state.

The other method valid in this regime is the zero-bandwidth approximation which produces exact results in the whole parameter range. This exact solution will be accompanied by a perturbative treatment. Applying perturbation theory allows us directly to interpret features we observe by the processes corresponding to the terms in the perturbativ expansion. The perturbative result furthermore also allows the generalization to the wide band limit. We can thus directly see whether a feature observed in the zero-bandwidth limit will also be present in the wide band limit.

In Eq. (4.24) we see that a series of four tunnel terms has to be considered. Each of these tunnel terms can be interpreted as a process. Because in the lead there is no conservation of number of electrons and also transitions between high energy states are possible the number of available processes is very high. To account for all of these processes and the matrix elements connected to those we developed a simple diagrammatic scheme. Before we describe this scheme in section 4.3.5 we want to describe the influence of certain processes first. We start by commenting on the structure of the ground state. We will then characterize the different processes and give their effect in the energy correction. This then also allows us to discuss the peculiarities that a change in the ground state has for the critical current.

In the unperturbed ground state, there are no excitations in the leads and the QDs have a well-defined charging state (N_1, N_2), where N_i is the number of electrons on QD i. Each charging state is spin degenerate

and can be realized by different quantum states, $|\alpha,\beta\rangle \equiv |\alpha\rangle_{\mathrm{QD1}} |\beta\rangle_{\mathrm{QD2}}$, all of which are completely decoupled because the model conserves the z projection of the total spin, S^z.

The only exception are the states in the $(1,1)$ sector with $S^z = 0$, where degenerate perturbation theory in the space spanned by the states $|\uparrow,\downarrow\rangle$ and $|\downarrow,\uparrow\rangle$ is required. Since the total spin is conserved, it is most intuitive to use a spin basis built from the nonlocal singlet and nonlocal triplet

$$|S\rangle = \frac{1}{\sqrt{2}}\Big(|\uparrow,\downarrow\rangle - |\downarrow,\uparrow\rangle\Big) \qquad |T\rangle = \frac{1}{\sqrt{2}}\Big(|\uparrow,\downarrow\rangle + |\downarrow,\uparrow\rangle\Big), \tag{4.29}$$

as these will remain eigenstates of the system. For the calculation of the matrix elements it is, however, easier to use $|\uparrow,\downarrow\rangle$ and $|\downarrow,\uparrow\rangle$ as a basis as the effect of the tunnel coupling on those states is easily understood. In this basis the effective model is not diagonal. The off diagonal elements correspond to processes that exchange the spins on the two QDs whereas the diagonal entries are processes that do not exchange the spins. As both spins are equivalent the spin conserving entries on the diagonal are the same. The effective Hamiltonian obtained from ground state perturbation theory can thus be written as

$$H_{\mathrm{eff}} = H_1 + H_2 + H_{\mathrm{sc}}\sigma_0 + H_{\mathrm{se}}\sigma_x, \tag{4.30}$$

where H_{sc} and H_{se} are the amplitudes for spin conserving and spin-exchanging processes and σ_i are the Pauli matrices σ_0 being the identity matrix. We see that the sign of H_{se} determines whether the singlet or the triplet is the ground state. The singlet–triplet splitting is thus given by $2H_{\mathrm{se}}$ and the singlet is the ground state if H_{se} is positive where the triplet is the ground state H_{se} it is negative. Note that the spin triplets with $S_z = \pm 1$ behave equivalently to $|T\rangle$ by spin-rotation invariance.

The terms in the perturbative expansion are local or nonlocal, where local processes involve only one of the QDs whereas nonlocal processes involve both QDs. Furthermore, we call all processes Josephson processes, in which entire Cooper pairs are removed from or added to the superconducting leads due to two single-particle tunnel events. In processes which are not Josephson processes as many carriers are added to each lead as are removed, so we call them cotunneling processes [3].

[3] As the charging state of the QDs must not change, Josephson processes and cotunneling processes do not mix to fourth order.

Summarizing all of the processes, we can write down the general form of the correction of the ground-state energy in perturbation theory,

$$\delta E_0(\Delta\varphi) = E^{\mathrm{loc}}_{\mathrm{CT},1} + E^{\mathrm{loc}}_{\mathrm{CT},2} + E^{\mathrm{loc}}_{J,1}(\Delta\varphi) + E^{\mathrm{loc}}_{J,2}(\Delta\varphi) + E^{\mathrm{nl}}_{\mathrm{CT,sc}} + E^{\mathrm{nl}}_{J,\mathrm{sc}}(\Delta\varphi) \pm \left[E^{\mathrm{nl}}_{\mathrm{CT,se}} + E^{\mathrm{nl}}_{J,\mathrm{se}}(\Delta\varphi)\right], \quad (4.31)$$

where the superscript denotes whether the correction is due to local (loc) or nonlocal (nl) processes and the subscripts denote whether the correction comes from a cotunneling (CT) or from a Josephson (J) process. For local processes, the second subscript denotes the QD which is involved in the process whereas for nonlocal processes, the second subscript denotes whether the process is a spin-exchanging (se) or spin-conserving (sc) process. The spin-exchange contributions are nonzero only in the $(1,1)$ sector. In the $(1,1)$ sector, Eq. (4.31) is thus the energy correction of the nonlocal triplet (upper sign) and the nonlocal singlet (lower sign).

In the charge sectors with a unique ground state or a degenerate ground state whose degeneracy is not lifted, the critical current is given directly by the amplitude of the phase-dependent corrections of the ground-state energy, which, in perturbation theory, are proportional to $\cos(\Delta\varphi)$. The amplitude is commonly referred to as the (phase-independent) Josephson energy E_J and the critical current is proportional to the Josephson energy, $I_c \propto E_J$. Since E_J decomposes into local and nonlocal contributions, so does I_c. The critical phase is always at $\Delta\varphi = \pm\pi/2$, where $\partial_{\Delta\varphi}\cos(\Delta\varphi)$ is maximized.

In the $(1,1)$-charge sector, the situation is more complicated. Both the energy of the singlet state and the energy of the triplet state, cf. Eq. (4.31), depend on the phase difference such that they may cross for suitable parameters and hence the ground state changes between singlet and triplet as a function of the phase difference $\Delta\varphi$. Three possible situations are shown in Fig. 4.3. If there is a singlet–triplet ground-state transition as a function of the phase difference, the cosinelike energy-phase relation of the ground state $\delta E_0(\Delta\varphi)$ becomes a piecewise function of the phase difference with two different amplitudes and with two different constant energy offsets for the singlet state and the triplet state, cf. right panels of Figs. 4.3 (a) and (b). This is different from the simple model given by Deacon *et al.* [Dea15] where they assume that the Josephson energy is independent of the phase difference. When the critical current is probed, the junction adjusts to the phase difference which maximizes the supercurrent. This is not necessarily at the conventional

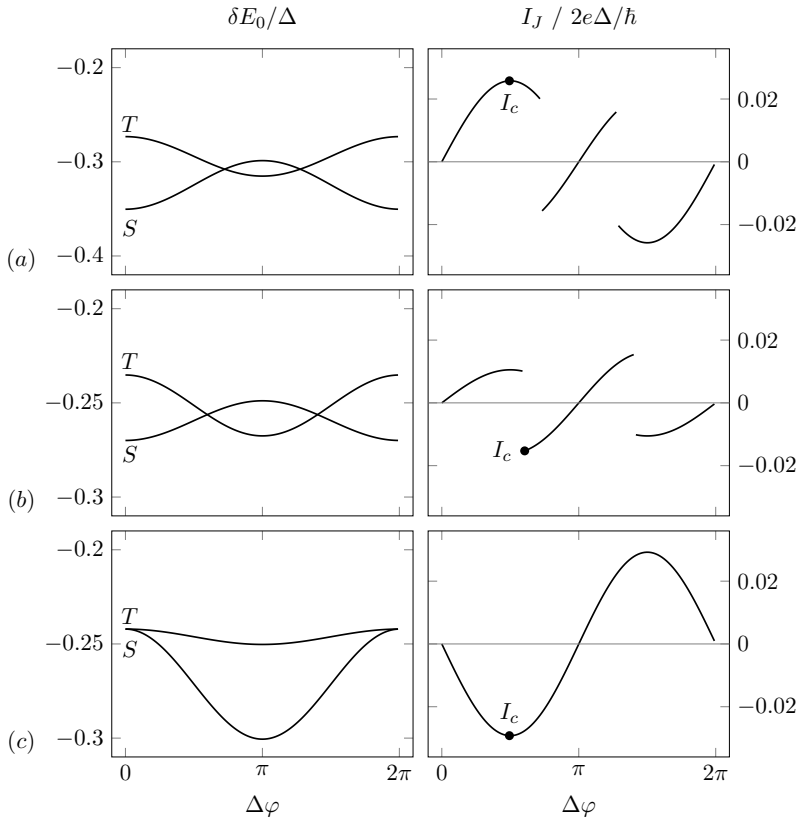

Figure 4.3: Phase dependence of the energy corrections δE_0 of the two lowest-lying states in the $(1,1)$-charge sector and the resulting supercurrent I_J in the ground state evaluated in the zero-bandwidth approximation. (a) Point A in Fig. 4.7. The critical current I_c is carried by the singlet ground state (S) at $\Delta\varphi = \pm\pi/2$. (b) Point B in Fig. 4.7. The critical current is carried by the triplet ground state (T) at $\Delta\varphi \neq \pm\pi/2$. (c) Point C in Fig. 4.7. At odd total tunnel parity, $\mathcal{P} = -1$, the ground state is a singlet at all $\Delta\varphi$ and the critical current has the conventional sinusoidal dependence on $\Delta\varphi$. The junction is in the π phase. Figure and caption reproduced from the original publication [Pro16].

value $\Delta\varphi = \pm\pi/2$. At $\Delta\varphi = \pm\pi/2$ there might be a singlet (triplet) ground state with a low amplitude $E_J(\Delta\varphi)$ which cannot carry as high a supercurrent as the triplet (singlet) ground state at a different phase difference $\Delta\varphi' \neq \pm\pi/2$ but with a larger amplitude $E_J(\Delta\varphi')$ such that $|E_J(\pm\pi/2)| < |E_J(\Delta\varphi')\sin(\Delta\varphi')|$. This is depicted in Fig. 4.3 (b). Then the junction will switch to the triplet (singlet) ground state and the critical phase locks to $\Delta\varphi'$.

An important reason that the critical current differs between the singlet phase and the triplet phase is the sign of the nonlocal Josephson current. As can be seen from Eqs. (4.24) and (4.37), it depends on the phase, on the parity, and on whether the ground state is a singlet or a triplet. So if the local supercurrents and the nonlocal supercurrent are flowing in opposite directions at $\Delta\varphi = \pm\pi/2$, it can be beneficial to switch to the other ground state at $\Delta\varphi' \neq \pm\pi/2$, where the individual supercurrents are smaller but flow in the same direction. Due to this interplay it is nontrivial to isolate nonlocal features from the critical current.

To determine whether the ground state changes and which ground state carries the critical current we need to evaluate the different terms in Eq. (4.31). To evaluate a specific term we need to use Eq. (4.22) and only sum over processes contributing to that term. As there are many processes contributing we have to find a way to write down the matrix elements in an efficient way. This can be achieved by using a simple diagrammatic technique explained in the next section.

4.3.5 Diagrammatic Technique for Matrix Elements

To organize all processes, we represent them by diagrams. We take the point of view of the DQD system. From this point of view, the DQD emits electrons to the leads or absorbs electrons from the leads. Due to the excitation gap of the superconductors, tunneling proceeds in pairs: the DQD can emit an electron into a superconductor which is later reabsorbed, absorb an electron from the Fermi sea and subsequently fill the hole which was created, emit two electrons which form a Cooper pair, or absorb two electrons by destroying a Cooper pair. At this point it does not matter which one of the leads enables the process as later on all possibilities are summed over. To keep track of which QD is affected by one tunneling event, we represent each QD by one horizontal line. Each tunnel event involving the QD is a vertex on this line. A line connecting two vertices indicates, which two tunnel events are connected by one of

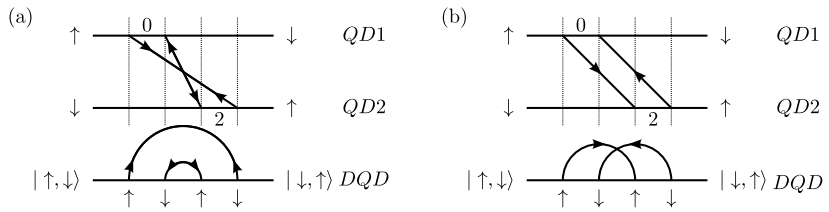

Figure 4.4: Example diagram of (a) a spin-exchange Josephson and (b) a spin-exchange cotunneling process with the same intermediate QD occupations (denoted by 0 and 2 electrons) read from the left to the right. The upper two horizontal lines represent the QDs and the lower horizontal line represents the DQD as a whole. The spin arrows at the beginning and at the end of the horizontal lines denote the initial state and the final state of the DQD and the arrows on the lead lines indicate the direction of the electrons flowing out of or into the DQD. Figure and caption reproduced from the original publication [Pro16].

the processes mentioned above. We name it a lead line. Two example diagrams are shown in Fig. 4.4. The process on the DQD is the same but it is mediated by two different lead processes; in Fig. 4.4 (a) the process is mediated by Josephson processes whereas it is mediated by cotunneling in Fig. 4.4 (b). The direction of the arrows on the lead lines indicates the flow of electrons onto or out of the QDs. So the lead lines of Josephson processes have two arrows and cotunneling processes have one arrow. The intermediate DQD occupations are given by numbers or by small spin arrows.

Since all processes conserve the total charge of the DQD, they are always a sequence of two creation and two annihilation events both in the DQD and in the leads. It can easily be checked that all possible sequences decompose into a part concerning the leads and a part concerning the DQD without acquiring an overall fermion-exchange sign. But within both of the subsystems, we need to account for possible signs due to fermion exchange. To determine the sign of the QD subsystem, the number of permutations is counted which would be required to arrange all vertices of QD 1 to the left of all vertices of QD 2. If the number is odd, a fermion-exchange sign results.

If the spin of the electron on a QD is changed in a spin-exchange process, another sign may occur. Changing the spin of a QD can be done either by removing the electron and filling the QD with an electron of

opposite spin (intermediate occupation number 0) or by adding another electron and removing the first electron afterwards (intermediate occupation number 2). In the second case, an additional exchange of fermions is necessary when removing the first electron, which we call spin flip via a local singlet. Such a spin flip introduces a sign.

To determine the sign of the processes on the DQD, we can thus summarize the following rules:

- Draw the diagram.
- Count the number of permutations which would be required to arrange all vertices of QD 1 to the left of all vertices of QD 2. If it is odd, add a sign.
- Count the spin flips via a local singlet (intermediate occupation number 2). Each contributes a fermion-exchange sign.

To determine the contributions due to the lead process, we construct an auxiliary diagram by collapsing the two lines of the QDs onto one. These auxiliary diagrams are the third horizontal line in Figs. 4.4 (a) and 4.4 (b). Now each crossing of lead lines corresponds to a commutation of lead operators. Furthermore, each lead line represents a normal or an anomalous superconducting correlation function. If, e.g., a lead line connects two events in which, read from the left to the right, first a spin-up electron is removed from the superconductors and then a spin-down electron is removed from the superconductors, the corresponding correlation function is $\langle c_\downarrow c_\uparrow \rangle$. All correlation functions can be calculated using the standard Bogoliubov transform summarized in section 4.3.2,

$$\begin{aligned}\langle c^\dagger_{\mathbf{k}\nu\uparrow} c^\dagger_{-\mathbf{k}\nu\downarrow}\rangle &= \langle c_{-\mathbf{k}\nu\downarrow} c_{\mathbf{k}\nu\uparrow}\rangle = -\langle c^\dagger_{-\mathbf{k}\nu\downarrow} c^\dagger_{\mathbf{k}\nu\uparrow}\rangle = -\langle c_{\mathbf{k}\nu\uparrow} c_{\mathbf{k}\nu\downarrow}\rangle \\ &= u_{\mathbf{k}\nu} v_{\mathrm{k}\nu} = \frac{\Delta_\nu}{2\sqrt{\varepsilon^2_{\mathbf{k}\nu} + \Delta^2}} \qquad (4.32a)\end{aligned}$$

$$\langle c^\dagger_{\mathbf{k}\nu\uparrow} c_{\mathbf{k}\nu\uparrow}\rangle = \langle c^\dagger_{\mathbf{k}\nu\downarrow} c_{\mathbf{k}\nu\downarrow}\rangle = |v_{\mathbf{k}\nu}|^2 = \frac{1}{2}\Big(1 - \frac{\varepsilon_{\mathbf{k}\nu}}{\sqrt{\varepsilon^2_{\mathbf{k}\nu} + \Delta^2_\nu}}\Big) \qquad (4.32b)$$

$$\langle c_{\mathbf{k}\nu\uparrow} c^\dagger_{\mathbf{k}\nu\uparrow}\rangle = \langle c_{\mathbf{k}\nu\downarrow} c^\dagger_{\mathbf{k}\nu\downarrow}\rangle = |u_{\mathbf{k}\nu}|^2 = \frac{1}{2}\Big(1 + \frac{\varepsilon_{\mathbf{k}\nu}}{\sqrt{\varepsilon^2_{\mathbf{k}\nu} + \Delta^2_\nu}}\Big), \qquad (4.32c)$$

where $\varepsilon_{\mathbf{k}\nu}$ is the normal-state dispersion of the lead electron measured from the Fermi level. Note that the order of the spins in the superconducting correlation functions is important since the order in which the electrons are put into the Cooper-pair condensate matters.

The lead part of the matrix element can thus be obtained by following these rules:

- Collapse the two-line diagram to the auxiliary diagram.
- Count the number of line crossings. Each crossing contributes a fermion-exchange sign.
- Write down the lead correlations following Eq. (4.32). Take care of fermion-exchange signs that might occur due to the spin-order of Cooper pairs. Use $\varepsilon_{\mathbf{k}\nu}$ for one lead line and $\varepsilon_{\mathbf{k}'\nu'}$ for the other line.

Finally, we need to determine the energies of the virtual states. The corresponding energies of the DQD can be read off from the two-line diagram. The energies of the three virtual states can be found by looking at the states in the three spaces between the dashed lines in the two line diagrams. Each lead line contributes an additional energy $\sqrt{\varepsilon_{\mathbf{k}\nu}^2 + \Delta_\nu^2}$ and $\sqrt{{\varepsilon_{\mathbf{k}'\nu'}}^2 + \Delta^2}$, for the two pairs of tunneling events, respectively.

By drawing all diagrams and inserting the corresponding matrix elements and the energies into Eq. (4.24), the fourth-order corrections of the ground state energy can be constructed explicitly.

As an illustration we will now calculate the matrix element for three examples. First we will reproduce the result by Spivak and Kivelson [Spi91] who calculated the Josephson current through a single QD and found that this QD builds a π-junction if the QD charge is odd. We then evaluate the example from Fig. 4.4 (a). Finally, we also check that the effective Hamiltonian from section 4.3.3 lowers the singlet and decouples from the triplet.

In their paper, Spivak and Kivelson consider one QD. This needs thus also be included in our formalism as having a single dot is equivalent to our definition of a local process. They furthermore also assume that Coulomb interaction is large such that virtual states involving double occupancies can be neglected. We focus on Josephson processes here. As we only have one QD line the only diagram contributing is the one shown in Fig. 4.5 (a). Looking at the lead lines we find that there is one crossing which contributes one sign. The order of the spins used to add a Cooper pair to the leads and the order of the spins used to extract a Cooper pair from the leads is not the same; injecting the Cooper pair into the lead starts with spin up whereas extracting the Cooper pair starts with spin down. Looking at Eq. (4.32) we see that the sign for these processes is the same and thus we have no additional sign such that the lead part

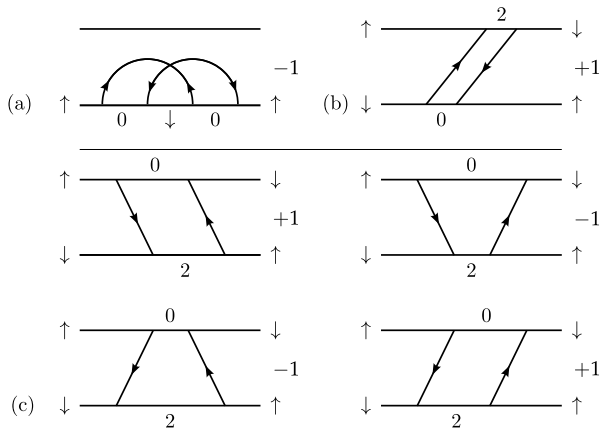

Figure 4.5: Diagrams for a local Josephson process (a), a cotunneling process including an spin exchange between the QDs (b) and cotunneling correction due to processes also present in the Cooper-pair-splitter regime (c).The processes illustrated in (a) and (b) are genuine fourth-order processes whereas the processes in (c) are higher order contributions of second-order processes. In local processes only one QD is involved whereas the other QD is not involved. Figure and caption reproduced from the original publication [Pro16].

of the process in general will contribute a sign. As we do not have a spin flip via a singlet in the QD part of the process it does not contribute a sign such that the total sign of the diagram is negative. Cooper pairs can be added and removed from the same lead or from different leads such that we have to sum over these possibilities. The diagram does not change structurally when changing the spin of the initial state such that it is the same for both spin states. All virtual states involve excitations in the lead such that we only have terms in the second sum of Eq. (4.24). Putting all these facts together we arrive at

$$E_J^{\mathrm{loc}} = -\sum_{\nu\nu'\mathbf{k}\mathbf{k}'} |t_\nu|^2 |t_{\nu'}|^2 e^{i(\varphi_\nu - \varphi_{\nu'})} \frac{\Delta^2}{4E_{\mathbf{k}}E_{\mathbf{k}'}} \frac{1}{\varepsilon - E_{\mathbf{k}}} \frac{1}{-(E_{\mathbf{k}} + E_{\mathbf{k}'})} \frac{1}{\varepsilon - E_{\mathbf{k}'}}, \quad (4.33)$$

where we already assumed that the superconductors are equivalent and only the tunnel coupling might differ. Because each of the energy factors is defined as the difference of the ground and the excited state they are negative such that the whole term is positive which agrees[4] with [Spi91].

As an example for a nonlocal process we consider the process depicted in Fig. 4.4 (b). Here an electron hops off QD1 and is immediately replaced such that two excitations remain in the leads. After that the excitations annihilate via tunneling to the other dot. The dot operators are already in the right order. On QD2 we have a spin flip via a singlet which contributes a sign. In the auxiliary diagram we have one line crossing which contributes a sign. As the lead also contributes a sign as well as the DQD, the total sign is positive. In the left lead line an electron is first emitted to the lead and then reabsorbed such that the excitation is particle like whereas the right line is hole like. Looking at Eq. (4.32) we see that these are not equivalent. Using the prime to denote the terms from the hole like excitation we find

$$E_{CT}^{\mathrm{nl}} = \sum_{\nu\nu'\mathbf{k}\mathbf{k}'} t_{\nu 1}^* t_{\nu' 2} t_{\nu 2} t_{\nu' 2}^* \, \mathcal{P}_\nu \, \mathcal{P}_{\nu'} \, \frac{1}{4} \, \frac{E_{\mathbf{k}\nu} + \varepsilon_{\mathbf{k}\nu}}{E_{\mathbf{k}\nu}} \frac{E_{\mathbf{k}'\nu'} - \varepsilon_{\mathbf{k}'\nu'}}{E_{\mathbf{k}'\nu'}} \times \frac{1}{\varepsilon_2 - E_{\mathbf{k}\nu}} \frac{1}{-E_{\mathbf{k}\nu} - E_{\mathbf{k}'\nu'}} \frac{1}{-\varepsilon_2 - U_2 - E_{\mathbf{k}'\nu'}}, \quad (4.34)$$

[4] Note that they defined the interaction in the Hamiltonian including a minus sign such that a negative J corresponds to a positive correction in the total energy

where $\mathcal{P}_\nu$ is the total tunnel parity for $\nu = R$ and 1 for $\nu = L$. We see that nonlocal processes can pick up the sign due to the parity whereas local terms cannot as they use tunnel couplings always twice. For this process the DQD returns into a ground state after two tunneling processes such that the second energy term is independent of the DQD parameters. A similar process without spin exchange also exists and only differs from this one in the spin of the second lead line. In this case the spin flip via a singlet is missing such that it just changes its total sign.

As a final example we can also use our technique to show that in the Cooper-pair-splitter regime the singlet is lowered. For this we need to show that the second order contributions do not lower the triplet. In section 4.4.2 we will show that all processes that lower the triplet are cotunneling processes. It is thus sufficient to focus on those cotunneling processes that are combinations of two second-order processes. These processes are shown in Fig. 4.5 (c) up to the exchange of the two QDs. In the Cooper-pair-splitter regime the only states the $(1,1)$-charge states couple to are the $(2,0)$ and the $(0,2)$ state. We discuss as an example the coupling to the $(0,2)$ state. In the Cooper-pair-splitter regime excitations in the leads are costly such that only processes contribute in which an excitation generated by a tunneling event is annihilated in the next tunneling event. In fourth order these are all diagrams with no lead line in the middle. We also call these diagrams reducible as they can be interpreted as higher orders of lower order corrections. All reducible diagrams that couple the $(1,1)$ to the $(0,2)$ state are shown in Fig. 4.5. We see that the neighboring diagrams only differ in the order in which the electrons are reinserted into the QDs, which induces a sign between them. In all diagrams the spin flip is mediated via a singlet such that another sign is introduced. As the lead lines never, cross the lead does not contribute another sign. This way we obtain the signs next to the diagrams. For the matrix element we thus find

$$E^{\mathrm{nl}}_{CP,se} = \sum_{\nu\nu'\mathbf{k}\mathbf{k}'} t^*_{\nu 1} t_{\nu 2} t_{\nu 1} t^*_{\nu' 2}\ \mathcal{P}_\nu\ \mathcal{P}_{\nu'}\ \frac{1}{4}\ \frac{1}{\varepsilon_1 - \varepsilon_2 - U_2}$$
$$\times \left(\frac{|u_{\mathbf{k}\nu}|^2}{\varepsilon_1 - E_{\mathbf{k}\nu}} \frac{|v_{\mathbf{k}'\nu'}|^2}{-\varepsilon_2 - U_2 - E_{\mathbf{k}'\nu'}} + \frac{|u_{\mathbf{k}'\nu'}|^2}{\varepsilon_1 - E_{\mathbf{k}'\nu'}} \frac{|v_{\mathbf{k}\nu}|^2}{-\varepsilon_2 - U_2 - E_{\mathbf{k}\nu}} \right.$$
$$\left. - \frac{|u_{\mathbf{k}\nu}|^2 |u_{\mathbf{k}'\nu'}|^2}{(\varepsilon_1 - E_{\mathbf{k}\nu})(\varepsilon_1 - E_{\mathbf{k}'\nu'})} - \frac{|v_{\mathbf{k}\nu}|^2 |v_{\mathbf{k}'\nu'}|^2}{(-\varepsilon_2 - U_2 - E_{\mathbf{k}\nu})(-\varepsilon_2 - U_2 - E_{\mathbf{k}'\nu'})} \right). \tag{4.35}$$

We used that the middle virtual state, and thus the term in the matrix element, is the $(0,2)$ state in all diagrams. The prime indicates that the term corresponds to the second lead line. After some simple algebra we find that

$$E^{\mathrm{nl}}_{CP,se} = -\frac{1}{\varepsilon_1-\varepsilon_2-U_2} \times \sum_{\nu\mathbf{k}} t^*_{\nu 1} t_{\nu 2}\, \mathcal{P}_\nu\, \frac{|u_{\mathbf{k}\nu}|^2(-\varepsilon_2-U_2-E_{\mathbf{k}\nu}) - |v_{\mathbf{k}\nu}|^2(\varepsilon_1-E_{\mathbf{k}\nu})}{(\varepsilon_1-E_{\mathbf{k}\nu})(-\varepsilon_2-U_2-E_{\mathbf{k}\nu})} \times \sum_{\nu'\mathbf{k}'} t_{\nu' 1} t^*_{\nu' 2}\, \mathcal{P}_{\nu'}\, \frac{|u_{\mathbf{k}'\nu'}|^2(-\varepsilon_2-U_2-E_{\mathbf{k}'\nu'}) - |v_{\mathbf{k}'\nu'}|^2(\varepsilon_1-E_{\mathbf{k}'\nu'})}{(\varepsilon_1-E_{\mathbf{k}'\nu'})(-\varepsilon_2-U_2-E_{\mathbf{k}'\nu'})}. \tag{4.36}$$

Both of these sums are the same and thus the final result is positive such that the singlet is lowered. Each of these terms is one of the cotunneling terms in Eq. (4.28) which shows that this diagrammatic formalism could also be used to calculate the second-order terms and that higher order of these terms are naturally included in the expansion Eq. (4.24).

In these examples we showed how local as well as nonlocal terms can be evaluated and also showed that the second-order terms are included and always lead to a singlet ground state. After this introduction to our diagrammatic technique we will now continue with the application to our problem. Knowledge of the structure of these terms will help us here to understand the behavior.

4.4 Results

In the previous section we defined three approaches; a simplified model reducing the lead to a single site, an effective model including Cooper-pair injection and cotunneling in Eq. (4.28) and a full fourth-order perturbation theory for the ground state using Eq. (4.24). By discussing the Cooper-pair splitter regime we will familiarize ourselves with the different transport regimes as function of the DQD parameters. We will then discuss the properties of the ground state in the $(1,1)$ sector if the superconducting gap is not larger than the on-site energies. Here we will use the perturbative approach to analyze the behavior of the model in zero-bandwidth approximation. The perturbative approach offers a possibility to interpret the results of the system in zero-bandwidth approximation, which stays valid even in regimes where the perturbation theory breaks

down. The perturbative result can then even be generalized to the wide band limit which expands the effect to more realistic systems. Here we will show the existence of a phase in which the supercurrent is carried by a triplet ground state and develop signatures of nonlocal transport. We will then also discuss a multi level DQD which is close to the situation described in the experiment of Deacon *et al.* [Dea15]. The model is solved in zero-bandwidth approximation and the results are interpreted using the ideas developed using perturbation theory.

4.4.1 Cooper-Pair-Splitter Regime

In the proposal by Choi *et al.* only a large Coulomb repulsion was assumed as they were focused more on the nonlocal spin correlations than on splitting the Cooper pair [Cho00]. They, however, found that if the superconducting gap is not large local processes also play an important role and that only for a large gap the nonlocal terms dominate. In their proposal Schroer *et al.* assumed an infinite superconducting gap to obtain an effective model describing a DQD coupled to two superconductors [Sch15a]. They, however, also show that a finite Coulomb repulsion does not invalidate the effective model but makes the expressions more complicated and also allows local Cooper pair contribution. With the experiment of Deacon *et al.* [Dea15] in mind we need to release the assumption of strong Coulomb repulsion as we especially want to understand the effect of different charging states.

The Coulomb repulsion is not essential to the effective model we introduced in section 4.3.3. In this model all further corrections are of higher orders of $t_{\nu i}/\Delta_\nu$ such that they are suppressed also by the large superconducting gap alone. In this model we also showed that the triplet decouples and the singlet gets lowered. We will see that reducing Δ_ν will enable fourth-order cotunneling processes that lower the triplet in section 4.4.2. Here those processes are suppressed.

If the superconducting gap is large the effective coupling parameters are furthermore independent of the DQD states and only depend on the coupling and lead parameters [Sch15a]. One contribution to $\tilde{t}$ was calculated as an example in section 4.3.5 and we arrived at Eq. (4.36). Each of the sums in the product is a contribution to $\tilde{t}$. For a large Δ_ν also $E_{\mathbf{k}\nu}$ is large such that we can neglect all dot energies ε_i and U_i and obtain the result by [Sch15a]. The only dependence of the Josephson current on the DQD parameters thus comes from the DQD terms in the Hamiltonian.

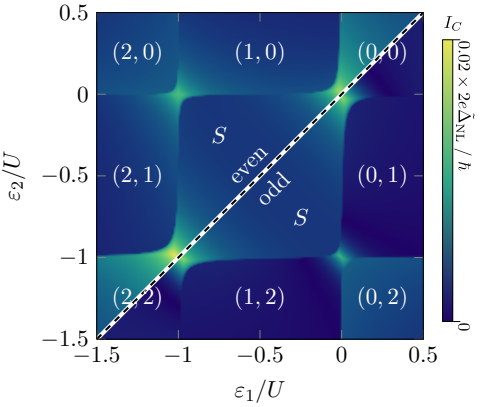

Figure 4.6: Critical current in the limit of large Δ, where $U_1 = U_2 \equiv U$, $\tilde{\Delta}_{\mathrm{L}} = 0.05U$, $\tilde{\Delta}_{\mathrm{NL}} = 0.025U$, and $\tilde{t} = 0.01U$. The plot for even and the plot for odd parity are separated by a dashed line. Electrons can leave or enter the superconducting leads only in pairs, so sequential transport is not possible and the single-particle resonances at the ground-state transitions are suppressed. In turn, if the Coulomb repulsion is large, two-particle resonances in the ground state are possible only at four points, where $\varepsilon_i = 0$ or $\varepsilon_i = -U_i$ is fulfilled simultaneously for both quantum dots $i = 1, 2$. At these points, nonlocal transport dominates. Parity has only quantitative influence. In particular, the singlet ground state (S) is stable in contrast to the situation shown in Fig. 4.2. Figure and caption reproduced from the original publication [Pro16].

It is thus vital to understand in which regime resonances between two states occur.

Each term of the Hamiltonian can lead to transport resonances. A resonance occurs if the states coupled by a process are close in energy. We will thus now discuss in which regimes each process is effective. As we are interested in the Josephson current, which is a ground-state property, we still need to understand whether the resonance involves a ground state.

For local Cooper-pair injection the QD needs to be in the empty state. After the Cooper pair is injected the QD is doubly occupied such that this resonance occurs for $\varepsilon_i = -U_i/2$. In this regime the QD ground state is the singly occupied state such that this resonance cannot be seen in the Josephson current.

As an example we will discuss the behavior of the $(1, 1)$-charge sector

which is the central state for an even number of electrons on the DQD. Nonlocal cotunneling can couple this sector only to the $(2,0)$-charge state and the $(0,2)$-charge state. These resonances are only possible for $\varepsilon_2 \mp \varepsilon_2 = U_{1/2}$. As the $(1,1)$-charge sector is only the ground state for $-U_i < \varepsilon_i < 0$ the only point where the resonance could appear is at the $(2,0)$–$(1,1)$ and the $(2,0)$–$(1,1)$ transition. Following similar arguments in the odd charge sectors we also find that cotunneling can lead to resonances at the $(0,1)$–$(1,0)$ point as well as the $(2,1)$–$(1,2)$ point in the charge diagram.

In the $(1,1)$ sector Cooper-pair injection is only possible in resonance with the $(0,0)$ state and the $(2,2)$ state. These resonances are possible at $\varepsilon_1 = -\varepsilon_2$ and $\varepsilon_1 + \varepsilon_2 = -U_1 - U_2$, respectively. The only points where these resonances are possible are thus the $(0,0)$–$(1,1)$ point and the $(2,2)$–$(1,1)$ point. Similar arguments show that in the odd charge sector at the $(2,1)$–$(1,0)$ point and the $(1,2)$–$(0,1)$ point these resonances also occur.

In Fig. 4.6 we show the resulting critical current for a DQD Josephson junction in the Cooper-pair-splitter regime. The parameters are chosen such that the local Cooper-pair amplitude is larger than the nonlocal Cooper-pair-injection amplitude and nonlocal cotunneling is even weaker. We can clearly see transitions in the ground state at $\varepsilon_i \approx -U_i$ and $\varepsilon_i \approx 0$. Because the nonlocal pair injection is larger than the cotunneling we see that in the corners of the $(1,1)$-charge sector the states coupled by Cooper-pair injection hybridize and the resonance is visible. The resonance due to nonlocal cotunneling is invisible as the resonant states are no ground states at the corresponding corner of the $(1,1)$ sector. Similar behavior can also be found for the other states in the odd charge sector. We also see that the parity has no qualitative influence on the critical current but only varies the strength.

These resonances in the even (odd) charge state are at the corner of four charge sectors of which only two comprise the resonance. This means that they only extend along the diagonal and are cut in all other directions by a ground-state transition to an odd (even) charge state. Due to this transition these resonances are well localized in the ε_1-ε_2 space. These localized features are a clear signature of nonlocal transport.

Local features can only lead to resonances between the empty and the doubly occupied QD and thus only lead to resonances along $\varepsilon_{1/2} = -U_{1/2}/2$. There the ground state is the singly occupied dot such that the resonance is between excited state of the QD. When these resonant

levels become ground states, however, we can still see the tails of this resonance or the tails of the nonlocal cotunneling resonances. These cut resonances tails might look like the resonances we will discuss in the next section but in contrast to those they are not resonant at the transition between different charge states.

4.4.2 Singlet–Triplet Ground-State Transition

To get closer to the experimental situation we have to decrease the superconducting gap Δ_ν. This regime can now be treated numerical exact in zero-bandwidth approximation which we also analyze using fourth-order perturbation theory. In Fig. 4.7, we present the results for the critical current of the DQD Josephson junction. In Fig. 4.7 (a), we plot the critical current and the total spin of the QD system in the ground state carrying the critical current depending on $U = U_1 = U_2$ and on ε_1 at fixed $\varepsilon_2 = -1.5\Delta$ in the zero-bandwidth limit. When the tunnel parity is even, $\mathcal{P} = 1$, (left panels), the total spin in the $(1,1)$ sector changes from a singlet to a triplet in a regime of finite charging energy U. This is true both in the zero-bandwidth limit (solid and dash-dotted phase boundaries) and in the wideband limit (dashed phase boundary) with no qualitative differences. In the wideband limit, the normal-state density of states in the superconducting leads is constant at all relevant QD energies. Then it affects the critical current only as a constant prefactor, which we choose to fit the zero-bandwidth results. With the tunnel couplings $|t_{\nu i}| = 0.5\Delta$, as chosen in Fig. 4.7, and a superconducting gap on the order of $\Delta = 0.1$ meV, we obtain a critical current of a few nanoamperes at the resonances. This agrees with the experimental data of Deacon *et al.* [Dea15], where aluminum electrodes were used.

In the wideband limit at very large Coulomb repulsion, $U_i \to \infty$, the parameter space is confined to what is the upper right corner of the $(1,1)$ sector in Fig. 4.2 (c) and the triplet ground state cannot be observed, consistent with earlier studies [Cho00]. In appendix G we reproduce their result and show that finite Coulomb repulsion as well as large band gap are essential for the anti ferromagnetic behavior they find. The triplet ground state can emerge if either the Coulomb repulsion or the bandwidth are not significantly larger than all other energy scales, which makes it rather the rule than the exception.

Intuitively, one could expect a singlet ground state in the $(1,1)$-charge sector, which could be justified by noting that only the nonlocal singlet

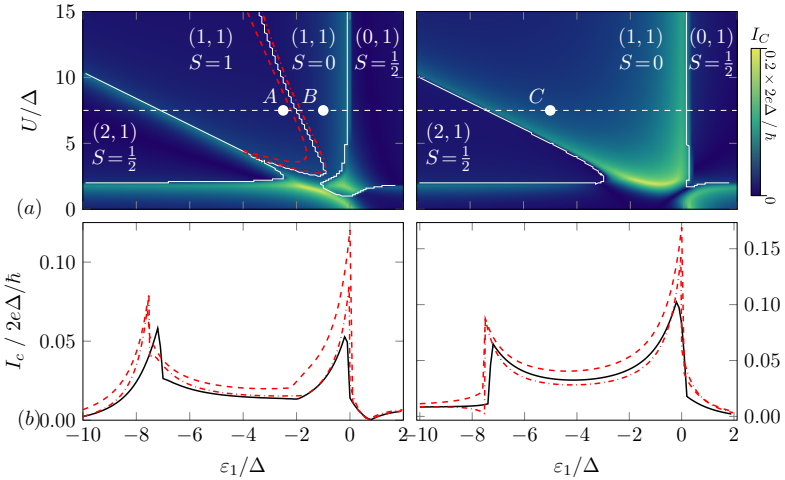

Figure 4.7: (a) Critical current and total spin of the Josephson junction depending on the on-site energy ε_1 on quantum dot 1 and on the Coulomb repulsion $U = U_1 = U_2$. Quantum dot 2 is kept at $\varepsilon_2 = -1.5\Delta$ and the tunnel couplings are $|t_{\nu i}| = 0.5\Delta$. Following the white dotted line from left to right, the quantum-dot occupation varies $(2,1) \to (1,1) \to (0,1)$. The critical current increases at each transition because the particle number fluctuates. Left: At even total tunnel parity, $\mathcal{P} = 1$, an additional ground-state transition between a nonlocal singlet and a nonlocal triplet occurs in the $(1,1)$ sector. It is caused by competing cotunneling processes between the quantum dots via the superconducting leads which give rise to an exchange interaction (text). The red lines indicate the phase boundary obtained in perturbation theory in the zero-bandwidth approximation (dash dotted) and in the wideband limit (dashed). Right: At odd total tunnel parity, $\mathcal{P} = -1$, the singlet–triplet transition is absent. (b) Cuts across the ε_1–U plane at $U = 7.5\Delta$ reveal that the shape of the current peaks depends strongly on the tunnel parity. This can be traced back to the singlet–triplet transition (text), which also immediately manifests as a kink in the critical current. Since singlet and triplet can be distinguished only by nonlocal transport, this kink constitutes immediate evidence of coherently split Cooper pairs. There is no qualitative difference between the zero-bandwidth approximation (exact result in solid black, perturbative result in dash-dotted red) and the wide-band limit (dashed red). In the wideband limit, the critical current scales with the density of states, which is chosen to agree with the result in the zero-bandwidth approximation. Figure and caption reproduced from the original publication [Pro16].

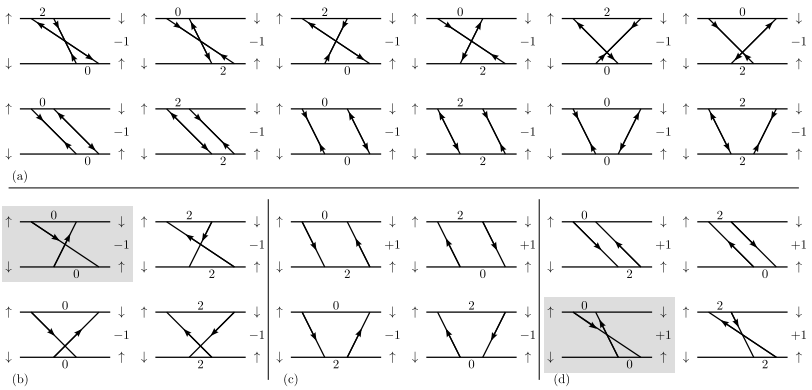

Figure 4.8: All diagrams contributing to (a) $\mathcal{M}^{\mathrm{nl}}_{\mathrm{J,se}}$ and (b)–(d) $\mathcal{M}^{\mathrm{nl}}_{\mathrm{CT,se}}$. (a) All Josephson processes have a negative overall sign and lower the singlet. (b) Cotunneling processes which lower the singlet. The process of Fig. 4.4 (a) is highlighted. (c) Higher orders of second-order cotunneling processes come with different signs but cannot lower the triplet since they are contained in the limit of large Δ. (d) Cotunneling processes which lower the triplet. The process of Fig. 4.4 (b) is highlighted. Figure and caption reproduced from the original publication [Pro16].

can tunnel into the leads to hybridize with the Cooper pairs in the s-wave superconductors and lower its energy. However, in addition to this second-order Cooper-pair tunneling process, there are genuine fourth-order terms with additional intermediate single-particle excitations in the superconducting leads. They cannot be decomposed into two Cooper-pair tunnel events and may favor the triplet ground state and thus are not present in the Cooper-pair-splitter regime.

The splitting of the nonlocal singlet and the nonlocal triplet is given by $2(E^{\mathrm{nl}}_{\mathrm{CT,se}} + E^{\mathrm{nl}}_{\mathrm{J,se}}(\Delta\varphi))$. Since the superconductors are identical, the energy corrections can be split into a matrix element $\mathcal{M}^{\mathrm{nl/loc}}_{\mathrm{CT/J,se/sc}}$ and the tunnel couplings to the leads. Because we associate the parity $\mathcal{P}$ and the phase difference $\Delta\varphi$ to the tunnel couplings $t_{\nu i}$, the matrix element is then independent of either. As demonstrated in section 4.3.5 each nonlocal process contributing to $E^{\mathrm{nl}}_{\mathrm{J,se}}(\Delta\varphi)$ can involve the same superconducting lead twice or both leads once. Summing all combinations

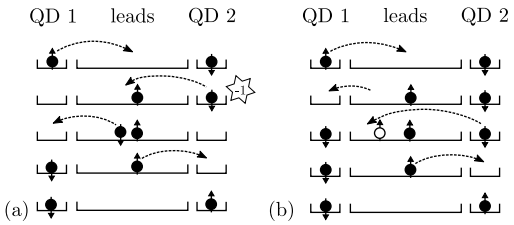

Figure 4.9: Two spin-exchange processes, which have a different overall sign and hence energetically favor (a) singlet states and (b) triplet states. Initially, one of two electrons (solid circles) with opposite spin resides on each quantum dot (left and right narrow tray). A final state with the spins swapped can be reached via intermediate virtual states (arranged top to bottom) connected by four tunnel processes (dashed arrows) between the quantum dots and the superconducting leads (wide tray). Every time the left-to-right order of two fermions is changed, a sign results. (a) If only electronlike states in the leads are involved, the two initial electrons have to be swapped. This kind of process with a negative sign energetically favors the singlet state. (b) If the exchange process involves a hole (open circle), it is possible to exchange the spins without anticommutation signs. This type of process energetically favors the triplet state. Figure and caption reproduced from the original publication [Pro16].

we obtain

$$E^{\mathrm{nl}}_{J,\mathrm{se}}(\Delta\varphi) = \mathcal{M}^{\mathrm{nl}}_{J,\mathrm{se}} \times \Big[(t_{R1}t_{R2})^2 + (t_{L1}t_{L2})^2 + 2\mathcal{P}t_{R1}t_{R2}t_{L1}t_{L2}\cos(\Delta\varphi)\Big]. \quad (4.37)$$

The matrix element can be determined using the diagrammatic technique described in section 4.3.5. All diagrams that contribute to a spin exchange are shown in Fig. 4.8. Looking at Fig. 4.8 (a) we see that all Josephson processes have the same sign such that $\mathcal{M}^{\mathrm{nl}}_{\mathrm{J,se}} > 0$ and thus $E^{\mathrm{nl}}_{\mathrm{J,se}}$ is strictly positive and favors the singlet ground state.

With the same arguments, we find

$$E^{\mathrm{nl}}_{\mathrm{CT,se}} = \mathcal{M}^{\mathrm{nl}}_{\mathrm{CT,se}}\Big[(t_{R1}t_{R2})^2 + (t_{L1}t_{L2})^2 + 2\mathcal{P}t_{R1}t_{R2}t_{L1}t_{L2}\Big] = \mathcal{M}^{\mathrm{nl}}_{\mathrm{CT,se}}(t_{R1}t_{R2} + \mathcal{P}t_{L1}t_{L2})^2, \quad (4.38)$$

so the sign of $E^{\mathrm{nl}}_{\mathrm{CT,se}}$ is determined solely by $\mathcal{M}^{\mathrm{nl}}_{\mathrm{CT,se}}$. This time, however, the perturbative analysis of $\mathcal{M}^{\mathrm{nl}}_{\mathrm{CT,se}}$ reveals that processes of both

signs exist. This can be seen by closer inspections of the diagrams in Fig. 4.8 (b)-(d). There are a few diagrams that contribute no sign and thus the corresponding processes lower the triplet. For illustration two processes are shown in detail in Fig. 4.9. Processes in which the electrons are exchanged via electronlike excitations in the leads [Fig. 4.9 (a)] have a different number of fermion-exchange signs than processes in which the electrons are exchanged via an electronlike and a holelike excitation [Fig. 4.9 (b)]. Processes involving only electronlike excitations lower the singlet while processes involving an electronlike and a holelike excitation lower the triplet.

For the existence of a triplet ground state the Josephson processes play a minor role as they are suppressed if $\Delta\varphi$ is chosen such that $\mathcal{P}\cos\Delta\varphi = -1$. The nonlocal triplet is thus driven by the sign of $E^{\mathrm{nl}}_{\mathrm{CT,se}}$, which is ultimately determined by the microscopic parameters.

The influence of Δ on the parameter space in which there may be a triplet ground state can be estimated. The matrix element of each process in the perturbative expansion is weighted by the product of the reciprocal virtual excitation energies (cf. Eq. (4.24)). In electronlike processes, which favor the singlet ground state, all virtual states involve excitations[5] on the QDs as can be seen from Fig. 4.8. They can be estimated by

$$\frac{1}{(\varepsilon_{\mathrm{DQD}}+\Delta)^2}\frac{1}{2\varepsilon_{\mathrm{DQD}}+2\Delta}, \tag{4.39}$$

where $\varepsilon_{\mathrm{DQD}}$ is a typical DQD-excitation energy. By using electronlike and holelike excitations, however, it is possible to restore the initial DQD state at the expense of two virtual excitations in the leads which corresponds to the diagrams in Fig. 4.8 (d). These processes, which favor the triplet ground state, are hence weighted by

$$\frac{1}{(\varepsilon_{\mathrm{DQD}}+\Delta)^2}\frac{1}{2\Delta}. \tag{4.40}$$

If Δ is comparable to or smaller than $\varepsilon_{\mathrm{DQD}}$, the ratio between triplet-favoring and singlet-favoring processes, $1+\varepsilon_{\mathrm{DQD}}/\Delta$, becomes large and a triplet ground state may emerge.

[5] Processes without an excitation in the middle virtual state are also present in the CPS regime. We already argued and showed for an example that these second-order terms lead to fourth-order corrections. As this can be seen in second-order perturbation theory and the triplet decouples, the singlet has to be lowered.

In general, second-order Cooper-pair tunneling restores the ground state of the superconducting leads in one intermediate virtual state, whereas the leads are excited in all three intermediate states of genuine fourth-order processes. So, genuine fourth-order processes have an additional suppression by Δ^{-1} compared to second-order Cooper-pair processes [6]. If the superconducting gap is very large compared to the other energy scales, the singlet character induced by the superconducting leads dominates and we recover the intuitive singlet ground state. This then restores the regime discussed in section 4.3.3.

The triplet ground state is absent in the regime of odd total tunnel parity, $\mathcal{P} = -1$, as can be seen in Fig. 4.7 (a), right panel. This is because different cotunneling processes interfere destructively, which reduces the magnetic exchange coupling. At negative tunnel parity, $\mathcal{P} = -1$, the parity-dependent factor in Eq. (4.38) is reduced and even vanishes in a symmetric setup, $t_{Li} = t_{Ri}$. This is different to the Josephson process. For $E^{\mathrm{nl}}_{\mathrm{J,se/sc}}(\Delta\varphi)$ this sign could be absorbed by a shift in $\Delta\varphi$ such that for Josephson processes this interference is not destructive. Without the exchange coupling, the nonlocal Josephson processes will always favor the singlet over the triplet, cf. Eq. (4.38) and Fig. 4.3 (c).

4.4.3 Peak Asymmetry and Signature of Nonlocal Transport

In the last section we established the existence of a triplet ground state and discussed their origin. This transition is inherently nonlocal. It thus offers a direct probe to identify nonlocal behavior. To identify nonlocal transport properties we will now discuss the implications for the critical current.

Figure 4.7 (b) shows the critical current as a function of ε_1 for a fixed on-site repulsion $U = 7.5\Delta$ in the $\mathcal{P} = \pm 1$ regimes. Red lines are the results from perturbation theory in the zero-bandwidth limit (dash dotted) and in the wideband limit (dashed), both of which agree with the exact results of the zero-bandwidth model (black solid). In general, the critical current is high at the charge neutrality points where the number of electrons on the QDs can fluctuate.

Both the singlet ground state and the triplet ground state can support

[6] When integrating out the momentum quantum number in the case of continuous leads, at large Δ, second-order Cooper-pair processes are independent of Δ so the relative suppression of genuine fourth-order processes may be even stronger.

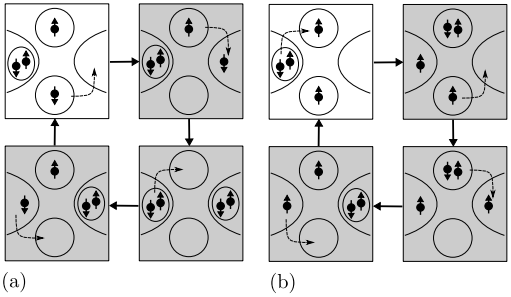

Figure 4.10: Typical Josephson transport processes via three intermediate virtual states (gray) in the $(1,1)$-charge sector. (a) In the singlet ground state, there are transport channels in which the two electrons initially localized on the DQD are absorbed as a Cooper pair in one lead. (b) In the triplet ground state (all triplets are equivalent by spin-rotation invariance and time-reversal symmetry), the electrons of the Cooper pair need to be transferred sequentially through the double quantum dot. Figure and caption reproduced from the original publication [Pro16].

a finite supercurrent. At first sight this seems to be contradicting. Processes that are blocked by the triplet have to exist in a spin exchanging and a spin conserving version. Looking at Fig. 4.8 those are all the diagrams in which the lead lines do not cross. If the lead lines do not cross the choice of the spin for the second lead line is free and a spin conserving version exists. As this involves either avoiding a spin flip via a singlet of changing the order of the creation or annihilation of a Cooper pair, the spin conserving and the spin exchanging version always differ by a sign only. For the triplet this sign leads to destructive interference whereas it is compensated by the singlet. All processes that involve no crossings of lead lines thus are possible for the singlet but blocked for the triplet. The processes with crossed lead lines are splitting the triplet and the singlet and thus also lead to transport for a triplet ground state.

In the singlet phase, the supercurrent tends to be higher because of these additional transport processes. One example of such processes is a process in which the two electrons of a Cooper pair are simultaneously added to or removed from the DQD. In the triplet ground state, this channel is blocked by the Pauli exclusion principle. At the resonance near $\varepsilon_1 = 0$ in Fig. 4.7 (b), the QD charging states $(1,1)$, $(1,0)$, $(0,1)$, and $(0,0)$ are almost degenerate so this type of transport is particularly strong

and in the singlet ground state the supercurrent is primarily carried by the process shown in Fig. 4.10 (a).

Following the above arguments and looking at the diagrams in Fig. 4.8 we see that there is no fourth-order transport process in the triplet ground state involving the $(0,0)$-charging state [7]. At the other resonance, however, $\varepsilon_1 \approx -U_1$, a Josephson process involving the almost-degenerate QD states $(1,1)$, $(1,0)$, $(2,1)$, and $(2,0)$ does exist in the triplet ground state. This transport process is depicted in Fig. 4.10 (b). So with increasing ε_1 in Fig. 4.7 (b), the singlet ground state has resonances both at the $(2,1)$–$(1,1)$ transition and at the $(1,1)$–$(0,1)$ transition but the triplet ground state has only one resonance at the $(2,1)$–$(1,1)$ transition. Hence, at even parity, with increasing ε_1 the critical current decreases in the $(1,1)$ sector as long as the system is still in the triplet ground state. Only once the ground state switches to a singlet, which happens close to the $(1,1)$–$(0,1)$ transition in Fig. 4.7 (a), the critical current rises again, producing a notable asymmetry between the resonance peaks. At odd parity, there is no asymmetry because the ground state remains a singlet throughout the entire $(1,1)$ sector.

We emphasize that the singlet–triplet transition of the ground state in the $(1,1)$ sector, realized in a large parameter window, leads to a kink in the critical current as a function of ε_2. This kink appears because, in the singlet phase, different processes contribute to the critical current compared to the triplet phase and, hence, the dependency on the on-site energies changes across the singlet–triplet transition. Since the distinction between triplet and singlet phases results from phase-coherent and nonlocal exchange, its observation in the critical current is a clear sign of coherent nonlocal Cooper-pair transport.

At odd tunnel parity, $\mathcal{P} = -1$, there is no singlet–triplet transition and hence no signature of nonlocal transport in the critical current. The other way around, if two neighboring resonance peaks belonging to the same level of a QD decay symmetrically in the off resonant regime between them, the level has odd parity. An asymmetric decay may be caused by a singlet–triplet transition and indicates even parity.

[7] It is helpful to consider the equivalent behavior of the fully-polarized triplet.

4.5 Multilevel Quantum Dot

In our discussion in this chapter we discussed several ways how different processes influence the behavior. We discussed how spin-exchange processes might split singlet and triplets in the $(1,1)$-charge sector and showed that these processes only split the ground state for negative tunnel parity. This tunnel parity is a property of the orbital level used to define our single level impurity. For different levels this parity might differ.

In the experiment by Deacon *et al.* [Dea15] the transition between several charging states is observed. This might indicate that several orbital levels are involved. These orbital levels might have a different tunneling parity. In order to make contact to the experiments we include one extra level in the model, e.g., on QD 2. In this way, we can study the evolution of the critical current along four consecutive resonances by continuously tuning ε_2. This scenario requires the substitution of H_2 in Eq. (4.13) by

$$H_2 = \varepsilon_2 d^\dagger_{21\sigma} d_{21\sigma} + (\varepsilon_2 + \delta) d^\dagger_{22\sigma} d_{22\sigma} + \sum_{(i\sigma)\neq(j\rho)} U_{ij} n_{2i\sigma} n_{2j\rho}, \quad (4.41)$$

where δ is the energy separation between the QD levels, and U_{ij} the Coulomb energy coming from the interaction of the occupation of the levels i and j on the second QD. We neglect the spin-exchange interaction within QD 2. Adding it, however, would not change our results because the device is in the single-level regime, $\delta \gg U_{2i}, t$. To couple this level to the leads, we also need to include an additional tunnel coupling to Eq. (4.16). Computationally, the addition of the extra level requires to extend the 256×256 Hamiltonian matrix to a 1024×1024 matrix, which remains tractable. Taking into account that the levels are well separated, we can still define the total tunnel parity close to a resonance as within the single-level model involving only the four relevant tunnel couplings.

Choosing the measurement presented in Fig. 4 by Deacon *et al.* [Dea15] as a specific example, we observe that two neighboring resonance peaks at lower gate voltages (higher on-site energies) are clearly more symmetric than two neighboring resonances at higher gate voltages (lower on-site energies). Within our model this is expected if the two lower peaks belong to one level with odd parity and the two higher peaks belong to one level with even parity. This was the behavior shown in Fig. 4.7. Note that concerning the occupation numbers this does not agree with Deacon *et al.* [Dea15], which seems to suggest that, in total, three levels on QD 2 are involved. Nevertheless, the model is clearly capable of reproducing

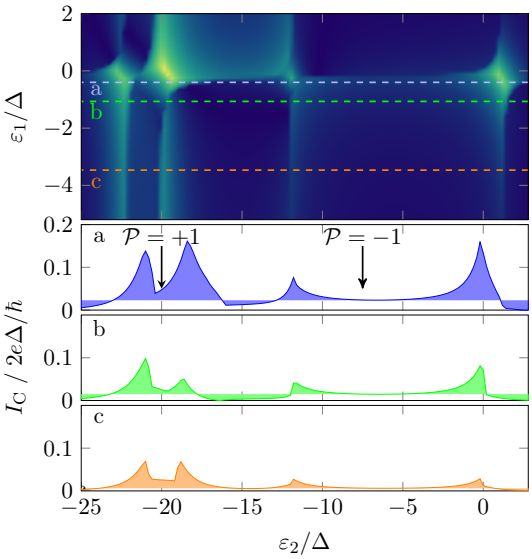

Figure 4.11: Critical current of the double-quantum-dot junction with two different levels of opposite parity on quantum dot 1. The parameters of the quantum dots are $\delta = 18.5\Delta$, $t_{R1} = t_{L1} = 0.45\Delta$, $t_{R21} = -t_{L21} = 0.45\Delta$, $t_{R22} = t_{L22} = 0.57\Delta$, $U_1 = 28\Delta$, $U_{11} = 12\Delta$, $U_{22} = 3\Delta$, and $U_{12} = 0.5\Delta$. Top panel: critical current as a function of the gate-controlled on-site energies ε_1 and ε_2. Bottom panel: Cuts at (a) $\varepsilon_1 = -0.9\Delta$, (b) $\varepsilon_1 = -1.8\Delta$, and (c) $\varepsilon_1 = -4.2\Delta$. In the absence of nonlocal transport, the three curves are expected to differ only by a constant. Instead, when approaching the resonance, $\varepsilon_1 \to 0$, the critical current grows more strongly at the peaks and less strongly between the peaks. Within our model this behavior is clearly attributable to nonlocal coherent transport and it was already observed experimentally [Dea15]. Figure and caption reproduced from the original publication [Pro16].

the qualitative features observed in the experiment when choosing the appropriate parameters.

In Fig. 4.11 we show the critical current as a function of ε_2 and ε_1 (top panel) and in the bottom panel we perform three cuts at different values of ε_1. Close to the resonance (blue and green curves), the results are basically equivalent to the results from the single-level model, once with even parity, and once with odd parity. Here, we recover the signature of nonlocal transport proposed by Deacon *et al.* [Dea15]: if there were only two independent transport channels, local transport through QD 1 and local transport through QD 2, the blue and the green curves would only differ from each other by being shifted along the vertical axis. This is because changing ε_1 would only affect the contribution of the critical current going through QD 1, which is independent from ε_2; i.e., it cannot influence the behavior of the critical current along the horizontal axis in the lower panel of Fig. 4.11. Choosing, however, an arbitrary reference point as indicated by the shaded areas, we can clearly see that there is crosstalk between ε_1 and ε_2. When QD 1 is brought closer to resonance, the resonance peaks of QD 2 grow, indicating an additional transport channel involving both QD 1 and QD 2. Moreover, there are interference effects which reduce the critical current between the two levels on QD 2, when QD 1 is brought closer to resonance. More strikingly, for values of $-\varepsilon_1 > t, U$, we observe that the resonance at $\varepsilon_2 \approx -18\Delta$, increases when effectively decoupling QD 1 (yellow curve). Now, the Cooper pairs tunnel locally through QD 2 but through two different levels. Note that this feature cannot occur in the simpler model with only two single-level QDs. Summing up, our model reproduces the signatures of nonlocal transport observed in [Dea15] even though, as we have argued in Sec. 4.3.4, the actual decomposition of the Josephson energy is more complicated than stated in their work.

4.6 Conclusion

In this chapter we discussed the setup of a double quantum dot Josephson junction. We extended the proposal by Choi *et al.* [Cho00] to contain all possible states of the double quantum dot and used the critical current to characterize the double dot Josephson junction. By extending their proposal and by focusing on the critical current this offers the possibility for a better understanding of the experiment by Deacon *et al.* [Dea15].

In our discussion we included all possible charging states of the dou-

ble quantum dot where we included on-site Coulomb interaction but neglected capacitive inter dot coupling. The tunnel coupling was described by the tunneling Hamiltonian where a possible sign of the product of all tunnel couplings defined the tunnel parity.

We discussed the system in three different approaches. In a first approach we reduced the superconductor to a single site which allowed us to diagonalize the system exactly numerically. In the second approach we derived an effective model for the double quantum dot valid for large superconducting gaps. This effective model contains second-order corrections in the tunnel coupling representing Cooper-pair injection and cotunneling of electrons between the quantum dots. In the third approach we released the need for the superconducting gaps being the largest energy scales and calculated the corrections to the ground state directly in fourth order in the tunnel coupling.

For large superconducting gaps we showed that nonlocal processes dominate the critical current. As the Coulomb interaction was finite local transport was not suppressed. These local Cooper-pair injection terms, however, only lead to resonances between states that are not the ground state such that this resonance is not visible in the critical current. The nonlocal processes can lead to resonances close to ground-state transitions. These points are localized where four charging states are nearly degenerate such that this leads to well localized transport features in the $\epsilon_1 - \epsilon_2$-plane.

When reducing the superconducting gap we found that the singlet ground state becomes unstable and a singlet–triplet transition is possible in the $(1,1)$-charging state. This singlet–triplet transition was found in the zero-bandwidth model. Using the perturbative expansion we showed that this singlet–triplet transition is driven by some nonlocal cotunneling processes. These processes are genuinely fourth order and are not higher orders of second-order corrections such that they vanish for large superconducting gap. For the existence of the triplet states the tunnel parity played a crucial role. Nonlocal processes pick up the parity sign such that nonlocal cotunneling processes interfere destructively whereas the superconducting phase difference avoids this cancellation in Josephson processes. The triplet ground state thus can only be observed for even tunnel parity.

Essential for the understanding of the triplet ground state was to interpret the behavior of the system in the zero-bandwidth approximation using a perturbative expansion of the ground-state energy. This expan-

sion allowed us to identify the relevant processes and thus to understand why processes lowering the triplet are possible. The perturbative treatment furthermore can be extended to the wide-band limit. We found that the triplet ground state is also stable in the wide-band limit. This seems to be in contrast to the findings by Choi *et al.* [Cho00] which find no singlet–triplet transition although also performing fourth-order perturbation theory. We were able to show that to suppress the triplet ground state an infinite Coulomb repulsion as well as a wide band are necessary.

The ground state of the double quantum dot Josephson junction also depends on the superconducting phase difference which makes determining the critical current more difficult. If the ground state does not change, the critical current is just given by the Josephson energy, but if the ground state changes between a singlet and a triplet, we need to look whether the maximum current is in the singlet or the triplet phase. By changing the phase the sign of the nonlocal currents also changes whereas the local current does not change sign. The critical current in the singlet and the triplet phase thus are very different. When just scanning the single level energy of one dot the other one being singly occupied we can see a singlet–triplet transition such that the critical current is not symmetric but asymmetric and develops a kink at the transition. This asymmetry and the kink are two clear signatures of a ground state transition and thus of the presence of nonlocal processes.

The ground-state transition thus makes the behavior more complicated than suggested in the simple model by Deacon *et al.* [Dea15]. In our model we see a lot of the phenomena described in their experiment. The phenomena, however, correspond to different tunnel parity. To combine these phenomena into one single model we added one level to one of the dots such that the levels have different tunnel parity. By choosing the on-site energies and the Coulomb repulsion such that the two levels are well separated we could find a set of parameters that shows all phenomena in one setup and also closely resembles the findings by Deacon *et al.* [Dea15]. Our proposal, however, underestimates the stronger transport resonance close to the single particle transitions and the total number of electrons reported in the experiment does not match our assumptions. This, however, could also indicate that another level is involved. Our findings thus motivate that the behavior could be more rich than anticipated. Despite the details of the setup being different we still think that our analysis helps understanding the qualitative features.

Chapter 5

Summary and Conclusion

In this thesis we discussed two systems in which spin played a crucial role in the interpretation of the behavior. First we discussed a quantum dot coupled to a helical edge states in which a magnetic field on the quantum dot introduces some interesting dynamics. In the second system we consider a double quantum dot coupled to two s-wave superconductors forming a double quantum dot Josephson junction.

In the first setup we considered a quantum dot in the cotunneling regime tunnel coupled to helical edge states. The quantum dot is assumed to be occupied by one electron such that we can use the Kondo model to describe the coupling. The quantum dot is described by the reduced density matrix obtained by tracing out the edge states degree of freedom. We derived a generalized master equation for the reduced density matrix. In this derivation we obtained an induced magnetic field on the quantum dot parallel to the spin quantization axis in the edge states and proportional to the bias applied to the edge state. We found that by defining an effective magnetic field including the induced and the external field the general master equation in secular approximation describes the behavior of the system very well compared to the full generalized master equation.

In general we found two interesting regimes. In the first regime the bias voltage is of the order of the effective Zeeman splitting for the quantum dot and in the second regime the induced field is of the order of the external magnetic field. In the first regime we found that the quantum dot relaxes to the ground state if the absolute value of the bias voltage is smaller than the Zeeman splitting whereas it becomes excited when exceeding this value. The state of the quantum dot was characterized by its spin polarization. If the external magnetic field is not perpendicular to the spin quantization direction of the helical edge states the amount of excitation of the quantum dot depends on the polarity of the bias applied to the edge states. The magnetic field enables spin conservation violating processes. By applying a bias to the edge state one type of

spin flip in the edge states is suppressed. The polarity of the bias thus determines whether the excitation process of the quantum dot conserves spin or not. When the external magnetic field is not perpendicular to the spin quantization direction in the helical edge states these two types of processes are not equally strong and thus we find this asymmetry in the strength of the excitation of the quantum dot and hence in its spin polarization.

In the second regime the direction of the effective magnetic field is influenced by the induced field and thus can be controlled electrically. Especially for large negative bias the direction of the effective field rotates until it antialigns with the spin quantization direction of the helical edge states. Because this regime is a high bias regime the amount of the spin polarization is completely determined by the relative orientation of effective magnetic field and spin quantization axis in the edge states. When going to very negative bias voltages the effective field eventually rotates and the excitation and relaxation process exchange their meaning such that the polarization forms a loop in the plane defined by the external magnetic field and the spin quantization direction in the helical edge states and ends up antialigned with the latter.

We also calculated transport for this setup. By transferring an electron through the quantum dot we change its spin and thus drive a backscattering current. In the second regime we found that during the rotation of the effective spin quantization axis on the dot the spin conservation violating processes lead to a strong current. When aligning the axis by a high bias, however, the backscattering current is blocked despite the large bias. In the first regime we found that due to the spin conservation violating processes transport is possible elastically and inelastically. The elastic processes contribute a constant offset to the differential conductance whereas the inelastic processes set in as soon as the absolute value of the bias exceeds the Zeeman splitting. The onset of this inelastic transport processes is asymmetric in strength and is associated with the relative orientation of the magnetic field and the spin quantization axis in the helical edge states. This asymmetry again is a consequence of the different strength of the spin conserving and spin non conserving processes.

Using full counting statistics we extended our investigation and also calculated the noise. We found that in the second regime the elastic tunneling lead to Poissonian noise whereas the inelastic processes in general lead to super-Poissonian noise. If the magnetic field is not perpendicular

to the spin quantization axis in the leads, however, for positive bias a sub-Poissonian region develops. By decomposing the dynamics into single scattering events we could show that this sub-Poissonian region is the consequence of the interplay of the change of strength in the inelastic scattering rates and the polarization of the quantum dot. By calculating the joined probability for two subsequent scattering events we could show that this sub-Poissonian behavior is associated with antibunching and the super-Poissonian behavior with bunching.

In order to obtain the behavior described here it was important that the external magnetic field was not aligned with the spin quantization axis in the helical edge states. This tilt enabled the electrons coming from the edge state to have a finite overlap with both spins on the quantum dot and thus enabled spin conservation violating processes. The relative strength of spin conserving and spin conservation violating processes was controlled by the angle between the effective field and the spin quantization axis in the edge states. The strength of a process is thus determined by a geometrical factor determined by whether spin is conserved or not and whether the process in the lead is suppressed by the applied bias voltage. Applying a bias to the edge state thus allowed to induce specific spin flip processes selectively. This then means that the amount of spin polarization can be tuned very precisely. Only for a large bias and thus strong induced magnetic field the direction changes. Then the amount of polarization is completely determined by the relative orientation of the effective field and the spin quantization direction in the edge states. This means that we are in some bounds able to manipulate the magnetization of the quantum dot electrically. Of central importance is here the external magnetic fields that tunes the relative strength of spin conserving processes and spin conservation violating processes. The behavior thus reflects the internal spin quantization direction of the helical edge state to an externally controllable field. As this orientation leaves clear signatures in the transport we cannot only manipulate the quantum dot but also use the quantum dot as a measurement probe for the internal spin quantization direction of the helical edge states.

Because helical edge states are intrinsically one dimensional and show a linear dispersion we could also include electron–electron interaction in the edge states exactly. Using bosonization we calculated the spin flip rates in our general master equation including electron–electron interaction in the edge states. The electron–electron interaction only influences the rates in the master equation and not the induced field and thus not the direc-

tion of the effective field. The qualitative behavior and the asymmetry in transport is not altered such that the interpretation does not change. In the noise we found that the electron–electron interaction leads to super-Poissonian noise that is not related to correlated scattering events. That uncorrelated events can lead to super-Poissonian noise is associated to the current being a bad measure for the total number of scattering events. This phenomenon could also be found without electron–electron interaction in the helical edges state but was enhanced by it. We showed that for positive bias we still find antibunching that is now masked by the super-Poissonian noise of the uncorrelated events by calculating the joined probability of two scattering events.

In the second system we considered a parallel double quantum dot without capacitive or direct tunnel coupling between the dots coupled to two s-wave superconductors and calculated the critical current. These setups are commonly used to find signatures of nonlocal transport of Cooper pairs. In contrast to Cooper pair splitters that separate the two electrons of a Cooper pair spatially here the two electrons are split and then again combined in a coherent manner. The supercurrent thus can show nonlocal signatures and additionally shows that after being nonlocally transported the electron pairs are still coherent.

We discussed two major regimes. In the first regime we considered the superconducting gap to be formally infinite whereas it was considered to be comparable to the other energy scales in the second regime. In contrast to previous studies we kept the Coulomb interaction finite and extended our studies to the whole range of charging states. This was motivated by recent experiments in the Tarucha group in Japan [Dea15].

In the first regime we used quasi degenerate perturbation theory to obtain second order corrections in the tunnel couplings from the quantum dots to the superconductors to the Hamiltonian. The superconducting gaps being large suppresses higher order corrections. In this regime we found that resonances due to local processes are only between states that are no ground states whereas resonances due to nonlocal processes can also involve the ground state. Because the critical current only picks up ground state properties this means that resonant features in this system always indicate nonlocal processes.

In the second regime more processes are possible because higher order tunneling processes are not suppressed anymore. In a first approach we used a simplified model in which the superconductors are represented by a single site with superconducting correlations. In this approximation the

system can be solved numerically exactly. The regime in which one electron can be found on each quantum dot is of special interest because a nonlocal singlet as well as triplets can be found there. We found that in this system a singlet–triplet transition in the ground state is possible that also leaves signatures in the critical current. Using fourth-order perturbation theory for the ground state we could identify the relevant processes leading to a triplet ground state. All of these processes are nonlocal cotunneling processes in which the electrons on the quantum dots are exchanged. Whether a triplet ground state exists crucially depends on the signs of the tunnel couplings. The perturbative result can be extended to a model in which the superconductors have a large bandwidth which also shows the singlet–triplet transition.

The nonlocal contribution to the supercurrent in the singlet and triplet ground states not only differs in strength but also in sign. This reflects that for the singlet more processes are possible and that singlet and triplets have different signs under exchange of the electrons. Together with the local contributions the current for the singlet and triplet ground state are different. A transition in the current carrying ground state thus leads to different dependences on the system parameters. When varying the single level energy of one dot the critical current shows a kink at the ground state transition. When this transition is between two transport resonances this leads to an asymmetric peak structure. The kink as well as the asymmetry of the peaks are signatures of nonlocal behavior.

Our interpretation supports the interpretation of Deacon *et al.* [Dea15] but also shows that the details can be more involved if a ground state transition is possible. Because the singlet–triplet transition in the ground state also depends on the phase difference of the superconductors and the supercurrent in each ground state depends on the phase difference differently, finding the maximal current becomes a nontrivial task. This makes the signatures of the singlet–triplet transition less apparent. In a SQUID geometry, however, one could also tune the phase difference of the superconductor and by that measure the phase dependence of the supercurrent directly in which the singlet–triplet transition should become more obvious.

Appendices

Appendix A

Diagonalization of the HLL

Solving systems of interacting fermions is not possible in general. Usually one tries to do perturbation theory to cover the interaction effects. In one dimension, however, perturbation theory does not work. It turns out that bosonization can be used in one dimension to solve some systems exactly. Spinless fermions with linear dispersion are one of the most prominent examples of the systems that can be diagonalized exactly. When introducing spin into this system one finds phenomena as spin charge separation. Then it is, however, not exactly solvable anymore. Using renormalization group methods one can still identify the relevant interactions.

The source of the problems with the spinful fermions comes from the fact that there are two kinds of left and two kinds of right movers that interact. For helical edge states there is only one kind of left and one kind of right mover. Because the interaction between the electrons is a density-density interaction the interaction is not spin sensitive. A helical edge state can thus be described by a spinless fermionic system.

We will first define the fermion operators and the electron density operator. This electron density operator then has bosonic commutation relations. After we defined these operators we will rewrite the Hamiltonian using these electron density operators thus representing it by bosonic excitations. This bosonic Hamiltonian will then be diagonalized using a Bogoliubov transform. In this section we basically follow the procedure and the calculation of von Delft and Schoeller [vD98] and thus also adopt their notation but choose a different normalization of the fields. Their notation differs from the notation used in other publications [Gra01, Gia07, Kan92a, Kan92b]. For better comparison and because it is more convenient when bosonizing the Kondo Hamiltonian we finally define fields that correspond to their conventions.

A.1 Definition of the Fermion and Boson Operators

Before we have a closer look at the Hamiltonian Eq. (2.2) we first define the fermion operators and the bosonic operators used to describe the electrons and the electron density operator. The operator describing a fermion in branch η is defined by

$$\Psi_\eta(x) = \frac{1}{\sqrt{L}} \sum_{k=-\infty}^{\infty} e^{i\eta kx} c_{k\eta}. \tag{A.1}$$

The Fock states can be grouped by the number of electron in each branch N_η. The system is then said to be in a state with $\vec{N} = (N_R, N_L)$ electrons. The ground state of these systems is the Fermi sea where all states are filled beginning from the bottom. All excitations are now defined with respect to this state. This is achieved by defining the normal ordering

$$:\bullet: \equiv \bullet - {}_0\langle\vec{N}|\bullet|\vec{N}\rangle_0, \tag{A.2}$$

where $\bullet$ is some operator and $|\vec{N}\rangle_0$ is the Fermi sea for $\vec{N}$ electrons. Using this normal ordering we can write the electron density by

$$\rho_\eta(x) \equiv \Psi_\eta^\dagger(x)\Psi_\eta(x) \tag{A.3a}$$

$$= \frac{1}{L} \sum_{k,k'=-\infty}^{\infty} e^{-i\eta(k-k')x} c_{k\eta}^\dagger c_{k'\eta} \tag{A.3b}$$

$$= \frac{\hat{N}_\eta}{L} + \frac{\sigma_\eta}{2\pi} \sum_{q>0} \frac{1}{\sqrt{n_q}} \partial_x \Big(e^{-i\eta qx} b_{q\eta}^\dagger + e^{i\eta qx} b_{q\eta} \Big), \tag{A.3c}$$

where $n_q = \frac{L}{2\pi} q$, $n_q \in \mathbb{Z}^+$, $\sigma_R = -\sigma_L = 1$ and the bosonic operators are defined by

$$b_{q\eta}^\dagger = \frac{i}{\sqrt{n_q}} \sum_{k=-\infty}^{\infty} c_{k+q\eta}^\dagger c_{k\eta}, \qquad b_{q\eta} = \frac{-i}{\sqrt{n_q}} \sum_{k=-\infty}^{\infty} c_{k-q\eta}^\dagger c_{k\eta}. \tag{A.4}$$

In this appendix and in all other appendices we set $e = \hbar = 1$. Restricting the operator to positive q allows us to define a real field

$$\tilde{\phi}_{L/R}(x) = -\sum_{n_q \in \mathbb{Z}^+} \frac{1}{\sqrt{n_q}} e^{-\alpha p/2} \Big[e^{\mp iqx} b_{qL/R} + e^{\pm iqx} b_{qL/R}^\dagger \Big], \tag{A.5}$$

where $\alpha > 0$ is a small regularization parameter. The price we pay is the additional $\hat{N}_\eta/L$ term which is a finite size term and will vanish in

the limit $L \to \infty$. The regularization parameter is effectively a high momentum cutoff which is later send to zero or set by the bandwidth. The commutation relation for $L \to \infty$ and $\alpha \to 0$ is given by

$$[\tilde{\phi}_{L/R}(x), \tilde{\phi}_{L/R}(x')] = \pm i\pi \ \mathrm{sign}(x - x'). \tag{A.6}$$

Using this operator the density operator now has a particular simple form

$$\rho_\eta(x) = \frac{\hat{N}_\eta}{L} - \frac{\sigma_\eta}{2\pi}\partial_x\tilde{\phi}_\eta(x). \tag{A.7}$$

The fermionic operators can now also be written by these bosonic fields using the bosonisation identity which is given by

$$\tilde{\Psi}_{L/R}(x) = \frac{1}{\sqrt{2\pi\alpha}} F_{L/R} e^{\mp i \frac{2\pi}{L}\hat{N}_{L/R}x} e^{-i\tilde{\phi}_{L/R}(x)}. \tag{A.8}$$

It is interesting to note that the direction of propagation is already incorporated in the definition of the field $\tilde{\phi}_{L/R}(x)$ or better in its spatial dependence. We can now start rewriting the Hamiltonian by means of these operators.

A.2 Diagonalization of the HLL

We will now use the bosonic representation of the fermion operators to diagonalize the Hamiltonian Eq. (2.2). We will though stick to a more general form where the Coulomb interaction is described using the g-ology. We start by representing the kinetic term in the bosonic fields. Then we define and bosonize the interaction terms. The resulting Hamiltonian is then diagonalized using a Bogoliubov transform.

The Coulomb interaction is a density-density interaction. Because we consider spinless fermions each density-density interaction has two types of interaction. To see this we write $\rho(x) = \rho_L(x) + \rho_R(x)$ and obtain

$$\begin{aligned}\rho(x)\rho(x') = \rho_R(x)\rho_R(x') + \rho_L(x)\rho_L(x') \\ + \rho_R(x)\rho_L(x') + \rho_L(x)\rho_R(x').\end{aligned} \tag{A.9}$$

To generalize this expression we define the terms in which densities of the same type interact to be of g_4 type whereas the mixed terms are of g_2

type. The Coulomb interaction is split into two Hamiltonians by

$$H_{\text{int}} = H_{\text{int},2} + H_{\text{int},4} \tag{A.10a}$$

$$H_{\text{int},2} = g_2 \int \mathrm{d}x \;\; \rho_L(x)\rho_R(x) \tag{A.10b}$$

$$H_{\text{int},4} = \frac{g_4}{2} \int \mathrm{d}x \sum_{\eta=L/R} \rho_\eta(x)\rho_\eta(x). \tag{A.10c}$$

The Hamiltonian defined in Eq. (2.2) can thus be obtained choosing $g_4 = g_2 = \lambda$. We now need to find a bosonic representation of the Hamiltonian.

The kinetic term is not bosonized by inserting the Bosonization identity but by showing that the excitations generated by $b_\eta^\dagger$ are eigenstates to the Hamiltonian and using that these excitations are a complete basis for the Hilbert space. Inserting the fermions from Eq. (A.1) into the kinetic part we find

$$\begin{aligned} H_{\text{kin}} &= v_F \int_{-L/2}^{L/2} \mathrm{d}x \;\; : \Big(\sum_\eta \Psi_\eta^\dagger(x)(-i\eta\partial_x)\Psi_\eta(x) \Big) : \\ &= v_F \sum_k k : c_{k,\eta}^\dagger c_{k,\eta} : . \end{aligned} \tag{A.11}$$

Using the definitions we can calculate the commutation relation

$$[H_{\text{kin}}, b_{q\eta}^\dagger] = v_F q b_{q\eta}^\dagger. \tag{A.12}$$

Using this relation we can show that

$$H_{\text{kin}} b_{q\eta}^\dagger |N\rangle_0 = (E_{0\eta} + v_F q) b_{q\eta}^\dagger |N\rangle_0 \tag{A.13}$$

where $E_{0\eta}$ is the energy contribution of the fermions in branch η of the ground state $|\vec{N}\rangle_0$. The excitations thus are eigenstates of the kinetic Hamiltonian. Because the bosonic excitations are a complete description of the Hilbert space the kinetic Hamiltonian can be represented in a bosonic basis by[1]

$$H_{\text{kin}} = v_F \sum_{q,\eta} q b_{q\eta}^\dagger b_{q\eta} + \frac{2\pi}{L}\frac{v_F}{2} \sum_\eta \hat{N}_\eta^2. \tag{A.14}$$

[1] For detail of this argument see von Delft and Schoeller [vD98].

The second term again comes from the energy of the $\vec{N}$-particle ground state[2] and is a finite size term that vanishes in the $L \to \infty$ limit. This way we managed to express the kinetic Hamiltonian, that is quadratic in the fermion operators, by bosonic operators such that the operator is also quadratic in these bosonic operators. That this is possible is not clear as each bosonic operator is already quadratic in the fermion operators. Because the interaction terms are quadratic in the electron densities, and hence also in the bosonic operators, the total Hamiltonian stays quadratic and can be diagonalized.

For the diagonalization we still need the representation of the Coulomb interaction terms which can be obtained by inserting Eq. (A.3) into Eq. (A.10). For the g_4 term we obtain

$$\begin{aligned} H_{\mathrm{int},4} &= \frac{g_4}{2} \int \mathrm{d}x \sum_{\eta=L/R} \rho_\eta(x)\rho_\eta(x) \\ &= g_4 \sum_{q>0} \frac{q}{2\pi} \Big(b^\dagger_{q\eta} b_{q\eta} + \frac{1}{2} \Big) + g_4 \hat{N}^2_\eta, \end{aligned} \tag{A.15}$$

and for the g_2 term

$$\begin{aligned} H_{\mathrm{int},2} &= g_2 \int \mathrm{d}x \;\; \rho_L(x)\rho_R(x) \\ &= -g_2 \sum_{q>0} \frac{q}{2\pi} \Big(b_{qR} b_{qL} + b^\dagger_{qR} b^\dagger_{qL} \Big) + 2g_2 \frac{\hat{N}_R \hat{N}_L}{L}. \end{aligned} \tag{A.16}$$

Here the restriction $q > 0$ is crucial as this reduces the terms a lot when performing the integral.The $q = 0$ component is included in the finite size term that vanishes for $L \to \infty$.

The total Hamiltonian is then given by

$$\begin{aligned} H_{\mathrm{HLL}} = v_F \sum_{q>0} q \Bigg[\Big(1 + \frac{g_4}{2\pi v_F} \Big) b^\dagger_{q\eta} b_{q\eta} \\ - \frac{g_2}{2\pi v_F} \Big(b_{qR} b_{qL} + b^\dagger_{qR} b^\dagger_{qL} \Big) \Bigg]. \end{aligned} \tag{A.17}$$

[2]For convenience we chose anti periodic boundary conditions. For details see von Delft and Schoeller [vD98].

This Hamiltonian can now be diagonalized using a Bogoliubov transformation. This transformation is defined by

$$B_{q1} = u_q\ b_{qL} - v_q\ b_{qR}^\dagger \tag{A.18a}$$

$$B_{q2} = -u_q\ b_{qR} + v_q\ b_{qL}^\dagger, \tag{A.18b}$$

where $u_q \equiv \cosh(\lambda_q)$ and $v_q \equiv \sinh(\lambda_q)$ ensure the bosonic commutation relations for the operators $B_{q\eta}$. Inserting these operators into Eq. (A.17) and requesting all non diagonal terms to vanish we obtain

$$\Big(1 + \frac{g_4}{2\pi v_F}\Big) 2u_q v_q = (u_q^2 + v_q^2)\frac{g_2}{2\pi v_F}, \tag{A.19}$$

which is independent of q. The resulting diagonal Hamiltonian is then

$$H_{\mathrm{HLL}} = v_F \sum_{q>0} q\Bigg[\Big(1 + \frac{g_4}{2\pi v_F}\Big)(u_q^2 + v_q^2) - \frac{g_2}{2\pi v_F} 2u_q v_q\Bigg]\big(B_{q1}^\dagger B_{q1} + B_{q2}^\dagger B_{q2}\big). \tag{A.20}$$

Using the parametrization for u_q and v_q we can solve Eq. (A.19). The resulting λ_q is found to be

$$\lambda_q = \ln\left(\sqrt[4]{\frac{2\pi v_F + g_4 + g_2}{2\pi v_F + g_4 - g_2}}\right). \tag{A.21}$$

By defining the interaction parameter K as

$$K \equiv e^{-2\lambda_q} = \sqrt{\frac{2\pi v_F + g_4 - g_2}{2\pi v_F + g_4 + g_2}} \tag{A.22}$$

the parameters u_q and v_q take a particular simple form

$$u_q = \frac{1}{2}\Big(\frac{1}{\sqrt{K}} + \sqrt{K}\Big) \qquad v_q = \frac{1}{2}\Big(\frac{1}{\sqrt{K}} - \sqrt{K}\Big). \tag{A.23}$$

In this particular model the interaction parameter K is momentum independent. Inserting these into Eq. (A.20) we find

$$H_{\mathrm{HLL}} = v \sum_{q>0} q\big(B_{q,1}^\dagger B_{q,1} + B_{q,2}^\dagger B_{q,2}\big) \tag{A.24}$$

where we defined a renormalized group velocity

$$v \equiv v_F \sqrt{\left(1 + \frac{g_4}{2\pi v_F}\right)^2 - \left(\frac{g_2}{2\pi v_F}\right)^2}. \tag{A.25}$$

The excitations $B_{q\eta}$ thus diagonalize the Hamiltonian and have again a linear dispersion relation with a renormalized group velocity v.

Finally we define the real field corresponding to the $B_{q\eta}$ by

$$\Phi_{1/2}(x) = -\sum_{q>0} \frac{e^{-\alpha q/2}}{\sqrt{n_q}} \left[e^{-iqx} B_{q1/2} + e^{iqx} B^\dagger_{q1/2} \right]. \tag{A.26}$$

In this expression one can insert the definition of the operators $B_{q\eta}$ in order to obtain a relation to the original fields

$$\Phi_{1/2}(x) = \frac{1}{2} \left(\left(\frac{1}{\sqrt{K}} \pm \sqrt{K} \right) \tilde{\phi}_R(\pm x) - \left(\frac{1}{\sqrt{K}} \mp \sqrt{K} \right) \tilde{\phi}_L(\pm x) \right). \tag{A.27}$$

Using the original commutation relation Eq. (A.6) we can calculate the commutation relation for these fields and find

$$[\Phi_{1/2}(x), \Phi_{1/2}(x')] = i\pi \ \mathrm{sign}(x - x'). \tag{A.28}$$

This commutation relation will be used later to define several canonical transformations.

To finish the diagonalization of the Hamiltonian we need to be able to represent the original fermions in terms of the bosonic eigenstates. This can be obtained by inverting this equation

$$\tilde{\phi}_{L/R}(x) = \frac{1}{2} \left(\left(\frac{1}{\sqrt{K}} \mp \sqrt{K} \right) \Phi_1(x) - \left(\frac{1}{\sqrt{K}} \pm \sqrt{K} \right) \Phi_2(-x) \right). \tag{A.29}$$

Inserting this field into the Bosonisation identity Eq. (A.8) we obtain a representation of the electrons in eigen states.

To finish this section we will give some handy definition of fields that will be needed later when bosonizing the Kondo Hamiltonian. We define two new fields

$$\varphi(x) = \Phi_1(x) + \Phi_2(-x) = \frac{1}{\sqrt{K}} \left(\tilde{\phi}_R(x) - \tilde{\phi}_L(x) \right) \tag{A.30a}$$

$$\vartheta(x) = \Phi_1(x) - \Phi_2(-x) = \sqrt{K} \left(\tilde{\phi}_R(x) + \tilde{\phi}_L(x) \right). \tag{A.30b}$$

These fields are also more directly connected to the notation of other works.

Appendix B

Correlation Functions of HLL

The general master equation is an equation of motion in which the transition rates are governed by the Fourier transforms or half sided Fourier transforms of the bath correlation functions. In this section we will give these correlation functions as well as the Fourier transforms. We will start by calculating the fundamental correlation function $\langle \Phi_\eta(x,t)\Phi_\eta(x',0)\rangle$ for edge states without bias voltage applied to them. The bias voltage will then be gauged from the statistical operator to the Hamiltonian used to describe the dynamics. The bias voltage will then contribute an oscillating phase factor to the fermion operators that shifts the Fourier transforms in frequency. We will then also calculate the Fourier transform. In this appendix, as in the other appendices, we set $e = \hbar = 1$.

B.1 Correlation Function of the Bosonic Fields $\Phi_{1/2}$

The correlation function of the fields $\Phi_{1/2}(x,t)$ have a special function as the Hamiltonian of the edge state is diagonal in these fields. Furthermore all other fields are linear combinations of these fields such that all other correlation functions can be written as a combination of these correlation functions.

The correlation function can be calculated as described in appendix H by von Delft and Schoeller [vD98]. We will sketch these calculations here and refer to their publication for the details. In the calculations first we calculate the $T = 0$ correlation function. After this is achieved we calculate the $T > 0$ correlation function using complex analysis. In this calculation a free parameter remains which is then fixed by the $T \to 0$ limit such that the $T = 0$ result is reproduced.

Because the Hamiltonian is diagonal in the bosonic operators $B_{q,\eta}$ and

we assume an equilibrium distribution we find

$$\langle B^\dagger_{q1/2} B_{q1/2}\rangle_{\rm HLL} = n_B(vp)$$
$$B_{q1/2}(t) = e^{-ivqt} B_{q1/2} \qquad B^\dagger_{q,1/2}(t) = e^{ivqt} B^\dagger_{q,1/2}, \quad \text{(B.1)}$$

where $n_B(\epsilon) = (e^{-\beta vq}-1)^{-1}$ is the Bose distribution function and $\langle \bullet \rangle_{\rm HLL}$ is the expectation value with respect to the helical Luttinger liquid (HLL) without a bias voltage applied to the edge states. Inserting the definition of the fields Eq. (A.26) we find as the basic expression

$$\langle \Phi_{1/2}(x,t)\Phi_{1/2}(0,0)\rangle_{\rm HLL} =$$
$$\frac{2\pi}{L}\sum_{q>0} \frac{e^{-\alpha q}}{q}\Big(e^{-i(x+vt)q}(1-n_B(q)) + e^{i(x+vt)q} n_B(q)\Big). \quad \text{(B.2)}$$

This expression now needs to be evaluated for $T = 0$ and $T > 0$.

For $T = 0$ the Bose function is $n_B(\epsilon) = -\theta(-q)$ such that Eq. (B.2) is easy to evaluate. We find

$$\langle \Phi_{1/2}(x,t)\Phi_{1/2}(0,0)\rangle_{{\rm HLL},T=0} = \frac{2\pi}{L}\sum_{q>0} \frac{e^{-\alpha q}}{q}\; e^{-i(x+vt)q}$$
$$= -\ln\Big(1 - e^{-i\frac{2\pi}{L}\left(x+vt-i\alpha\right)}\Big), \quad \text{(B.3)}$$

which in the limit $L \to \infty$ becomes

$$\langle \Phi_{1/2}(x,t)\Phi_{1/2}(0,0)\rangle_{{\rm HLL},T=0} \approx -\ln\left(i\frac{2\pi}{L}\Big(x+vt-i\alpha\Big)\right). \quad \text{(B.4)}$$

This will now hold as a benchmark for the result for $T > 0$ that has to reproduce this limit.

For $T > 0$ we first rewrite the sum in Eq. (B.2) using an integral and obtain

$$\langle \Phi_{1/2}(x,t)\Phi_{1/2}(0,0)\rangle_{\rm HLL} =$$
$$\int_{\frac{2\pi}{L}}^{\infty} \frac{1}{q}\left[\frac{e^{-i(x+vt-i\alpha)q}}{1-e^{-\beta vq}} + \frac{e^{i(x+vt+i\alpha)q}}{e^{\beta vq}-1}\right]{\rm d}q\,. \quad \text{(B.5)}$$

The convergence of these integrals is ensured by $\alpha > 0$. In the second term, however, this task could also be taken over by the Bose function. For $\alpha \ll \beta$ we can thus change the sign of α without making a large errors.

In this form we can now change the sign in the integration variable of the second term to obtain

$$\langle\Phi_{1/2}(x,t)\Phi_{1/2}(0,0)\rangle_{\mathrm{HLL}} = P\int_{-\infty}^{\infty}\frac{1}{q}\frac{e^{-i(x+vt-i\alpha)q}}{1-e^{-\beta vq}}\mathrm{d}q + C, \quad \text{(B.6)}$$

where the P means Cauchy's principal value. In Eq. (B.5) we set the lower boundary of the integral to $2\pi/L$ which also cuts the UV divergence. So in general these integrals have to diverge as $\ln(L/\alpha)$. By introducing Cauchy's principal value we basically ignored this behavior and assumed to be in the $L\to\infty$ limit. The divergent terms are then collected in the constant C which we fix later by comparing to the $T=0$ case.

The principal value can be evaluated using complex analysis [Arf13, Fre06]. It is expressed using the residues of the integrand. This method, however, only applies for simple singularities on the real axis. Here the singularity is of second order. Terms in the Laurent series representing higher order poles will obtain a L dependence and will be absorbed in the constant C. For the poles q_n we find

$$q_0 = 0 \qquad\qquad q_n = i\frac{2n}{\beta v} \quad \text{(B.7)}$$

and for the corresponding residues

$$\mathrm{Res}\left(\frac{1}{q}\frac{e^{-i(x+vt-i\alpha)q}}{1-e^{-\beta vq}}, q_0\right) = -i\frac{\ln\bar{y}}{2\pi} \quad \text{(B.8a)}$$

$$\mathrm{Res}\left(\frac{1}{q}\frac{e^{-i(x+vt-i\alpha)q}}{1-e^{-\beta vq}}, q_n\right) = -i\frac{\bar{y}^n}{2\pi n}, \quad \text{(B.8b)}$$

where

$$\bar{y} \equiv \exp\left(\left(x+vt-i\alpha\right)\frac{2\pi}{\beta v}\right). \quad \text{(B.9)}$$

The real part of the exponent determines whether the contour has to be closed in the upper or lower complex half plane. Using these we can evaluate the principal value and find

$$\begin{aligned}\langle\Phi_{1/2}(x,t)\Phi_{1/2}(0,0)\rangle = &-\theta(x+vt)\left(2\pi i\sum_{n=-\infty}^{-1}\frac{-i\bar{y}^n}{2\pi n} + \pi i\frac{\ln\bar{y}}{2\pi i}\right)\\ &+\theta(-x+vt)\left(2\pi i\sum_{n=1}^{\infty}\frac{-i\bar{y}^n}{2\pi n} + \pi i\frac{\ln\bar{y}}{2\pi i}\right) + C. \quad \text{(B.10)}\end{aligned}$$

The sums can be evaluated using the series representation of the logarithm via $\sum_{n=1}^{\infty}(-1)^{n-1}(-\bar{y})^n/n = \ln(1-\bar{y})$. One needs to ensure that $|\bar{y}| < 0$ which can be achieved by using $\bar{y}^{-1}$ in the second term. This yields

$$\langle\Phi_{1/2}(x,t)\Phi_{1/2}(0,0)\rangle = -\ln\left(\mathrm{sign}\Big(x+vt\Big)\Big(\bar{y}^{1/2}-\bar{y}^{-1/2}\Big)\right)+C = -\ln\left(e^{-C}\mathrm{sign}(x+vt)2\sinh\left(\frac{\pi}{\beta v}\Big(x+t-i\alpha\Big)\right)\right). \quad \text{(B.11)}$$

Choosing C appropriately we find as a result with the right $L\to\infty$ and $T\to 0$ limit

$$\langle\Phi_{1/2}(x,t)\Phi_{1/2}(0,0)\rangle_{\mathrm{HLL}} = -\ln\left(i\,\frac{\beta v}{L}\sinh\left(\frac{\pi}{\beta v}(x+v-i\alpha)\right)\right). \quad \text{(B.12)}$$

This correlation function is the correlation function for the system in equilibrium without a bias voltage applied to the edge states. With these functions we could calculate the correlation functions for $V=0$. Before calculating the lead correlation functions we first introduce the bias voltage into the system.

B.2 Bias Voltage in HLL Systems

The bias voltage is included using a transformation described by Peça *et al.* [Peç03]. The basic idea is to obtain the bias term in the statistical operator by a gauge transformation from H_{HLL} and then not apply the transformation to the statistical operator including H_{HLL} but to the operator in the correlation function. This way the bias voltage term does not appear in the statistical operator but in the propagators and the operators. This means that we can use the correlation function for the system without bias voltage applied to the edge states as described above.

In this gauge transform we use the $1/L$ terms to generate the bias term by shifting the particle numbers with respect to each other. Peça *et al.* [Peç03] argue that they gauge the zero mode. Following von Delft and Schoeller [vD98] this argumentation is somehow dangerous as the zero mode is no field in the conventional sense. We argue with shifting particle numbers rather than by gauging the zero mode. This corresponds to adding and removing particles using the Klein factors.

We assume that the interactions are only active in a small part of the edge state and that the statistics of the electrons are determined in the noninteracting part. This corresponds to the picture that the zero modes span the whole system and that only a smaller part of the system is affected by the interactions. When defining the unitary transformation we thus only consider the $1/L$ terms of H_{kin}.

To obtain a term describing the bias voltage we shift the particle numbers by $N_{L/R} \to N_{L/R} \pm N_V/2$ such that

$$N_R^2 + N_L^2 \to N_R^2 + N_L^2 + N_V(N_R - N_L) + \frac{N_V^2}{2}. \tag{B.13}$$

The second term thus has the right form for a bias term. The way N_V is introduced here it needs to be an even integer. A transformation having such an effect can be build by a series of Klein factors. We define this transformation to be U_{N_V}. The effect on the kinetic part is now

$$U_{N_V} H_{\mathrm{kin}} U_{N_V}^\dagger = H_{\mathrm{kin}} + \frac{\pi v_F}{L} N_V(\hat{N}_R - \hat{N}_L) + \mathcal{C}, \tag{B.14}$$

where $\mathcal{C}$ is a constant. The bias term in the statistical operator is defined to be $\hat{V} = V/2\ (\hat{N}_R - \hat{N}_L)$. By choosing $N_V = LV/2\pi v_F$ we thus find

$$U_V^\dagger H_{\mathrm{kin}} U_V = H_{\mathrm{kin}} + \frac{V}{2}(\hat{N}_R - \hat{N}_L) + \mathcal{C} = H_{\mathrm{kin}} + \hat{V} + \mathcal{C}, \tag{B.15}$$

where U_V is the transformation generating the right number of electrons. As mentioned above this way only discrete values of V can be obtained. In the limit of $L \to \infty$ these values become dense. Using this transform we find that

$$U_V^\dagger \frac{e^{\beta H_V}}{Z} U_V = \frac{e^{-\beta H_{\mathrm{HLL}}}}{Z_{\mathrm{HLL}}}, \tag{B.16}$$

where $Z_{\mathrm{HLL}} \equiv \mathrm{Tr}(\exp(-\beta H_{\mathrm{HLL}}))$ and the constant $\mathcal{C}$ canceled as it appears in the nominator as well. For any operator we thus find

$$\frac{1}{Z}\mathrm{Tr}\Big(e^{-\beta H_V} e^{iHt} \hat{\mathcal{O}} e^{-iHt}\Big) = \frac{1}{Z_{\mathrm{HLL}}}\mathrm{Tr}\Big(e^{-\beta H_{\mathrm{HLL}}} e^{i(H+\hat{V})} U_V^\dagger \hat{\mathcal{O}} U_V e^{-i(H+\hat{V})}\Big), \tag{B.17}$$

where we used the cyclic property of the trace to bring the transformation U_V to the operator $\hat{\mathcal{O}}$ whose time evolution was written out. This way we managed to obtain an expression where the statistical operator is given

by the equilibrium without bias voltage applied to the edge states and an propagator in which the Hamiltonian now contains an additional bias term.

The other change is the transformation of the operator $\hat{\mathcal{O}}$ such that we have to have a closer look at the effect on our lead operators $A_\eta(t)$. To generate the imbalance between right and left movers the operator U_V is basically a series of Klein Factors which make left movers to right movers or vice versa. They thus commute with the spin flip operators $A_\pm(t)$.

To find the effect on the operator $A^z(t)$ we have to go to its bosonized representation and keep the $1/L$ terms. In the definition of A_z in Eq. (2.21) also the expectation value of J^z appears. In the bosonized form the operator can be written by

$$\begin{aligned} J^z &= \frac{1}{2}\Big(\rho_R(0) - \rho_L(0)\Big) \\ &= \frac{1}{2}\left(\frac{\hat{N}_R - \hat{N}_L}{L} + \frac{1}{2\pi\sqrt{K}}\partial_x\vartheta(x)|_{x=0}\right). \end{aligned} \tag{B.18}$$

Using this expression and we find

$$\begin{aligned} \mathrm{Tr}\left(\frac{e^{-\beta H_V}}{Z}J^z\right) &= \frac{1}{2}\mathrm{Tr}\left(\frac{e^{-\beta H_{\mathrm{HLL}}}}{Z_{\mathrm{HLL}}}\Big(\frac{\hat{N}_R - \hat{N}_L + N_V}{L} + \frac{1}{2\pi\sqrt{K}}\partial_x\vartheta(0)\Big)\right) \\ &= \frac{N_V}{2L}, \end{aligned} \tag{B.19}$$

where we used that the Hamiltonian is symmetric under exchange of $\hat{N}_R$ and $\hat{N}_L$ such that the expectation value of $\hat{N}_\eta$ does not depend on η. The $\hat{N}_R - \hat{N}_L$ thus has a vanishing expectation value. The $\theta(x)$ term changes the number of bosonic excitations such that the expectation value also vanishes.

The full bosonic representation of A_z thus is

$$A_z = \frac{\hat{N}_R - \hat{N}_L - N_V}{L} + \frac{1}{2\pi\sqrt{K}}\partial_x\vartheta(x)|_{x=0}. \tag{B.20}$$

Applying the transform U_V now we thus find

$$U_V^\dagger A_z U_V = \frac{\hat{N}_R - \hat{N}_L}{L} + \frac{1}{2\pi\sqrt{K}}\partial_x\vartheta(x)|_{x=0}. \tag{B.21}$$

The way we defined A_z in Eq. (2.21), by construction, the expectation value vanishes which holds for this expression. In the definition of Δ_S,

however, the expectation value of J^z appears. For the completeness we give this value. It can be easily calculated by inserting the right N_V into Eq. (B.19) yielding

$$\langle J^z \rangle_V = \frac{V}{4\pi v_F}, \tag{B.22}$$

where $\langle \bullet \rangle_V$ is the expectation value with respect to the HLL with bias applied to the helical edge states. Now that we gauged the bias voltage into the operators we can now express any expectation value as an expectation value of the unbiased system with bias voltage dependent operators.

B.3 Correlation Functions

Having included the bias voltage into the expressions we will now use these to calculate the correlation functions $G_{\alpha\bar{\alpha}}$ and G_{zz} using the bosonized expression. Those two functions will require two different approaches.

B.3.1 $G_{\pm\mp}(\tau)$

Here we will first show that the bias term leads to an oscillating phase factor and then use bosonization. To understand the effect we start by gauging the bias into the spin flip operators

$$G_{\nu\bar{\nu}}(t) = \mathrm{Tr}_B \left(\frac{e^{-\beta(H_{\mathrm{HLL}} - \hat{V})}}{Z} e^{iH_{\mathrm{HLL}}t} A_\nu e^{-iH_{\mathrm{HLL}}t} A_{\bar{\nu}} \right) \tag{B.23a}$$

$$= \mathrm{Tr}_B \left(\frac{e^{-\beta H_{\mathrm{HLL}}}}{Z_{\mathrm{HLL}}} e^{i(H_{\mathrm{HLL}} + \hat{V})t} A_\nu e^{-i(H_{\mathrm{HLL}} + \hat{V})t} A_{\bar{\nu}} \right), \tag{B.23b}$$

where we used that the spin flip operators are not affected by the gauge transform. The bias term now commutes with all operators but the Klein factors. The commutation relations are given by von Delft and Schoeller [vD98]

$$[\hat{N}_\eta, F_\eta^\dagger] = F_\eta^\dagger \qquad [\hat{N}_\eta, F_\eta] = -F_\eta. \tag{B.24}$$

Using these commutators we find

$$\begin{aligned} e^{i\hat{V}t} A_\nu e^{i\hat{V}t} &= \frac{J}{2\pi\alpha} e^{-i\sigma_\nu \sqrt{K}\phi(t)} e^{i\hat{V}} F_{\bar{\nu}}^\dagger F_\nu e^{i\hat{V}} \\ &= \frac{J}{2\pi\alpha} e^{-i\sigma_\nu \sqrt{K}\phi(t)} e^{-i\sigma_\nu V t}. \end{aligned} \tag{B.25}$$

Inserting this into Eq. (B.23) we find

$$G_{\nu\bar{\nu}}(t) = \frac{J^2}{4\pi^2\alpha^2} e^{-i\sigma_\nu V} \langle e^{-i\sigma_\nu\sqrt{K}\phi(t)} e^{i\sigma_\nu\sqrt{K}\phi(0)}\rangle_{\mathrm{HLL}} \tag{B.26}$$

where $x = 0$ is implied.

To evaluate this expression we need a combination of the famous Baker-Campbell-Hausdorff formula and an identity sometimes referred to as Debye-Waller factor. This factor simplifies the expectation value of the exponential of bosonic operators. In appendix C theorem 4 from [vD98], we find that for a Hamiltonian $H = \sum_n \omega_n (b_n^\dagger b_n + 1/2)$, where b_n are bosonic operators for any operator $\hat{B} = \sum_n \lambda_n b_n^\dagger + \tilde{\lambda}_n b_n$

$$\langle e^{\hat{B}}\rangle = \exp\left(\frac{1}{2}\langle \hat{B}^2\rangle\right), \tag{B.27}$$

where the expectation value is for the density matrix defined by H. This relation thus expecially is valid for the bosonic fields used to diagonalize H_{HLL}. We thus find

$$\begin{aligned}\langle e^{-i\sigma_\nu\sqrt{K}\phi(t)} e^{i\sigma_\nu\sqrt{K}\phi(0)}\rangle_{\mathrm{HLL}} \\ = \exp\left(\frac{1}{K}\Big(\langle\varphi(t)\varphi(0)\rangle_{\mathrm{HLL}} - \langle\varphi(0)^2\rangle_{\mathrm{HLL}}\Big)\right),\end{aligned} \tag{B.28}$$

where the Baker-Campbell-Hausdorff formula is used to combine the two exponentials and that $\langle\varphi(t)\varphi(t)\rangle_{\mathrm{HLL}} = \langle\varphi(0)\varphi(0)\rangle_{\mathrm{HLL}}$. By inserting the definition of $\varphi(x,t)$ from Eq. (A.30a) we find

$$\begin{aligned}\langle\varphi(t)\varphi(0)\rangle_{\mathrm{HLL}} &= \sum_{\nu=1,2} \langle\phi_\nu(t)\phi_\nu(0)\rangle_{\mathrm{HLL}} \\ &= 2\langle\phi_{1/2}(t)\phi_{1/2}(0)\rangle_{\mathrm{HLL}},\end{aligned} \tag{B.29}$$

where we used that the correlation function of the $\phi_\nu(x)$ fields does not depend on the type η. Inserting Eq. (B.12) here and inserting the result to Eq. (B.28) we find

$$G_{\nu\bar{\nu}}(t) = \frac{J^2}{\beta^2 v^2}\, e^{-i\sigma_\nu V t}\, \frac{\Big(\sin\big(a\big)\Big)^{2K}}{a^2} \left(\frac{i}{\sinh\big(ia - \frac{\pi t}{\beta}\big)}\right)^{2K}, \tag{B.30}$$

where $a = \pi\alpha/\beta v$. In the case of $K = 1$ this expression becomes independent of the regularization parameter a and gives the $1/\sinh^2(\pi t/\beta)$ dependence expected for non interacting fermions.

B.3.2 $G_{zz}(\tau)$

Because the operator A_z is given directly by one of the fields here we do not need to go the detour via the exponential but can rather calculate the correlation function directly. For the product of the two operators we find

$$A_z(t)A_z(0) = J^2\Bigg(\frac{(\hat{N}_R-\hat{N}_L)^2}{L^2} + \frac{\hat{N}_R-\hat{N}_L}{2\pi\sqrt{K}L}(\partial_x\vartheta(x,t)|_{x=0}+\partial_x\vartheta(x,0)|_{x=0}) + \frac{1}{4\pi^2K}\partial_x\partial_{x'}\vartheta(x,t)\vartheta(x',0)|_{x=x'=0}\Bigg)\Bigg), \quad \text{(B.31)}$$

where we already used that the number operators do not have any dynamics. We will first discuss the expectation values of the first two terms.

For the second term a similar argument as used previously for $\langle J^z\rangle_{\mathrm{HLL}}$ applies. The theta fields change the number of bosons and thus the expectation value has to vanish. For the first term we need to have a closer look at the expectation value for $\hat{N}_R\hat{N}_L$ and $\hat{N}_\eta^2$ because

$$(\hat{N}_R-\hat{N}_L)^2 = \hat{N}_R^2+\hat{N}_L^2-2\hat{N}_R\hat{N}_L. \quad \text{(B.32)}$$

In the Hamiltonian only the $1/L$ terms depend on $\hat{N}_{R/L}$ explicitly. Because $\hat{N}_{R/L}$ commute with the boson fields and amongst each other we just have to consider terms of the type

$$\mathrm{Tr}\left(\frac{\hat{N}_\eta}{L}\frac{e^{-\beta\pi v_F\hat{N}_\eta^2/L}}{Z_{N_\eta}}\right) \quad \text{(B.33)}$$

and

$$\mathrm{Tr}\left(\frac{\hat{N}_\eta^2}{L^2}\frac{e^{-\beta\pi v_F\hat{N}_\eta^2/L}}{Z_{N_\eta}}\right), \quad \text{(B.34)}$$

where

$$Z_{N_\eta} = \mathrm{Tr}\Big(\exp(-\beta\pi v_F\hat{N}_\eta^2/L)\Big). \quad \text{(B.35)}$$

In the limit $L\to\infty$ we can transform the sum defined by the trace into an integral such that

$$Z_{N_\eta} = L\int_0^\infty \mathrm{d}x\,\exp(-\beta\pi v_F L x^2) = \frac{1}{2}\sqrt{\frac{L}{\beta v_F}}. \quad \text{(B.36)}$$

using the same trick we find that

$$\mathrm{Tr}\left(\frac{\hat{N}_\eta}{L}\frac{e^{-\beta\pi v_F\hat{N}_\eta^2/L}}{Z_{N_\eta}}\right)=\frac{1}{\pi\sqrt{L\beta v_F}} \tag{B.37a}$$

$$\mathrm{Tr}\left(\frac{\hat{N}_\eta^2}{L^2}\frac{e^{-\beta\pi v_F\hat{N}_\eta^2/L}}{Z_{N_\eta}}\right)=\frac{1}{2\pi L\beta v_F}. \tag{B.37b}$$

Using these we find

$$\mathrm{Tr}\left(\frac{e^{-\beta H_{\mathrm{HLL}}}}{Z_{\mathrm{HLL}}}\frac{(\hat{N}_R-\hat{N}_L)^2}{L^2}\right)=\frac{\pi-2}{\pi L v_F\beta} \tag{B.38}$$

such that the first term in Eq. (B.31) vanishes in the $L\to\infty$ limit.

The correlation function is thus given by

$$G_{zz}(\tau)=\frac{J^2}{4\pi^2K}\partial_x\partial_{x'}\langle\vartheta(x-x',\tau)\vartheta(0,0)\rangle_{\mathrm{HLL}} \tag{B.39}$$

Using the definitions of Eq. (A.30) we find

$$\begin{aligned}G_{zz}(\tau)&=-\frac{J^2}{2\pi^2K}\partial_x\partial_{x'}\langle\Phi_{1/2}(x-x',\tau)\Phi_{1/2}\rangle_{\mathrm{HLL}}\\&=\frac{J^2}{\beta^2v^2K}\left(\frac{i}{\sinh\left(-\frac{\pi t}{\beta}+ia\right)}\right)^2.\end{aligned} \tag{B.40}$$

After we now have the correlation functions we still need their Fourier transforms.

B.4 Fourier Transforms of the Correlation Functions

The correlation functions in general are of the form

$$\left(\frac{i}{\sinh(ia-\tau)}\right)^\gamma, \tag{B.41}$$

where $a,\gamma>0$. To calculate the Fourier transforms and the half sided Fourier transforms we thus can stick to this expression. We will first give the expressions for the half sided Fourier transform and then continue with the Fourier transform.

The half sided Fourier transform of Eq. (B.41) can be obtained by using the binominal series. This series is also given by Eq. (C4) of Virtanen

and Recher [Vir11]. For this series representation the half sided Fourier transform can be carried out and by rewriting the result one obtains

$$\int_0^\infty e^{iz\tau}\left(\frac{i}{\sinh(ia-\tau)}\right)^\gamma \mathrm{d}\tau = \frac{2^\gamma i^{-\gamma} e^{ia\gamma}}{\gamma - iz}\ {}_2F_1\Big(\gamma, \frac{\gamma}{2} - i\frac{z}{2}, \frac{\gamma}{2} - i\frac{z}{2} + 1, e^{i2a}\Big), \quad \text{(B.42)}$$

where ${}_2F_1$ is the hypergeometric function [Abr65]. The other half sided Fourier transform can be obtained by complex conjugation and replacing $z \to -z$ such that we find

$$\int_0^\infty e^{iz\tau}\left(\frac{i}{\sinh(ia+\tau)}\right)^\gamma \mathrm{d}\tau = \frac{2^\gamma (-i)^{-\gamma} e^{-ia\gamma}}{\gamma - iz}\ {}_2F_1\Big(\gamma, \frac{\gamma}{2} - i\frac{z}{2}, \frac{\gamma}{2} - i\frac{z}{2} + 1, e^{-i2a}\Big). \quad \text{(B.43)}$$

We can thus summarize these formulas by

$$\int_0^\infty e^{iz\tau}\left(\frac{i}{\sinh(ia+\sigma\tau)}\right)^\gamma \mathrm{d}\tau = \frac{2^\gamma (-\sigma i)^{-\gamma} e^{-i\sigma a\gamma}}{\gamma - iz}\ {}_2F_1\Big(\gamma, \frac{\gamma}{2} - i\frac{z}{2}, \frac{\gamma}{2} - i\frac{z}{2} + 1, e^{-i\sigma 2a}\Big). \quad \text{(B.44)}$$

These expressions can now be applied to the half sided Fourier transforms.

In section 2.2.5 the half sided Fourier transforms have been defined by

$$F^\sigma_{\alpha\bar{\alpha}}(z) = \int_0^\infty \mathrm{d}\tau\, e^{iz\tau} G_{\alpha\bar{\alpha}}(\sigma\tau) \quad \text{(B.45a)}$$

$$F^\sigma_{zz}(z) = \int_0^\infty \mathrm{d}\tau\, e^{iz\tau} G_{zz}(\sigma\tau). \quad \text{(B.45b)}$$

The identity Eq. (B.44) can now be used to express the Half sided Fourier transforms of the lead correlation functions Eq. (B.30) and Eq. (B.40).

The resulting functions are

$$F^{\sigma}_{zz}(z) = \frac{1}{\hbar\beta}\left(\frac{\hbar J}{v}\right)^2 \frac{2}{K}\frac{e^{i2\sigma aK}}{2\pi - iz\beta}\ {}_2F_1\Big(2, 1 - i\frac{z\beta}{\pi}, 2 - i\frac{z\beta}{\pi}, e^{i2\sigma aK}\Big) \tag{B.46a}$$

$$F^{\sigma}_{\alpha\bar{\alpha}}(z) = F^{\sigma}(z - \sigma_\alpha V) \tag{B.46b}$$

$$F^{\sigma}(z) = \frac{1}{\hbar\beta}\left(\frac{\hbar J}{v}\right)\frac{(2\sin a)^2}{(2a)^2}\frac{(\sigma i)^{-2K}e^{i\sigma 2aK}}{2\pi K - iz\beta} \\ {}_2F_1\Big(2K, K - i\frac{z\beta}{\pi}, K + 1 - \frac{z\beta}{\pi}, e^{i2\sigma aK}\Big) \tag{B.46c}$$

where we used that the oscillating pre factor of $G_{\alpha\bar{\alpha}}(\tau)$ only contributes a frequency shift.

Using those half sided Fourier transforms the exact Fourier transforms can easily be expressed by

$$F(\omega) = F^{+}(\omega) + F^{-}(-\omega) \qquad F_z(\omega) = F^{+}_{zz}(\omega) + F^{-}_{z}(\omega). \tag{B.47}$$

In general we are interested in the wide band limit which corresponds to the limit $\alpha \to 0$. In this limit the expressions for the Fourier transforms can be simplified significantly.

For the case of $a = 0$ the hypergeometric functions can be rewritten using Eq. (15.1.20) from [Abr65]. Using Eq. (6.1.17) from the same publication and addition theorems we find

$$\int_{-\infty}^{\infty} \mathrm{d}\tau\, e^{i\omega\tau}\left(\frac{i}{\sinh\left(ia - \tau\right)}\right)^{\gamma} = \\ e^{\pi\omega/2}\frac{2^{\gamma}\pi^2}{\Gamma(\gamma)|\Gamma\big(1 - \frac{\gamma}{2} + \frac{i\omega}{2}\big)|^2\big(\cosh(\pi\omega) - \cos(\pi\gamma)\big)}. \tag{B.48}$$

The formula Eq. (15.1.20) from [Abr65], however, is only valid if γ is no integer. If γ is integer the hypergeometric function diverges for $a \to 0$. For the Fourier transform, however, we can use the residue theorem for integer γ to evaluate the integral and find that the integral exist an thus the divergence in the $F^{+}(\omega)$ and the $F^{-}(\omega)$ term cancel. We can use this replacement in the $a \to 0$ limit also for integer γ.

Using this formula to express the Fourier transforms we find

$$F_z(\omega) = \frac{1}{\hbar\beta}\left(\frac{\hbar J}{v}\right)^2 \frac{1}{2\pi K}\ \omega\beta\ \frac{e^{\omega\beta/2}}{\sinh(\omega\beta/2)} \tag{B.49a}$$

$$F(\omega) = \frac{1}{\hbar\beta}\left(\frac{\hbar J}{v}\right)^2 \frac{\pi\ e^{\omega\beta/2}}{\Gamma(2K)|\Gamma(1-K+u\omega\beta/2\pi)|^2(\cosh(\omega\beta)-\cos(2\pi K))}. \tag{B.49b}$$

In the noninteracting case we can use again Eq. (6.1.29) from [Abr65] and we find

$$F(\omega) = \frac{1}{\hbar\beta}\left(\frac{\hbar J}{v}\right)^2 \frac{\omega\beta}{4\pi}\frac{e^{\omega\beta/2}}{\sinh(\omega\beta/2)}. \tag{B.50}$$

Using these formulas the correlation functions needed in chapter 2 and chapter 3 can be given. In section 2.2.8 we also give the asymptotic behavior for large $|\omega\beta|$ which can be found using Sterling's formula.

Appendix C

Schrieffer–Wolff and the Kondo Hamiltonian

In the cotunneling regime the processes changing the number of electrons on the quantum dot are strongly suppressed. This is usually achieved by making the energy costs very high. In section 2 we introduced the single impurity Anderson model. In the cotunneling regime we find that $\epsilon < 0$ and $\epsilon + U > 0$. Furthermore they are much larger than $k_{\mathrm{B}}T$ and the level broadening due to the coupling to the leads. As the tunnel coupling always changes the number of electrons on the QD it increases the energy regardless of whether an electron is added or removed. Sequential tunneling processes thus are suppressed exponentially. Higher order tunneling processes, however, are only suppressed algebraically and thus can be dominant deep in the Coulomb blockade regime.

There are several methods to account for these higher order tunneling processes. Schrieffer and Wolff used a canonical transformation to obtain the Kondo model as a low energy model [Sch66]. Another approach to obtain a low energy model is presented by Hewson where he introduces a projection operator to the low energy space and then obtaining an eigenvalue problem for the low energy part only [Hew93]. In this approach the inverse of an operator is obtained by a series expansion. A similar approach for Hubbard models is also found in the literature [Fra91, Ess05]. In this thesis we make use of quasi degenerate perturbation theory as presented in an appendix of the book by Winkler [Win03]. It enables us to define a low energy space and then derive a low energy model. This approach is equivalent to the approach by Schrieffer and Wolff.

In his book Winkler presents a technique known as Löwdin partitioning. In this method a canonical transformation is used to remove the coupling in lower orders and move it to higher orders in the interaction Hamiltonian [Win03]. For this the Hamiltonian is split into a diagonalizable part H^0 and an off diagonal part H'. The resulting Hamiltonian $\tilde{H} = H^{(0)} + H^{(1)} + \cdots$ can now be decomposed into parts that have corrections of

the same order of the perturbation. Up to second order he gives for the matrix elements

$$H^{(0)}_{m,m'} = H^{0}_{m,m'} \tag{C.1a}$$

$$H^{(1)}_{m,m'} = H'_{m,m'} \tag{C.1b}$$

$$H^{(2)}_{m,m'} = \frac{1}{2}\sum_{l} H'_{m,l}H'_{l,m'}\left(\frac{1}{E_m - E_l} + \frac{1}{E_{m'} - E_l}\right), \tag{C.1c}$$

where m is the index of the low energy state $|m\rangle$, l is the index of the high energy state $|l\rangle$, $H_{m,n} = \langle m|H|n\rangle$ are the matrix elements. These expressions along with higher order terms are also used in section 4.3.2. The part of the Hamiltonian that connects the low energy states is given by $H_Z + H_{\mathrm{HLL}}$ whereas the coupling to the higher energies is given by the tunnel Hamiltonian H_T.

The separation into an interaction H' and a diagonalizable part H^0 does not restrict the interaction to terms that couple to higher orders. It may as well contain matrix elements between low energy states or high energy states among each other. If such couplings are possible also odd orders contribute.

C.1 Kondo Hamiltonian Using Perturbation Theory

Our main interest in the calculations here is to see whether or to what degree the Zeeman splitting modifies the result of other derivations [Sch66, Fra91, Hew93, Ess05] which found an isotropic Kondo model. We are interested in deriving a low energy and low temperature model. We will thus only consider excitations in the lead that are much smaller than the excitation energies of the quantum dot. In this regime the states with excitations in the quantum dot can be assumed to be well separated in energy from the states in which the quantum dot is in its ground state, which allows the use of quasi degenerate perturbation theory.

In a wide-band limit, however, this separation of energies is not given strictly as the energies of the excitations in the lead can be very large. The processes discussed here are only possible close to the Fermi-energy. In the vicinity of the Fermi-energy the energy of the excitations in the lead can be neglected in comparison to the energies of the excitations on the quantum dot. We thus restrict the summation over the states in the lead to the states close to the Fermi-energy. By restricting the behavior to the

vicinity of the Fermi-energy we thus achieve the necessary assumptions needed for the application of quasi degenerate perturbation theory.

Some remark on the lead operators is, however, in place as the interaction in the lead cannot be treated perturbatively. When allowing interactions amongst the high energy excitations we basically include the perturbative expansions for the interaction in the general scheme which has to fail for $1D$ electrons. The proper way would be to use a bosonic basis instead of the fermionic for the lead part instead and rewrite the tunnel operator accordingly. The main difference, however, would be that the sum over these bosonic states would be weighted by the by different energies of the corresponding excitations in the lead in the denominator. Being close to the Fermi-energy we ignore these contributions such that this weighting does not appear. We thus can ignore whether the interaction was mediated by bosonic or fermionic excitations. We will thus use the fermionic formulation of the tunneling here and insert the bosonic field later when bosonizing the resulting model.

We choose the diagonal part $H_0 = H_{QD} + H_{\mathrm{HLL}}$ and the interaction $H' = H_Z + H_T$. In this formulation the tunneling operator couples low and high energy states whereas the Zeeman Hamiltonian also couples the states in one energy block amongst each other. Inserting these Hamiltonians into Eq. (C.1) we find

$$H^{(0)}_{m,m'} = \delta_{m,m'}\epsilon_m + H_{HLL} \tag{C.2a}$$

$$H^{(1)}_{m,m'} = \langle m|H_Z|m'\rangle \tag{C.2b}$$

$$H^{(2)}_{\uparrow,\downarrow} = -\frac{|t|^2}{L}\sum_{k,k'} c^\dagger_{k\downarrow}c_{k'\uparrow}d^\dagger_\uparrow d_\downarrow\left(\frac{1}{\epsilon-\epsilon_s}+\frac{1}{\epsilon}\right) \tag{C.2c}$$

$$H^{(2)}_{\downarrow,\uparrow} = -\frac{|t|^2}{L}\sum_{k,k'} c^\dagger_{k\uparrow}c_{k'\downarrow}d^\dagger_\downarrow d_\uparrow\left(\frac{1}{\epsilon-\epsilon_s}+\frac{1}{\epsilon}\right) \tag{C.2d}$$

$$H^{(2)}_{\uparrow,\uparrow} = \frac{|t|^2}{L}\sum_{k,k'}\left(c^\dagger_{k\downarrow}d_\downarrow d^\dagger_\downarrow c_{k'\downarrow}\frac{1}{\epsilon-\epsilon_s} + d^\dagger_\uparrow c_{k'\uparrow}c^\dagger_{k\uparrow}d_\uparrow\frac{1}{\epsilon}\right) \tag{C.2e}$$

$$H^{(2)}_{\downarrow,\downarrow} = \frac{|t|^2}{L}\sum_{k,k'}\left(c^\dagger_{k\uparrow}d_\uparrow d^\dagger_\uparrow c_{k'\uparrow}\frac{1}{\epsilon-\epsilon_s} + d^\dagger_\downarrow c_{k'\downarrow}c^\dagger_{k\downarrow}d_\downarrow\frac{1}{\epsilon}\right). \tag{C.2f}$$

As a next step we will have a closer look at $H^{(2)}_{\uparrow\uparrow}$ and $H^{(2)}_{\downarrow\downarrow}$. Here we bring the operator in normal ordering. In this normal ordering we can define $\hat{n}_\sigma = d^\dagger_\sigma d_\sigma$. In the subspace considered here we find $\hat{n}_\uparrow + \hat{n}_\downarrow = 1$. Using

this we obtain

$$H^{(2)}_{\uparrow\uparrow} + H^{(2)}_{\downarrow\downarrow} = \frac{|t|^2}{L}\sum_{k,k'}\Big(\hat{n}_\uparrow(c^\dagger_{k\uparrow}c_{k'\uparrow} - c^\dagger_{k\downarrow}c_{k'\downarrow})\Big(\frac{1}{\epsilon+U} - \frac{1}{\epsilon}\Big) - c^\dagger_{k\uparrow}c_{k'\uparrow}\frac{1}{\epsilon+U} - c^\dagger_{k\downarrow}c_{k'\downarrow}\frac{1}{\epsilon} + \delta_{k,k'}\frac{1}{\epsilon}\Big). \quad \text{(C.3)}$$

The sum over k and k' can be carried out. Using that $2S^z = \hat{n}_\uparrow - \hat{n}_\downarrow$, $J^z = (\Psi^\dagger_\uparrow(0)\Psi_\uparrow(0) - \Psi^\dagger_\downarrow(0)\Psi_\downarrow(0))/2$ and $\rho(x) = \sum_\sigma \Psi^\dagger_\sigma(x)\Psi_\sigma(x)$ we find that

$$H^{(2)}_{\uparrow\uparrow} + H^{(2)}_{\downarrow\downarrow} = |t|^2\Big(2S^zJ^z\Big(\frac{1}{\epsilon+U} - \frac{1}{\epsilon}\Big) - \frac{1}{2}\Big(\frac{1}{\epsilon+U} + \frac{1}{\epsilon}\Big)\rho(0) + \frac{1}{d\epsilon}\Big), \quad \text{(C.4)}$$

where d is the lattice constant. Together with the other two terms we thus have

$$H^{(2)} = |t|^2\Big(\frac{1}{\epsilon+U} - \frac{1}{\epsilon}\Big)(J^-S^+ + J^+S^- + 2J^zS^z) - \frac{|t|^2}{2}\Big(\frac{1}{\epsilon+U} + \frac{1}{\epsilon}\Big)\rho(0) \quad \text{(C.5)}$$

and a constant energy shift. By defining the Kondo parameter

$$J = |t|^2\Big(\frac{1}{\epsilon+U} - \frac{1}{\epsilon}\Big) \quad \text{(C.6)}$$

we obtain the Kondo Hamiltonian and a potential scattering term. The resulting Hamiltonians are now

$$H_K = J(J^+S^- + J^-S^+ + 2J^zs^z) \quad \text{(C.7a)}$$

$$H_{\text{pot}} = V_{\text{pot}}\rho(0), \quad \text{(C.7b)}$$

where

$$V_{\text{pot}} \equiv \frac{|t|^2}{2}\Big(\frac{1}{\epsilon+U} + \frac{1}{\epsilon}\Big) \quad \text{(C.8)}$$

is the strength of the potential impurity at $x = 0$. In this appendix, as in all appendices, we set $e = \hbar = 1$.

Here we did not assume that the Hamiltonian H^0 is diagonal and already mentioned that this introduces several further matrix elements. One

important difference to the other treatment is the additional Zeeman term that functions as a nondiagonal term here. Lookling at $H^{(3)}$ as defined by Winkler [Win03] we find that the corrections add an additional factor of $\Delta_Z/\min(\epsilon, \epsilon+U)$ to the Kondo term. As ϵ as well as $\epsilon+U$ are much larger than Δ_Z we can safely neglect these contributions.

C.2 Bosonized Kondo Hamiltonian

In order to calculate the correlation functions of the operators in the Kondo Hamiltonian we need to find the bosonic representation. The operator as presented in Eq. (2.10) is already normal ordered. We can thus add normal ordering without obtaining any additional terms. Inserting the bosonization identity Eq. (A.8) into the definition of the Kondo Hamiltonian we find

$$H_{\mathrm{K}} = \frac{J}{2\pi} : \Big(\frac{F_L^\dagger F_R}{\alpha} e^{-i\sqrt{K}\varphi(0)} S^+ + \frac{F_R^\dagger F_L}{\alpha} e^{i\sqrt{K}\varphi(0)} S^- - \frac{2}{\sqrt{K}} \partial_x \vartheta(0) S^z \Big) : \tag{C.9a}$$

$$H_{\mathrm{pot}} = -\frac{V_{\mathrm{pot}}\sqrt{K}}{2\pi} \ : \partial_x \varphi(0) :, \tag{C.9b}$$

where the $1/L$ terms in the exponent do not show up as we chose $x = 0$ and we explicitely used that the operators commute when being evaluated at the same position.

In a next step we will remove the potential term using a unitary transformation. We define this transformation by

$$U_{\mathrm{pot}} = e^{-i\frac{2}{v\sqrt{K}}\vartheta(0)}. \tag{C.10}$$

Because all commutation relations vanish when the fields are at the same position the Kondo Hamiltonian is not affected by this transformation. Applying this transformation to H_{HLL} will generate a term that can will cancel the potential term. To see this we use the commutator

$$[B_{q\eta}, \Phi_\eta(x)] = -\frac{1}{\sqrt{n_q}} e^{-\alpha q/2 + iqx} \tag{C.11}$$

and the Baker-Campbell-Hausdorff relation to show that for a generic transform $U_\lambda \equiv e^{i\lambda\Phi_\eta(x)}$ the Hamiltonian transforms as

$$U_\lambda H_{\mathrm{HLL}} U_\lambda^\dagger = H_{\mathrm{HLL}} - \lambda \frac{v}{2\pi} \partial_x \phi(x). \tag{C.12}$$

Choosing the λ as indicated above thus removes the potential scattering term.

In general one could also use the same trick to remove the J^z terms from the Kondo Hamiltonian. This is used for example by [Mac09, Tan11]. They also introduce a magnetic field to mimic the behavior of a bias voltage applied to the edge states. In our case, however, this transformation will not commute with the Zeeman field as the field is not necessarily parallel to the z axis. We thus don't remove this term but rather deal with it in the master equation.

Appendix D

Kernel of GME

In section 2.2 we derived a self-consistency equation for a density matrix. This equation contained a Kernel. The Kernel here is a superoperator, which is an operator acting on operators. In order to give a matrix representation we have to vectorize the density matrix. Here we choose

$$\rho = \begin{pmatrix} \rho_{\uparrow\uparrow} & \rho_{\downarrow\downarrow} & \rho_{\uparrow\downarrow} & \rho_{\downarrow\uparrow} \end{pmatrix}^T, \tag{D.1}$$

where the first two entries are the diagonal entries and the last two entries are the off diagonal entries. Using this vectorization we can represent the effect of the spin operators and the time propagation in Eq. (2.42) matrix form. The correlation functions then are the prefactor and the sum can be represented in a matrix. In this matrix we can distinguish entries that couple diagonal and off diagonal terms amongst each other and terms that couple those with each other. This way we can split the Kernel by

$$\mathcal{K}(\tau) = \begin{pmatrix} \mathcal{K}_{dd}(\tau) & \mathcal{K}_{do}(\tau) \\ \mathcal{K}_{od}(\tau) & \mathcal{K}_{oo}(\tau) \end{pmatrix}, \tag{D.2}$$

where o indicates off diagonal and d indicates diagonal. We find for our system

$$\mathcal{K}_{dd}(\tau) = \begin{pmatrix} e^{-i\Delta_S\tau}\mathcal{G}_{+-}(-\tau) + e^{i\Delta_S\tau}\mathcal{G}_{+-} & -e^{i\Delta_S\tau}\mathcal{G}_{-+}(\tau) + e^{i\Delta_S\tau}\mathcal{G}_{-+} \\ -e^{-i\Delta_S\tau}\mathcal{G}_{+-}(-\tau) - e^{i\Delta_S\tau}\mathcal{G}_{+-} & e^{i\Delta_S\tau}\mathcal{G}_{-+}(\tau) + e^{i\Delta_S\tau}\mathcal{G}_{-+} \end{pmatrix} \tag{D.3a}$$

$$\mathcal{K}_{do}(\tau) = \begin{pmatrix} -e^{-i\Delta_S\tau}\frac{\mathcal{G}_{-z}(\tau)+\mathcal{G}_{z-}(-\tau)}{2} & -e^{i\Delta_S\tau}\frac{\mathcal{G}_{+z}(\tau)+\mathcal{G}_{z+}(-\tau)}{2} \\ e^{-i\Delta_S\tau}\frac{\mathcal{G}_{-z}(\tau)+\mathcal{G}_{z-}(-\tau)}{2} & e^{i\Delta_S\tau}\frac{\mathcal{G}_{+z}(\tau)+\mathcal{G}_{z+}(-\tau)}{2} \end{pmatrix} \tag{D.3b}$$

$$\mathcal{K}_{od}(\tau) = \begin{pmatrix} \frac{\mathcal{G}_{z+}(-\tau) - \mathcal{G}_{+z}(\tau)}{2} - e^{-i\Delta_S\tau}\mathcal{G}_{+z}(-\tau) & \frac{\mathcal{G}_{z+}(-\tau) - \mathcal{G}_{+z}(\tau)}{2} - e^{-i\Delta_S\tau}\mathcal{G}_{z+}(\tau) \\ \frac{\mathcal{G}_{-z}(\tau) - \mathcal{G}_{z-}(-\tau)}{2} - e^{i\Delta_S\tau}\mathcal{G}_{z-}(\tau) & \frac{\mathcal{G}_{-z}(-\tau) - \mathcal{G}_{z-}(-\tau)}{2} - e^{i\Delta_S\tau}\mathcal{G}_{-z}(-\tau) \end{pmatrix} \tag{D.3c}$$

$$\mathcal{K}_{oo}(\tau) = \begin{pmatrix} \mathcal{G}_{-+}(-\tau)+\mathcal{G}_{+-}(\tau)+e^{-i\Delta_S\tau} \times \frac{\mathcal{G}_{zz}(-\tau)+\mathcal{G}_{zz}(\tau)}{2} & -(\mathcal{G}_{++}(-\tau) + \mathcal{G}_{++}(\tau)) \\ -(\mathcal{G}_{--}(-\tau) + \mathcal{G}_{--}(\tau)) & \mathcal{G}_{+-}(-\tau)+\mathcal{G}_{-+}(\tau)+e^{i\Delta_S\tau} \times \frac{\mathcal{G}_{zz}(-\tau)+\mathcal{G}_{zz}(\tau)}{2} \end{pmatrix}. \tag{D.3d}$$

In this appendix as in all appendices we set $e = \hbar = 1$. To determine the steady state we need the Laplace transform of this superoperator. This is defined by

$$\mathcal{K}(z) = \int_0^\infty \mathrm{d}\tau \; e^{iz\tau}\mathcal{K}(\tau). \tag{D.4}$$

Using the definition of the half sided Fourier transforms Eq. (2.56) and

$$\mathcal{K}(z) = \begin{pmatrix} \mathcal{K}_{dd}(z) & \mathcal{K}_{do}(z) \\ \mathcal{K}_{od}(z) & \mathcal{K}_{oo}(z) \end{pmatrix}, \tag{D.5}$$

we find

$$\mathcal{K}_{dd}(z) = \begin{pmatrix} \mathcal{F}^-_{+-}(z-\Delta_S) + \mathcal{F}^+_{+-}(z+\Delta_S) & -(\mathcal{F}^-_{-+}(z+\Delta_S) + \mathcal{F}^+_{-+}(z-\Delta_S) \\ -(\mathcal{F}^-_{+-}(z-\Delta_S) + \mathcal{F}^+_{+-}(z+\Delta_S)) & \mathcal{F}^-_{-+}(z+\Delta_S) + \mathcal{F}^+_{-+}(z-\Delta_S) \end{pmatrix} \tag{D.6a}$$

$$\mathcal{K}_{do}(z) = \begin{pmatrix} -\frac{\mathcal{F}^+_{-z}(z-\Delta_S)+\mathcal{F}^-_{z-}(z-\Delta_S)}{2} & -\frac{\mathcal{F}^+_{+z}(z+\Delta_S)+\mathcal{F}^-_{z+}(z+\Delta_S)}{2} \\ \frac{\mathcal{F}^+_{-z}(z-\Delta_S)+\mathcal{F}^-_{z-}(z-\Delta_S)}{2} & \frac{\mathcal{F}^+_{+z}(z+\Delta_S)+\mathcal{F}^-_{z+}(z+\Delta_S)}{2} \end{pmatrix} \tag{D.6b}$$

$$\mathcal{K}_{od}(z) = \begin{pmatrix} \frac{\mathcal{F}^{-}_{z+}(z) - \mathcal{F}^{+}_{+z}(z)}{2} - \mathcal{F}^{-}_{+z}(z - \Delta_S) & \mathcal{F}^{+}_{z+}(z - \Delta_S) + \frac{\mathcal{F}^{-}_{z+}(z) - \mathcal{F}^{+}_{+z}(z)}{2} \\ \frac{\mathcal{F}^{+}_{-z}(z) - \mathcal{F}^{-}_{z-}(z)}{2} - \mathcal{F}^{+}_{z-}(z + \Delta_S) & \mathcal{F}^{-}_{-z}(z + \Delta_S) + \frac{\mathcal{F}^{+}_{-z}(z) - \mathcal{F}^{-}_{z-}(z)}{2} \end{pmatrix} \tag{D.6c}$$

$$\mathcal{K}_{oo}(z) = \begin{pmatrix} \frac{\mathcal{F}^{-}_{-+}(z) + \mathcal{F}^{+}_{+-}(z)}{2} + \frac{\mathcal{F}^{-}_{zz}(z - \Delta_S) + \mathcal{F}^{+}_{zz}(z - \Delta_Z)}{2} & -(\mathcal{F}^{-}_{++}(z) + \mathcal{F}^{+}_{++}(z)) \\ -(\mathcal{F}^{-}_{--}(z) + \mathcal{F}^{+}_{--}(z)) & \frac{\mathcal{F}^{+}_{-+}(z) + \mathcal{F}^{-}_{+-}(z)}{2} + \frac{\mathcal{F}^{-}_{zz}(z + \Delta_S) + \mathcal{F}^{+}_{zz}(z + \Delta_Z)}{2} \end{pmatrix}. \tag{D.6d}$$

Noting that the Fourier transforms are defined by

$$\mathcal{F}_{kl}(\omega) = \mathcal{F}^{+}_{kl}(\omega) + \mathcal{F}^{-}_{kl}(-\omega) \tag{D.7}$$

we can see that the $\mathcal{K}_{dd}$ block can be written using Fourier transforms and directly produces the rate equation. In the secular approximation all terms containing other correlation functions than $\mathcal{F}^{\sigma}_{k\bar{k}}$ vanish such that the diagonal entries and the off diagonal entries vanish.

Appendix E

Transport Statistics and Transport Properties

The starting point for our derivation of FCS was the probability distribution $P(N,T)$ for N electrons being transferred in a time interval T. This is not directly connected to transport properties as current or noise. That the average number of electrons transferred, which is the first cumulant of $P(N,T)$, is given by the average current multiplied by T can still be understood intuitively. How the current noise is connected to $P(N,T)$ is less intuitive. We will thus show how to obtain the transport properties from the cumulants of the function $P(N,T)$. The main idea here is to exploit that the current is defined as the rate of change of electrons in the reservoir and thus the number of electrons transferred is the integral of the current.

To calculate the cumulants we use the CGF. The cumulants can conveniently obtained from $S(\chi,T)$. Using Eq. (3.2) we can easily find

$$S(\chi,T) = -\ln\left(\mathrm{Tr}\Big(\rho_0 e^{i\chi\hat{N}}\mathcal{U}(0,T)e^{-i\chi\hat{N}}\mathcal{U}(T,0)\Big)\right). \tag{E.1}$$

In this form we can check that the derivatives directly reproduce the cumulants of the distribution $P(N,T)$.

E.1 Current

From the definition of the CGF it is straightforward to show that

$$\partial_\chi S(\chi,T)|_{\chi=0} = -i\big(\langle\hat{N}(T)\rangle - \langle\hat{N}(0)\rangle\big), \tag{E.2}$$

where $\langle X(t)\rangle = \mathrm{Tr}(\rho_0 X(t))$ is the expectation value of an operator $X(t)$ in the Heisenberg picture. The current is defined as the rate of change

of the number of electrons in a reservoir. We can use this and the fundamental theorem of calculus and find

$$\partial_\chi S(\chi,T)|_{\chi=0} = -i\int_0^T \mathrm{d}\tau\,\langle\dot{\hat{N}}(\tau)\rangle = -\frac{i}{e}\int_0^T \mathrm{d}\tau\, I(\tau) \equiv -i\frac{T}{e}\bar{I}, \quad \text{(E.3)}$$

where $\bar{I}$ is the average current averaged over the time interval T. This average current is thus

$$\bar{I} = i\frac{e}{T}\,\partial_\chi S(\chi,T)|_{\chi=0}, \quad \text{(E.4)}$$

which corresponds to the definition in Eq. (3.13). For the mean value using the interpretation of the current as rate of change of the number of electrons transferred is still intuitive. To identify the current noise to be the second cumulant of the distribution will be slightly more complicated.

E.2 Current Noise

One assumption made here is particularly important in the context of noise. In the derivation of Eq. (3.2) it is explicitly assumed that the density matrix is diagonal in the number operator. This assumption is also at the heart of the master equation approach. In a way it is also at the heart of FCS as $P(N,T)$ assumes that the number of electrons is at any time well defined. We assume here that the initial state ρ_0 is diagonal in a particle number representation and thus commutes with the number operator. Using this we find

$$\partial_\chi^2 S(\chi,T)|_{\chi=0} = \big(\langle\hat{N}(T)-\hat{N}(0)\rangle\big)^2 - \langle\big(\hat{N}(T)-\hat{N}(0)\big)^2\rangle. \quad \text{(E.5)}$$

Each of these terms can now be represented by an integral over the current such that

$$\partial_\chi^2 S(\chi,T)|_{\chi=0} = \frac{1}{e^2}\int_0^T \mathrm{d}\tau \int_0^T \mathrm{d}\tau'\Big(\langle\hat{I}(\tau)\hat{I}(\tau')\rangle - \langle\hat{I}(\tau)\rangle\langle\hat{I}(\tau')\rangle\Big). \quad \text{(E.6)}$$

Defining the deviation of the current from its expectation value as $\delta\hat{I}(t) = \hat{I}(t) - \langle\hat{I}(t)\rangle$ we can rewrite this expression by

$$\partial_\chi^2 S(\chi,T)|_{\chi=0} = \frac{1}{e^2}\int_0^T \mathrm{d}\tau \int_0^T \mathrm{d}\tau'\,\langle\delta\hat{I}(\tau)\delta\hat{I}(\tau')\rangle. \quad \text{(E.7)}$$

As no term in the Hamiltonian has an explicit time dependence the correlation function will only depend on the difference of the two times τ and τ' such that

$$\partial_\chi^2 S(\chi,T)|_{\chi=0} = \frac{1}{e^2}\int_0^T \mathrm{d}\tau \int_0^T \mathrm{d}\tau' \,\langle \delta\hat{I}(\tau-\tau')\delta\hat{I}(0)\rangle. \tag{E.8}$$

Defining $s = \tau - \tau'$ this expression becomes

$$\partial_\chi^2 S(\chi,T)|_{\chi=0} = \frac{1}{e^2}\int_0^T \mathrm{d}\tau \int_{-T}^T \mathrm{d}s \;\langle \delta\hat{I}(s)\delta\hat{I}(0)\rangle. \tag{E.9}$$

Assuming that the current correlators decay faster than the time T the inner integral becomes independent of T and we can carry out the outer integral to obtain the final form for the zero frequency noise S_I

$$\partial_\chi^2 S(\chi,T)|_{\chi=0} = \frac{T}{e^2}\int_{-\infty}^{\infty} \mathrm{d}s \;\langle \delta\hat{I}(s)\delta\hat{I}(0)\rangle \equiv \frac{T}{e^2} S_I. \tag{E.10}$$

A simple calculation then restores the form of the definition in Eq. (3.13)

$$S_I = \frac{e^2}{T}\frac{\partial^2}{\partial\chi^2} S(\chi,T). \tag{E.11}$$

By interpreting the current as rate of change of the number of particles in the reservoir we could show that the cumulants that can be obtained by the derivatives of $S(\chi,T)$ are connected to the transport properties by Eq. (3.13).

Appendix F

Perturbation Theory for Superoperators

In section 3.2 we used the analytical properties of the eigenvalue with the lowest real part of the Liouvillian $\Lambda_0(\chi)$ to calculate the transport properties. We thus need a expansion of Λ_0 in χ up to second order. As the Liouvillian is not Hermitian and the dependence on the counting field is not Hermitian we will carefully repeat the derivation of the perturbative expression here. We follow the derivation given in [Sak09] and check that all the steps also work for non-Hermitian operators.

In section 3.1.1 we already argued that Λ_0 is the eigenvalue corresponding to the steady state. We also argued that for $\chi = 0$ the right eigenvector is the steady state density matrix which has no dynamics and that the left eigenvector is the trace which is conserved. The left and the right eigenvectors are defined to be $\langle\tilde{\phi}_0(\chi)|$ and $|\phi_0(\chi)\rangle$. Using these eigenvectors we defined the projector onto the unperturbed state $\mathcal{P} = |\tilde{\phi}_0\rangle\langle\phi_0|$ and the projector onto the complement $\mathcal{Q} = \mathbb{1} - \mathcal{P}$, where dropping the argument in the eigenstates implies $\chi = 0$.

The starting point for the perturbative treatment is decomposing the eigenvalue problem by splitting the perturbation and the unperturbed part by

$$\big(\mathcal{L}(0) + \tilde{\mathcal{L}}(\chi)\big)|\phi_0(\chi)\rangle = \big(\Lambda_0(0) + \Delta(\chi)\big)|\phi_0(\chi)\rangle, \tag{F.1}$$

where $\tilde{\mathcal{L}}(\chi)$ and $\Delta(\chi)$ are the deviations from the unperturbed state. Multiplying this equation from the left by $\langle\tilde{\phi}_0|$ we find

$$0 = \Delta(\chi)\langle\tilde{\phi}_0|\phi_0(\chi)\rangle - \langle\tilde{\phi}_0|\tilde{\mathcal{L}}(\chi)|\phi_0(\chi)\rangle. \tag{F.2}$$

Now we expand all quantities in χ up to second order in χ

$$\mathcal{L}(\chi) = \mathcal{L}(0) + \mathcal{L}'\chi + \frac{\chi^2}{2}\mathcal{L}'' \tag{F.3a}$$

$$\Lambda_0(\chi) = \Lambda_0(0) + \chi\Lambda_0' + \frac{\chi^2}{2}\Lambda_0'' \tag{F.3b}$$

$$|\phi_0(\chi)\rangle = |\phi_0(0)\rangle + \chi|\phi_0'\rangle + \frac{\chi^2}{2}|\phi_0''\rangle, \tag{F.3c}$$

where the prime denotes derivatives with respect to the counting field. Inserting this into Eq. (F.2) and sorting by orders of χ we find

$$\Lambda_0' = \langle\tilde{\phi}_0|\mathcal{L}'|\phi_0\rangle \tag{F.4a}$$

$$\Lambda_0'' = 2\langle\tilde{\phi}_0|\mathcal{L}'|\phi_0'\rangle + \langle\tilde{\phi}_0|\mathcal{L}''|\phi_0\rangle - 2\Lambda_0'\langle\tilde{\phi}_0|\phi_0'\rangle. \tag{F.4b}$$

This expression already contains the final expression for Λ_0'. The expression for Λ_0'', however, still contains the first correction to the state, $|\phi_0'\rangle$. In order to eliminate this we have a closer look at Eq. (F.1). By bringing all unperturbed quantities to the right we find

$$\big(\mathcal{L}(0) - \Lambda_0(0)\big)|\phi_0(\chi)\rangle = \big(\Delta(\chi) - \tilde{\mathcal{L}}(\chi)\big)|\phi_0(\chi)\rangle. \tag{F.5}$$

It is straightforward to check that

$$\mathcal{Q}\big(\mathcal{L}(0) - \Lambda_0(0)\big)\mathcal{Q} = \mathcal{L}(0) - \Lambda_0(0). \tag{F.6}$$

This shows that $\big(\Delta(\chi)-\tilde{\mathcal{L}}(\chi)\big)|\phi_0(\chi)\rangle$ has no overlap with $|\phi_0(0)\rangle$, which is the kernel of the linear map $\mathcal{L}(0) - \Lambda_0(0)$. This means we use a pseudoinverse to isolate $|\phi_0(\chi)\rangle$ in Eq. (F.5) on the left hand side. This leads to

$$\mathcal{Q}|\phi_0(\chi)\rangle = \mathcal{Q}\frac{1}{\mathcal{L}(0) - \Lambda_0(0)}\mathcal{Q}\big(\Delta(\chi) - \tilde{\mathcal{L}}(\chi)\big)|\phi_0(\chi)\rangle, \tag{F.7}$$

where the pseudoinverse does not depend on χ and $\Delta(\chi) - \tilde{\mathcal{L}}(\chi)$ is in leading order linear in χ. This means that this equation gives a hierarchy for the expansion coefficients of $|\phi_0(\chi)\rangle$. Inserting the expansion of $|\phi_0(\chi)\rangle$ and comparing coefficients we find

$$|\phi_0'\rangle = \mathcal{Q}\frac{1}{\mathcal{L}(0) - \Lambda_0(0)}\mathcal{Q}|\mathcal{L}'|\phi_0\rangle. \tag{F.8}$$

Inserting this into Eq. (F.4) we find the final expression

$$\Lambda_0'' = \langle\tilde{\phi}_0|\mathcal{L}''|\phi_0\rangle - \langle\tilde{\phi}_0|\mathcal{L}'\mathcal{Q}\frac{2}{\mathcal{L}(0) - \Lambda_0(0)}\mathcal{Q}\mathcal{L}'|\phi_0\rangle. \tag{F.9}$$

These expressions now allow the calculations of the current and the current noise just by knowing the analytical dependence of the Liouvillian on the counting field.

Appendix G

Comparison to the Result by Choi *et al.*

In the paper by Choi *et al.* [Cho00] the same setup as in our case is considered. They find an effective model in which two spins are coupled antiferromagnetically. The different terms can be categorized using Aharonov-Bohm oscillations and superconducting phase oscillations. They assume that the Coulomb repulsion is large such that they can neglect double occupancies on the quantum dots. Furthermore they assume that the levels of the two quantum dots have the same energy ε.

We found that there is also a regime in which the coupling is ferromagnetic and we could show that this ferromagnetic regime is driven by the nonlocal cotunneling processes. To compare our result to theirs we look at these contributions in their result. We will show that in their result a wide band is essential.

The cotunneling corrections leading to a splitting of the singlet and triplet are included in their J_1. The other terms J and J_0 are higher orders of second order terms and genuine fourth order Josephson processes respectively. The diagrams for the processes contributing to the splitting of singlet and triplet are depicted in Fig. G.1. We will now decompose the result by Choi *et al.* such that we can see that it corresponds to the diagrams shown. Choi *et al.* define the Heisenberg exchange coupling parameter due to cotunneling as

$$J_1 = \frac{\Gamma^2}{\Delta} \int \frac{\mathrm{d}x\,\mathrm{d}y}{\pi^2} \frac{g(x)[f(x)+f(y)] - 2\zeta g(y)}{g(x)^2 g(y)[g(x)+g(y)][f(x)+f(y)]}, \tag{G.1}$$

where $\Gamma = \pi t^2 N(0)$, $N(0)$ is the normal state density of states for one spin at the Fermi edge, $\zeta = \varepsilon/\Delta$ is the single level energy in units of the superconducting splitting, $f(x) = \sqrt{1+x^2}$ and $g(x) = \sqrt{1+x^2}+\zeta$. The functions $f(x)$ can be identified as $E_{\mathbf{k}\nu}/\Delta_\nu$ where $x = \varepsilon_{\mathbf{k}\nu}/\Delta_\nu$. To better understand this expression for J_1 we insert

$$\zeta = \frac{1}{2}\Big((g(x)+g(y)) - (f(x)+f(y))\Big) \tag{G.2}$$

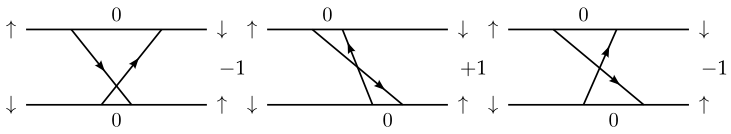

Figure G.1: Cotunneling diagrams contributing to J_1 from Choi *et al.* [Cho00]. The sign next to the diagramm is the sign contributed by the diagram. Two of the diagrams lower the singlet whereas the middle one lifts the singlet in energy.

and split the sum not separating $f(x) + f(y)$ and $g(x) + g(y)$. In most of the terms the fractions can be reduced and we obtain

$$J_1 = \frac{\Gamma^2}{\Delta} \int \frac{\mathrm{d}x\,\mathrm{d}y}{\pi^2} \left[\frac{1}{g(x)[g(x)+g(y)]g(y)} + \frac{1}{g(x)[g(x)+g(y)]g(x)} - \frac{1}{g(x)[f(x)+f(y)]g(x)} \right]. \quad \text{(G.3)}$$

This expression can be reproduced using our diagrammatic technique.

In Fig. G.1 all cotunneling diagrams splitting the singlet and the triplet not involving double occupancy of one dot are shown. All of these diagrams contain particle and/or hole excitations in the leads. These factors contribute a factor of $|u_{\mathbf{k}\nu}|^2$ and $|v_{\mathbf{k}\nu}|$ respectively. These expressions, however, do not appear in Eq. (G.3). To see this we have to have a closer look at the integral over all states. In the wide-band limit the density of states is considered to be constant such that we can also parametrize $|u_{\mathbf{k}\nu}|^2$ and $|v_{\mathbf{k}\nu}|^2$ by the energy alone. Particle and hole excitations then are connected by a change in the sign of the energy and especially

$$\int_{-\infty}^{\infty} \mathrm{d}\varepsilon_\nu\, h(|\varepsilon_\nu|)|u_{\varepsilon_\nu\nu}|^2 = \int_{-\infty}^{\infty} \mathrm{d}\varepsilon_\nu\, h(|\varepsilon_\nu|)|v_{\varepsilon_\nu\nu}|^2 \quad \text{(G.4)}$$

where $h(|\varepsilon_\nu|)$ is a function that does not depend on the sign of ε_ν. This can be seen by changing the sign of the energy and exchange the boundaries of the integral. Adding the left side to both sides of this equation and using Eq. (4.26) we then find

$$\begin{aligned} \int_{-\infty}^{\infty} \mathrm{d}\varepsilon_\nu\, h(|\varepsilon_\nu|)|u_{\varepsilon_\nu\nu}|^2 &= \frac{1}{2} \int_{-\infty}^{\infty} \mathrm{d}\varepsilon_\nu\, h(|\varepsilon_\nu|) \Big(|v_{\varepsilon_\nu\nu}|^2 + |u_{\varepsilon_\nu\nu}|^2 \Big) \\ &= \frac{1}{2} \int_{-\infty}^{\infty} \mathrm{d}\varepsilon_\nu\, h(|\varepsilon_\nu|), \end{aligned} \quad \text{(G.5)}$$

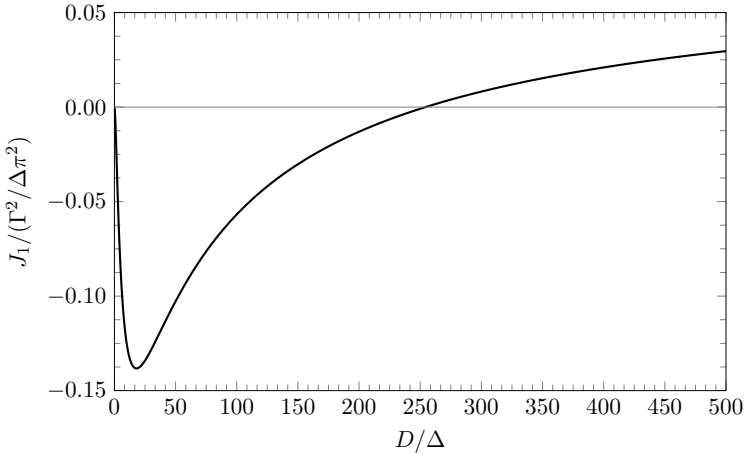

Figure G.2: Dependence of the coupling parameter J_1 from Choi *et al.* [Cho00] on a energy cutoff D for $\varepsilon = -10\Delta$. For small energies the integrand can be negative such that for small cutoff D the resulting coupling is ferromagnetic. Only if D is large enough the coupling becomes antiferromagnetic.

which works for integrals over $|v_{\varepsilon_\nu \nu}|^2$ as well. As long as the energy does not depend on the sign of the free electron energy and we integrate over all energies we can thus replace these factors by $1/2$.

When setting up the energy terms corresponding to the diagrams in Fig. G.1 we make use of the notation defined by Choi *et al.*. As ε is the same on their QDs they cannot distinguish whether the electron was removed on the first or the second QD. Because they exclude double occupancies the quantum dot can only be singly occupied or empty and thus an empty dot has to be associated with an excitation in the lead. The energy difference to the ground state of an excitation in the lead and an empty dot is $g(x)$, where $x = \varepsilon_\nu/\Delta_\nu$ is the free single particle energy parameterizing this excitation. It is, however, possible to have excitations in the lead with the dot being in the ground state. This energy difference is then given by $f(x)$. Having that in mind we can identify the terms in Eq. (G.3) to correspond to the diagrams in Fig. G.1 from left to right.

As we can reproduce their result the method used cannot be the reason why we find a triplet ground state where they have none. Looking closer at Eq. (G.3) we see that also in their expression it is not clear that the

integrand is positive as the last term has a negative sign. The middle virtual state has no excitation in the DQD such that it is only regularized by the superconductor, which we identified as one of the reasons for a triplet ground state.

To understand the influence of possible negative values in the integrand we introduce a cutoff D for the integral and calculate J_1. The result is shown in Fig. G.2. We see that for small values of the cutoff the result is a ferromagnetic model. This means that for small energies of the lead excitation the last term in Eq. (G.3) dominates. In this regime the first terms are approximately $1/\varepsilon^3$ whereas the last term is approximately $1/(\varepsilon^2\Delta)$. As $\varepsilon \gg \Delta$ we find negative values in the integrand. In the tail of the terms the second and the third term are similar and cancel each other approximately. The first term, however, will eventually overcome the negative values. This, however, demands a rather large cutoff.

When comparing the processes listed in Fig. G.1 to the processes listed in Fig. 4.8 we see that for infinite U there is one out of three spin exchange processes favoring the triplet whereas for finite U there are six out of twelve. An infinite U thus seems to suppress spin exchange processes lowering the triplet stronger than those that lower the singlet. This shows that for the antiferromagnetic Heisenberg term of Choi *et al.* [Cho00] a large bandwidth as well as infinite U are necessary. Dropping either could enable a ferromagnetic interaction.

Bibliography

[Abr65] M. Abramowitz and I. A. Stegun. *Handbook of Mathematical Functions with Formulas, Graphs, and Mathematical Tables*. Dover, New York, ninth dover printing, tenth gpo printing edition (1965).

[Aff00] I. Affleck, J.-S. Caux, and A. M. Zagoskin. *Andreev scattering and Josephson current in a one-dimensional electron liquid*. Phys. Rev. B **62** (2000), 1433–1445.

[Ale02] I. Aleiner, P. Brouwer, and L. Glazman. *Quantum effects in Coulomb blockade*. Physics Reports **358** (2002), 309–440.

[Alt97] A. Altland and M. R. Zirnbauer. *Nonstandard symmetry classes in mesoscopic normal-superconducting hybrid structures*. Phys. Rev. B **55** (1997), 1142–1161.

[Ami16] E. Amitai, R. P. Tiwari, S. Walter, T. L. Schmidt, and S. E. Nigg. *Nonlocal quantum state engineering with the Cooper pair splitter beyond the Coulomb blockade regime*. Phys. Rev. B **93** (2016), 075421.

[Arf13] G. Arfken, H. J. Weber, and F. E. Harris. *Mathematical methods for physicists*. Academic Press, Amsterdam, Heidelberg, seventh edition (2013).

[Asp82a] A. Aspect, J. Dalibard, and G. Roger. *Experimental Test of Bell's Inequalities Using Time-Varying Analyzers*. Phys. Rev. Lett. **49** (1982), 1804–1807.

[Asp82b] A. Aspect, P. Grangier, and G. Roger. *Experimental Realization of Einstein-Podolsky-Rosen-Bohm Gedankenexperiment: A New Violation of Bell's Inequalities*. Phys. Rev. Lett. **49** (1982), 91–94.

[Aus00] O. M. Auslaender, A. Yacoby, R. de Picciotto, K. W. Baldwin, L. N. Pfeiffer, and K. W. West. *Experimental Evidence for*

Resonant Tunneling in a Luttinger Liquid. Phys. Rev. Lett. **84** (2000), 1764–1767.

[Aus02] O. M. Auslaender, A. Yacoby, R. de Picciotto, K. W. Baldwin, L. N. Pfeiffer, and K. W. West. *Tunneling Spectroscopy of the Elementary Excitations in a One-Dimensional Wire*. Science **295** (2002), 825–828.

[Ave92] D. V. Averin and Y. V. Nazarov. *Macroscopic Quantum Tunneling of Charge and Co-Tunneling*. In H. Grabert and M. H. Devoret, editors, *Single Charge Tunneling - Coulomb Blockade Phenomenain Nanostructures*. Plenum Press, London, 217–248 (1992).

[Bag03] D. A. Bagrets and Y. V. Nazarov. *Full counting statistics of charge transfer in Coulomb blockade systems*. Phys. Rev. B **67** (2003), 085316.

[Bai88] M. N. Baibich, J. M. Broto, A. Fert, F. N. Van Dau, F. Petroff, P. Etienne, G. Creuzet, A. Friederich, and J. Chazelas. *Giant Magnetoresistance of (001)Fe/(001)Cr Magnetic Superlattices*. Phys. Rev. Lett. **61** (1988), 2472–2475.

[Bee91a] C. Beenakker and H. van Houten. *Quantum Transport in Semiconductor Nanostructures*. In H. Ehrenreich and D. Turnbull, editors, *Semiconductor Heterostructures and Nanostructures*, volume 44 of *Solid State Physics*. Academic Press, 1–228 (1991).

[Bee91b] C. W. J. Beenakker. *Theory of Coulomb-blockade oscillations in the conductance of a quantum dot*. Phys. Rev. B **44** (1991), 1646–1656.

[Bee03] R. Beerends, H. Morsche, J. van den Berg, and E. van de Vrie. *Fourier and Laplace transforms*. Cambridge Univ. Press, Cambridge (2003).

[Bel03] W. Belzig. *Full Counting Statistics of Superconductor–Normal-Metal Heterostructures*. In Y. V. Nazarov, editor, *Quantum noise in mesoscopic physics*, volume 97 of *NATO Science Series II. Mathematics, Physics and Chemistry*. Kluvert Academic Publishers Dordrecht, 463–496 (2003).

[Bel05] W. Belzig. *Full Counting Statistics in Quantum Contacts*. In K. Busch, A. Powell, C. Röthig, G. Schön, and J. Weissmüller, editors, *CFN Lectures on Functional Nanostructures Vol 1.*, Lecture Notes in Physics. Springer-Verlag Berlin Heidelberg, 123–143 (2005).

[Ben02] C. Bena, S. Vishveshwara, L. Balents, and M. P. A. Fisher. *Quantum Entanglement in Carbon Nanotubes*. Phys. Rev. Lett. **89** (2002), 037901.

[Ber06a] B. A. Bernevig, T. L. Hughes, and S.-C. Zhang. *Quantum Spin Hall Effect and Topological Phase Transition in HgTe Quantum Wells*. Science **314** (2006), 1757–1761.

[Ber06b] B. A. Bernevig and S.-C. Zhang. *Quantum Spin Hall Effect*. Phys. Rev. Lett. **96** (2006), 106802.

[Ber07] F. S. Bergeret, A. L. Yeyati, and A. Martín-Rodero. *Josephson effect through a quantum dot array*. Phys. Rev. B **76** (2007), 174510.

[Bin89] G. Binasch, P. Grünberg, F. Saurenbach, and W. Zinn. *Enhanced magnetoresistance in layered magnetic structures with antiferromagnetic interlayer exchange*. Phys. Rev. B **39** (1989), 4828–4830.

[Bla00] Y. Blanter and M. Büttiker. *Shot noise in mesoscopic conductors*. Physics Reports **336** (2000), 1–166.

[Blu96] K. Blum. *Density matrix theory and applications*. Physics of atoms and molecules. Plenum Press, New York, 2. ed edition (1996).

[Bra03] B. Bransden and C. Joachain. *Physics of Atoms and Molecules*. Pearson, 2nd edition (2003).

[Bra04] M. Braun, J. König, and J. Martinek. *Theory of transport through quantum-dot spin valves in the weak-coupling regime*. Phys. Rev. B **70** (2004), 195345.

[Bra13] B. Braunecker, P. Burset, and A. Levy Yeyati. *Entanglement Detection from Conductance Measurements in Carbon Nanotube Cooper Pair Splitters*. Phys. Rev. Lett. **111** (2013), 136806.

[Bre02] H.-P. Breuer and F. Petruccione. *The theory of open quantum systems*. Oxford Univ. Press, Oxford (2002).

[Bru04] H. Bruus and K. Flensberg. *Many-Body Quantum Theory in Condensed Matter Physics*. Oxford University Press (2004).

[Bru12] C. Brune, A. Roth, H. Buhmann, E. M. Hankiewicz, L. W. Molenkamp, J. Maciejko, X.-L. Qi, and S.-C. Zhang. *Spin polarization of the quantum spin Hall edge states*. Nat. Phys. **8** (2012), 485–490.

[Bud12] J. C. Budich, F. Dolcini, P. Recher, and B. Trauzettel. *Phonon-Induced Backscattering in Helical Edge States*. Phys. Rev. Lett. **108** (2012), 086602.

[Bur16] P. Burset, B. Lu, H. Ebisu, Y. Asano, and Y. Tanaka. *All-electrical generation and control of odd-frequency s-wave Cooper pairs in double quantum dots*. Phys. Rev. B **93** (2016), 201402.

[Cay08] J. Cayssol. *Crossed Andreev Reflection in a Graphene Bipolar Transistor*. Phys. Rev. Lett. **100** (2008), 147001.

[Cho00] M.-S. Choi, C. Bruder, and D. Loss. *Spin-dependent Josephson current through double quantum dots and measurement of entangled electron states*. Phys. Rev. B **62** (2000), 13569–13572.

[CN09] A. H. Castro Neto, F. Guinea, N. M. R. Peres, K. S. Novoselov, and A. K. Geim. *The electronic properties of graphene*. Rev. Mod. Phys. **81** (2009), 109–162.

[Cré12] F. Crépin, J. C. Budich, F. Dolcini, P. Recher, and B. Trauzettel. *Renormalization group approach for the scattering off a single Rashba impurity in a helical liquid*. Phys. Rev. B **86** (2012), 121106.

[Dat97] S. Datta. *Electronic transport in mesoscopic systems*. Cambridge studies in semiconductor physics and microelectronic engineering. Cambridge University Press (1997).

[Dea15] R. S. Deacon, A. Oiwa, J. Sailer, S. Baba, Y. Kanai, K. Shibata, K. Hirakawa, and S. Tarucha. *Cooper pair splitting in*

parallel quantum dot Josephson junctions. Nat. Commun. **6** (2015), 7446.

[DM13] A. Del Maestro, T. Hyart, and B. Rosenow. *Backscattering between helical edge states via dynamic nuclear polarization*. Phys. Rev. B **87** (2013), 165440.

[Dol11] F. Dolcini. *Full electrical control of charge and spin conductance through interferometry of edge states in topological insulators*. Phys. Rev. B **83** (2011), 165304.

[Dol12] G. Dolcetto, S. Barbarino, D. Ferraro, N. Magnoli, and M. Sassetti. *Tunneling between helical edge states through extended contacts*. Phys. Rev. B **85** (2012), 195138.

[Dol13] G. Dolcetto, F. Cavaliere, D. Ferraro, and M. Sassetti. *Generating and controlling spin-polarized currents induced by a quantum spin Hall antidot*. Phys. Rev. B **87** (2013), 085425.

[Dol16] G. Dolcetto and T. L. Schmidt. *Emission of entangled Kramers pairs from a helical mesoscopic capacitor*. Phys. Rev. B **94** (2016), 075444.

[Ema12] C. Emary, C. Pöltl, A. Carmele, J. Kabuss, A. Knorr, and T. Brandes. *Bunching and antibunching in electronic transport*. Phys. Rev. B **85** (2012), 165417.

[Eri12] E. Eriksson, A. Ström, G. Sharma, and H. Johannesson. *Electrical control of the Kondo effect in a helical edge liquid*. Phys. Rev. B **86** (2012), 161103.

[Eri13] E. Eriksson. *Spin-orbit interactions in a helical Luttinger liquid with a Kondo impurity*. Phys. Rev. B **87** (2013), 235414.

[Ess05] F. H. L. Essler. *The one-dimensional Hubbard model*. Cambridge University Press, Cambridge (2005).

[Fer08] A. Fert. *Nobel Lecture: Origin, development, and future of spintronics*. Rev. Mod. Phys. **80** (2008), 1517–1530.

[Fer13] D. Ferraro, G. Dolcetto, R. Citro, F. Romeo, and M. Sassetti. *Spin current pumping in helical Luttinger liquids*. Phys. Rev. B **87** (2013), 245419.

[Fra91] E. Fradkin. *Field theories of condensed matter systems*. Number 82 in Frontiers in physics. Addison-Wesley, Reading, Mass. (1991).

[Fre06] E. Freitag and R. Busam. *Funktionentheorie 1*. Springer-Lehrbuch. Springer-Verlag, Berlin, Heidelberg, vierte, korrigierte und erweiterte auflage edition (2006).

[Ger22a] W. Gerlach and O. Stern. *Das magnetische Moment des Silberatoms*. Zeitschrift für Physik **9** (1922), 353–355.

[Ger22b] W. Gerlach and O. Stern. *Der experimentelle Nachweis der Richtungsquantelung im Magnetfeld*. Zeitschrift für Physik **9** (1922), 349–352.

[Ger22c] W. Gerlach and O. Stern. *Der experimentelle Nachweis des magnetischen Moments des Silberatoms*. Zeitschrift für Physik **8** (1922), 110–111.

[Ger10] F. Gerhard. *Magnetfeld- und Temperaturabhängigkeit des Quanten-Spin-Hall-Effekts*. Master's thesis, Physikalisches Institut Julius-Maximilians-Universität Würzburg (2010).

[Gia07] T. Giamarchi. *Quantum physics in one dimension*. Number 121 in International series of monographs on physics. Clarendon Press, Oxford (2007).

[Giu15] M. Giustina, M. A. M. Versteegh, S. Wengerowsky, J. Handsteiner, A. Hochrainer, K. Phelan, F. Steinlechner, J. Kofler, J.-A. Larsson, C. Abellán, W. Amaya, V. Pruneri, M. W. Mitchell, J. Beyer, T. Gerrits, A. E. Lita, L. K. Shalm, S. W. Nam, T. Scheidl, R. Ursin, B. Wittmann, and A. Zeilinger. *Significant-Loophole-Free Test of Bell's Theorem with Entangled Photons*. Phys. Rev. Lett. **115** (2015), 250401.

[Gra01] H. Grabert. *Transport in Single Channel Quantum Wires*. In S. Sarkar, editor, *Exotic States in Quantum Nanostructures*, Exotic States in Quantum Nanostructures. Springer, Dotrecht, 1–52 (2001).

[Grü86] P. Grünberg, R. Schreiber, Y. Pang, M. B. Brodsky, and H. Sowers. *Layered Magnetic Structures: Evidence for Antiferromagnetic Coupling of Fe Layers across Cr Interlayers*. Phys. Rev. Lett. **57** (1986), 2442–2445.

[Grü08] P. A. Grünberg. *Nobel Lecture: From spin waves to giant magnetoresistance and beyond*. Rev. Mod. Phys. **80** (2008), 1531–1540.

[Gus06] S. Gustavsson, R. Leturcq, B. Simovič, R. Schleser, T. Ihn, P. Studerus, K. Ensslin, D. C. Driscoll, and A. C. Gossard. *Counting Statistics of Single Electron Transport in a Quantum Dot*. Phys. Rev. Lett. **96** (2006), 076605.

[Haa10] F. Haake. *Quantum signatures of chaos*. Springer series in synergetics. Springer, Berlin ; Heidelberg, 3., rev. and enlarged ed. edition (2010).

[Hak04] H. Haken and H. C. Wolf. *Atom- und Quantenphysik*. Springer-Verlag, Berlin Heidelberg (2004).

[Han07] R. Hanson, L. P. Kouwenhoven, J. R. Petta, S. Tarucha, and L. M. K. Vandersypen. *Spins in few-electron quantum dots*. Rev. Mod. Phys. **79** (2007), 1217–1265.

[Hen15] B. Hensen, H. Bernien, A. E. DrÃ©au, A. Reiserer, N. Kalb, M. S. Blok, J. Ruitenberg, R. F. L. Vermeulen, R. N. Schouten, C. AbellÃ¡n, W. Amaya, V. Pruneri, M. W. Mitchell, M. Markham, D. J. Twitchen, D. Elkouss, S. Wehner, T. H. Taminiau, and R. Hanson. *Loophole-free Bell inequality violation using electron spins separated by 1.3 kilometres*. Nature **526** (2015), 682.

[Hew93] A. C. Hewson. *The Kondo Problem to Heavy Fermions*. Number 2 in Cambridge studies in magnetism. Cambridge Univ. Press, Cambridge, 1. publ. edition (1993).

[Hus16] R. Hussein, L. Jaurigue, M. Governale, and A. Braggio. *Double quantum dot Cooper-pair splitter at finite couplings*. Phys. Rev. B **94** (2016), 235134.

[Inh13] A. Inhofer and D. Bercioux. *Proposal for an on-demand source of polarized electrons into the edges of a topological insulator*. Phys. Rev. B **88** (2013), 235412.

[Ish95] S. Ishizaka, J. Sone, and T. Ando. *dc Josephson current through a quantum dot coupled with superconducting leads*. Phys. Rev. B **52** (1995), 8358–8362.

[Jac15] R. Jacquet, J. Rech, T. Jonckheere, A. Zazunov, and T. Martin. *Cooper pair splitting and recombination in a nanoSQUID geometry at high transparency*. Phys. Rev. B **92** (2015), 235429.

[Jos62] B. Josephson. *Possible new effects in superconductive tunnelling*. Physics Letters **1** (1962), 251–253.

[Jos65] B. Josephson. *Supercurrents through barriers*. Advances in Physics **14** (1965), 419–451.

[Kan92a] C. L. Kane and M. P. A. Fisher. *Transmission through barriers and resonant tunneling in an interacting one-dimensional electron gas*. Phys. Rev. B **46** (1992), 15233–15262.

[Kan92b] C. L. Kane and M. P. A. Fisher. *Transport in a one-channel Luttinger liquid*. Phys. Rev. Lett. **68** (1992), 1220–1223.

[Kan05a] C. L. Kane and E. J. Mele. *Quantum Spin Hall Effect in Graphene*. Phys. Rev. Lett. **95** (2005), 226801.

[Kan05b] C. L. Kane and E. J. Mele. *Z_2 Topological Order and the Quantum Spin Hall Effect*. Phys. Rev. Lett. **95** (2005), 146802.

[Kli03] I. Klich. *An Elementary Derivation of Levitov's Formula*. In Y. V. Nazarov, editor, *Quantum Noise in Mesoscopic Physics*, volume 97 of *NATO Science Series II. Mathematics, Physics and Chemistry*. Kluvert Academic Publishers Dordrecht, 397–402 (2003).

[Kol10] S. Koller, M. Grifoni, M. Leijnse, and M. R. Wegewijs. *Density-operator approaches to transport through interacting quantum dots: Simplifications in fourth-order perturbation theory*. Phys. Rev. B **82** (2010), 235307.

[Kön07] M. König, S. Wiedmann, C. Brüne, A. Roth, H. Buhmann, L. W. Molenkamp, X.-L. Qi, and S.-C. Zhang. *Quantum Spin Hall Insulator State in HgTe Quantum Wells*. Science **318** (2007), 766–770.

[Kön08] M. König, H. Buhmann, L. W. Molenkamp, T. Hughes, C.-X. Liu, X.-L. Qi, and S.-C. Zhang. *The Quantum Spin Hall Effect: Theory and Experiment*. Journal of the Physical Society of Japan **77** (2008), 031007.

[Lai15] E. A. Laird, F. Kuemmeth, G. A. Steele, K. Grove-Rasmussen, J. Nygård, K. Flensberg, and L. P. Kouwenhoven. *Quantum transport in carbon nanotubes*. Rev. Mod. Phys. **87** (2015), 703–764.

[Lee10] M. Lee, T. Jonckheere, and T. Martin. *Josephson effect through a multilevel quantum dot near a singlet-triplet transition*. Phys. Rev. B **81** (2010), 155114.

[Les01] G. Lesovik, T. Martin, and G. Blatter. *Electronic entanglement in the vicinity of a superconductor*. Eur. Phys. J. B **24** (2001), 287–290.

[Lev04] L. S. Levitov and M. Reznikov. *Counting statistics of tunneling current*. Phys. Rev. B **70** (2004), 115305.

[Lik79] K. K. Likharev. *Superconducting weak links*. Rev. Mod. Phys. **51** (1979), 101–159.

[Los98] D. Loss and D. P. DiVincenzo. *Quantum computation with quantum dots*. Phys. Rev. A **57** (1998), 120–126.

[LY07] A. Levy Yeyati, F. S. Bergeret, A. Martín-Rodero, and T. M. Klapwijk. *Entangled Andreev pairs and collective excitations in nanoscale superconductors*. Nat. Phys. **3** (2007), 455–459.

[Mac09] J. Maciejko, C. Liu, Y. Oreg, X.-L. Qi, C. Wu, and S.-C. Zhang. *Kondo Effect in the Helical Edge Liquid of the Quantum Spin Hall State*. Phys. Rev. Lett. **102** (2009), 256803.

[Mac12] J. Maciejko. *Kondo lattice on the edge of a two-dimensional topological insulator*. Phys. Rev. B **85** (2012), 245108.

[McN10] R. P. G. McNeil, R. J. Schneble, M. Kataoka, C. J. B. Ford, T. Kasama, R. E. Dunin-Borkowski, J. M. Feinberg, R. J. Harrison, C. H. W. Barnes, D. H. Y. Tse, T. Trypiniotis, J. A. C. Bland, D. Anderson, G. A. C. Jones, and M. Pepper. *Localized Magnetic Fields in Arbitrary Directions Using Patterned Nanomagnets*. Nano Letters **10** (2010), 1549–1553.

[Mia15] G.-X. Miao and J. S. Moodera. *Spin manipulation with magnetic semiconductor barriers*. Phys. Chem. Chem. Phys. **17** (2015), 751–761.

[Mic11] P. Michetti and P. Recher. *Bound states and persistent currents in topological insulator rings*. Phys. Rev. B **83** (2011), 125420.

[Mic12a] P. Michetti, J. C. Budich, E. G. Novik, and P. Recher. *Tunable quantum spin Hall effect in double quantum wells*. Phys. Rev. B **85** (2012), 125309.

[Mic12b] P. Michetti, P. H. Penteado, J. C. Egues, and P. Recher. *Helical edge states in multiple topological mass domains*. Semiconductor Science and Technology **27** (2012), 124007.

[Naz03] Y. V. Nazarov, editor. *Quantum noise in mesoscopic physics*, volume 97 of *NATO Science Series II. Mathematics, Physics and Chemistry*. Kluwer Acad. Publ., Dordrecht (2003).

[Naz09] Y. V. Nazarov and Y. M. Blanter. *Quantum Transport: Introduction to Nanoscience*. Cambridge University Press (2009).

[Nie10] M. A. Nielsen and I. L. Chuang. *Quantum computation and quantum information*. Cambridge Univ. Press, Cambridge [u.a.], 10. anniversary ed. edition. Hier auch später erschienene, unveränderte Nachdrucke (2010).

[Nig15] S. E. Nigg, R. P. Tiwari, S. Walter, and T. L. Schmidt. *Detecting nonlocal Cooper pair entanglement by optical Bell inequality violation*. Phys. Rev. B **91** (2015), 094516.

[Oli02] W. D. Oliver, F. Yamaguchi, and Y. Yamamoto. *Electron Entanglement via a Quantum Dot*. Phys. Rev. Lett. **88** (2002), 037901.

[Pau27] W. Pauli. *Über Gasentartung und Paramagnetismus*. Zeitschrift für Physik **41** (1927), 81–102.

[Peç03] C. S. Peça, L. Balents, and K. J. Wiese. *Fabry-Perot interference and spin filtering in carbon nanotubes*. Phys. Rev. B **68** (2003), 205423.

[Pik14] D. I. Pikulin, T. Hyart, S. Mi, J. Tworzydło, M. Wimmer, and C. W. J. Beenakker. *Disorder and magnetic-field-induced breakdown of helical edge conduction in an inverted electron-hole bilayer*. Phys. Rev. B **89** (2014), 161403.

[Pra04] E. Prada and F. Sols. *Entangled electron current through finite size normal-superconductor tunneling structures*. Eur. Phys. J. B **40** (2004), 379–396.

[Pro15] B. Probst, P. Virtanen, and P. Recher. *Controlling spin polarization of a quantum dot via a helical edge state*. Phys. Rev. B **92** (2015), 045430.

[Pro16] B. Probst, F. Domínguez, A. Schroer, A. L. Yeyati, and P. Recher. *Signatures of nonlocal Cooper-pair transport and of a singlet-triplet transition in the critical current of a double-quantum-dot Josephson junction*. Phys. Rev. B **94** (2016), 155445.

[Rab37] I. I. Rabi. *Space Quantization in a Gyrating Magnetic Field*. Phys. Rev. **51** (1937), 652–654.

[Ram50] N. F. Ramsey. *A Molecular Beam Resonance Method with Separated Oscillating Fields*. Phys. Rev. **78** (1950), 695–699.

[Rec01] P. Recher, E. V. Sukhorukov, and D. Loss. *Andreev tunneling, Coulomb blockade, and resonant transport of nonlocal spin-entangled electrons*. Phys. Rev. B **63** (2001), 165314.

[Rec02] P. Recher and D. Loss. *Superconductor coupled to two Luttinger liquids as an entangler for electron spins*. Phys. Rev. B **65** (2002), 165327.

[Rec03] P. Recher. *Correlated spin transport in nanostructures: entanglement creation and spin filtering*. Ph.D. thesis, Universität Basel. Ref.: Daniel Loss, C.J.W. Beenakker, Christoph Bruder (2003).

[Rot09] A. Roth, C. Brüne, H. Buhmann, L. W. Molenkamp, J. Maciejko, X.-L. Qi, and S.-C. Zhang. *Nonlocal Transport in the Quantum Spin Hall State*. Science **325** (2009), 294–297.

[Rot10] D. G. Rothe, R. W. Reinthaler, C.-X. Liu, L. W. Molenkamp, S.-C. Zhang, and E. M. Hankiewicz. *Fingerprint of different spin–orbit terms for spin transport in HgTe quantum wells*. New Journal of Physics **12** (2010), 065012.

[Roz01] A. Rozhkov, D. Arovas, and F. Guinea. *Josephson coupling through a quantum dot*. Phys. Rev. B **64** (2001), 233301.

[Saf96] I. Safi and H. J. Schulz. *Transport through a single-band wire connected to measuring leads*. In B. Kramer, editor, *Quantum transport in semiconductor submicron structures*, volume 326 of *NATO ASI Series (Series E: Applied Sciences)*. Kluwer, Dordrecht, 159–172 (1996).

[Sai98] R. Saito, G. Dresselhaus, and M. S. Dresselhaus. *Physical Properties of Carbon Nanotubes*. Imperial College Press, London (1998).

[Sak09] J. J. Sakurai. *Modern quantum mechanics*. Addison-Wesley Longman, Reading Mass., Bonn, rev. ed. edition. San Fu Tuan ed. (2009).

[Sat10] K. Sato, D. Loss, and Y. Tserkovnyak. *Cooper-Pair Injection into Quantum Spin Hall Insulators*. Phys. Rev. Lett. **105** (2010), 226401.

[Sch66] J. R. Schrieffer and P. A. Wolff. *Relation between the Anderson and Kondo Hamiltonians*. Phys. Rev. **149** (1966), 491–492.

[Sch97] H. Schoeller. *Transport Theory of Interacting Quantum Dots*. In L. L. Sohn, L. P. Kouwenhoven, and G. Schön, editors, *Mesoscopic Electron Transport*. Kluvert Academic Publishers, 291–330 (1997).

[Sch08] A. P. Schnyder, S. Ryu, A. Furusaki, and A. W. W. Ludwig. *Classification of topological insulators and superconductors in three spatial dimensions*. Phys. Rev. B **78** (2008), 195125.

[Sch12a] B. Scharf, A. Matos-Abiague, and J. Fabian. *Magnetic properties of HgTe quantum wells*. Phys. Rev. B **86** (2012), 075418.

[Sch12b] J. Schindele, A. Baumgartner, and C. Schönenberger. *Near-Unity Cooper Pair Splitting Efficiency*. Phys. Rev. Lett. **109** (2012), 157002.

[Sch12c] T. L. Schmidt, S. Rachel, F. von Oppen, and L. I. Glazman. *Inelastic Electron Backscattering in a Generic Helical Edge Channel*. Phys. Rev. Lett. **108** (2012), 156402.

[Sch15a] A. Schroer and P. Recher. *Detection of nonlocal spin entanglement by light emission from a superconducting $p-n$ junction*. Phys. Rev. B **92** (2015), 054514.

[Sch15b] A. Schroer, P. G. Silvestrov, and P. Recher. *Valley-based Cooper pair splitting via topologically confined channels in bilayer graphene*. Phys. Rev. B **92** (2015), 241404.

[Scu97] M. O. Scully and M. S. Zubairy. *Quantum optics*. Cambridge Univ. Press, Cambridge. Literaturangaben (1997).

[Sha11] W.-Y. Shan, J. Lu, H.-Z. Lu, and S.-Q. Shen. *Vacancy-induced bound states in topological insulators*. Phys. Rev. B **84** (2011), 035307.

[Shi98] Y. Shimizu, H. Horii, Y. Takane, and Y. Isawa. *Multilevel Effect on the Josephson Current through a Quantum Dot*. Journal of the Physical Society of Japan **67** (1998), 1525–1528.

[Soh97] L. Sohn, L. Kouwenhoven, and G. Schön. *Mesoscopic electron transport*. NATO ASI series: Applied sciences. Kluwer Academic Publishers (1997).

[Spi91] B. I. Spivak and S. A. Kivelson. *Negative local superfluid densities: The difference between dirty superconductors and dirty Bose liquids*. Phys. Rev. B **43** (1991), 3740–3743.

[Sto38] E. C. Stoner. *Collective electron ferronmagnetism*. Proceedings of the Royal Society of London A: Mathematical, Physical and Engineering Sciences **165** (1938), 372–414.

[Str09] A. Ström and H. Johannesson. *Tunneling between Edge States in a Quantum Spin Hall System*. Phys. Rev. Lett. **102** (2009), 096806.

[Str15] A. Ström, H. Johannesson, and P. Recher. *Controllable spin entanglement production in a quantum spin Hall ring*. Phys. Rev. B **91** (2015), 245406.

[Suk01] E. V. Sukhorukov, G. Burkard, and D. Loss. *Noise of a quantum dot system in the cotunneling regime*. Phys. Rev. B **63** (2001), 125315.

[Tan11] Y. Tanaka, A. Furusaki, and K. A. Matveev. *Conductance of a Helical Edge Liquid Coupled to a Magnetic Impurity*. Phys. Rev. Lett. **106** (2011), 236402.

[Ted86] P. M. Tedrow, J. E. Tkaczyk, and A. Kumar. *Spin-Polarized Electron Tunneling Study of an Artificially Layered Superconductor with Internal Magnetic Field: EuO-Al*. Phys. Rev. Lett. **56** (1986), 1746–1749.

[Teo09] J. C. Y. Teo and C. L. Kane. *Critical behavior of a point contact in a quantum spin Hall insulator*. Phys. Rev. B **79** (2009), 235321.

[Tho82] D. J. Thouless, M. Kohmoto, M. P. Nightingale, and M. den Nijs. *Quantized Hall Conductance in a Two-Dimensional Periodic Potential*. Phys. Rev. Lett. **49** (1982), 405–408.

[Tin96] M. Tinkham. *Introduction to superconductivity*. McGraw-Hill international editions. McGraw-Hill, New York, 2. ed edition (1996).

[Tka10] G. Tkachov and E. M. Hankiewicz. *Ballistic Quantum Spin Hall State and Enhanced Edge Backscattering in Strong Magnetic Fields*. Phys. Rev. Lett. **104** (2010), 166803.

[Tka11] G. Tkachov and E. M. Hankiewicz. *Transition between ordinary and topological insulator regimes in two-dimensional resonant magnetotransport*. Phys. Rev. B **83** (2011), 155412.

[Väy13] J. I. Väyrynen, M. Goldstein, and L. I. Glazman. *Helical Edge Resistance Introduced by Charge Puddles*. Phys. Rev. Lett. **110** (2013), 216402.

[Väy14] J. I. Väyrynen, M. Goldstein, Y. Gefen, and L. I. Glazman. *Resistance of helical edges formed in a semiconductor heterostructure*. Phys. Rev. B **90** (2014), 115309.

[vD98] J. von Delft and H. Schoeller. *Bosonization for beginners — refermionization for experts*. Annalen der Physik **7** (1998), 225–305.

[vD06] J. A. van Dam, Y. V. Nazarov, E. P. A. M. Bakkers, S. De Franceschi, and L. P. Kouwenhoven. *Supercurrent reversal in quantum dots*. Nature **442** (2006), 667–670.

[Vec03] E. Vecino, A. Martín-Rodero, and A. L. Yeyati. *Josephson current through a correlated quantum level: Andreev states and π junction behavior*. Phys. Rev. B **68** (2003), 035105.

[Vir11] P. Virtanen and P. Recher. *Dephasing of spin and charge interference in helical Luttinger liquids*. Phys. Rev. B **83** (2011), 115332.

[Vir12] P. Virtanen and P. Recher. *Signatures of Rashba spin-orbit interaction in the superconducting proximity effect in helical Luttinger liquids*. Phys. Rev. B **85** (2012), 035310.

[vW88] B. J. van Wees, H. van Houten, C. W. J. Beenakker, J. G. Williamson, L. P. Kouwenhoven, D. van der Marel, and C. T. Foxon. *Quantized conductance of point contacts in a two-dimensional electron gas*. Phys. Rev. Lett. **60** (1988), 848–850.

[Wan11] Z. Wang and X. Hu. *Interference and Switching of Josephson Current Carried by Nonlocal Spin-Entangled Electrons in a SQUID-Like System with Quantum Dots*. Phys. Rev. Lett. **106** (2011), 037002.

[Wei13] L. Weithofer and P. Recher. *Chiral Majorana edge states in HgTe quantum wells*. New Journal of Physics **15** (2013), 085008.

[Wey05a] I. Weymann, J. Barnaś, J. König, J. Martinek, and G. Schön. *Zero-bias anomaly in cotunneling transport through quantum-dot spin valves*. Phys. Rev. B **72** (2005), 113301.

[Wey05b] I. Weymann, J. König, J. Martinek, J. Barnaś, and G. Schön. *Tunnel magnetoresistance of quantum dots coupled to ferromagnetic leads in the sequential and cotunneling regimes*. Phys. Rev. B **72** (2005), 115334.

[Win03] R. Winkler. *Spin-orbit Coupling Effects in Two-Dimensional Electron and Hole Systems*, volume 191 of *Springer Tracts in Modern Physics*. Springer, Berlin (2003).

[Wu06] C. Wu, B. A. Bernevig, and S.-C. Zhang. *Helical Liquid and the Edge of Quantum Spin Hall Systems*. Phys. Rev. Lett. **96** (2006), 106401.

[Xia11] D. Xiao, W. Zhu, Y. Ran, N. Nagaosa, and S. Okamoto. *Interface engineering of quantum Hall effects in digital transition metal oxide heterostructures*. Nat. Commun. **2:596** (2011), 5.

[Xu06] C. Xu and J. E. Moore. *Stability of the quantum spin Hall effect: Effects of interactions, disorder, and $\mathbb{Z}_2$ topology*. Phys. Rev. B **73** (2006), 045322.

[Xu13] Y. Xu, B. Yan, H.-J. Zhang, J. Wang, G. Xu, P. Tang, W. Duan, and S.-C. Zhang. *Large-Gap Quantum Spin Hall Insulators in Tin Films*. Phys. Rev. Lett. **111** (2013), 136804.

[Zha14] H. Zhang, Y. Xu, J. Wang, K. Chang, and S.-C. Zhang. *Quantum Spin Hall and Quantum Anomalous Hall States Realized in Junction Quantum Wells*. Phys. Rev. Lett. **112,** (2014), 216803.

[Zho08] B. Zhou, H.-Z. Lu, R.-L. Chu, S.-Q. Shen, and Q. Niu. *Finite Size Effects on Helical Edge States in a Quantum Spin-Hall System*. Phys. Rev. Lett. **101** (2008), 246807.

[Zho14] M. Zhou, W. Ming, Z. Liu, Z. Wang, Y. Yao, and F. Liu. *Formation of quantum spin Hall state on Si surface and energy gap scaling with strength of spin orbit coupling*. Scientific Reports **4** (2014), 7102.